Doctoral Thesis

ADAMTS1 ACTIVITY IN THE TUMOUR MICROENVIRONMENT AND THE VASCULAR NICHE: FOCUSING ON SUBSTRATES

FRANCISCO JAVIER RODRÍGUEZ BAENA

Granada, 2017

UNIVERSIDAD
DE GRANADA

PROGRAMA OFICIAL DE DOCTORADO EN BIOMEDICINA

_____

DEPARTAMENTO DE BIOQUÍMICA Y BIOLOGÍA MOLECULAR III E INMUNOLOGÍA

TESIS DOCTORAL

ADAMTS1 ACTIVITY IN THE TUMOUR MICROENVIRONMENT AND THE VASCULAR NICHE: FOCUSING ON SUBSTRATES

Francisco Javier Rodríguez Baena

Director de la tesis:
Juan Carlos Rodríguez-Manzaneque Escribano

Granada 07 de Abril del 2017

Ea!

AGRADECIMIENTOS

Tras escribir este libro que estás sujetando, puedo reconocer que esta es, sin duda, la parte más complicadas. Agradecer a todas las personas que de algún modo me han ayudado al desarrollo de este proyecto, ya sea profesional o personalmente, es muy difícil. En esta etapa he cambiado mucho, no puedo decir que me he hecho a mí mismo, porque en realidad todos nos hacemos de lo que nos rodea, de nuestro entorno. A día de hoy soy quien soy gracias a todos los que habéis pasado por mi vida y me siento muy agradecido y orgulloso.

Es necesario empezar dando las gracias a Juan Carlos, mi director de tesis, por darme la oportunidad y confiar en mi desde el principio y animarme a embarcarme en esta aventura, cuando sabías que no lo tenía nada claro. Aunque no lo parezca, han pasado muchos años y te he conocido profesionalmente, pero tengo claro que eres una gran persona y esta etapa ha quedado muy marcada por ti. Por esto y por todo, gracias.

Esta tesis la he realizado en el centro de investigación GENyO y no tengo hojas suficientes para describir lo que tengo que agradecer a todas las personas que están y que han pasado por aquí. Tengo que empezar por el grupo de investigación, porque más que un grupo ha sido una familia para mi durante 5 años. Empiezo por ti, MD, así me quito el nudo de la garganta… ¿qué puedo decirte? o ¿qué me queda por decirte?. No te puedo agradecer lo suficiente las horas de tu paciencia, aguantando mi carácter y mi humor. Eres el soporte humano del grupo y sin ti, ese laboratorio no llegaría muy lejos. A Estefanía, aunque coincidimos poco fui tu relevo y dejaste el nivel muy alto, gracias por toda la ayuda y tu amistad. A Rubén, que hayamos tenido nuestras diferencias, aprendí de ti y eso no se olvida. A Silvia, me quedo corto con lo que te pueda decir aquí, gracias por aguantarme en todos los sentidos y sobre todo, gracias por quedarte. Eres increíble y vas a llegar muy lejos, espero tenerte cerca siempre. A Peris, pelocho, gracias por aportar tu buen rollo y energía al grupo, voy a echar de menos tus bailes con la cabeza de fondo en mi pantalla. A Orlando, que también ha sufrido mi humor y aguantado como un valiente y una sonrisa.

A los vecinos del laboratorio 5 y 6, a Gabi y su guasa argentina, a Juani y su microondas, que risas… a Alba, Pili y Agustín. Los cristales no aportan discreción pero si unión, gracias por hacer esas largas horas de laboratorio más cortas.

Quería agradecer especialmente a mis compañeros de sala; Rosi, Antonio, Javi, Carmen, Luz, Almudena, Victoria, Diego, Angélica, Óscar, Suyapa, Joan y Fede, porque al fin y al cabo pasamos muchas horas allí encerrados, pero hacerlo con vosotros, ha sido un placer.

A muchos otros compañeros de GENyO con los que he vivido muy buenos momentos, es un placer estar rodeado de grandes profesionales y mejores personas; Thomas, Meri,

ACKNOWLEDGMENTS

El doctorando / *The doctoral candidate*: **Francisco Javier Rodríguez Baena** y el director de la tesis / *and the thesis supervisor*: **Juan Carlos Rodríguez-Manzaneque Escribano**

Garantizamos, al firmar esta tesis doctoral, que el trabajo ha sido realizado por el doctorando bajo la dirección del director de tesis y hasta donde nuestro conocimiento alcanza, en la realización del trabajo, se han respetado los derechos de otros autores a ser citados, cuando se han utilizado sus resultados o publicaciones.

/ /

Guarantee, by signing this doctoral thesis, that the work has been done by the doctoral candidate under the direction of the thesis supervisor and, as far as our knowledge reaches, in the performance of the work, the rights of other authors to be cited (when their results or publication have been used) have been respected.

Lugar y fecha / *Place and date*:
España, Granada, 07 de Abril de 2017

Tutor y Director de Tesis / *Thesis supervisor*;   Doctorando / *Doctoral candidate*
Juan Carlos Rodríguez-Manzaneque Escribano   Francisco Javier Rodríguez Baena

Firmado / *Signed*   Firmado / *Signed*

QUALITY CRITERIA TO AIM FOR THE DEGREE OF "INTERNATIONAL Ph.D" FROM THE UNIVERSITY OF GRANADA:

1. An accepted or published scientific article in a relevant journal on the field of the knowledge of the doctoral thesis, here signed by the candidate, including part of the thesis results.

> Fernández-Rodríguez, R., **Rodríguez-Baena, F.J**., Martino-Echarri, E., Peris-Torres, C., Plaza-Calonge, M.C., and Rodríguez-Manzaneque, J.C. (2016). **Stroma-derived but not tumor ADAMTS1 is a main driver of tumor growth and metastasis**. *Oncotarget 2016; 7(23):34507.*
> Impact factor: 5,008 (Q1).

2. International stay in a foreign research centre.

> A six months period working in the department of Paediatrics and Reproductive Health, Faculty of Medicine, University of Adelaide, South Australia, Australia. This research fellowship has been funded by the Endeavour Research Fellowship Program from the Ministry of Education of Australia. The receptor laboratory was lead by Dr. Darryl L. Russell.
> From June 2015 to December 2015.

NOTA

El grueso del texto ha sido desarrollado en inglés debido a que se opta para la distinción de "doctorado internacional" y por la lógica del desarrollo de la mayoría de la investigación en este idioma. En la mayoría de textos científicos, los términos, acrónimos y abreviaturas que se utilizan día a día están en inglés. Para evitar confusión y aportar coherencia dentro de lo posible, el texto de la tesis se ha desarrollado íntegramente en inglés, y de la misma forma será presentada ante el tribunal. Además se incluye un apartado donde se describen las abreviaciones y conceptos que puedan dar lugar a duda en caso de que el lector no esté familiarizado con ellos.

NOTE

According to University of Granada's requirements to obtain an "international doctorate" degree, this thesis has been written in English and it will be defended in that language as well. As the vast majority of scientific texts, English have been selected as the language to avoid misconception within scientific terminology, abbreviation and acronyms. Nevertheless, there is included an abbreviation table to facilitate the reader to go through the text in case they are not familiar with the terminology used.

TABLE OF CONTENTS

RESUMEN

Muchos estudios han demostrado la importancia del entorno extracelular y su dinamismo. Su propia complejidad y la respuesta a diferentes estímulos demuestran su importancia en procesos como el desarrollo, angiogénesis, regeneración tisular, y la progresión tumoral, entre muchos otros. Entre los componentes de la matriz extracelular (MEC), las proteasas cobran una vital importancia por su contribución al dinamismo característico. Cualquier cambio puede afectar a procesos celulares básicos como la proliferación, migración, invasión y diferenciación. Este trabajo se enfoca en la proteasa extracelular ADAMTS1 (<u>A</u> <u>D</u>isintegrin <u>an</u>d <u>M</u>etalloproteinase with <u>Thrombos</u>pondin Motifs <u>1</u>), primer miembro descrito de la familia ADAMTS. Sus funciones son variadas, encontrando referencias a sus acciones moduladoras de la angiogénesis y una participación dual durante la progresión tumoral y metástasis.

Durante los últimos años, este equipo de investigación ha estudiado a fondo ADAMTS1, contribuyendo al descubrimiento de sustratos, como Nidógenos y Versicano, importantes componentes de la matriz extracelular. Más recientemente sus esfuerzos han girado en torno a la función de estas proteínas y su procesamiento por ADAMTS1 en eventos como homeostásis y progresión tumoral.

Esta tesis ha estudiado ambos Nidógeno 1 y Nidógeno 2 en distintos contextos. Por un lado, en una serie de modelos tumorales en los que se ha modificado genéticamente ADAMTS1, se ha encontrado un importante incremento de la deposición de Nidógeno 1 alrededor de vasos tumorales cuando ADAMTS1 no está presente en el entorno tumoral, o cuando su expresión de inhibe en las células tumorales. En algunos de los modelos estudiados, esta mayor deposición de Nidógeno está acompañada del bloqueo de la progresión tumoral, y más en general se han encontrado alteraciones de la red vascular del tumor, pero sin consecuencias para su crecimiento. En adición, se han estudiado los efectos de la sobreexpresión de ambos Nidógenos, independientemente, en un modelo de melanoma murino (B16F1). Aparte de la inhibición de propiedades miméticas de endotelio de estas células *in-vitro*, por la citada sobreexpresión, también se ha observado una drástica reducción del crecimiento tumoral, pero solo con Nidógeno 1. Este hallazgo tiene importantes similitudes con lo ocurrido con células B16F1 parentales en ratones *Adamts1* Knockout, destacando el incremento de hipoxia que indica la disfuncionalidad de los vasos, aunque más alteraciones de la vasculatura también han sido encontradas.

Por otro lado, detallados estudios en ratones ADAMTS1 knockout revelan sugerentes alteraciones de Nidógeno 1 en órganos como el riñón y el bazo, al igual que ocurre para el Versicano, pero no coincidiendo exactamente en los mismos órganos. Distintos motivos han provocado estudios más detallados en órganos como el bazo y la médula ósea por su importancia reguladora del sistema inmune, descubriendo de hecho una importantísima conexión funcional con *Adamts1*. En esta línea de conocimiento, un último estudio incluye la generación de tumores (melanoma murino B16F1 y Carcinoma de pulmón de Lewis LLC), en ratones controles y ADAMTS1 knockouts, para estudiar las alteraciones del sistema inmune también en el bazo y la médula ósea. Importantes datos muestran que el ratón deficiente en *Adamts1* genera un microambiente inmunosupresor con consecuencias para la distinta progresión de cada modelo tumoral ensayado.

ABSTRACT

Past and recent studies have shown the importance of the extracellular microenvironment and its dynamism. Its complexity and the response to different stimuli denote its importance in processes such as development, angiogenesis, tissue regeneration, and tumour progression among many others. Within the extracellular matrix (ECM), proteases are important components given their contribution to dynamism. A single action would affect basic cellular processes as proliferation, migration, invasion and differentiation. Our main focus is the extracellular protease ADAMTS1 (A Disintegrin and Metalloproteinase with Thrombospondin Motifs 1), the first described member of ADAMTS family. Its roles vary, with reports about the modulatory activity of angiogenesis and also suggesting a dual participation during tumour progression and metastasis.

During the last years, this research team has focused its work on ADAMTS1, contributing to the discovery of substrates, as Nidogens and Versican, main components of the extracellular matrix. More recently their efforts were devoted to unveil the function of these substrates and their proteolytic cleavage by ADAMTS1, mostly during homeostasis and tumour progression.

This thesis project reports studies on Nidogen 1 and Nidogen 2 in different biological scenarios. In one side, using a variety of tumour models with genetically-modified

Adamts1, it has been found a significant increase of the deposition of Nidogen 1 in tumour vessels when *Adamts1* is not present in such context. In some of these models, such increase correlated with a striking blockade of tumour progression and impaired vasculature. Furthermore, it has been approached the overexpression of *Nidogen 1* and *Nidogen 2* in a melanoma murine tumour model (B16F1). In addition to the inhibition of capillary-like properties *in-vitro* provoked by such overexpression, in the case of nidogen 1 there is also a clear reduction of tumour growth. This finding displays relevant similarities to the effects observed with parental B16F1 in the *Adamts1* null mouse model, highlighting in both cases the induction of hypoxia that implies a major vascular dysfunctionality. Further alterations of the vasculature have been found.

Moreover, a thoughtful evaluation of *Adamts1* null mice exhibited changes for Nidogen 1 in organs such as kidney and spleen, as also occurred for Versican but no exactly in the same organs. A series of results encouraged the focus in organs as spleen and bone marrow, according to their importance as regulators of immune system. In fact, it has been observed an unexpected functional connection with *Adamts1*. In line with these insights, a last study includes the induction of tumours (murine melanoma B16F1 and Lewis lung carcinoma LLC), in wild type and *Adamts* KO mice, studying alterations of the immune system in those tumours, together with spleen and bone marrow. Relevant data show that the deficiency of *Adamts1* induces an immunosuppressive environment with consequences for the distinct tumour output of every tumour model.

ABBREVIATIONS AND ACRONYMS

ABREVIATURE	DEFINITION
ADAM	A Disintegrin and Metalloprotease
ADAMTS	A Disintegrin and Metalloprotease with Thrombospondin motifs
ADAMTS1	A Disintegrin and Metalloprotease with Thrombospondin motif 1
ANG-1	Angiopoietin - 1
APC	Antigen presenting cell or accessory cell
Arg1	Arginase - 1
B-Cell	B lymphocyte cell
B16F0	B16F0 mouse melanoma cell line
B16F1	B16F1 mouse melanoma cell line
BL	Basal Lamina
BM	Basement membrane or Bone marrow (context dependent)
BMDM	Bone marrow derived macrophages
BRG1	Transcription activator BRG1 or ATP-dependent helicase SMARCA4
C57BL/6	C57BL/6 mouse strain
CA125	Ovarian cancer prognosis marker CA125
CAFs	Cancer associated fibroblasts
CAT	Catalytic domain
CC	Cancer cell
CD11b	Cluster of differentiation molecule 11b o Integrin alpha M (ITGAM)
CD144/VE-CAD	Cluster of differentiation molecule 144 or Vascular endothelial cadherin
CD163	Cluster of differentiation molecule 163
CD3	Cluster of differentiation molecule 3
CD31 or PECAM	Cluster of differentiation molecule 31 or Platelet endothelial cell adhesion molecule
CD34	Cluster of differentiation molecule 34
CD44	Cluster of differentiation molecule 44 or Homing cell adhesion molecule
CD45	Cluster of differentiation molecule 45 or Protein tyrosine phosphatase, receptor type, C
CD45R	Cluster of differentiation molecule 45 receptor or Protein tyrosine phosphatase, receptor type, C receptor
CD8	Cluster of differentiation molecule 8
cDNA	Complementary Deoxyribonucleic acid
CHO	Chinese hamster ovary cell line
CL	Cell lysate
CM	Conditioned Media
Col IV	Collagen IV
CS	Chondroitin sulphate

CSCs	Cancer stem cells
Ct	Cycle threshold
CVM-1118	phenyl-quinoline derivative, vasculogenic mimicry drug
Cy	Cytoplasmic region
DNA	Deoxyribonucleic acid
DPEAAE	Aspartic acid-Proline-Glutamic acid-Alanine-Alanine-Glutamic acid (Cleavage product from Versican)
ECM	Extracellular matrix
ECs	Endothelial cells
EGF	Epithelial growth factor
EGFR	Epithelial growth factor receptor
EMT	Epithelial to mesenchymal transition
EPCs	Endothelial progenitor cells
EPHA2	Ephrin A2
ETV5	Transcription factor ETV5
EZH2	Enhancer of zeste homolog 2
F4/80	EGF-like module-containing mucin-like hormone receptor-like 1
FAK	Focal adhesion kinase
FGF	Fibroblast growth factor
FNs	Fibronectins
G1	Nidogen G1 domain
G2	Nidogen G2 domain
G2-G3	Nidogen G2-G3 domains
G3	Nidogen G3 domain
GAGs	Glycosaminoglycans
GENyO	Pfizer-University of Granada-Junta de Andalucía Centre for Genomics and Oncological Research
GR1	Lymphocyte antigen 6 complex locus G6D
H3K27	Histone H3 lysine 27
HEK-293T	Human embryonic kidney 293T
IGF-1/2	Insulin growth factor 1 or 2
IIC	Infiltrating immune cells
IL-10	Interleukin 10
IL-12	Interleukin 12
IL-6	Interleukin 6
IL-1	Interleukin 1
iMCs	Immature myeloid cells
iNOS/NOS2	Inducible nitric oxide synthase
IRF8	Interferon regulatory factor 8
ISH	*In-situ* hybridization
KD	Knockdown regulation
kDa	kiloDalton

KO	Knockout
LAMC2	laminin 5 γ2-chain
LDL	Low density lipoprotein
LLC	Lewis Lung Carcinoma cell line
MDC	Myeloid derived cell
MDSC	Myeloid derived suppressor cell
MEC	From Spanish "*Matriz extracelular*", Extracellular matrix
MLEC	Mouse lung endothelial cells
MMPs	Matrix metalloproteases
MMTV-PYMT	mouse mammary tumour-virus promoter with the polyoma middle T-antigen
MSCs	Mesenchymal stromal or stem cell
MT	Transmembrane domain
MT-MMP	Transmembrane domain metalloprotease
MUM2B	Human uveal melanoma MUM2B cell line
NG2	Neural/glial antigen 2
NID1	Nidogen 1
NID2	Nidogen 2
NIDO	Nidogen-like domain
NK	Natural killer
Notch/Dll4	notch – Delta like-ligand 4
PAS	periodic acid-shiff
PCs	Pericyte cell
PDGFC	platelet derived growth factor c
PDGFβ	platelet derived growth factor β
PDGFβR2	platelet derived growth factor β receptor 2
PGK	Phosphoglycerate kinase
PGs	Proteoglycans
PI3K	phosphatidylinositol 3-kinase
PRE	Signal peptide
PRO	Pro domain
PTEN	phosphatase and tensin homolog
qPCR	Quantitave polymerase chain reaction
RGD	Arginine-Glycine-Aspartic acid
RNA	Ribonucleic acid
Rod	Rod domain
SH-SY5Y	Human bone marrow neuroblast cell line
SM-MHC	Smooth muscle-myosin heavy chain
SMA	Smooth muscle actin
T-Cell	Lymphocyte T-cell
TAM	Tumour associated macrophage
TEM	Tie 2 expressing monocyte

TEM7	PLXDC1 - Plexin Domain Containing 1
TFPI	Tissue factor pathway inhibitor
TGFβ	Transforming growth factor beta
TICs	Tumour initiating cells
Tie2	Tyrosine kinase angiopoietin receptor 2
TIMPs	Tissue inhibitor of metalloproteases
TLR2	Toll-like receptor 2
TME	Tumour microenvironment
TNFα	Tumour necrosis factor alpha
TSP	Thrombospondin
TY	Thyroglobulin type-1
UGR	University of Granada
vBM	Vascular basement membrane
VCAN	Versican
VEGF	Vascular endothelial growth factor
VEGF-A	Vascular endothelial growth factor A
VEGFR2	Vascular endothelial growth factor receptor 2
VM	Vasculogenic mimicry
VKIN	Versikine
vSMC	Vascular smooth muscle cell
vWF	Von Willebrand factor
WT	Wild type
αSMA	Alpha smooth muscle actin
3LL	Lewis lung carcinoma cell line

FIGURES AND TABLES INDEX

INTRODUCTION

1. CANCER HETEROGENEITY

1.1 KEY CONCEPTS

Cancer is the name given to a series of related malignancies. The origin of these diseases coincides with the abnormal proliferation of cells which loses the capability to stop that process. The generation and renewal of normal cells take place in a harmonious manner. This process is determined by a surveillance system that detects failures, mutations and apoptotic cells and determines their fate. When a normal cell cannot stop dividing and skip this monitoring system then becomes neoplastic and it may develop a tumour due to its uncontrolled growing capacities (Nowell, 1976).

A cancer cell accumulates mutations that will be inherited to the cells that arise from it. These changes induced by genetic variations, provide a positive or negative feature that will make this cell population to grow or shrink within the tumour. Metabolic disadvantages and the immune system are the common reasons for the failure of these populations to proliferate. Divergence emerge with the result of variant subclones that progress distinctly. The thesis of the tumour origin from a single cell has been accepted taking into consideration Darwinian evolutionary patterns (**Figure 1a**). However, we should remember that the exposure to carcinogens may alter and turn into neoplastic several cells within a tissue (Greaves, 2010; Marusyk and Polyak, 2010).

Since the nineteenth century, when modern microscopes were used to study human tissue, the age of cellular pathology busted to provide a scientific basis to the already observed anomalies and diseases. Cancer, among them, surprised physicians since early Greek and Roman times. The reductionist model of cancer has been based on the fact of out-of-control neoplastic cells that arise tumours rapidly. Nowadays we know that tumours, as other organs in our bodies, have a heterogeneous population of cells that are not only tumour cells (Hanahan and Weinberg, 2000).

During the development of a tumour, clonal evolution will create a heterogenic intra-tumour environment in which cancer cells will differ from each other in specific mutations (**Figure 1b**). The tissue environment, an ecosystem evolved during a billion of years to adapt the multicellular function, also participates during this clonal evolution (Greaves and Maley, 2012). It is very important to distinguish between clonal heterogeneity and tumour heterogeneity. While the first concept refers to the cancer subclone variation obtained from a rich genetic tumour cell landscape, tumour heterogeneity refers to the variety of cells from different origins within the tumour microenvironment.
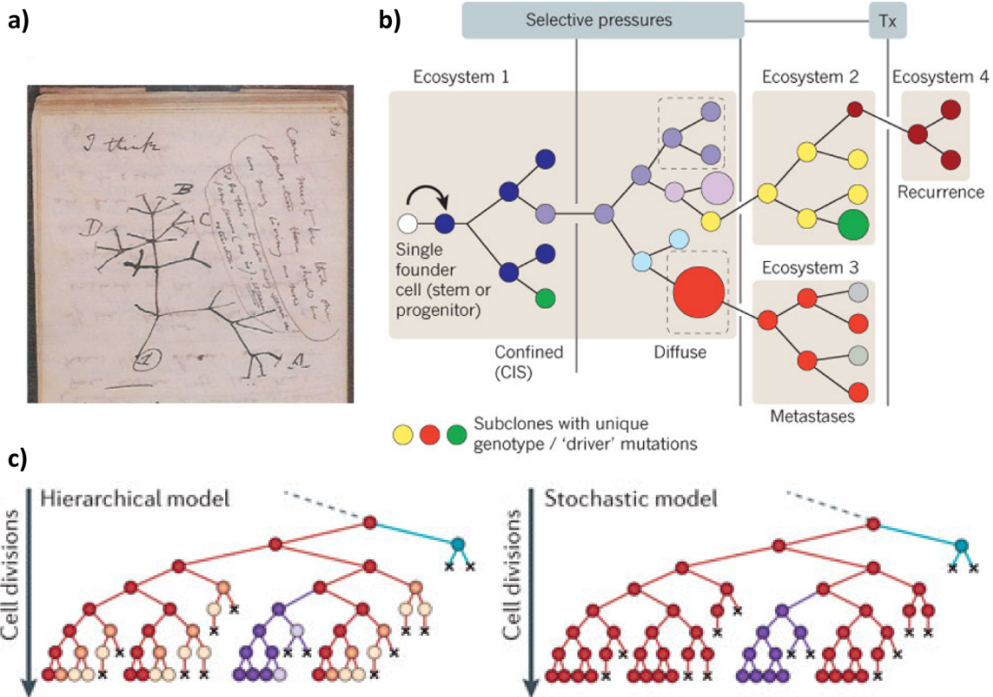
Figure 1. The branching architecture of tumour evolution. a) Evolutionary tree of speciation from Charles Darwin's 1837 notebook. b) Cancer clones suffer a selection which determines which tumour cell type will evolve above other which will die or remain dormant, creating a defined ecosystem before or after treatment (Tx) (Greaves and Maley, 2012). c) Comparison of the stochastic and hierarchical model explaining tumour heterogeneity (Nguyen et al., 2012)

In regard to the tumour origin, it is thought that a single cell has the ability to start a single neoplasia through a series of transformation but it is still unknown whether this cell remains genetically similar to its origins or it changes during tumour progression. In the literature we can find authors who refers to these cells as cancer stem cells (CSCs) and/or tumour initiating cells (TICs) even though there is a bit of a controversy in this topic (Kelly et al., 2007). CSCs were first described by John. E. Dick in the late 90s studying a model of human acute leukaemia (Bonnet and Dick, 1997; Lapidot et al., 1994). They first described them as cells with different differentiative and proliferative capacities and with a high capacity of self-renewal expected from a stem cell. Since then, cancer research has also focused on the fight against this rare population within the tumour, as they were thought to be responsible for most of the relapse in treated patients (Dick, 2008).

Regarding this it is important to mention the two actual models that try to explain tumour heterogeneity. The first model lays on the theory that all the cells in a tumour are biologically equivalent and their behaviour depends on intrinsic and extrinsic factors (stochastically) and this is unpredictable (**Figure 1c**). The second model is based on

hierarchy and it postulates the existence of biologically distinct cell subtypes with different abilities, as in CSCs that may be able to form tumours (Dick, 2008, 2009; Nguyen et al., 2012).

For many decades, it has been believed that cancer cells were the main drivers of carcinogenesis and tumour progression. Nowadays it is well known the role of the microenvironment and the tumour-cell-interactions as key events in order to generate a tumour. The cross-talk between tumour cells and the stroma (including cell and non-cellular components) have risen in prominence now becoming a flourishing field of study (Hanahan and Coussens, 2012). While a tumour is developing, depending on the tissue and surrounding area, the stroma found by neoplastic cells influences the tumour fate. This is the initial barrier that cells have to overcome to create a well formed tumour tissue. In order to do so, tumour cells generate changes in their surrounding that affect the environment. They have the ability to tune the stroma turning the situation to a favourable scenario for the tumour growth. Among the orchestration of all these changes is included the recruitment of immune cell populations, association of fibroblasts, the remodelling of the extracellular matrix (ECM) and finally the generation of a proper vascular network (Junttila and de Sauvage, 2013).

Out of this, we can certainly affirm that a tumour is not a simply mass of cloned cancer cells that arose from a cell without replication control, they are abnormal organs with a structure and an organisation of cell types and a complex matrix. The development of a tumour could be seen as a tissue developing organ and also as a remodelling process. Although they resemble normal organs, their chaotic structure makes them non-functional compared with the rest of the tissues. Of note is the lack of integration with the rest or organism. As the rest of the organs have a functionality and a role in the organism maintenance, a tumour doesn't have a specific function and doesn't support the individual survival, the effect of the tumour growth on the surrounding and distant organs is what ultimately would kill the host (Egeblad et al., 2010).

1.2 TUMOUR MICROENVIRONMENT

As we have previously described, the tumour is not only composed by cancer cells but also by a complex tumour microenvironment (TME) in which we can find tumour associated cells and non-cellular components (**Figure 2**). More importantly we can find cells from different origins, these are the main TME constituents grouped into four general classes (Hanahan and Coussens, 2012):

- Angiogenic endothelial cells
- Supporting vascular cells
- Cancer associated fibroblastic cells
- Infiltrating immune cells

The role of these cells within the TME differs regarding their physiological role and main functions. In a tumour we find endothelial cells forming blood vessels which supply nutrients, remove the undesired metabolites and support metastasis. Enhancing the role of endothelial cells, we can find supporting cells such as pericytes and smooth muscle cells which basically add complexity and strength to forming blood vessels apart from the modification and restructuration of the vascular ECM. In the TME we also find cancer associated fibroblasts (CAFs), with important implications in tumour fate. Last but not least are infiltrating immune cells (IICs), which constitute a very important cell type within the tumour (**Figure 2**), and their nature could determine the tumour fate. In a very nice work, Hannahan and Coussens review the role of different TME cell types in a wide spectrum of the cancer hallmarks (Hanahan and Coussens, 2012).

1.2.1 ANGIOGENIC ENDOTHELIAL CELLS

Angiogenic endothelial cells are known to participate in multiple processes apart from angiogenesis (creation of new blood vessels from pre-existing ones). Among them, the migration and activation of invasive properties of immune cell subsets, matrix remodelling and tumour suppression. It is well established that neovascularisation recurs in an increment in tumour proliferation, progression and metastatic events. Furthermore, the angiogenic phenomenon helps to prevent tumour cell death and escape from apoptotic events. The tumour vasculature is known to be abnormal and leaky (De Bock et al., 2011), facilitating the escape of tumour cells and allowing the dissemination to distant organs to form metastasis. Furthermore, abnormal tumour vascularisation does not support the immune cell influx, allowing the tumour to escape from immune destruction (Manzur et al., 2008). These cell types will be extensively described in the section 2.

1.2.2 SUPPORTING VASCULAR CELLS

Maintaining the vascular architecture, we can find vascular supporting cells such as pericytes. These cells are present at different degrees in most of the tumours, and their main function is still keeping the vessel structure and deposit a rich ECM (Ribatti et al.,

2011). Its function is very relevant for tumour progression, the lack of these cells would end up in a chaotic and less structured vessel network, impacting in the tumour fate. There are cases of pericyte transdifferentiating tumour cells, which reflect the real value of this cell type (Krishna Priya et al., 2016). This and other related subtypes will be described in the section 2.1.2.
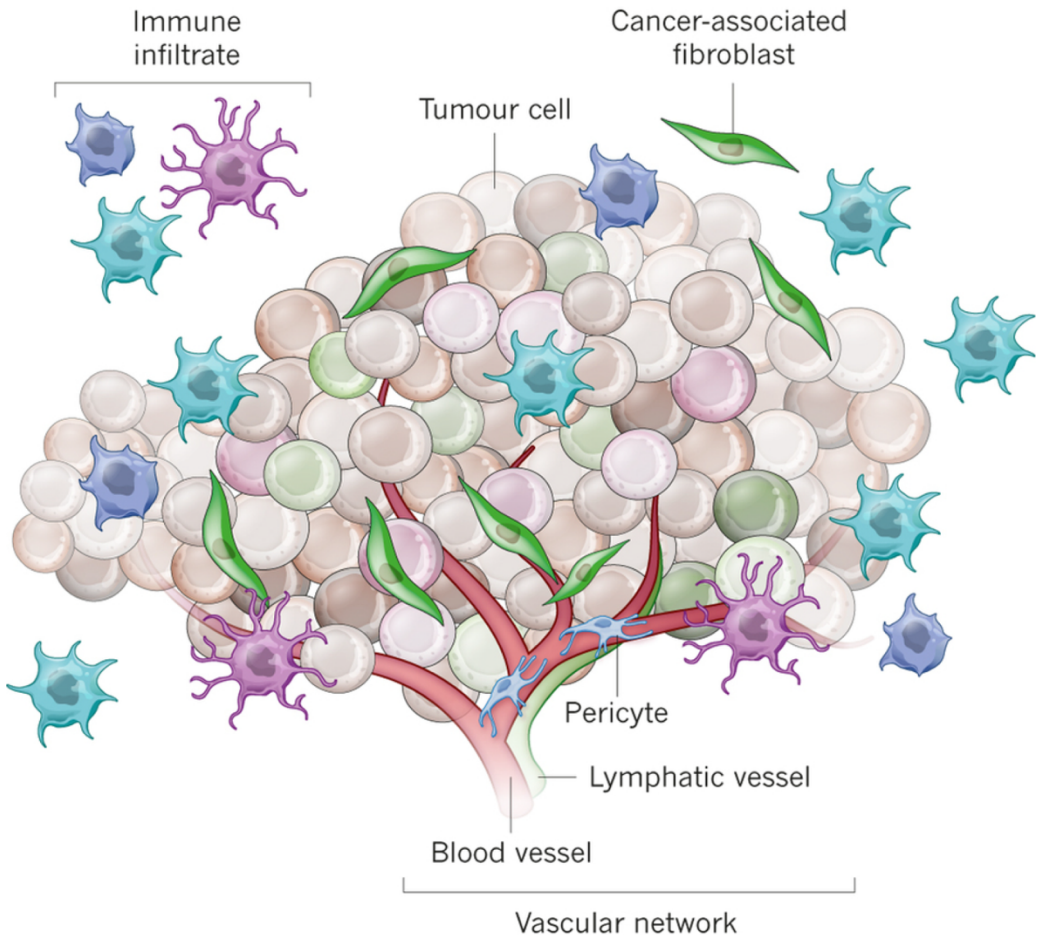
Figure 2. Schematic representation of the intra tumour heterogeneity. This image shows the composition of a heterogenic tumour view where neoplastic cells together with vascular endothelium, fibroblasts, pericytes, stromal and immune cells coexist in the same environment (Junttila and de Sauvage, 2013).

1.2.3 CANCER ASSOCIATED FIBROBLASTIC CELLS

CAFs are important components of the stroma and their interaction with tumour cells have a great relevance in the tumour architecture. Fibroblasts, mesenchymal stem cells (MSC) and/or bone marrow-derived cells can be recruited within the TME and also induced to differentiate intro myofibroblasts, adipocytes and other cell types. Even

though their different nature, all these cells are included into the CAF definition. These cells can secrete signalling molecules as epithelial growth factor members (EGF), fibroblast growth factors (FGF), insulin-like growth factor (IGF-1/2) that would drive tumorigenesis. These cells are also known to produce factors involved in the epithelial to mesenchymal transition (EMT) relevant for metastatic events (Chaffer and Weinberg, 2011). Still how cancer cells fine-tune these cells to become CAFs is not well understood. For example, researchers have shown how normal fibroblast are able to inhibit tumour growth and on the other hand, CAFs have the ability to promote this progression (Bissell and Hines, 2011). CAFs and normal fibroblast are one of the main sources of the ECM that will serve as the tumour scaffold, thus the regulation and remodelling of this matrix is a process that needs to be under a tight control. Some works have described the regulation of the ECM by CAFs and the repercussion on tumour biology (Lu et al., 2011). CAFs are also interacting with the tumour angiogenesis events, they can produce a number of pro-angiogenic factors such as the vascular endothelial growth factor (VEGF), FGF and platelet derived growth factor beta (PDGFβ) which could rescue angiogenesis in case of anti-VEGF tumour treatments. These cells can also produce chemoattractant for proangiogenic macrophages and myeloid cells that would finally impact in tumour angiogenesis (Crawford et al., 2009). Finally, CAFs are known to interact with the infiltrating immune component of tumour. Several studies reports how production of transforming growth factor β (TGFβ) can inhibit cytotoxic T-cells and NK-suppressors, this way, inhibiting tumour destructive immune responses that will benefit the tumour growth (Stover et al., 2007).

1.2.4 INFILTRATING IMMUNE CELLS

Links between the immune system and tumour biology were first given in the nineteenth century when the surgeon Rudolf Virchow observed leukocytes in neoplastic tissue. Since then many studies have proved the relationship between inflammation and cancer (Balkwill and Mantovani, 2001). While tumours grow and a vascular network develops, the blood supply is loaded with nutrients, metabolites but also brings a flux of immune cells that forms part of the surveillance system of the organism. These cells either infiltrate the tumour because they recognise the tumour mass as an offense, or can be recruited via factors produced by tumour cells.

IICs include both the innate response against tumour growth and also cells that are recruited by the tumour to its niche (**Figure 3**). The tumour immune infiltrate varies depending on the tumour type, aggressiveness and organ location. For example, either lymphoid or myeloid lineages could be found and their activation state also depends on

the tissue location and state of the malignancy (Mantovani et al., 2008; Ruffell et al., 2012). IICs can supply direct factors required for the tumour growth, among the stimuli we can find the tumour necrosis factor α (TNFα), TGFβ, EGF, FGF and many interleukins (ILs). IICs can also secrete proteases that modify their environment as they infiltrate. These modifications allow them to migrate easier but also impact cell-cell and cell-ECM interactions, that results in apoptotic events or facilitate an EMT transition, thus modifying the tumour scenario (Lu et al., 2011). Importantly, endothelial cells and IICs interact with each other. Endothelial cells express surface markers that are recognised by immune cells so they can extravasate but also IICs can prepare endothelial cells through paracrine production of factors that induce an specific cell behaviour (De Bock et al., 2011).
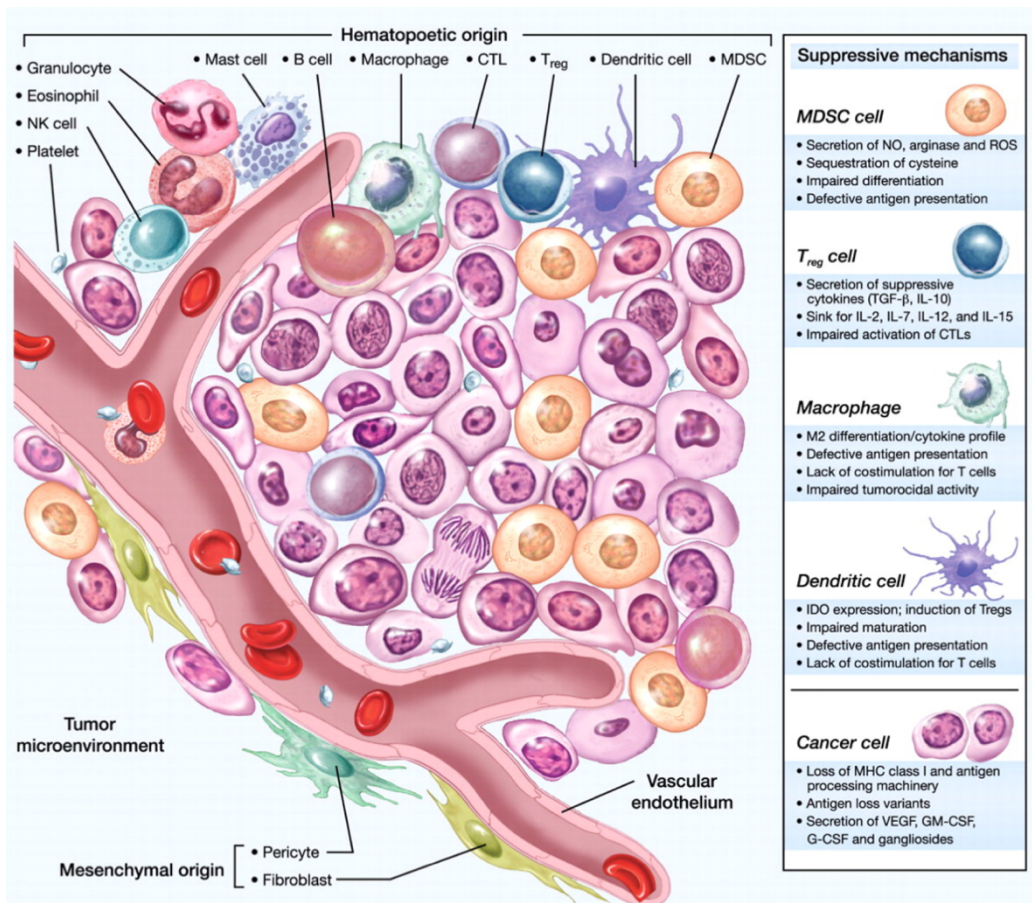
Figure 3. Representation of the immune infiltrates in the tumour microenvironment. Different immune subset that can contribute to tumour growth. Representation of both innate and acquired immunity such as MDSC, T-cells, Macrophages, Dendritic cells and their mechanisms of action (Kerkar and Restifo, 2012).

IICs also contribute to one of the most important cancer hallmarks, the immune destruction. The recruited IICs create an immunosuppressive scenario which is not suitable for cytotoxic T-cells (Ruffell et al., 2012).

Within the immune infiltrate, a very interesting subset of cells are macrophages. There are many classifications of macrophages but we are not going to recapitulate them in this introduction. They originate mainly from bone-marrow myeloid-derived cells that circulate the blood flow as immature monocytes. Macrophages are very heterogeneous and plastic so, depending on the microenvironment, they can orchestrate a different immune response favouring or inhibiting tumour progression (Porta et al., 2011). With special interest, the tumour-associated-macrophages (TAMs) play an important role in the tumour biology. The term TAM should not be misunderstood with *Tie2*-expressing monocytes (TEMs), an alternative classification of macrophages which are neither tissue resident or inflammatory macrophages. Among the varied functions of TAMS, they can produce VEGF-A and thus have the ability to modulate angiogenesis (Lin et al., 2007). Other studies have related the ability to tune up the ECM by expressing proteases as MMP9 (Matrix Metalloproteinase 9) which facilitates VEGF release, hence, modulating tumour angiogenesis. TAMs became a new target for tumours that acquired resistance to certain treatments (Mantovani et al., 2002).

Another subset of immune-related myeloid cells are the immature myeloid cells (iMCs), characterised by the co-expression of CD11b^{+} surface marker. More importantly a heterogeneous and somewhat undifferentiated population including granulocytes, terminally differentiated monocytes and immature myelomonocytic cells, englobed in the term, myeloid derived suppressor cells (MDSC) (Gallina et al., 2006) (**Figure 3**). iMCs and MDSCs are known to inhibit T-cell proliferation by the production of Arginase 1 (Arg I) and inducible nitric oxide expression (NOS2 or iNOS), and at the same time inducing T regulatory cell induction (Bronte et al., 2000; Shojaei et al., 2007). The presence of these cells also participate in the creation of an immunosuppressive scenario which could drive tumour progression and facilitate processes as angiogenesis, tumour treatment scape, EMT and metastatic events (Liu et al., 2014a; Ostrand-Rosenberg, 2008) (Yang et al., 2004).

2. VASCULARIZATION

The vascular system is composed by vessels that carry blood and lymph throughout the body. A healthy individual has a very well established vascular network that delivers oxygen, nutrients and metabolites to every organ and tissue in the organism except to avascular tissues as the cartilage, epithelial layers of the skin and cornea.

The vascular system evolved more than 400 millions years ago. During evolution, as the organism complexity increased the nutrients distribution had to adjust and evolve as well. This is the theory and explanation of the origin of the vascular system in the *Metazoa* kingdom (Monahan-Earley et al., 2013). Early in vertebrate development, during ontogeny, the vascular system is the first to appear. There is a moment in which the embryo nourishes itself by simple diffusion. This situation disappears when the first vascular plexus starts forming and connecting with the primitive and developing heart. The creation of a vascular system is a hierarchy process in which mesoderm-derived endothelial precursors (Endothelial Precursor Cells, EPCs or angioblast) are recruited to create a primitive vessel network (Flamme et al., 1997). This early process is called vasculogenesis and it should not be confused with the term angiogenesis. Next, the process of angiogenesis, both normal and tumour-induced, will extensively be described along with the most important cell types involved and also key players as ECM components. Finally, we will introduce alternative mechanisms to angiogenesis, also important for tumour development.

2.1 ANGIOGENESIS

The term angiogenesis derives from the Greek form *angeion,* which means "a vessel receptacle". It is described as the creation of a blood vessel from a pre-existing one. Angiogenesis is necessary for the development of a proper vascular network in a mature and/or developing organism and it is needed to continue the blood vessel trails from the primitive vascular plexus initiated by vasculogenesis (Flamme et al., 1997; Potente et al., 2011). This phenomenon occurs in homeostasis and pathological processes, and it is fundamental for the creation of tissues and organs during development. Alternative mechanisms for the creation of blood vessels will be described in the section 2.2.

The creation of a new blood vessel need a start, a triggering moment and location which is determined by correct balance of stimuli, pro- and anti-angiogenic factors in this case

(Table 1). This process is orchestrated by the stroma in which many different types of cells are involved (Adams and Alitalo, 2007). The induction of pro-angiogenic factors and thus the initiation of angiogenesis can be triggered by different processes as for example hypoxic events, wound healing, menstruation or the development of a tumour mass. In a mature organism the vascular network remains quiescent unless one of these last events happens (Gupta and Zhang, 2005).
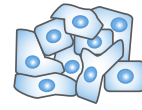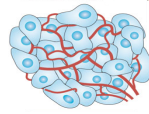
Pro-Angiogenic molecules	Anti-angiogenic molecules
VEFG	TSP1/2
FGF-2	Angiostatin
PDGFb	Endostatin
Angiopoietins	TIMPs
TGFb	PEDF
HGF	IFNa
Ephrins	IL-4 & 12
TNFa	

Table 1. The most studied pro- and anti-angiogenic molecules. This table recapitulate the most important molecules that act favouring or against the angiogenic process and finally can have an impact in the tumour fate.

Although blood vessels could be classified by its size and role (Tennant and McGeachie, 1990), basic components remains the same. A blood vessel is composed mainly by a monolayer of endothelial cells (ECs), supporting vasculature cells as pericytes (PCs), vascular smooth muscle cells (vSMCs), and a basement membrane (BM) which is a specialised extracellular matrix. While small blood vessels (capillaries, post-capillary venules and arterioles) only contain ECs, PCs and a BM, as the vessel increases its size and complexity the BM and PCs start being surrounded of rich stroma layers of cells and ECM. It may have up to 3 different layers: intima, media and adventitia (from inner to outer layer), the last two containing a higher proportion of vSMCs (Tennant and McGeachie, 1990). To describe the creation a blood vessel, next we briefly introduce its components.

2.1.1 ENDOTHELIAL CELLS

These cells form the lumen of the blood vessel, the part in touch with the blood stream. The alteration of these cells would compromise the vessel architecture and so the functionality of the nurtured-being area (Risau, 1997). ECs form a monolayer of cells with tight junctions to maintain the architecture of the tube. Normally ECs have a thin cytoplasm and a conspicuous nucleus and are covering a big surface within the tube lumen. Both cell-cell and cell-ECM interaction are now well studied and allow us to understand the behaviour of the ECs during different processes as angiogenesis. The endothelium can be considered as an endocrine and paracrine organ itself. In addition to act as a blood barrier, endothelium can be stimulated but they also regulate

themselves many other cell types, which will finally have an effect in vessel tone, immune cell attraction and inflammatory responses (Sumpio et al., 2002). Among some important molecules secreted by ECs, there is nitric oxide, a molecule related to the regulation of vasodilation and platelet activating factor (PAF), which acts in the adhesion of platelets and neutrophils to the endothelium which will finally enhance the production of leukocyte adhesion molecules in an inflammatory situation (Thienel et al., 1999). Nonetheless, the main activator of ECs is VEGF-A (vascular endothelial growth factor-A, thereafter called VEGF). Even though the stroma is the main producer of VEGF, ECs can generate this factor in stress conditions as in hypoxia (Crawford and Ferrara, 2009a; Herbert and Stainier, 2011).

2.1.2 VASCULAR SUPPORTING CELLS

In this point we are describing the most important supporting cells that are pericytes (PCs) and vascular smooth muscle cells (vSMCs), both with mesoderm origin. These cells line up in the outer surface of the blood vessel. The interaction with ECs are mediated through the shared BM and cell-ECM interactions, which orchestration helps to the creation and stabilization of capillaries and post-capillary venules (Armulik et al., 2010; Ribatti et al., 2011). Both cells types differ in their functions, properties and the scenario where they appear. However, they can be identified by the same protein expression markers alpha smooth muscle actin (αSMA) or neural/glial protein 2 (NG2). There is an extensive review of the identification of these cells types in which, markers as smooth muscle-myosin heavy chain (SM-MHC) and smoothelin A/B that seems to be specific for the vSMC (Owens et al., 2004; Rensen et al., 2007; Stapor et al., 2014).

Pericytes are the most common supporting vascular cells. During the developing of a blood vessel, ECs produce molecules as PDGFβ (platelet derived growth factor beta) to attract PCs to the developing tube. Other molecules as TGFβ or angiopoietin 1 (Ang-1) can stimulate migratory capacities to facilitate PC coverage. Among their functions, PCs are known to modulate the vessel diameter (due to their ability to contract) and physically influence EC behaviour. A lack of PCs covering can result into a vessel hyperplasia and leakiness of the blood vessel. It is still unclear if pericytes can divide from the ones that already surround the tissue, can differentiate from vSMCs or from stromal or mesenchymal stem cells (MSCs) in the surrounding area due to the angiogenic pressure (Stapor et al., 2014).

Vascular smooth muscle cells are found on arterioles and venules. Generally, their shape is thinner and more stretched through the vessel in comparison to PCs. Their contractile

abilities may regulate the lumen diameter and so controlling the blood flow and pressure. Two forms or states of vSMCs can be found, synthetic and contractile. Both derive from same cells but a balance of factors secretion mediated from the endothelium can switch between them. Particularly the synthetic vSMC play an important role in the deposition of the rich ECM that surrounds ECs and supporting cells. They take an important part during vessel remodelation in situations of wound healing, menstruation and/or exercise (Rensen et al., 2007).

2.1.3 VASCULAR BASEMENT MEMBRANE

We already introduced the ECM and we have also talked about BM and its importance during angiogenesis and blood vessel homeostasis. The vascular basement membrane (vBM) is an organised and specialised ECM typical from blood vessels. It is the non-cellular compartment of the endothelial tissue and it plays a vital role during processes as vasculogenesis, angiogenesis, wound healing and immune extravasation. The vBM is a complex network of extracellular proteins with different origins, depending on the vessel nature. Its main function is structural, helping to maintain ECs and PCs together with cell-cell and cell-BM interactions. But it also functions as a molecule reservoir, signalling mediator, migration barrier and as a regulator or biomechanical forces (Lu et al., 2012). Importantly, this organisation can be disrupted during disease or abnormal development (Eble and Niland, 2009).

The main components of the vBM are common for most of the BMs and they will be described in the section 3.1 devoted to ECM. Its control and deposition in the vascular stroma is an interesting feature that we are particularly interested in.

2.1.4 THE CREATION OF A NEW BLOOD VESSEL

In a normal situation, ECs are stably governed by a balanced presence of pro- and anti-angiogenic factors. When this balance is disrupted, different phenomena can occur. In the process of the sprouting, selected endothelial cells will become a tip or initiating endothelial cell (**Figure 4a**). This is something crucial because if every ECs would respond similarly to this stimuli, the tissue structure would be compromised. It is now well understood that endothelial cells and the regulation of VEGF-A expression is under control of the Notch/Dll4 (notch – Delta like-ligand 4) signalling pathway but how the tip cell is selected is still poorly understood.

The activation of an endothelial tip cell provokes a change in their behaviour. These cells become more active and their motile, migratory and/or invasive capacities are

enhanced. They also need to detach from the surrounding PCs, modulating the cell-cell interaction with their neighbouring ECs. There is an upregulation of the VEGFR2 (VEGF receptor-2) in the tip cells, which correlates with their sensibility to VEGF-A. In this scenario, the tip cell is more likely to invade the microenvironment through filopodia extension. The secretory profile is very important in this context because the ECM must be degraded and tuned in its path.

Multiple matrix proteases are involved in the degradation of this complex niche. As the tip cell progresses in search for another sprouting event to converge, there is also a modulation of the remaining ECs (**Figure 4b**). Even though the tip cell is leading the way, the sprout needs more ECs that will form the stalk. Tip-cell-peripheral ECs enhance their replication capacities, however is known that tip cells are not likely to divide. In this process a new ECM must be organised and tip cells are also leading a new PC attachment to the newly formed sprout in order to maintain its stability. This regulation is known to be mediated by soluble factors as PDGFβ. The encounter of two tip cells is essential for the formation of the final sprout. Repulsion, adhesion and anastomosis occur at the same time (**Figure 4c**).
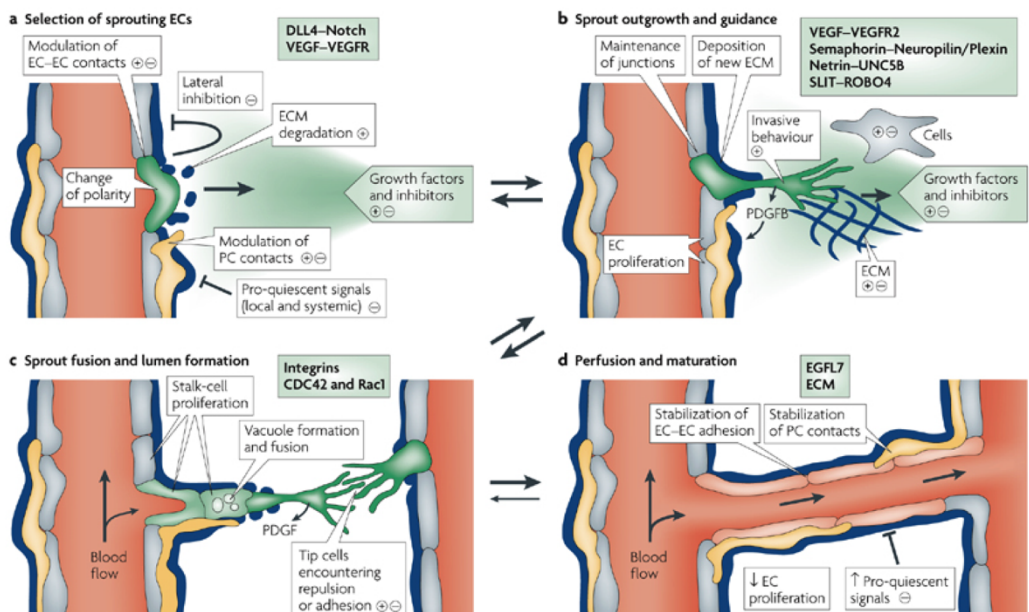
Figure 4. Schematic representation of the typical angiogenesis process. Explanation of the angiogenesis phenomenon with the fusion of two tip cells from two branching vessels. The main characteristics outlined in the representation are explained in the introduction as it follows (Adams and Alitalo, 2007).

This is very important because it can lead to the fusion between incompatible parts of the vasculature, e.g. the formation of arteriovenous shunts (**Figure 4d**). Vascular

junctions between ECs, a well-established ECM and BM and a good coverage of pericytes are also overdue in the process of the formation of the vessel and at the final stage. In this scenario, the angiogenic signalling profile is very different, more pro-quiescent signals are present and also cells have stop dividing in order to maintain the vessel stability (Adams and Alitalo, 2007; Carmeliet and Jain, 2011a)

2.2 ALTERNATIVE MECHANISMS TO ANGIOGENESIS

Even though the previously described angiogenesis is the most likely and known to form new blood vessels, there are been identified other alternatives. In this section we recapitulate the best described, regarding normal and physiological conditions.

2.2.1 ENDOTHELIAL PROGENITOR RECRUITMENT

Endothelial progenitor cells (EPCs) were first discovered as CD34^{+} cells in the bone marrow (Asahara et al., 1997). EPCs can be attracted to highly angiogenic areas where they are inserted within ECs of blood vessels under progression and become ECs. Since then, the concept of vascularisation changed, there were more options rather than traditional angiogenesis to form blood vessels (**Figure 5b**). EPCs also express VEGFR2, cluster of differentiation 31 (CD31) and tyrosine kinase angiopoietin receptor 2 (TIE2). This recruitment can be facilitated by the secretion of angiogenic factors as VEGF-A that allow them to change their secretory profile in order to leave the bone marrow, their primary niche. This can be considered to be a mechanism that is happening together with angiogenesis in new developing sprouts and not just by itself and it can be driven by stress situations and hypoxic conditions (Hillen and Griffioen, 2007; Potente et al., 2011).

2.2.2 VESSEL INTUSSUSCEPTION

There are also processes related to more mature and bigger blood vessels as arterioles and venules. In this case, intussusception stands for the split of an already formed blood vessel (**Figure 5c**). This is thought to happen in order to extend the vascular network rather than to create new branches. It is a very quick process that has been observed early in development, and it is very rare to happen as the organism ages. Very little is known about the molecular mechanisms that underlie this phenomenon, but what is known is that the creation of endothelial pillars in the middle of the vessel is necessary. This may occur due to the presence of vSMC or PCs in the outer layers that somehow

apply a determined pressure over the tube, arranging a new contact between different ECs that cover the lumen (Flamme et al., 1997).

2.3 TUMOUR ANGIOGENESIS

A tumour, as another organ, needs a blood supply to grow and proliferate. This blood supply is provided by different mechanisms, being angiogenesis the most important. When a neoplasia reaches 2-4 mm^3, diffusion is not enough to feed tumour cells with nutrients and oxygen. Hence, blood vessels are created (Hillen and Griffioen, 2007). It was not until the early 70s when a group of medical doctors reported the first phenomena of angiogenesis in neoplastic solid tissues, years before VEGF was even discovered. They also described how tumour and endothelial cells may constitute an integrated ecosystem where a cross-talk between them exists (Folkman, 1971).

After this lumen contacts, a reorganisation must take place in order to form two different vessels. Signalling of VEGF-A, PDGFβ and Ephrins have found to be related to this phenomenon. Triggering signals for this mechanism are still unknown but some authors state that the inhibition of angiogenesis could induce these processes, so they appear directly related to the drug-resistance of antiangiogenic treatments (Hillen and Griffioen, 2007).

A tumour is an abnormal situation because tumour cells produce more pro-angiogenic factors as VEGF, FGF-2, PDGFβ and EGF under stress situations as in hypoxia and nutrient depravation (**Figure 6a**). This setting induces the angiogenic switch, triggering new sprouting as described in the introduction (**Figure 5a**) (Folkman and Hanahan, 1991; Weis and Cheresh, 2011). However, this scenario in which angiogenesis takes place is not ideal to generate a hierarchic and organised vascular network. Tumour vessels are aberrant because cell-cell contact between ECs is not as tight as in a vessel created in physiological conditions. Also, the coverage of pericytes and vascular smooth muscle cells is insufficient, which makes the vessels more likely to leak and more permeable. In general, the ECM is altered (**Figure 6b**), creating an unstable vascular network in which the capillary system seems to be bigger, dilated and more disorganised than average (Goel et al., 2011; Jain, 2005; Weis and Cheresh, 2011). Thus, a non-homogeneous nurture is taking place in different tumour areas, were necrosis and hypoxia can appear. Importantly, tumour cells under hypoxia undergo epigenetic changes which makes them more resistant to tumour treatments and favour epithelial to mesenchymal transition (EMT), which enhances metastatic events. Also, leakiness and lack of consistency

between ECs and PCs facilitates the creation of enema which increases the inner tumour pressure, impeding the right nutrient and oxygen diffusion (**Figure 6b**).
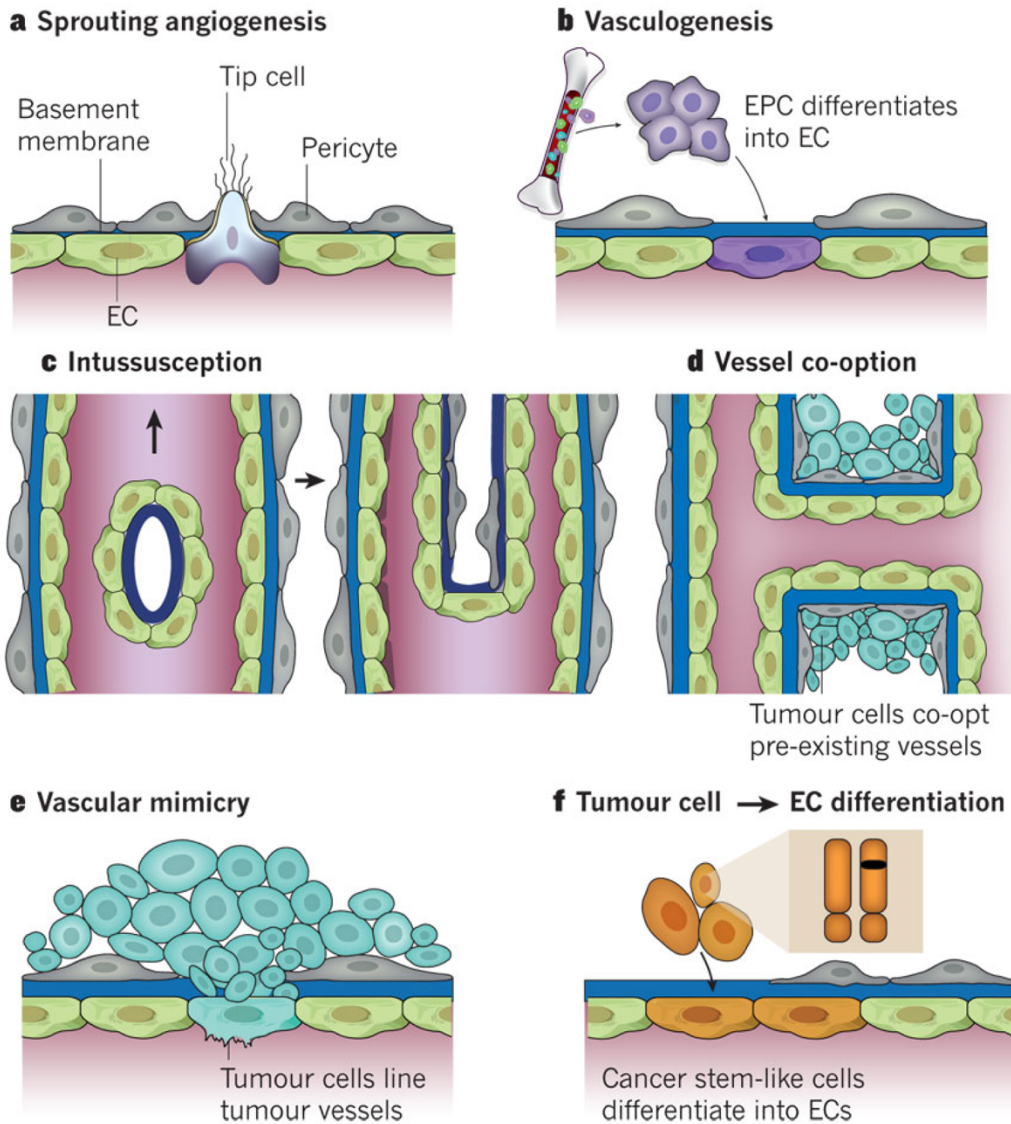
Figure 5. Different modalities of vessel formation. This representation includes angiogenesis and the different alternative to these mechanisms generally accepted for tumour biology (Carmeliet and Jain, 2011b).

This situation enhances other properties of tumour cells as the ease of extravasation and migration to distant organs in order to metastasise. In this scenario the remodelling of the ECM is an important event. Tumour cells also express matrix degrading molecules

to facilitate the incoming sprouting towards the tumour mass (Nagy et al., 2010; Ziyad and Iruela-Arispe, 2011).
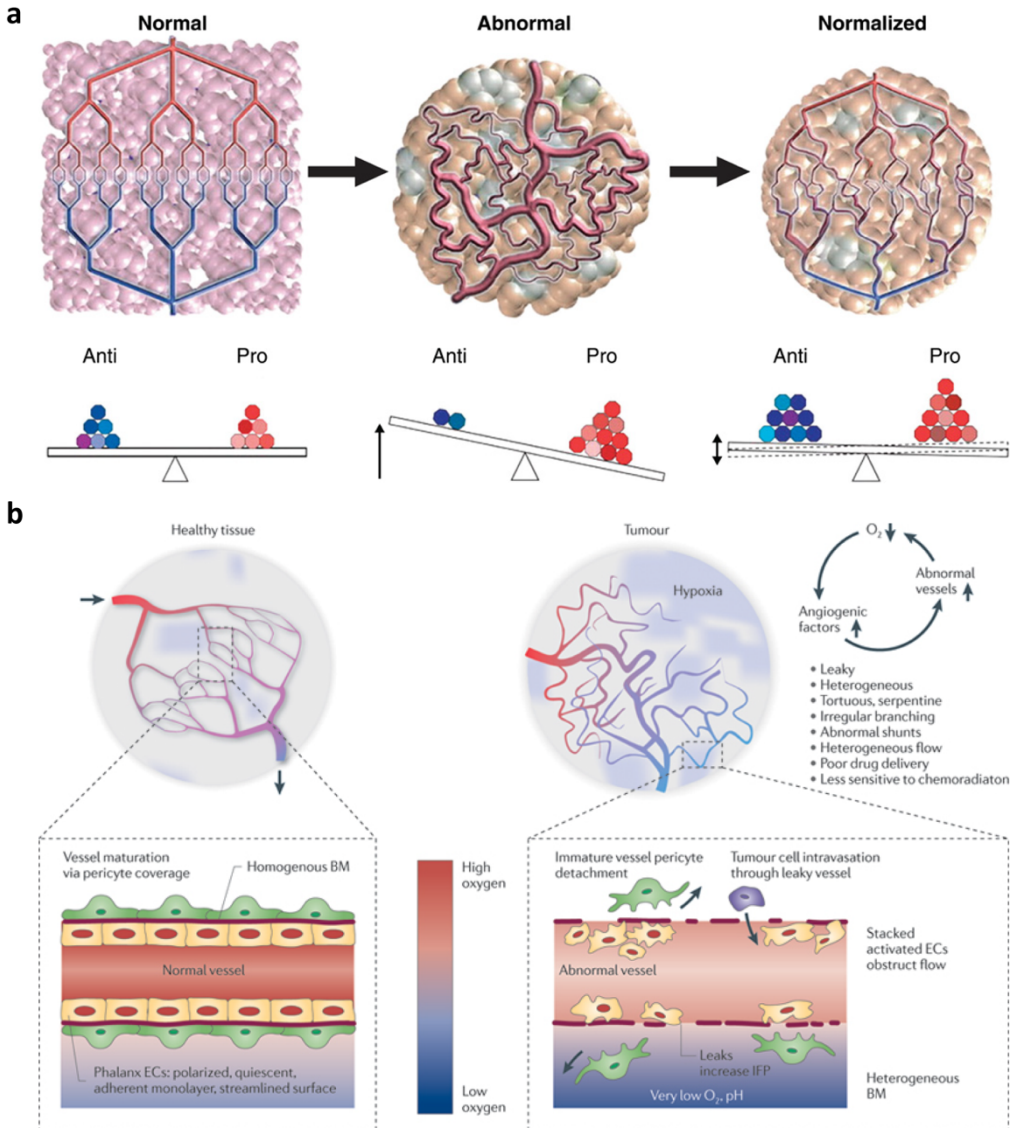
Figure 6. Tumour angiogenesis homeostasis. a) This figure represents the importance of the balance of mitogens that are necessary for the formation of a well-defined vascular network. The disruption of the balance ends in an abnormal situation. b) Cell and molecular changes suffered by the bad organisation of the tumour vessel formation in comparison with a normal physiological condition (Carmeliet and Jain, 2011b; Goel et al., 2011).

Tumour angiogenesis have been studied for many decades now. The mechanisms and molecular pathways involved are very similar to physiological angiogenesis and this made it very favourable to study and thus, become a therapeutic target. It was thought

that if tumour vasculature could be inhibited and impaired, the lack of blood supply would suffocate the tumour and even make it disappear. In the late 80s, Napoleone & Henzel described for the very first time a mitogen named VEGF that was activating ECs (Ferrara and Henzel, 1989). Right after, this molecule became an important target for anti-angiogenic therapies to treat tumour malignancies. The attempts to block VEGF against tumour progression grew rapidly during the following years and many studies showed how it positively impaired tumour progression. As for humans, the first treatment was a monoclonal antibody against the molecule VEGF-A, *bevacizumab* (Ferrara et al., 2005). This agent showed exceptional results *in-vitro* and *in-vivo* but side effects started to appear, showing resistance episodes and increasing aggressiveness in certain tumour types (Bergers and Hanahan, 2008; Ellis and Hicklin, 2008).

The selection of monotherapies did not show good results, thus, *Bevacizumab* have been used in combination with chemotherapies, showing an improved efficacy and limiting the traditional non-selective toxicities (Crawford and Ferrara, 2009b; Weis and Cheresh, 2011). Concurrently, additional targets were the focus for the development of drugs, such as VEGF receptors, angiopoietins, and others.

Taking into consideration the abnormal nature of tumour vasculature, it was also hypothesized that chemotherapies and different tumour treatments might be not as efficient due to non-homogenous distribution. Different authors already describe the need to normalise the tumour vasculature to acquaint a better treatment efficiency. Such normalisation would fall into the compensation of the balance of pro- and anti-angiogenic factors which is clearly tilted (Jain, 2005). The normalised vasculature is characterised by a less tortuous system with less leakiness together with a better organisation of ECs, more coverage of PCs and a good deposition of a vBM. This would be accompanied by changes affecting the blood flow which would subsequently decrease the tumour inner pressure and so the oxygenation and nutrient diffusion would be restored. With these changes the penetration of therapeutic anti-tumour drugs should be improved (Goel et al., 2011).

2.3.1 ALTERNATIVE MECHANISMS TO TUMOUR ANGIOGENESIS

It has been reported that tumours can bypass the blockade of angiogenesis by alternative mechanisms not directly related with sprouting. Tumour vascularisation can include the already described in the section 2.2 (vessel intussusception and endothelial progenitor recruitment) (**Figure 5**) and, in addition, vessel cooption and vasculogenic mimicry.

Vessel cooption is a process that has not been found in physiological conditions (Thompson et al., 1987). It was first described as the ability of certain tumours growing in vascularised areas, to hijack the vascular network of the surrounding tissue and incorporate the vessels to its own environment (**Figure 5d**). Its frequency would depend on the nature of the tumour and the tissue which is invading (Holash et al., 1999). The new endothelium must be maintained and regulated by its own new microenvironment and thus tumour cells must control the ECs line up, PCs coverage and the deposition of an ECM. Some studies have shown that angiopoietin-1 (Ang-1) and Tie2 mediate in this maintenance responses that arise from the tumour (Brooks et al., 1994).

A second alternative, named vasculogenic mimicry (VM), raised a good scientific debate at the verge of the XXI century. Maniotis et al, reported for the first time events of "vascular channel formation by human melanoma cells *in-vivo* and *in-vitro*". They described it as the ability of certain tumour cells to behave like ECs, forming part of a pre-existing endothelium (**Figure 5e**). There is no information about this mechanism happening in normal healthy tissues or remodelling processes, although the generation of vascular channels by cytotrophoblasts in placental tissue could be related (Zhou et al., 1997). Other authors described a very similar situation, identified as tumour cell transdifferentiation to ECs, in this case linked to the existence of tumour stem-like subpopulations (CSCs). There is a bit of confusion in the literature regarding these two terms (**Figure 5f**).

VM has been confirmed in cell culture and in melanoma models *in-vivo* (Maniotis et al., 1999). Additional tumour types also presented VM: glioblastoma, sarcoma, prostate and breast cancer are some examples (Misra et al., 2012; Wang et al., 2016; Yao et al., 2013; Zhang et al., 2014). These structures are functional and can transport a blood flux. More importantly, their architecture and biochemical composition have been studied and interestingly the tumour cells lining the vessel lumen are also covered by PCs and have a regular deposition of a specialised vBM. The literature shows that VM+ vessels can be identified by their rich polysaccharide and proteoglycan structures by using the periodic acid-shiff (PAS) staining. Furthermore, researchers have shown how these tumour cells can express endothelial-related molecules as CD31 or vascular endothelial cadherin (VE-CAD or CD144) (Dunleavey et al., 2014; Lai et al., 2012). The expression of other genes has been linked to the VM phenomena. Among them, we can find: erythropoietin-producing hepatocellular carcinoma-A2 (*EphA2*), phosphatidylinositol 3-kinase (*PI3K*), VE-CAD, focal adhesion kinase (*Fak*) and laminin 5 γ2-chain (*LamC2*) (Hess et al., 2001, 2003). It is also important to remark that the ECM can also tune how these aggressive

tumour cells behave as the implication of certain MMPs show in poorly aggressive melanoma (Seftor et al., 2001).

The identification of these alternative mechanisms are of high importance to improve the current use of anti-angiogenic agents, given its direct relation with resistance phenomena. The blockade of new angiogenic sprouts may trigger the VM phenomena due to the stress that the tumour is going through. Researchers have shown how tumour cells can exhibit more plastic phenotypes when they undergo stress situations as hypoxia and nutrient depravation (Liang et al., 2016; Liu et al., 2014b). Many other studies shed light over the correlation of VM events with bad prognosis, encouraging the need of VM inhibition or treatments directed to it (Cao et al., 2013; Liu et al., 2012; Yang et al., 2016). Noteworthy, it is a recent study using a novel anti-VM agent named CVM-1118. This is a plant-derived compound (phenyl-quinoline derivative) that has shown its inhibitory properties *in-vitro* in different human tumour cells. They show interesting data about the alteration of molecular pathways related to stem-cell genes (*Nodal2* and *Notch2*) and the *Vegf* pathway. So far, this compound has reached the first stages for clinical trials (Hendrix et al., 2016).

3. THE EXTRACELLULAR SCENARIO

The extracellular scenario is the non-cellular compartment present in every organ, tissue and structure of the organism. It is mainly composed by highly modified proteins, so it is different in every organ, due to the cell nature and origin.

When referring to the extracellular scenario, we are mostly going to refer to extracellular matrix (ECM) as a broader concept, and the more specific basement membrane (BM) and basal lamina (BL). In fact, ECM can comprise both BM and BL (**Figure 7**). The BM is composed by the BL and another layer mainly made of connective tissue. The BL itself can be defined as a layer of specialised ECM secreted by epithelial cells and is commonly mistaken with BM. When observed under electron microscopy these 3 compartments can be easily differentiated by the density of the layer (Paulsson, 1992). In this section we will describe the main components of the ECM, with special regard to proteases, and their functions in important processes as angiogenesis and tumorigenesis.

3.1 THE EXTRACELLULAR MATRIX: COMPONENTS AND FUNCTIONS

The main components of the ECM are macromolecules as glycoproteins, proteoglycans (PGs) and fibrous proteins. The most important fibrous proteins are Collagens, Fibronectin (FNs), Elastins, Laminins and Tenascins. PGs have exceptional properties that allow them to retain water, taking most of the interstitial space (Frantz et al., 2010). Collagen is the most abundant protein, representing up to the 30% of the total protein mass of a multicellular organism. With more than 28 different Collagens, it also provides tensile strength by binding to other components as Elastins (Gordon and Hahn, 2010). Among the non-collagenous proteins of the ECM we find FN, Tenascins, Laminins and Elastins. These families share functions and structural domains that have been preserved during evolution, for example the RGD (Arg-Gly-Asp) binding domain, critical for the interaction with Integrins, and so, for ECM-cell contact (Rozario and DeSimone, 2010).

ECM functions may vary depending on the location and/or its origin. In general, it works as a substrate for cells, and it can define a migratory track for cells. As a main scaffold, it provides the structure and integrity of tissues, defining the boundaries, limits and shapes. It also acts as a signal reservoir, by storing growth factors and mitogens, which release would be modulated by cell-mediated forces and/or proteolytic activities. In line with this, mechanical forces are also transduced along its structure, allowing cell differentiation by engaging their cytoskeletal machinery. All these features explain the

need of the link between the extracellular scenario and the cell compartment (Lu et al., 2011, 2012).
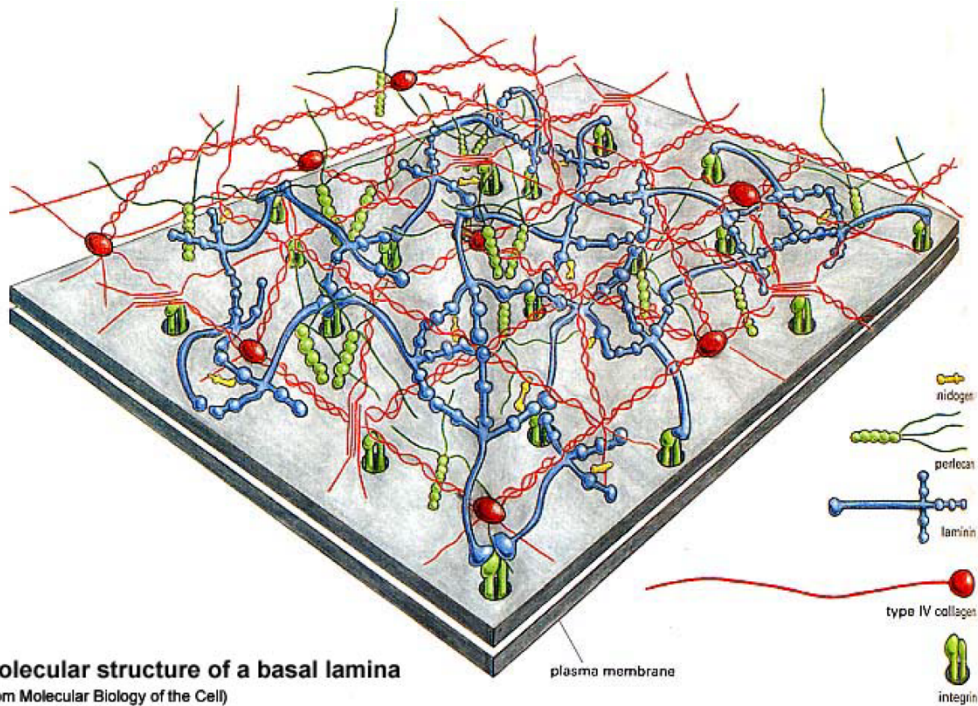
Figure 7. The molecular structure of the basal lamina. Figure representing the tri-dimensionality of the ECM and the assembly of the most representative elements (Bruce Alberts, Alexander Johnson et al., 2002)

As introduced above, the BM is a very specialised ECM that covers every epithelial, muscle, fat, endothelium and nervous tissue in the organism. It lays as a very thin layer of non-cellular components that separates cells from the interstitial matrix. Its main constituents are Collagen IV (COL IV), Perlecan, Laminin, Nidogen 1 (NID1), Nidogen 2 (NID2) and Fibulin-1 (**Figure 7**). COL IV and Laminin form two independent networks highly organised and linked between each other by Nidogens and Perlecan. The complex interactions among all the molecules is what gives integrity and strengthen this scaffolding structure (Kruegel and Miosge, 2010).

3.2 EXTRACELLULAR MATRIX PROTEASES

An extracellular protease is defined as a hydrolytic enzyme that acts cleaving peptides links of a protein in the extracellular milieu. These molecules can be soluble or transmembrane. For many years, proteases have been categorised as gastric juice

proteolytic enzymes that were involved in the non-specific proteolysis of proteins of our daily food intake.

As another component of the extracellular milieu, the extracellular matrix proteases have an important function in the deposition and maintenance of the ECM components so its study and comprehension is overdue. Proteolysis gained a key role during evolution and its biological significance has driven the raise of the multiple protease families that have been discovered in mammals and other organisms (Puente et al., 2003). Importantly, the Degradome project was initiated to get a full picture of the catalytic activity of all proteases, studying their substrates in health and disease (López-Otín and Overall, 2002). Updated data show the complexity of this field and the relevance of proteases for homeostasis. There are up to 588 human and 672 mouse proteases, with a 90% of orthologues and representing more than 2% of the genome. The high conservation among species also highlights the importance of these molecules during ontogeny (Auld, 2013). According to the main domain of these enzymes, a classification includes: aspartyl-, cysteine-, metallo-, serine- and threonine proteases (Puente et al., 2003; Quesada et al., 2009).

For the focus of this thesis we provide next a deeper introduction for the group of metalloproteases and more specifically about the ADAMTS family. They are members of a super-family under the name of metzincin zinc-proteases. All metzincin zinc-proteases share the zinc-binding motif **HE**XX**H**XX**G**XX**H** (Gomis-Rüth, 2009). Within this group, a sub-classification includes: matrix metalloproteases (MMPs), a disintegrin and metalloprotease domain (ADAMs) and, a disintegrin and metalloprotease with thrombospondin motifs (ADAMTS) (Bode et al., 1996). These three families possess homologies which makes their biochemistry very interesting (**Figure 8**). From N- to C-terminus, their basic structure consists of a signal peptide (Pre), a pro-peptide (Pro) and a catalytic domain (Cat) with a zinc binding motif (Shiomi et al., 2010), followed by the most variable C-term part. Thus, the N-terminus region is responsible of substrate cleavage specificity, and the C-terminus region will determine its location (soluble, anchored to the membrane or to ECM).

Finally, it is important to mention that these families have common inhibitors, identified as tissue inhibitor of metalloproteases (TIMPs). They can specifically bind and block the catalytic domain of MMPs, ADAMs and ADAMTSs with their N-terminus region (Nagase et al., 2006). Henceforth, we will briefly describe the most important protease families.

3.2.1 MATRIX METALLOPROTEASES

Matrix metalloproteases (MMPs) or Matrixins share common domains with all the proteases. Specifically, they have a linker or hinge region followed by the C-terminus region with hemopexin domains (**Figure 8**). Some members, first named MT-MMP, were found to be anchored to the membrane by a transmembrane domain (MT). The nomenclature can result confusing but nowadays, every MMP have its own official name in addition to other alternative or former nomenclatures. So far, 23 human and 24 mouse members have been identified. As an overview, this family includes well-known collagenases (MMP1, -8 and -13), gelatinases (MMP2 and -9), matrilisins (MMP7 and -26) and stromelysins (MMP3, -10 and -11), named after the specificity of their main substrates. Except all the anchored-membrane members, the rest are soluble. For all of them, in order to become active, they need to be cleaved by other proteases (as furin endopeptidases) (Klein and Bischoff, 2011)

In general, the matrix turnover provoked by these proteases has a severe impact in health and disease. From angiogenesis to cancer and metastasis, the wide horizon of action of this group and its substrate keep widening as more functions are discovered (Klein and Bischoff, 2011; Nagase et al., 2006)

3.2.2 A DISINTEGRIN AND METALLOPROTEASES

Originally known as MDC proteases (Metalloproteinase-Disintegrin-Cysteine rich). Approximately up to 38 members have been cloned in several species but only 25 genes have been identified in humans and not all of them exhibit protease activity. While the N-terminus domain is similar to the rest of the metzincins, ADAMs contain a disintegrin with cysteine-rich domain. In the C-terminus region they also possess a TM and a cytoplasmic (Cy) domain, so all members are transmembrane (**Figure 8**). Many functions have been described for ADAMs but a remarkable one is the ectodomain shedding of membrane proteases (Shiomi et al., 2010).
Cell adhesion, EGFR transactivation, and relevance in fertility are also associated to this family. Collagen, FN, gelatins and factors as TNFα are some of their substrates. Nevertheless, there are many members for which their proteolytic function is yet to be discovered (Giebeler and Zigrino, 2016). The upregulation of some members of this family (ADAM-8, -9, -10, -15 and -17) in multiple cancers enhances its biological importance in health an pathology (Duffy et al., 2011; Mullooly et al., 2016).

According to our interest in ADAMTS1, this is the most important group of proteases for the pipeline of this thesis. In their structure, they are very similar to ADAMs but right after the disintegrin domain we can find a single thrombospondin repeat (TSP), giving it also the name to the family. Very well conserved during ontogeny for all members of the family, are the cysteine-rich region and the spacer. The main difference among members is the number of TSP repeats in the carboxyl-end and other specific domains. Significantly, their carboxyl-end (including TSP repeats) provides specific binding properties to ECM molecules that makes them unique (Apte, 2009; Kumar et al., 2012; Tang and Hong, 1999).
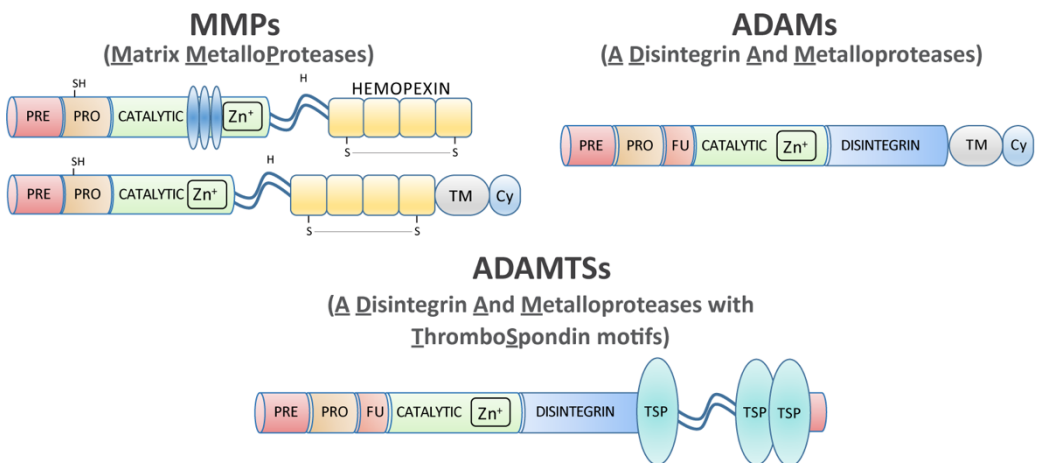
Figure 8. Schematic representation of the structure of the different metzincin families. In this representation the following motifs are showed: the signal peptide (Pre), the prodomain (Pro), the furin cleaving site (Fu), the Zn^+ dependent catalytic domain, the hinge (H) or linker region, the disintegrin domain, the thrombospondin repeats (Tsp), the transmembrane domain (Tm) and the cytoplasmic region (Cy).

Both human and mouse families comprise a total of 19 ADAMTSs that can be classified in five sub-groups regarding their substrates. They are: aggrecanases or proteoglycanases (ADAMTS1, 4, 5, 8, 9, 15 and 20), procollagen N-propeptidases (ADAMTS2, 3 and 14), cartilage oligomeric matrix protein-cleaving enzymes (ADAMTS7 and 12), von-Willebrand Factor proteinase (ADAMTS13) and a group of orphan enzymes with unknown function (ADAMTS6, 10, 16, 17, 18 and 19) (Kelwick et al., 2015).

All ADAMTSs contain a catalytic motif, and least in theory all the members are proteolytically active. Despite containing a site for furin-like convertases, some members as ADAMTS1 have been shown to be initially cleaved in the *trans*-golgi network and, leading to the secretion of a fully active form (Rodriguez-Manzaneque et al., 2000).

3.2.3.1 ADAMTSs in angiogenesis, cancer and other diseases.

The expression of ADAMTS proteases is wide and tissue-dependent. They have important roles during development, so it has been described that its dysregulation may result in mendelian inherited diseases and other pathologies related to cancer, the vascular system or arthritis (Kelwick et al., 2015). For example, the organisation and processing of a proteoglycan named Versican (VCAN) has been highlighted. It is known that ADAMTS1, 4, 5, 9, 15 and 20 can cleave this ECM component and this processing can have further consequences during cardiac organogenesis, palate development, urogenital organ development and even fetal lethality (Kern et al., 2010; Mittaz et al., 2004; Nandadasa et al., 2014).

In general, ADAMTSs can impair a series of processes as cell migration, adhesion, regulation of phosphorylation, angiogenesis and maturation of stromal cells which would finally impact in the tumour biology. Regarding the field of cancer research, ADAMTSs have been reported to display both pro- and anti-tumorigenic functions (Cal and Lopez-Otin, 2015). For example, in human breast carcinomas opposite actions have been attributed to different members of the family. ADAMTS1, 3, 5, 8, 9, 10 and 18 are down-regulated compared to normal tissue, while only ADAMTS4, 6, 14 and 20 are up-regulated (Porter et al., 2004). In spite its brief mention here, ADAMTS1 will be extensively described in the next section. This protease is a good example with both pro- and anti-tumorigenic capacities (Fernández-Rodríguez et al., 2016; Martino-Echarri et al., 2013) while other proteases as ADAMTS4 and 5 have been linked just to the promotion of cancers as glioblastoma (Held-Feindt et al., 2006). Nonetheless, many other members of the family stand by their anti-tumour capacities as ADAMTS8 in brain tumours (Dunn et al., 2006) and ADAMTS9 in pancreatic and colorectal cancers (Liu et al., 2012). (**Figure 9**).

Noteworthy is the increasing amount of literature regarding the angiogenic tuning capabilities of this family of proteases. Indeed, the link to their implication in various diseases but also physiological activities is appealing. Again, different ADAMTSs have been found to exert both pro- or anti-angiogenic properties depending on the context and situation. Originally their anti-angiogenic capacities were linked to the TSP repeats. ADAMTS1, 2, 4, 5, 8 and 12 have inhibitory angiogenic effects even though all members have at least one TSP motif. Not only the C-terminus region but also the N- part of the protease, where the catalytic domain is located, can have a role during angiogenesis (**Figure 9**). The cleave of substrates as versican, TSPs, and other ECM components can have further effects during the formation of the vascular system (Rodríguez-Manzaneque et al., 2015).
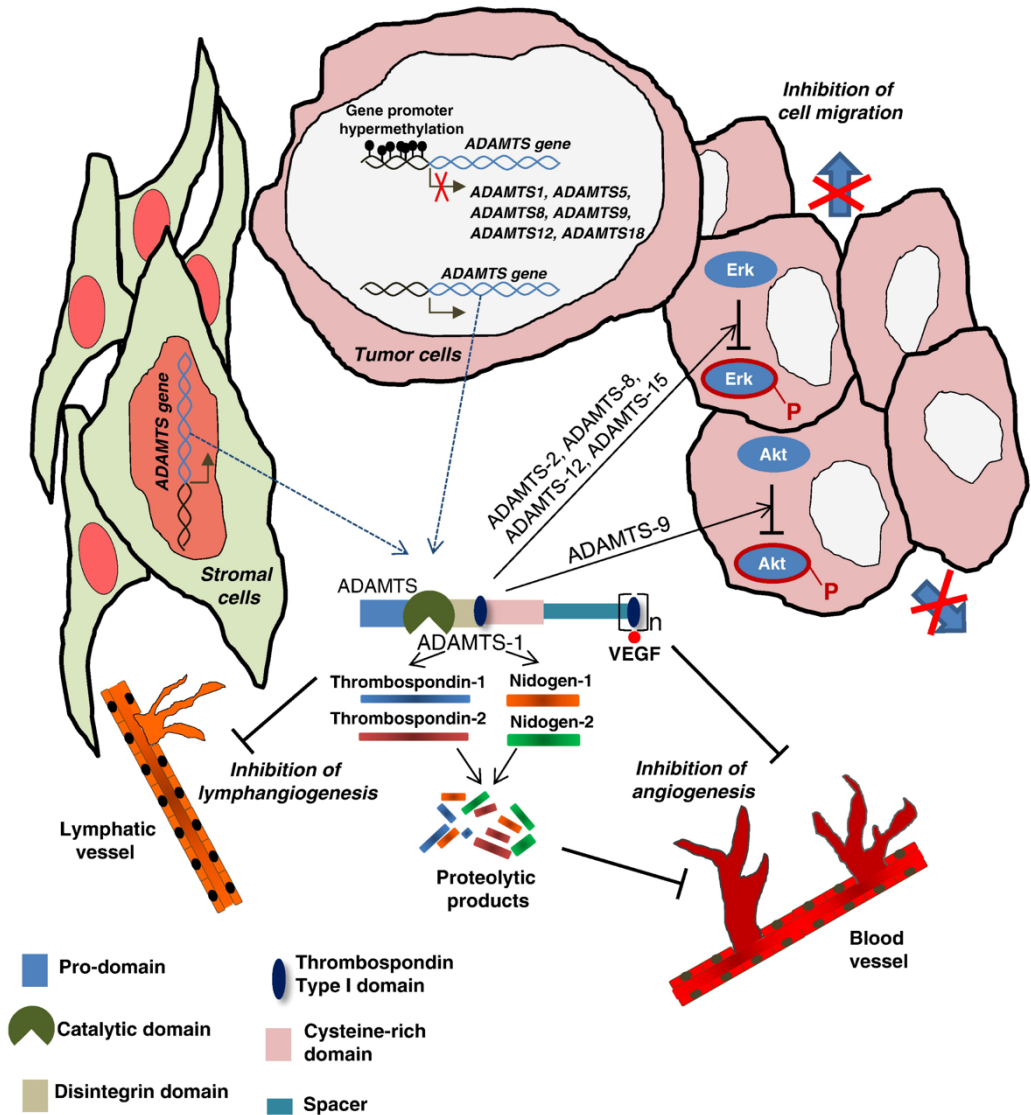
Figure 9. Anti-tumour effects mediated by ADAMTS proteases. This figure represents the mechanisms of action of ADAMTS proteases in relation to the tumour progression. This figure recapitulates both the cleaving power and the catalytic-independent effects that this protease family can exert within the tumour microenvironment (Cal and Lopez-Otin, 2015).

3.3 ROLE OF THE ECM IN ANGIOGENESIS

The vBM has already been described in the section 2.1.3 as another component of the blood vessel structure. During the process of the creation of a new sprout or blood vessel, the remodelling of the ECM and their BM must be under a tight control.

In normal physiological conditions, ECs and PCs remain quiescent when they are attached or in contact with the vBM. When the degradation of the vBM starts, these cells acquire a different behaviour and they become more motile and invasive. Furthermore, there is a secretion of a new ECM surrounding the tracking area where the new tip cells are spreading the filopodia, in order to further invade the area. This new ECM differs in composition, so the cells do not recover from its quiescent state. In this case Collagen I, Vitronectin and Thrombin can be found. In this process, not only ECs and PCs but also fibroblasts and immune cells play a role, producing matrix metalloproteases, VEGF and other vascular related factors (Kalluri, 2003).

3.4 ROLE OF THE ECM IN CANCER PROGRESSION

In the beginning of the XXI century, Hanahan and Weinberg reviewed again the hallmarks of cancer (Hanahan et al., 2011). Interestingly they show and remark that tumour must be seen as heterogeneous mass of cells instead of the reductionist view that was originally accepted (Figure 8a). They show the importance of the different subsets of cells present in the tumour scenario, such as endothelial, fibroblasts and immune cells. Interestingly, the ECM was not included in their "heterotypic cell model" (Hanahan and Weinberg, 2000). In a newer version, the same authors gave a key role to the ECM in the process of tumorigenesis and metastasis (Hanahan et al., 2011). More recently, researchers have shown the similarities between the ECM of primary tumours and metastases, instead of the resemblance with the organ that has been invaded (**Figure 10**). This cue stands out the importance of the tumour cells fine tuning of the ECM (Naba et al., 2014).

Accordingly, a dysregulated ECM also acquired the status of hallmark of cancer. The deposition and regulation of the ECM is a very uptight controlled process and any defect in its assembly or production can promote malignancies as occurs in cancer (Lu et al., 2011). Not only ECM regulation itself but others hallmarks, such as sustained angiogenesis, evasion of growth suppression, enhanced invasiveness and so on, are modulated somehow by the ECM state (Hanahan and Weinberg, 2000; Hanahan et al., 2011; Pickup et al., 2014). Considering this, extracellular proteases appear as important and main regulators of the matrix homeostasis. The modulation of these enzymes at translational and post-translational levels in the stromal and/or tumour cells will have an impact in the constitution of a proper ECM.
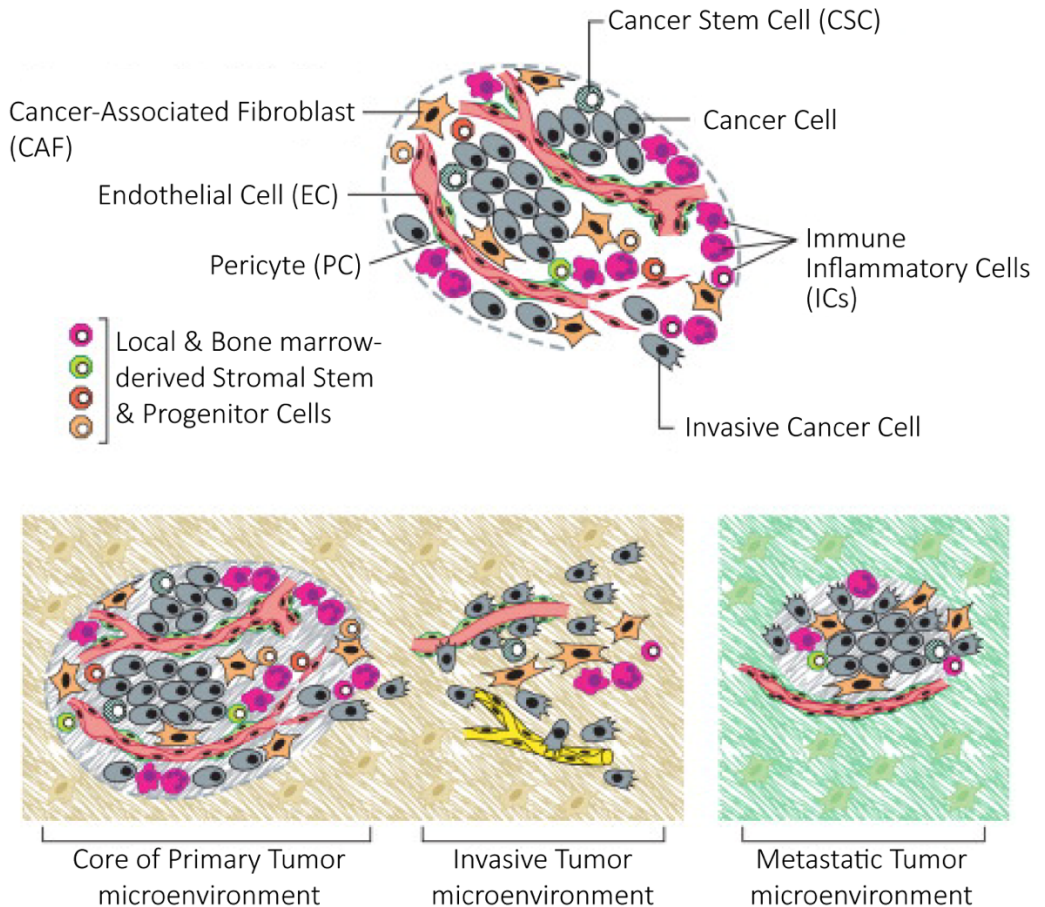
Figure 10. The reductionist and renewed ECM tumour model. This figure covers the first observations that Hanahan & Weinberg took of the tumour concept in which the ECM was not included (upper image). In the next review (bottom images) they update their point of view including the ECM as a key player in primary tumour and metastatic events (Hanahan et al., 2011).

Fibroblast, endothelial, vasculature supporting, immune cells and tumour cells are their main contributors, and thus they can tune up the whole process (Bhowmick et al., 2004). During aging or disease, the regulation and expression of extracellular proteases and thus the deposition of the ECM can be altered despite the multiple controlling mechanisms. Indeed, the amount of ECM components that are deposited, their degradation and additional post-translational modifications would affect ECM dynamics in general, turning to be one of the first cues of the malignancies (Lu et al., 2011, 2012). One of the main characteristic of tumour ECM is the stiffness. Many studies have related the stiffness of the matrix with tumorigenesis via the trans-differentiation to mesenchyme (EMT) and is also associated with a poor prognosis value in breast cancer patients (Seewaldt, 2014; Wei et al., 2015).

As a final point, ECM also has a role in the maintenance of the cancer stem niche. Modifications in ECM components can modify the cell-cell and cell-matrix attachment, altering the tumour niche architecture and thus compromising the tumour cell fate (Raymond et al., 2009). Other features that impacts in tumorigenesis is the tissue polarity. Studies show how modifying the ECM dynamics can compromise the BM stability and lead to EMT, thus increasing the risk of developing a cancer. This was also corroborated by studies in which mice overexpressed matrix metalloproteinases (MMPs) and this led to cancer events (Sternlicht et al., 1999). Last but not least, is the impact in tumour angiogenesis, described in the section 2.3. However, it is known that in tumours, the vascularisation process is different from the physiological and the ECM components are key molecules within these processes. For example, the result of de degradation of Collagen IV and XVIII (Endostatin, Tumstatin and Aresten) can have pro- or anti-angiogenic effects, potentiated by the interaction with VEGF and also the production of MMPs and other extracellular proteases by tumour cells, thus modulating tumour angiogenesis (Mott and Werb, 2004).

4. ADAMTS1

ADAMTS1 (A Disintegrin and Metalloprotease with Thrombospondin motif-1) is the first member of this family (Kuno et al., 1997a, 1997b). It was first named METH-1 (as MEtalloprotease with THrombospondin motifs-1), and it was thought to be an ADAM protease with TPS repeats (Vázquez et al., 1999). The mouse orthologous was found in a murine colon adenocarcinoma model associated to cachexia. ADAMTS1 is well conserved during evolution, showing 82% of homology between the human and mouse genes (Puente et al., 2003).

4.1 STRUCTURE AND REGULATION.

ADAMTSs structure has been already described in the section 3.2.3. Compared to its relatives, ADAMTS1 is one of the smallest members, with two TSP repeats after the cysteine-rich region (Vázquez et al., 1999). ADAMTS1 protein has been found in different isoforms, named according to their molecular weight: the pro-active form (p110) containing the pro-domain that will be cleaved by furin-peptidases to generate the active form. This process occurs in the *trans*-golgi network. The first active isoform, p87, can also be cleaved by MMP2, 8 and 12 in the spacer region, after the cysteine-rich region, where the two TSP repeats are found, making this active form less fond to bind heparin (**Figure 11b**) (Rodriguez-Manzaneque et al., 2000). Nevertheless, it was shown how the protease could auto-cleave itself, regulating its own cleaving activity, in this case in a cancer context (Liu et al., 2006).

The gene expression regulation of *Adamts1* has not been fully characterised but its influence has been depicted in diverse scenarios. First, it was demonstrated that *Adamts1* is an *IL-1* inducible gene in a colon 26 adenocarcinoma cachexia model, the same model where it was discovered (Kuno et al., 1997a; Sasaki et al., 2001). Similarly, same effects where observed for *IL-1β* in human decidual stromal cells (Ng et al., 2006). On the other hand, some works suggest that the cytokine *Tgfβ* negatively regulates the expression of *Adamts1* (Cross et al., 2005; Ng et al., 2006). Later on, *Adamts1* was found to promote the migration of human umbilical vein endothelial cells (HUVEC) under hypoxic conditions. Further characterisation discovered three putative hypoxia-inducible factor (HIF) binding sites in the promoter region of *Adamts1* (Hatipoglu et al., 2009).
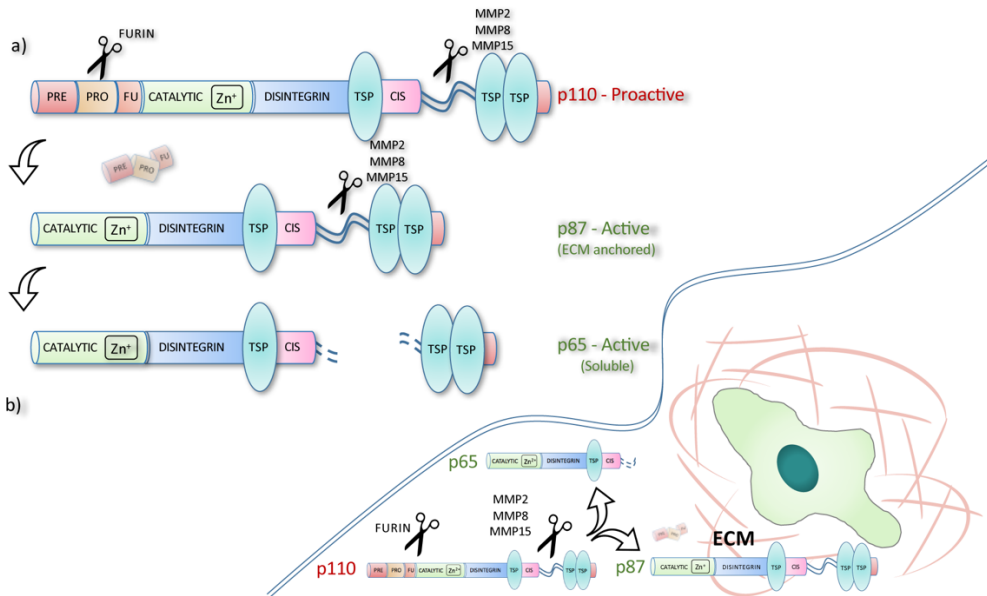
Figure 11. Structure and maturation of ADAMTS1. a) The structure of ADAMTS1 in the three different isoforms: p110 – Proactive, p87 – Active and p65 – Active. b) protease location in the ECM in regard to its processing. Adapted from (Rodriguez-Manzaneque et al., 2000).

Finally, chromatin remodelling proteins as Brg1, involved in cardiac development, repressed *Adamts1* expression in order to support the formation of the cardiac tube (Stankunas et al., 2008). Lastly, one study shows how the sustained *Adamts1* expression involves the loss of the Enhancer of zeste homolog 2 (*Ezh2*) a histone-lysine N-methyltransferase enzyme thus, enhancing the trimethylation of H3K27 histones. This was demonstrated by using an inhibitor of the PI3K-Akt pathway, which significantly downregulated the expression of *Adamts1* in fibroblasts (Tyan et al., 2012).

Apart from the cleavage of ECM substrates, the proteolytic activity of ADAMTS1 also have important biological functions. Interestingly, the release from latent to active-TGFβ has been linked to ADAMTS1 in a hepatic stellate cell model (Bourd-Boittin et al., 2011). In a different scenario, the lutein hormone induced transcription factor PR is required for the production of this protease. Moreover, the action of this protease also required in the reorganisation of the ECM of the follicle wall and angiogenic modulation in the ovary (Robker et al., 2000).

It is also important to mention that this protease was first described to be inhibited mainly by TIMP2 and TIMP3, being this last one the most effective one (Rodríguez-Manzaneque et al., 2002).

4.2 ADAMTS1 SUBSTRATES

Since its discovery in 1997, more than 13 substrates have been described to be cleaved by ADAMTS1. The first identified were proteoglycans such as: Aggrecan (Rodríguez-Manzaneque et al., 2002), Brevican (Matthews et al., 2000) and versican (Sandy et al., 2001). While the processing of versican has been related to organ development and cancer progression, the digestion of Aggrecan is linked to osteoarthritis, and Brevican with neural development (**Table 2**). Syndecan-4 is another ADAMTS1 substrate and this controls cell-cell and cell-ECM junctions, whose cleavage provokes changes in cell adhesion (Rodríguez-Manzaneque et al., 2009). Finally, other proteoglycans identified were: Dystroglycan, Desmocollin-3 and Mac-2 binding protein (M2BP) (Canals et al., 2006).

PROTEIN	SUBSTRATE	FUNCTION	LITERATURE
GLYCOPROTEINS	Aggrecan Versican Brevican Syndecan-4 Dystroglycan Desmocollin-3 Mac-2 binding protein	Cartilage-specific ECM component Surface of neurons Cell-cell/ECM bonds Skeletal-muscle Cell-cell junctions Cell-ECM adhesion	Rodriguez-Manzaneque et al., 2002 Sandy et al., 2001 Rodriguez-Manzaneque et al., 2009 Canals et al., 2006
SOLUBLE PROTEIN OR ECM-ANCHORED	Semaphorin 3C Gelatins TPFI-2 TSP1/2 IGFBP2	Nervous System Collagen I degradation ECM Scenario Anti-angiogenic IGF biodisponibility	Esselens et al., 2006 Lind et al., 2006 Torres-Collado et al., 2006 Lee et al., 2006 Martino-Echarri., 2014
BASEMENT MEMBRANE	Nidogen 1 Nidogen 2	ECM component binding	Canals et al., 2006
EGF FAMILY	Amphiregulin TGF Alpha Heparin binding EGF	EGF-Like Growth factors	Lu. X et al., 2009

Table 2. Updated list of ADAMTS1 substrates. Table recovering an updated information of all the known substrates of the protease ADAMTS1 indicating the protein type, its main function and also the most relevant literature.

Soluble proteins or ECM-anchored components with important biological functions are also cleaved by ADAMTS1. Among them, Semaphorin 3C (Sem3C) have a central role in neuron development but its cleavage has been associated to tumour progression and metastatic events (Esselens et al., 2010). Gelatins, products of Collagen I denaturation, were found to be degraded by ADAMTS1 in conditioned media from an insect cell line (Lind et al., 2006) as well as the suggested Collagen I fibers degradation in rat osteoblasts (Rehn et al., 2007). Interestingly, TSP-1 can also be cleaved by ADAMTS1 releasing single anti-angiogenic molecules to the milieu (Lee et al., 2006b). During the search of new

substrates of ADAMTS1, the molecule tissue factor pathway inhibitor 2 (TFPI-2) was first identified and also included in the list of substrates. TFPI-2 acts on initiation of the coagulation process but also acts as an endogenous serine protease inhibitor. More recently, the insulin growth factor binding protein 2 (IGFBP2) cleavage by ADAMTS1 was discovered by this research group, associated with poor prognosis in gliomas (Martino-Echarri et al., 2014) (**Table 2**).

In addition, Rodríguez-Manzaneque's group found Nidogen 1 (NID1) and Nidogen 2 (NID2) as ADAMTS1's substrates (Canals et al., 2006). On account of the relevance of these 2 substrates, together with Versican, for this thesis, they will be profoundly described in the section 5 and 6, respectively, of this introduction (**Table 2**). Finally, in this wide list of substrates, ADAMTS1 is known to participate in the release of EGF-like ligands including TGFα and heparin binding EGF from tumour cells (Lu et al., 2009).

4.3 THE ADAMTS1 KNOCKOUT MOUSE MODEL

To date, four mouse models of the *Adamts1* K.O have been developed using similar methodologies (Lee et al., 2005; Mittaz et al., 2004; Shindo et al., 2000). By homologous recombination, the *Adamts1* mouse gene was substituted by a PGK vector. All the models used a PGK cassette to substitute different exons of the gene except the model of Mittaz et al., in which they only deleted the exon 2, obtaining a truncated and non-functional ADAMTS1 protease. As presented in this thesis project, our research group have been working with the model described in Lee et al., 2005. This is the model in which the deletion of the largest number of exons was taken.

All models can be accessed by http://www.informatics.jax.org a "mouse genomic information" free access database where most of the phenotypic details and information is reported (**Table 3**):

Mouse origin strain	Strain Designation	MGI: ID	Reference
129S6/SvEvTac	129S6-Adamts1[tm1Hku]	2156168	Shindo et al., 2000
129/Sv	129/Sv-Adamts1[tm1Mapr]	3574351	Mittaz et al., 2003
129X1/SvJ	129X1/Sjv-Adamts1[tm1Mlia]	3609982	Lee et al., 2005
129P2/OlaHsd	B6;129P2-Adamts1[tm1Dgen]	5427602	Oller et al., 2017

Table 3. Current *Adamts1* knockout mouse models. In the table is included the mouse origin strain and the international strain designation as well as the MGI ID number to find more information about the model and the first references.

The deepest morphological characterisation was done by the team of Shindo et al. According to published reports, the most important phenotype relates with the urogenital system and fertility. During ovulation, null ovaries could not further develop because the mature oocytes remained trapped in the ovarian follicles impacting in the fertility of *Adamts1* KO females (Mittaz et al., 2004). The *Adamts1* deficiency also was accompanied by polyuria (increased amount of urine produced), lower amount of sodium and potassium in urine and abnormal ureter morphology were observed in the null littermates. Also notably is the morphology of the kidney itself, with absent papilla, its morphology results aberrant.

More generally accepted among all the *Adamts1* KO models was the reduction of body size and epididymal fat mass, accompanying with leaner bodies (30% of body mass reduction in 9 months' individuals). Although not deeply assessed, researchers also observed a significant lethality at the intraembryonic/neonatal stage, with about 40% of homozygous null mice not recovered (Mittaz et al., 2004; Shindo et al., 2000).

This model has been very significant and valuable for this research group. The use of the animal biology in the study of tumour progression allow us to unravel the duality of the protease in cancer as well as depicting its functions related to angiogenesis. Even though there has been an extensive description of this animal in the literature, we use it as a powerful tool to describe the importance of the ADAMTS1 substrate cleavage during organogenesis and non-pathological conditions, which is one of the main aims of this thesis.

4.4 MAIN FUNCTIONS OF ADAMTS1

As introduced above, ADAMTS1 is a complex molecule which actions not only depend on its catalytic activity but also displays relevant functions by its carboxyl-end region. Here we recapitulate the most important functions highlighting their relation with our research project. Nevertheless, it is important to know the general levels of expression of the protease. *Adamts1* is expressed in multiple tissues and cell types; ovary, bronchial epithelial cells, fetal lung, placenta, smooth muscle, uterus, adrenal cortex, adipocyte, ciliary ganglion, prostate, olfactory bulb, breast stromal fibroblasts and myoepithelial cells. Generally, its expression is moderate to low but it increases in specific processes as development, angiogenesis and pathological conditions as cancer, inflammation and arthritis (De Arao Tan et al., 2013).

4.4.1 ADAMTS1 & ANGIOGENESIS

The protease was first described as an anti-angiogenic factor according to the presence of three TSP motifs (Vázquez et al., 1999). The full length of the protease was shown to have anti-angiogenic capacities, but it was proven how the cleavage of the p87 into p65, releasing two TSP repeats had also important anti-angiogenic effects (Rodriguez-Manzaneque et al., 2000). A few years later another mechanism by which ADAMTS1 inhibited the formation of new blood vessels was described, based on the sequestering of the VEGF165, so hampering the activity of VEGFR2 (Luque et al., 2003). The majority of the studies and research show and support the anti-angiogenic effects of the molecule (Rodríguez-Manzaneque et al., 2015). A very recent study has linked the heritable thoracic aortic aneurysms and dissections including Marfan's syndrome with the expression of *Adamts1*. In the null mice the aortic dilation and degeneration is more evident, being this related with higher levels of inducible nitric oxide synthase (NOS2) (Oller et al., 2017).

On the other hand, ADAMTS1 is also necessary for the process of sprouting. It is a protease required for the cleavage of the ECM in regard of the tip cell to facilitate its migration towards the other sprout, but its activation is later inhibited to avoid anti-angiogenic effects (Su et al., 2008). *Adamts1* expression is driven together with hypoxia in an *in-vitro* model, also potentiating the migratory capacities of ECs, thus, showing a pro-angiogenic role (Hatipoglu et al., 2009).

4.4.2 ADAMTS1 & CANCER

For many years now the association of ADAMTS1 and tumour progression have long been accepted. The dual role of this molecule has been recognised with remarks to its interesting nature as a tumour modulator. The first study associated the protease with tumour cachexia and inflammation in a murine colon adenocarcinoma model (Kuno et al., 1997a).

There are studies in which *Adamts1* was associated with tumour progression and metastasis. Some of these studies are linked to the anti-angiogenic properties that ADAMTS1 glance, but others outline the proteolysis of several ECM components as the main driver. The first work were this link was observed, studied tumours in a model of pancreatic cancer in which they saw that the expression of the molecule promoted tumour pancreatic cells progression and also metastasis to lymph nodes (Masui et al.,

2001). Similarly, other studies added strength to this hypothesis; an upregulation of *Adamts1* was found in bone metastasis (Kang et al., 2003). In agreement with the previous work, researchers studied a breast cancer tumour with bone metastasis in which *Adamts1* was upregulated in primary tumours with the worst prognosis and also in the majority of the metastasis (Casimiro et al., 2012). As mentioned, the proteolytic activity of ADAMTS1 was the main contributor to the tumour progression findings. In this case it was associated with high-risk metastasis patients in regard to the ECG-like ligands cleavage (Lu et al., 2009).

In line with the tumour progression role, and being very relevant for this thesis, other studies added interesting data using more functional models. Studies by our collaborators, using the *Adamts1* KO in a MMTV-PyMT mouse strain that develops spontaneous breast tumours, implies the lack of ADAMTS1 with reduced tumour burden (Ricciardelli et al., 2011). More recently, and constituting the main published work of this thesis, our laboratory demonstrated the tumour progression impairment of a B16F1 mouse melanoma cell line with the *Adamts1* KO model (Fernández-Rodríguez et al., 2016).

A few years later than the pro-tumorigenic side of *Adamts1* was described, some studies showed how this molecule also exhibited anti-tumorigenic capacities. First, a researcher found a positive upregulation of *Adamts1* in human breast cancer patient samples in comparison to non-neoplastic mammary tissue. However, no direct correlation was found between this expression and the progression of the disease (Porter et al., 2004). Very closely, another study over-expressed *Adamts1* or the carboxyl-end in a Chinese hamster ovary (CHO) cell line. This time, the anti-metastatic role of the TSP- loaded C-terminus of the protease was proven in a xenograft assay (Kuno et al., 2004). Similarly, other studies started to relate the anti-angiogenic properties of the protease with the anti-tumorigenic effects seen *in-vivo*. A reduction in the tumour size (Reynolds et al., 2010) and affected metastasis efficiency (Lee et al., 2010) were assessed in this case. In line with the rationale of this thesis, this research group also looked at the possible anti-tumoral side of the protease in a xenograft assay in which the ADAMTS1 over-expression showed a clear tumour growth delay, linked to their Nidogens processing in the perivascular niche (Martino-Echarri et al., 2013).

Given all the information about the tumorigenic capacities of *Adamts1*, it is clear now that this protease has a dual role in this scenario. The literature itself show how there are more studies that could be thought to be contradictory but nothing further than that, they imply the complexity of the nature of ADAMTS1, particularly, driving tumour progression. Some studies found this particular duality within the same models. The first

study showed an increased metastatic potential with the over-expression of the full length of ADAMTS1 in a murine mammary carcinoma and a lung carcinoma cell lines. When they assessed the same approach but with the ADAMTS1 fragments instead, the metastatic events were reduced (Liu et al., 2006). Since then, several studies published by this research group highlighted the importance of ADAMTS1 in the context, the tumour origin and also the stromal nature (Casal et al., 2010; Fernández-Rodríguez et al., 2016; Martino-Echarri et al., 2013).

4.4.3 ADAMTS1 & THE IMMUNE SYSTEM

As already introduced, mouse *Adamts1* was first associated to inflammation and thus, the immune system by the moment of its discovery. The positive regulation of ADAMTS1 by *Il-1* and the downregulation by *Tgfβ* has long been described (Kuno et al., 1997a; Ng et al., 2006; Sasaki et al., 2001). It is also necessary to mention the role of the proteolytic activity of ADAMTS1 showed in the release of active TGFβ in a hepatic stellate cell model (Bourd-Boittin et al., 2011). Nevertheless, no functional alterations in immune cells have been attributed to either the cleaving activity ECM components that may have an impact in immune cell maturation or the functionality that its carboxyl-end gives to this protease. The functional studies of the *Adamts1* KO mouse models did not challenge appropriately the immune landscape in order to find possible alterations. Since the first approaches to the *Adamts1*-immune system relationships, we still have not found an explanatory mechanism of action for ADAMTS1 within the immune landscape.

The expression of *Adamts1* in the different immune subsets has not been well studied and characterised. Interestingly, there is a study which showed colocalisation of the protease within a subset of F4/80[+] macrophages. In this work they use a CX3 chemokine receptor 1 (CX3CR1) deficient animal which showed a downregulation of *Adamts1* and also *Tsp1*, remarking the importance of this macrophage subset in angiogenic processes (Lu et al., 2008). A recent study shows the relationship between ADAMTS1, Versican and the tolerogenic polarisation of antigen-presenting-cells (APCs) and T-cells through the Toll-like receptor (TLR2) in a myeloma model (Hope et al., 2016). ADAMTS1 can cleave Versican creating a molecule called Versikine (VKIN) which induces pro-inflamatory IL-6 and IL-12, attracting T-cell to the bone marrow and the tumour niche. Also Versikine can induce interferon regulatory factor 8 (IRF8) which makes tumour cells prone to apoptosis (Schmitt et al., 2016). This phenomenon is driven by the cleavage of versican by ADAMTS1, so the regulation of this protease in this tumour niche is necessary for the maturation of certain immune populations (Hope et al., 2016; Schmitt et al., 2016).

Relevant for our ongoing interest on the connection ADAMTS1/immune system, recent research has showed how *Adamts5* is necessary for virus-specific T-cell infection. The *Adamts5* null mice takes longer to clear the virus from their system and they propose a model in which Versican cleavage due to the absence of ADAMTS5 creates a physical barrier that impedes t-cells function. (McMahon et al., 2016). The biochemical structure of ADAMTS1 and 5 are very similar, sharing also some cleavage affinities as in the case of Versican. In relation with the previous study of the tolerogenic polarisation of APCs in the myeloma model and the induction of the pro-inflammatory environment, these two molecules proteases could share a role. This would help to depict the impact of *Adamts1* in the immune system landscape.

5. NIDOGENS

In addition to a brief introduction in section 3.1 we consider to devote a whole chapter to Nidogens due to its importance in this research project. Nidogens, formerly known as Entactins, are extracellular sulphated glycoproteins that form part of the basement membrane and basal lamina. There are 2 members: Nidogen 1 (NID1) and Nidogen 2 (NID2) and between the human and mouse sequences there is a high similarity > 85%. Following a time line, NID1 was the first discovered, produced by cells isolated from an embryonal carcinoma (Bender et al., 1981, 1982; Carlin et al., 1981). NID2 was found 17 years later using a osteoblast-like murine cell line; they isolated several cDNA clones and one of them was termed entactin-2 (Kimura et al., 1998). A few months later another research team confirmed that it was *Nidogen 2* cDNA and it had a high similarity with *Nidogen 1* (Kohfeldt et al., 1998).

5.1 STRUCTURE AND PROTEOLYSIS

Nidogens are triglobular proteins, 150 and 200 kDa for NID1 and NID2 respectively. The globular domains are connected to each other by a linker and a rod domain (**Figure 12**). Both molecules show a strong homology, higher in the globular domains. Although with differences, each globular domain provides specific binding affinities to ECM molecules (**Figure 12**). The globular domain 1 (G1) is composed by a NIDO domain (Nidogen-like), which is separated from the rest of the molecule by proteolysis-sensible spacer region (Mayer et al., 1993). This domain presents differences, more precisely a binding sequence to Fibulin-2 in NID1 but not in NID2 (Kohfeldt et al., 1998). The globular domain 2 (G2) contains an EGF-like domain and the main G2F domain. The rod domain connects the G2 and G3 domains and is composed by five EGF-like and one thyroglobulin type-1 motif (TY) for Nid1 and five EGF-like and 2 TY for Nid2. The rod structure has been found to be very stable and not sensible to proteolysis. The globular domain 3 (G3) is composed of four low-density-lipoprotein-like receptor type-1 (LDL) and one EGF-like for Nid1 and five LDL without EGF-like for Nid2. The G3 region is also sensitive to proteolytic activity (**Figure 12**).

On the other hand, Collagen XIII only binds Nid2, this molecule is present in the BM of musculoskeletal tissue and its relationship with NID2 seems important to the assembly of this tissue (Ho et al., 2008). Both Nidogens can bind Laminin, one of the main components of the BM (**Figure 13**).
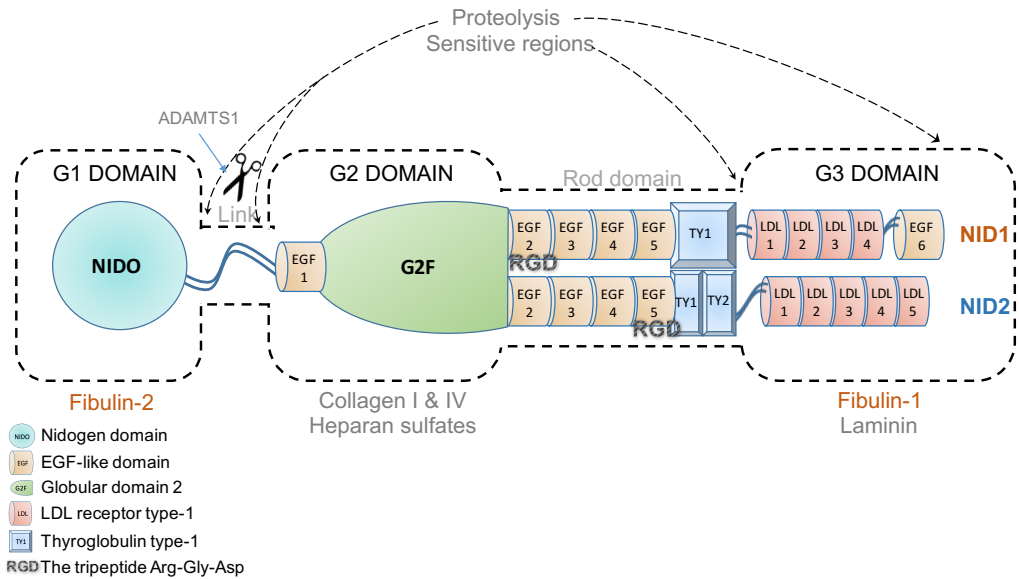
Figure 12. Nidogens structure. Representation of all the all the available information about differences between both Nidogens molecules in structure and composition. Also the proteolysis sensitive regions and specifically to ADAMTS1 are included apart from the binding regions that varies within both molecules.

This interaction is the most relevant for the deposition of the molecules in the BM. The blockade of the binding sites of laminins in the G3 domains, completely wipes Nidogens from this environment (Mokkapati et al., 2008). Nidogens also possess RGD sequences that makes them able to bind Integrins. NID1 has the RGD in the first EGF-like domain of the rod-domain and NID2 in the last one. Among all Integrins, the α3β1 is the most relevant binding both Nidogens (Dedhar et al., 1992). A research showed more affinity on cell-adhesion via Integrins for NID2 rather than NID1 in an adhesion approach with different cell lines in culture (Salmivirta et al., 2002a).

The proteolysis of Nidogens is a topic of high interest to us giving the relevant effects that may provoke in their structural and binding properties (**Figure 13**). Both Nidogens are found cleaved in healthy tissue, suggesting that such process is necessary for their functionality. NID1 proteolysis was reported right after its discovery (Paulsson et al., 1986). In a different study they test several proteases including serin- and metallo-proteases. Among them, MMP3 and MMP7 were found to cleave NID1 in the link domain and the G3 domain. These researchers stands the importance of the proteolytic form of NID1 in the apoptotic events of epithelial cells (Alexander et al., 1996; Mayer et al., 1993). MMP19 was also found to cleave NID1 and its biological consequence affected to the formation of tubular-like structure *in-vitro* in a matrigel matrix (Titz et al., 2004). ADAMTS1 was described to cleave both NID1 and NID2, for NID2 was the first

time shown to be cleaved by a protease (Canals et al., 2006). The process happens between the G1 and G2 regions generating 2 different fragments for NID1 (110 kDa – G2/G3 and 40 kDa – G1) and NID2 (140 kDa – G2/G3 and 40 kDa – G1). Another protease from the cysteine-protease family, Cathepsin S, was found to cleave NID1 even though its main action is intracellular. This cleavage impairs the molecule to bind its BM partners (Sage et al., 2012). More recently, this cleavage showed interesting properties during tumour progression vascularisation. The lack of cleavage in the tumour perivascular niche led to the hypothesis that this processing might be necessary to drive tumourigenesis (Martino-Echarri et al., 2013).
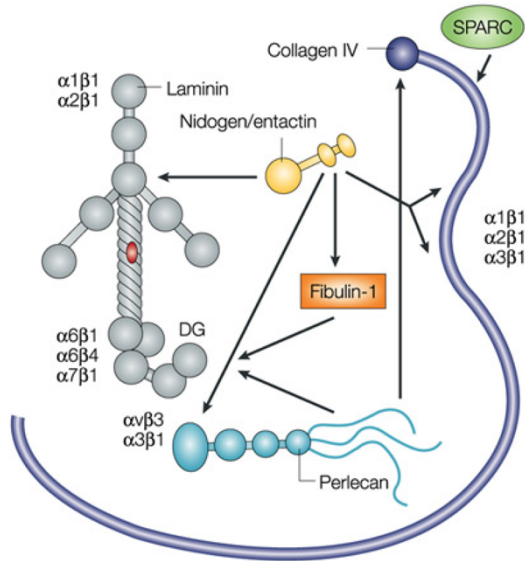
Figure 13. Nidogen interaction relationship with other ECM components. This figure represents the multiple interactions with molecules as Perlecan, Fibulin-1, Collagen IV and Laminin (Kalluri, 2003)

5.2 MAIN FUNCTIONS

NIDOGENS are components of the BM produced mainly by mesenchymal cells (Pujuguet et al., 2000). Their main described role by now is the bridging between the two main layers of proteins of the BM, the network of Laminin and Collagen IV. Nidogens create bonds between both Laminin and Collagen IV, strengthening their interactions and unifying both networks. As introduced above, Nidogens also bind other ECM proteins, indicating extra functions apart from the stabilisation of the two main protein networks of the BM (Ho et al., 2008).

Its biological importance during development and organogenesis has been approached in mouse studies. Significantly, the complete ablation of both Nidogens causes basement membrane defects and perinatal lethality in mice. Both molecules have shown their relevance during late stages of lung and cardiac tissue maintenance (Bader et al., 2005). Nevertheless, when only NID1 is ablated in the mice, there is a compensation phenomenon that does not effect NID2 (Miosge et al., 2002; Schymeinsky et al., 2002). However, the NID1 null mice can assemble a proper BM (Murshed et al., 2000) but has

several reported defects as impaired wound healing (Baranowsky et al., 2010) and neurological deficits in the central nervous system (Dong et al., 2002).

Studies related to human diseases are highlighting Nidogens in various scientific research areas. Bio-informatics approaches discovered mutations in NID1 related to neurological disorders (autosomal dominant Dandy-Walker malformation) (Darbro et al., 2013; Vasudevan et al., 2010). In a recent study, Nidogens were found to act in the binding of the tetanus toxin at the neuromuscular junction. When blocking or ablating Nidogens the toxin did not bind at all, turning the molecule into a possible target for the toxin blockade (Bercsenyi et al., 2014). NID1 was also associated with the micro-RNA, miR-192/215. This microRNA is known to inhibit cell migration *in-vitro* and it targets NID1 as well. Rescuing *Nidogen 1* expression, restored migration of a human embryonic kidney (HEK-293T) and human bone marrow neuroblast (SH-SY5Y) in the Hirschsprung's disease model (Zhu et al., 2015).

5.2.1 ROLE OF NIDOGENS IN ANGIOGENESIS

Although both Nidogens are main components of the BM, their role in angiogenesis and vascularisation is still not well defined and the literature shows controversial findings. The first study relating Nidogens and angiogenesis was in 1994 in a rat aortic ring assay in collagen matrices. The high density of Laminin-Nid1 in the matrices inhibited the sprouting but stabilised their structure, and when the concentration decreased the sprouting was increased (Nicosia et al., 1994). Its cleavage also revealed important changes during angiogenesis *in-vitro* assays. The cleavage of NID1 by MMP19 releasing the G3 fragment impairs its ECM-binding capabilities thus inhibiting the formation of tubular-like structures (Titz et al., 2004). Similarly, in a co-culture assay with ECs and PCs the authors show an upregulation of NID1, FN and Laminin in the co-culture, the greater BM assembly resulted in longer and stronger sprouts (Stratman et al., 2009).

In a study of the identification of the endothelial-cell tip-enriched genes signatures in a rat-retina *ex-vivo* model for Dll4 [+/-], the mutants show over-expression of *Adamts1* and both *Nidogens*. More importantly, the *in-situ hybridisation* (ISH) revealed how *Nidogen 2* was transcribed at higher levels at the tip cells in comparison to the stalk and the rest of the vasculature. *Nidogen 1* was also over-expressed but it was more vasculature-wide (del Toro et al., 2010).

More recently in a study of choroidal neovascularization with the NID1 and NID2 null mice models, NID1 is seen as a stabiliser of the BM during the angiogenesis process but

it provides an anti-angiogenic environment to the already established vessels (Semkova et al., 2014). In spite, and in relationship with the next section, there is an interesting association between NID1 and tumour endothelial cells that might be key in tumour progression. TEM7 a protein found to be overexpressed in tumour endothelium has NID1 as one of the major ligands and the interaction enhanced tumour cell spreading and adhesion *in-vitro* (Lee et al., 2006a).

5.2.2 ROLE OF NIDOGENS IN CANCER

Finally, the functional relationship of Nidogens with tumour progression and metastasis might be associated to the already described functions such as BM assembly and angiogenesis-related or new roles that are yet to be discovered. Paulsson et al, already isolated Nidogens from mouse tumour models in 1996 and they were found to be deposited in vascular tumour BM in several tumour models (Baluk et al., 2003; Paulsson et al., 1986). Both molecules have been found as biomarkers for several cancers. NID2 serum levels in ovarian cancer patients correlated with other cancer prognosis markers as CA125 (Kuk et al., 2010). NID1 was found to be a good candidate in a study with 268 patients of ovarian serous cancer (Li et al., 2015; Zhang et al., 2012). Another study found a significant reduction of NID2 in serum for hepatocarcinoma patients, correlating with a decrease in the expression of the primary tumour (Cheng et al., 2012).

The expression and/or deposition of both nidogens in primary tumours is something that has not been very well examined. Early experiments with xenografts observe an upregulation of *Nidogen 1* in pancreatic and renal cell carcinomas (Oivula et al., 1999). In other study of hepatocellular carcinoma they determined that *Nidogen 1* is over-expressed in PDGFC and PTEN null mice models (Lai et al., 2011). Some reports also find an association with metastases and tumour cell aggressiveness. The expression of *Nidogen 1* was found upregulated in highly metastatic melanoma cells (Valente et al., 1996). On the other hand, the ablation of *Nidogen 2* was associated with an increase of lung metastases (Mokkapati et al., 2012). This last evidence has recently been supported with another study in nasopharyngeal and oesophageal squamous cell carcinoma (Chai et al., 2016). In addition, several studies report that the metilation of *Nidogens* is altered in different human cancers. The downregulation of *Nidogen 1* was associated to melanoma cancer risk (Nan et al., 2011). Particularly, the downregulation of both genes can be a risk association in colon and stomach (Ulazzi et al., 2007) and bladder tumorigenesis (Yegin et al., 2013).

The transcription factor ETV5 is known to increase endometrial cancer cell invasion through EMT and *Nidogen 1* is one of the direct transcriptional targets. When *Nidogen*

1 was inhibited in this cell line under study, cell migration and cancer invasiveness was reduced (Pedrola et al., 2015).

Our research team has shed light over the controversy that already exists in the topic of tumour progression and/or inhibitory properties of nidogens. More importantly, the relationship of Nidogens and ADAMTS1 speaks by itself when we show the contribution of the cleavage during tumorigenesis in breast cancer. Nidogens cleavage is reduced in tumour human samples, in line with the reduction of ADAMTS1 and linking it to tumour progression (Martino-Echarri et al., 2013). This work is very important to the thesis that is proposed in this thesis as it is the basis and support the main aims and objectives. A deeper and high-throughput analysis of the localisation and the cleavage of these proteins is required in order to understand their biological role during tumour progression.

6. VERSICAN

Additionally, to the information already introduced about this ECM component, we decided to include a section explaining the most important aspects of Versican in regard to its importance in this thesis. VCAN is a complex proteoglycan whose structure integrates a protein core with a variety of carbohydrates chain named glycosaminoglycans (GAGs), highly poly-ionic, unbranched and with polymeric-side chains. Both the protein core and GAGs participate in the binding to other ECM proteins, mitogens and chemokines. The Versican human and mouse aminoacid sequence share >89% of homology. The structure of Versican consists of an N-terminus G1 domain and a G3-terminal domain and chondroitin sulfate (CS) chains between G1 and G3. Alternative splicing of the *Versican* mRNA encoding GAG, generate the following isoforms; V0, V1, V2 and V3 with molecular weight of 370 kDa, 263 kDa, 180 kDa and 74 kDa respectively, being the V0 the largest isoform of them all (**Figure 14a**) (Naso et al., 1995; Rahmani et al., 2006).

According to its structure, Versican provides hygroscopic properties to the matrices that create a loose and hydrated environment, becoming an important molecule during development and organogenesis. Versican is expressed widely among organs and tissues and its biological functions are very important. Given the virtue of its modular nature, it can direct or indirectly contact with cells or other molecules thus, playing a role proliferation, migration, adhesion and the ECM deposition itself (Wight, 2002). There is a broad spectrum of molecules to which Versican can interact with: Collagen, Fibronectin, Hyaluronan, Tenascin-R, Fibulins-1, CD44, Integrin-β1 and EGFR (Wu et al., 2005).

The Versican interplay is very broad and we would like to focus on the role of this molecule in cancer progression, linking its cleavage by ADAMTS1 to important phenomena related to immunomodulation. ADAMTS1 and other members of the family can cleaves Versican at the peptidic sequence DPEAAE^{441}-A^{442}RRGQ, within the G1 domain of V1 (Sandy et al., 2001) more recently named Versikine (Nandadasa et al., 2014). This Versican fragment is able to elicit biological functions including cell apoptosis promotion during development (McCulloch et al., 2009).

6.1 VERSICAN IN TUMOUR PROGRESSION AND IMMUNE INFILTRATION

The upregulation of *Versican* have been reported in a wide variety of malignancies as in melanoma, glioma, osteosarcoma, breast, prostate and lung cancers (Nikitovic et al.,

2006; Paulus et al., 1996; Ricciardelli et al., 1998, 2002) and in non-solid tumours as leukemia (Makatsori et al., 2003). The biggest contributor to the secretion of VCAN are the stromal cells, however, it has demonstrated how some tumour cells can also secrete it (Kodama et al., 2006). This outstands its importance in the regulation of tumour progression.

More importantly for this thesis aim, is the relationship of the expression of *Versican* in the TME, its cleavage by proteases as ADAMTS1 and the immunomodulatory role of the fragments. The roles of VCAN and its proteolysis in the TME are still unknown but some studies demonstrate certain correlations between these molecules and the immune infiltration. A study with human cervical carcinomas demonstrated an increase of *Versican* and a reduction of CD8^{+} T-cells (Gorter et al., 2010).
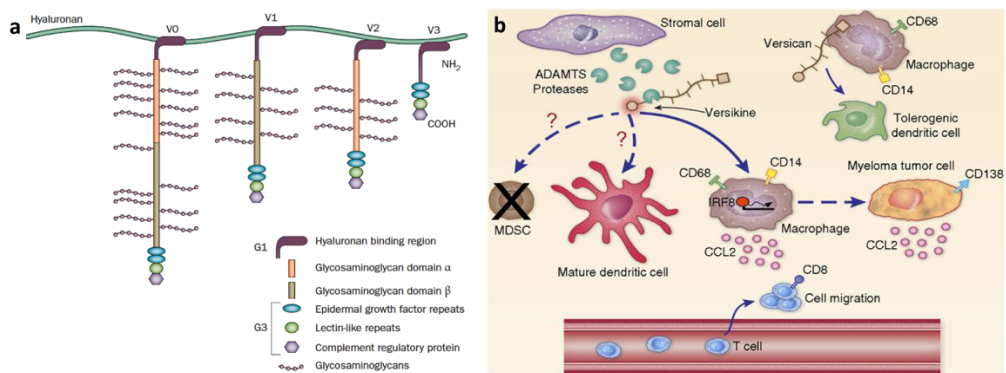
Figure 14. Versican structure and its implication in the immune system in a myeloma cancer model. a) Representation of the different forms of Versican and its main structural components (Edwards, 2012). **b)** The production of ADAMTS proteases by stromal cells and the processing of Versican, producing Versikine affects resident population of macrophages which produce a tolerogenic response attracting CD8 T-cells to the tumour niche (Hope et al., 2016).

More recent studies have shown how the processing of VCAN into these immune-active fragments had an impact in the myeloma tumour niche (Hope et al., 2016). The expression of ADAMTS1 by stromal cells in the tumour environment generates Versikine, thus, promoting the maturation of cytotoxic CD8^{+} T-cells and its recruitment to the TME. These studies suggest that Versikine could become an active therapeutic target as an adjuvant in T-Cell epitope peptide vaccination and other therapies (Hope et al., 2016; Schmitt et al., 2016). Not only the fragment Versikine but also VCAN elicits important effects on tumour burden when inhibited in two of the mouse tumour models that we use in this project, B16F1 melanoma and Lewis lung carcinoma. This study suggests that the differential processing of VCAN in the TME would finally impact in the immunosuppressive environment and thus the tumour progression. A higher VCAN

cleavage by proteases as ADAMTS1 or 5 can induce resident macrophages to produce pro-inflammatory cytokines as IL-6 or CCL2 which pave the niche for a cytotoxic CD8^{+} T-cells infiltration (Wang et al., 2015).

7. ADAMTS1 DEPENDENT TUMOUR MODELS

Throughout the development of this research we have used and managed a series or complex mouse models, or samples derived from them. Accordingly, we decided to provide some introductory details about them together with a rationale behind their study. There is a brief explanatory introduction of each model and a final **table 4** that summarise all the facts.

7.1 B16F1 MOUSE MELANOMA

This is the main model that we have used in this research project. It basically consists in the syngeneic subcutaneous implantation of the B16F1 mouse melanoma cells in mice and the study of the tumour progression, generating palpable melanomas of 1 cm^3 within 15-21 days (Overwijk and Restifo, 2001). The cell line B16F1 is a melanoma derived from a spontaneous tumour in a C57BL/6 mouse strain. The original cell line was termed B16F0 and sub consequent tumour bearing assays generated the following lines (B16F1, B16F2…) isolating the cells from lung metastases and thus increasing its metastatic capacities (Hu, 1965; Poste et al., 1980). This is a worldwide used model to study tumour progression and metastasis and the supporting literature is a great advantage. Very importantly, the background of this cell line makes possible to complement these studies with the use of the *Adamts1* KO model, also in a C57BL/6 background. The immunocompetent status of the mouse model offers also a great opportunity to study immune-associated phenomena, which an important point for this thesis research pipeline.

In addition, B16F1 cells presented a very interesting phenotype as it is the ability to create tubular-like structures when growth in 3D-like matrices *in-vitro*. They have the ability to mimic endothelial structures, outstanding its plastic properties (Huuzer et al., 1995). This characteristic allows us to study and compare these capacities in different scenarios where ADAMTS1 and Nidogens are modified (**Table 4**).

7.2 LEWIS LUNG CARCINOMA

Lewis lung carcinoma (LLC, 3LL) cells were originated from a lung carcinoma of a C57BL mouse (Bertram and Janik, 1980), Its growth properties makes it ideal for tumour

transplantation assays. Subcutaneous syngeneic implantation of LLC in mice, allow the development of palpable tumour within 15 days. The compatibility with our *Adamts1* KO mouse model was one of the main reasons for eligibility of this cell line. Furthermore, the immune compatibility of the cell line and the animal background allowed us to study the immune landscape within the TME.

The LLC cell line does not form endothelial-like structures *in-vitro* when is cultured on Matrigel, indicating somehow its poor plastic potential. Despite this fact we still wanted to work with the cell line because we needed to explore the behaviour of cell lines with different plastic phenotypes (**Table 4**).

7.3 MMTV-PYMT ADAMTS1 KNOCKOUT

This mouse model samples comes from a very generous donation from Dr. Darryl L. Russell in the University of Adelaide, Australia. The mouse mammary tumour-virus promoter with the polyoma middle T-antigen (MMTV-PYMT) model is a mouse transgenic strain generated to produce spontaneous mammary adenocarcinomas (Schoenenberger et al., 1988; Stewart et al., 1984). This mouse strain was bred with the *Adamts1* null C57/Bl6/129SvxFvBN to create the PYMT-ADAMTS1 null mice model. The cell hyperplasia in the mammary tissue is initiated by the expression of the PyMT antigen and tumours spontaneously progress to metastatic disease. The *Adamts1* null animals reduced primary tumour size and grade, as well as metastatic burden (Ricciardelli et al., 2011).

These tumour samples were of high interest to us because the development of the tumour was independent of a cell line injection. The expression of ADAMTS1 within the tumour bulk is completely absent and the tumour cell behaviour is very different from the previous models (Ricciardelli et al., 2011). The background of the PYMT-ADAMTS1 KO cell lines derivate from the tumours and its characterisation have been taken into consideration for the discussion and the results analyses (De Arao Tan et al., 2013).

7.4 MUM2B HUMAN MELANOMA

The MUM2B cell line originated from hepatic metastases from a human uveal melanoma. They are considered to be aggressive and highly metastatic (Folberg et al., 2008). The generation of the tumours consisted in the subcutaneous implantation of the MUM2B human cell line into the mice, developing palpable xenograft tumours within 21

days. The mouse background chosen was the Swiss nude strain, a athymic mouse in which the immune scenario is limited and thus we have not studied in depth.

To approach the effects of the downregulation of ADAMTS1, *Adamts1* was inhibited using a short-hairpin technology, thus, generating the MUM2B-shATS1. With this approach we can compare this models to the previous ones, where *Adamts1* was downregulated in the background. Nevertheless, we need to consider that stromal *Adamts1* remains untouched in this model, turning it into a different model.

Interestingly this cell line has been reported to form tubular-like structures *in-vitro* when cultured in Matrigel matrices. Actually the first study describing the vasculogenic mimicry phenomena was carried with this human cell line (Maniotis et al., 1999).

	MELANOMA	LEWIS LUNG CARCINOMA	BREAST CANCER	UVEAL MELANOMA
Mouse Strain	C57BL/6 ADAMTS1 $^{+/+}$ ADAMTS1 $^{-/-}$	C57BL/6 ADAMTS1 $^{+/+}$ ADAMTS1 $^{-/-}$	MMTV-PyMT ADAMTS1 $^{+/+}$ ADAMTS1 $^{-/-}$	Swiss Nude (immunodeficient)
Assay Type	Allograft	Allograft	Spontaneous	Xenograft
Cell line Used	B16F1 mouse melanoma	Lewis Lung carcinoma	- -	MUM2B and MUM2BshATS1
Vasculature Signature	Tubulogenesis Assay positive	Tubulogenesis Assay negative	Tubulogenesis Assay negative	Tubulogenesis Assay positive

Table 4. Tumour models included in this thesis. A table summarising the most relevant information about the four tumour models. Information as the mouse strain, the cell line (if any), assay type and also the vasculature network phenotype is included.

RATIONALE AND MAIN AIMS

-

THESIS RATIONALE

During tumour development most of the cancer hallmarks are depicted. Many efforts are ongoing in order to disrupt tumour fate to increase the patient lifespan and wellbeing. Some decades now have passed since the introduction of the ECM as a cornerstone in tumour progression and metastasis. In fact, its study is still an expanding field and, although most components of ECM have already been described, their physiological roles in health and disease require still to be investigated.

In the context of tumour biology and the ECM, angiogenesis and vascularization in general are crucial events for tumour progression. The dynamics of the vascular basement membrane during new vessel sprouting have been under research for many years and its contribution in tumorigenesis has been highlighted. The tune of the vascular BM, and the vascular niche in general, depends on the effects of extracellular proteases. In this thesis we focus on the study of the protease ADAMTS1, which displays a particular dual role driving or arresting tumour growth and angiogenesis.

Our interest covers the evaluation of the ADAMTS1 substrates Nidogens (NID1 and NID2) and Versican, including their impact in the development of tumour vasculature and further tumour progression. Led by previous studies that show the relevance of these substrates in vascular-related niches, we wanted to unravel their functionality approaching the genetic alteration of ADAMTS1 itself and also of such substrates.

Furthermore, the use of ADAMTS1 null mice would allow to obtain a biological perspective during organogenesis but also during tumour progression.

THESIS MAIN AIMS

1. STUDY THE PERIVASCULAR NICHE OF DISTINCT TUMOUR MODELS WITH MODIFIED LEVELS OF ADAMTS1 IN THE STROMA AND/OR TUMOUR CELLS

    i. Characterize the vasculature in different tumour models considering *Adamts1* expression.

    ii. Study specific vBM components of the tumour perivascular area with regard to *Adamts1*.

2. EVALUATION OF THE CONSEQUENCES OF THE ALTERATION OF ADAMTS1 SUBSTRATES *IN-VIVO*

    i. Engineer B16F1 melanoma cell lines to overexpress *Nidogens*, and study the *in-vitro* phenotypes.

    ii. Study the *in-vivo* phenotypes and cell behaviour of *Nidogen*-overexpressing cell lines in WT and *Adamts1* null murine model.

    iii. Assess the status of the vBM and overall vasculature with regard to Nidogens overexpression.

3. ASSESSMENT OF THE IMPORTANCE OF THE PROTEASE ADAMTS1 IN THE MURINE KNOCKOUT MODEL IN HEALTH AND TUMOUR MODELS

    i. Characterize and compare the vasculature of various organs in healthy WT and *Adamts1* knockout mice.

    ii. Study the deposition and cleavage of Nidogens and VERSICAN in the vBM and stroma of various organs of WT and *Adamts1* knockout mice.

    iii. Study the relationship between *Adamts1* and the immune system, by the evaluation of spleen, bone marrow and distinct tumours (B16F1 and LLC), in WT and Adamts1 knockout mice.

RESULTS

1. ANALYSIS OF THE VASCULATURE IN DIFFERENT ADAMTS1-DEPENDENT TUMOUR MODELS

As part of our main aim, we study the role of ADAMTS1 as a protease and angiogenesis-related molecule in tumour progression in a series of *Adamts1*-dependent tumour models (described in Introduction, section 7). These tumours would display a distinct scenario where stromal and/or tumour ADAMTS1 is absent or reduced. With their respective controls, the breast cancer model includes a complete knockout of the protease, B16F1 and LLC models comprise a lack the *Adamts1* just in the stroma, and the uveal melanoma studies involved the downregulation of tumour *Adamts1*. This heterogeneity adds more complexity to the study in order to assess the possible roles of tumour and/or stromal ADAMTS1. We evaluated parameters that would allow the study of vascular impairments during tumour progression. A protein and gene expression analyses to unravel possible differences in the different tumour sets has been also included. More precisely we focused our attention in the status of the deposition of ADAMTS1 substrates in the perivascular area to understand if there is a contribution to the vascular network with consequences to the tumour fate.

1.1 CHARACTERIZATION OF THE TUMOUR VASCULATURE

An initial analysis of the macroscopic characteristics of the tumours was assessed (**Figure 15**). The first model, the mouse breast cancer model (MMTV-PyMT), was already described by our collaborators at the University of Adelaide, Australia (Ricciardelli et al., 2011). They observed a tumour size and volume reduction in the complete absence of *Adamts1*. The following models, B16F1 and LLC, showed distinct outputs.
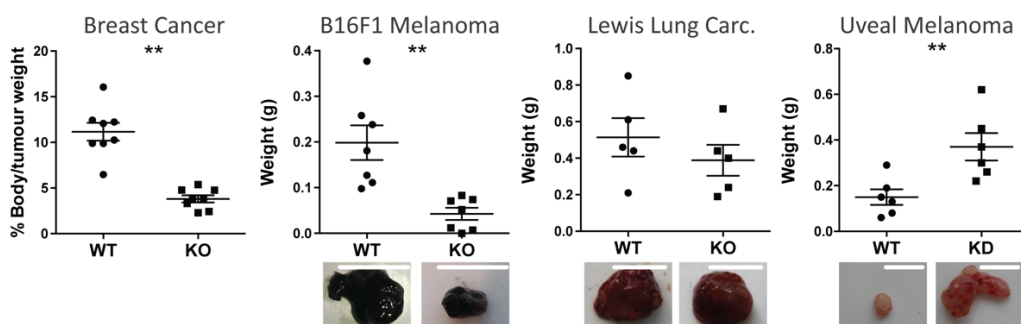
Figure 15. Morphological characterisation of the different *Adamts1* dependent tumour models. The breast cancer model represents the percentage of the body/tumour weight; the data has been obtained from (Ricciardelli et al., 2011). The rest of the models are represented for its tumour weight (grams). Representative WT and KO *Adamts1* or Knockdown (KD) tumour pictures are included (White bars = 1 cm)

While B16F1 displayed a relevant reduction of tumour size and volume in *Adamts1* KO tumours, LLC model was not affected. Finally, the inhibition of tumour *Adamts1* in the uveal melanoma cell line provoked an opposite effect, increasing tumour size, in line with previous work by our research group (Martino-Echarri et al., 2013). In general, these highlight remark again ADAMTS1 dual role during tumour progression (**Figure 15**).

To evaluate the vasculature within these tumours, we performed an immunoanalysis of CD31$^+$ vessels on tumour sections. Relevant parameters, such as total number of vessels per area (vascular density in figures) and vessel perimeter were assessed according to materials and methodology section (**Figure 16**).
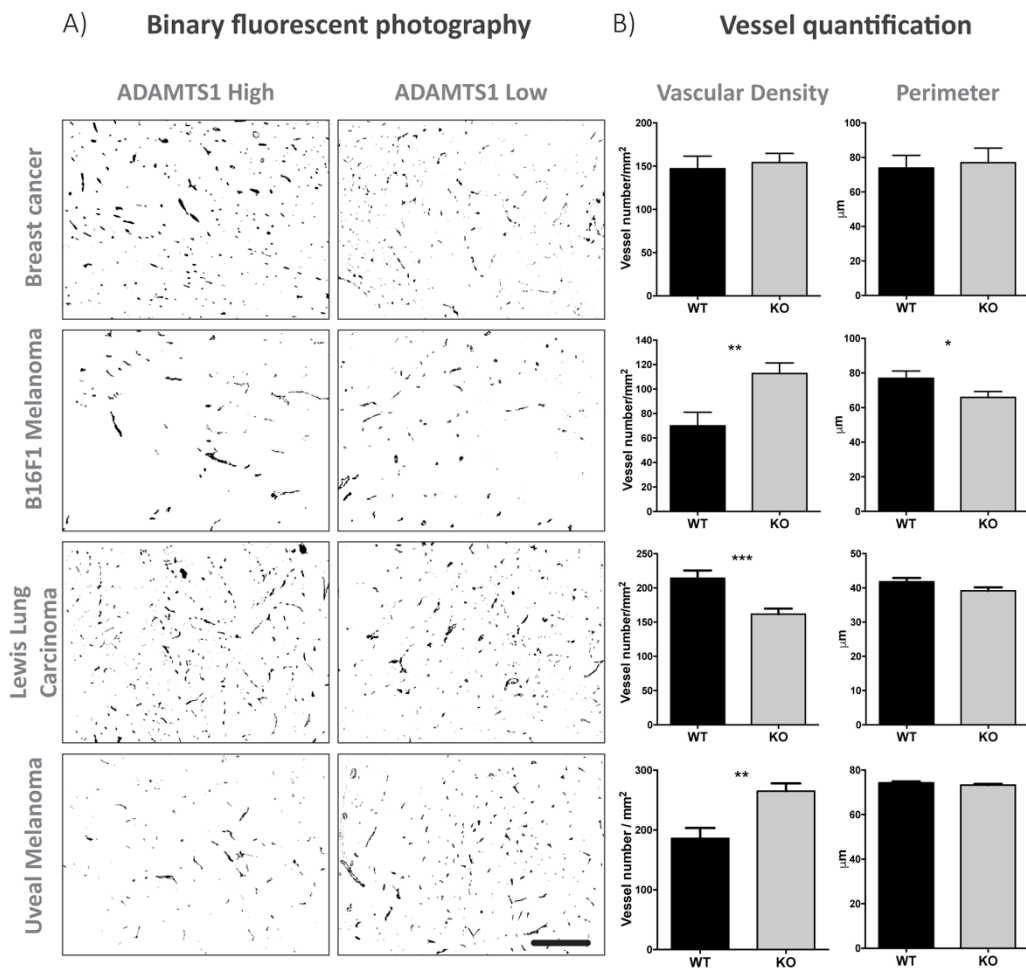
Figure 16. Analysis of the tumour vasculature by immunofluorescence and vessel quantification. Tissue sections were assessed with α-CD31 and a secondary antibody AF488 to visualize the vasculature. On the left, there are representative images (10x) captured with an epi-fluorescence microscope and converted to a binary image for proper analysis, as detailed in materials and methodology section 10 (black bar = 200

μm). Graphs on the right represent the quantification of vascular density. WT indicates Wild type and KO, *Adamts1* KO tumours (vessels per mm^2) and vessel perimeter (μm) (n ≥ 8 tumour samples).

The breast cancer model did not show a differential vascular patterning within the tumours. Regardless, vasculature of the B16F1 and LLC models were differently altered in relationship to stromal *Adamts1*. B16F1 tumours in *Adamts1* KO showed an increased vessel density accompanied by a perimeter size reduction, whereas LLC tumours displayed a decreased vascular density with no perimeter alterations, always comparing with their respective WT mates. Finally, the uveal melanoma model showed a higher vessel density with downregulated tumour *Adamts1*, in this case matching the differences in tumour growth (**Figure 16**).

From these results, we can conclude that the lack of stromal and/or tumour *Adamts1* infers differently in the development of the vasculature and tumour progression in general. At this point, many mechanisms could be attributed to the variability in these changes but we also aimed to continue further research into this interesting phenomena and whether alternative mechanisms to angiogenesis that may be contributing to the interpretation of these results.

1.2 STUDYING ALTERNATIVE MECHANISMS OF ANGIOGENESIS

Here we evaluated the possible influence of vasculogenic mimicry (VM) phenomena during tumour progression and vascular changes associated to ADAMTS1 expression. Indeed, these further studies were just performed in the B6F1 and LLC models given their higher availability.

Although the current bibliography indicates that the most appropriate methodology to detect vasculogenic mimicry events is PAS staining together with localization of endothelial markers CD31 or VE-CAD, this characterization still does not distinguish from non-pathological vessels and has provoked multiple discrepancies (Maniotis et al., 1999). In an attempt to improve the study of VM, we developed tumour-bearing mice with GFP-tagged tumour cells to discriminate from host cells. Our first goal was to find, by flow cytometry, B16F1 tumour-GFP$^+$ cells that also co-expressed endothelial markers, such as CD31. Interestingly, we found that the endothelium represented approximately the 2-3% of total number of cells in the tumour (**Figure 17**). From the total of endothelial cells, approximately 60-70% express also GFP signal. Overall, the analysis of the tumour population revealed an approximate 0,5-1,5% of GFP$^+$/CD31$^+$, representing VM cases, a little bit higher in tumours from *Adamt1* KO mice (**Figure 17B**).

A)

B)

%	WT		Adamts1 KO	
	Total cells	Tumour cells	Total cells	Tumour cells
Total cells	100	87	100	85,6
Tumour cells	87	100	85,6	100
Endothelial cells	2,7	65	1,9	67,5
VM	0,8	1,35	1,3	2,75

C)
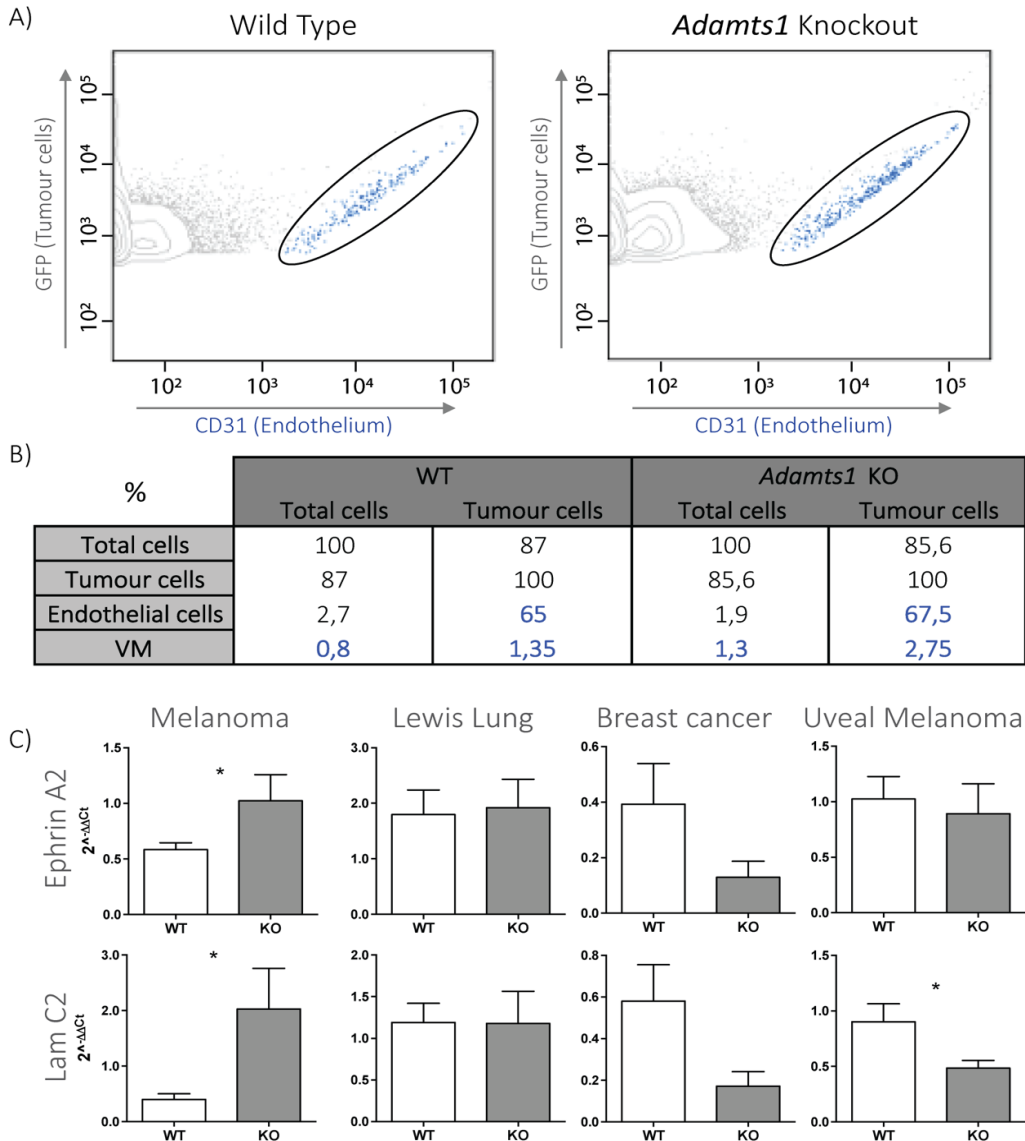
Figure 17. Characterization of the vasculogenic mimicry events by flow cytometry and qPCR. A) Flow cytometry of B16F1-GFP tumours in WT and *Adamts1* KO mice. Antibody α-CD31-PE (representing endothelium) was assessed in the samples (n= 2 WT and 2 KO). The gated population corresponds to CD31^{+} and GFP^{+} signal. B) Table presenting percentages of tumour (GFP^{+}), endothelial (CD31^{+}), and VM (GFP^{+}/CD31^{+}) events from flow cytometry analyses, this last group highlighted in blue. C) Graphs representing quantitative PCR analyses ($2^{-\Delta\Delta Ct}$ value) for the genes *EphrinA2* and *LamC2*. Mouse primers were used for the B16F1, LLC and breast cancer models. Human primers were used for the uveal melanoma model. t-student test performed and SEM are represented, *p value < 0,05, n = 2 tumour samples per group.

In addition, we evaluated gene expression of endothelial-related molecules such as *EphA2* and *LamC2*, as the literature showed its relevance in the identification of VM cases (Dunleavey et al., 2014; Lai et al., 2012). The nature of these studies made possible

to assess all the tumour sets comparing WT and *Adamts1* KO/downregulated. Importantly, while we used mouse specific gene primers for the B16F1, LLC and breast cancer models, in the case of our uveal melanoma model, we used human specific gene primers to assess just the tumour contribution. Interestingly, only in the B16F1 melanoma model, both genes are upregulated in the *Adamts1* null tumours which agrees with the slight increase found in the flow cytometry analysis (**Figure 17B-C**).
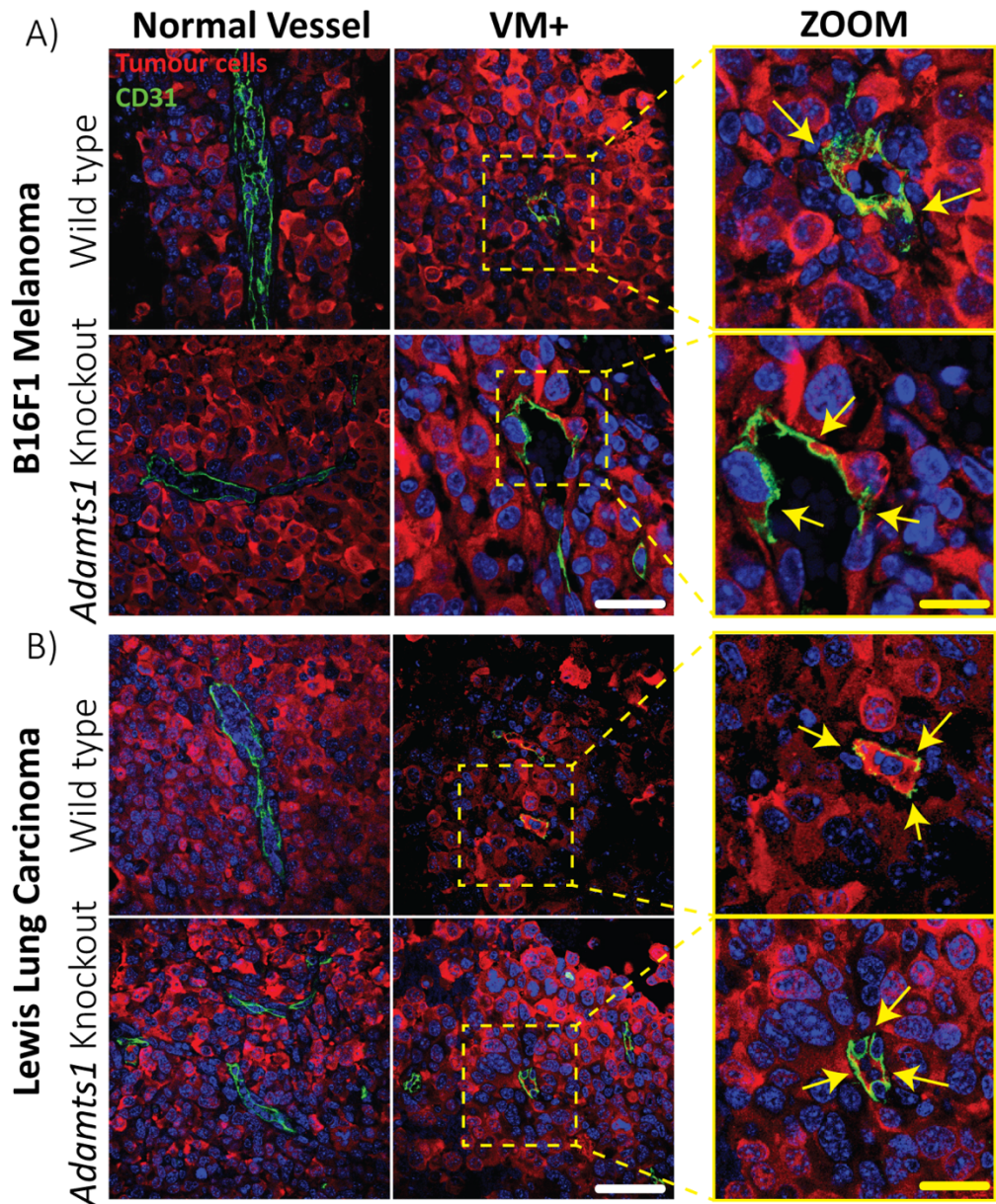
Figure 18. Immunofluorescence analysis of vasculogenic mimicry in B16F1 and LLC tumours. Sections from B16F1-GFP (A) and LLC-GFP (B) tumours, from WT and *Adamts* KO mice, were assessed with α-GFP (red)

and α-CD31 (green). Left panels show representative non-vasculogenic mimicry vessel. Middle panels show positive cases, and right panels are magnifications (63x). VM events are pointed with yellow arrows, identified by the green signal coexisting with the tumour red signal. White bars scale = 20 µm, yellow bars scale = 10 µm.

Finally, we performed immunofluorescence of B16F1 and LLC tumours in search of colocalisation of markers of tumour cells and endothelium, thus reinforcing the results found by flow cytometry.

Indeed, this technique could not be considered quantitative as flow cytometry, but it provides a relevant qualitative input. We successfully observed positive vasculogenic mimicry events in both models. As showed in our immunofluorescence staining (**Figure 17**), we detect tumour cells (in red) and CD31+ cells (in green), representing endothelial or endothelial-like cells. The overlapping of both positive signals, in an endothelial standard disposition, provides a new insight confirming the VM phenomenon. It is necessary to mention that we did not identify totally independent VM$^+$ cases forming tumour vessels; instead they were located as a mosaic with normal endothelium, closer to reported transdifferentiating tumour cells (Hess et al., 2003) (**Figure 18**). In general, the identification of these events was easier in our B16F1 model than in the LLC, however no differences between WT or *Adamts1* KO samples could be assessed with this methodology.

All these results suggest that *Adamts1* expression in tumour cells is indeed relevant for the VM phenomena. At least in the B16F1 melanoma model, in which the expression of *Adamts1* is very relevant and which vascular phenotype is clearly altered, the *Adamts1* KO tumours display higher amount of VM events.

1.3 GENE EXPRESSION ANALYSIS OF ADAMTS1, SUBSTRATES AND OTHER RELATED MOLECULES

Given our results about tumour progression and vascular characterization, we wanted to assess a broad gene expression panel, including *Adamts1* itself, together with some of its substrates, and additional molecules related to vasculature.

Prior to the analysis of tumours, we wanted to determine the basal expression of *Adamts1* and substrates in all the tumour cells associated to each different model. Hence we have looked at the Ct value of the qPCR outcome (more details in materials and methodology section 12). For the breast cancer model, we tested a tumour-derived

primary culture from WT mice. We also used B16F1 and LLC parental cell lines, and last, for our uveal melanoma model, we included parental and *Adamts1*-downregulated MUM2B. In general, *Adamts1* is highly expressed in all parental or control cell lines. *Nidogen 1* levels are high in all the cells excepting B16F1. The expression of *Nidogen 2* only appears to be high in the breast cancer derived-cell line. Last, *Versican* is highly expressed in LLC and breast cancer with a moderate expression in B16F1 and MUM2B cells (**Figure 19**).
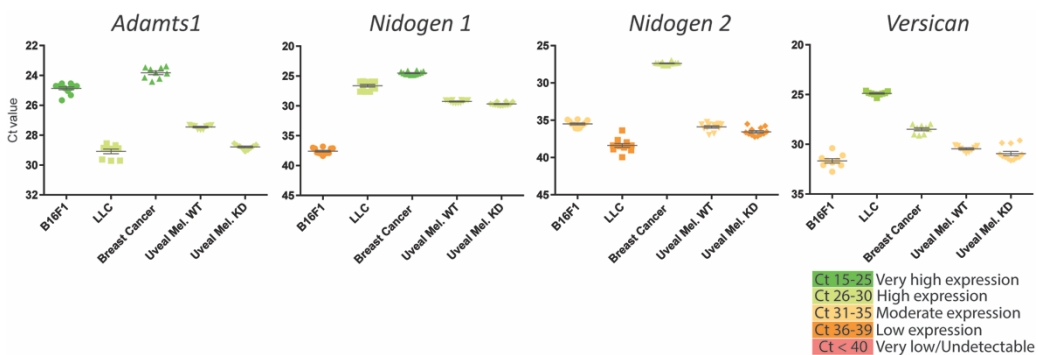
Figure 19. Gene expression analysis of the original/derivate cell lines of the different tumour models. Graph represents a quantitative PCR analysis showing Ct values (more details in materials and methodology section 12). For the breast cancer model (spontaneous) the primary cells were isolated from a WT tumour. The genes assessed were *Adamts1* and its substrates *Nidogen 1*, *Nidogen 2* and *Versican*. A colour legend indicates the level of expression by the Ct value. Error bars represent the SEM, n = 6 samples per group.

The next step included the analysis of our tumour samples. We characterised and categorised the genes under study in a series of groups: i) *Adamts1* and its inhibitor, *Timp3*; ii) Substrates such as *Nidogens* and *Versican;* and iii) endothelial-related genes, such as CD31 and Ng2, representing both the endothelium and vascular-supporting cells. As already introduced, for the uveal melanoma model, given its human origin in a mouse environment, our qPCR included the analysis of both species with specific primers.

Adamts1 expression was logically inexistent in the *Adamts1* KO breast cancer model, and very low levels were found in LLC-derived tumours from *Adamts1* KO, reminiscent of the endogenous expression in the cell line. Interestingly, B16F1-derived tumours presented an upregulation in *Adamts1* KO mice, probably due to the increased hypoxic levels of these tumours, and directly related to the observed vasculature defects (Fernández-Rodríguez et al., 2016). No significant changes were observed in the uveal melanoma model. Interestingly, the expression of its inhibitor, *Timp3,* was found to be downregulated for the models were stromal *Adamts1* is absent, with no significant changes in the uveal melanoma model (**Figure 20A**).
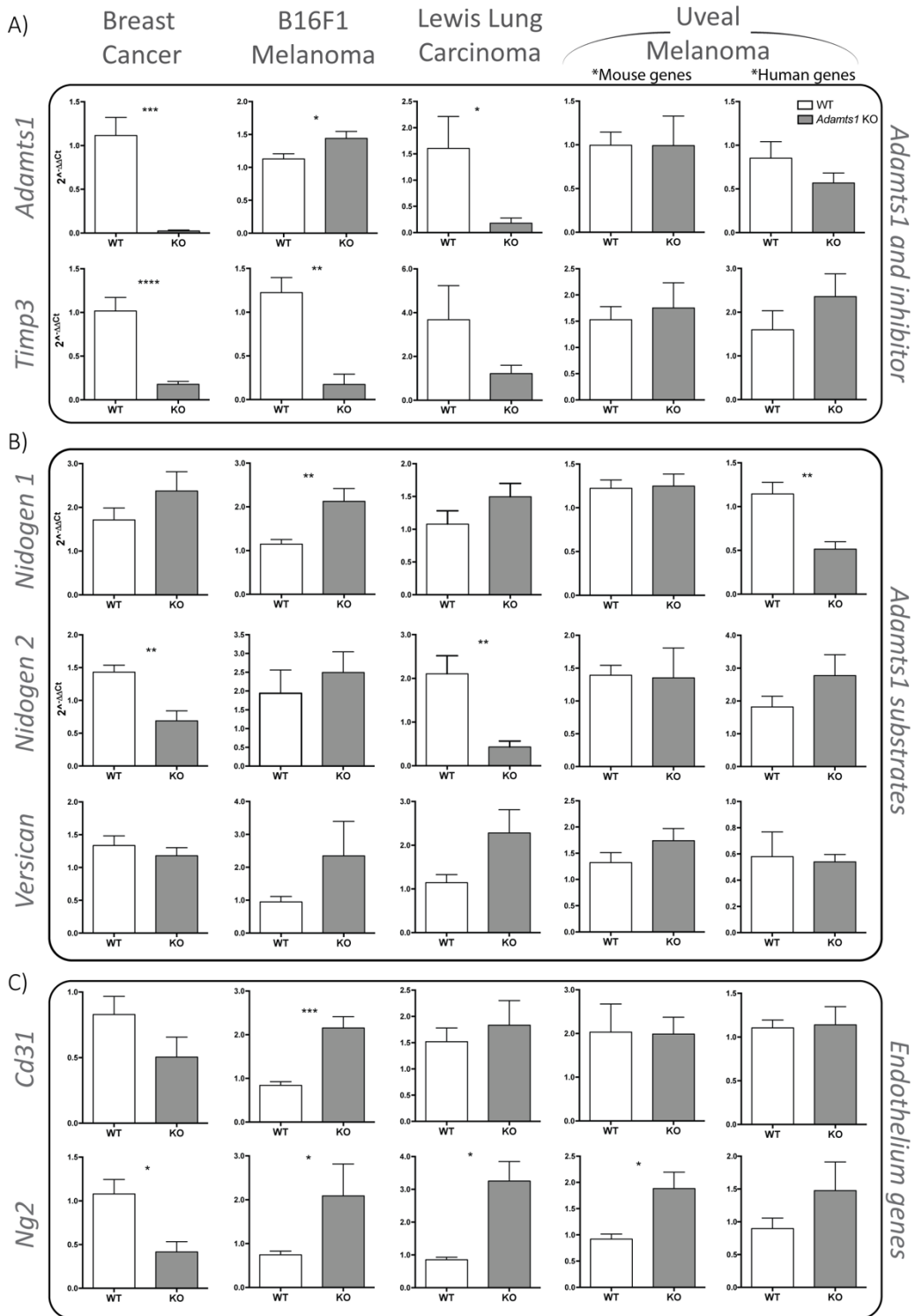
Figure 20. Gene expression analysis of the different WT and *Adamts1* KO tumour models. A quantitative PCR

analysis for: A) *Adamts1* and its inhibitor *Timp3*, B) *Adamts1* substrates as *Nidogen 1*, *Nidogen 2* and *Versican*, C) Endothelium related genes as *Cd31* and *Ng2*. Mouse primers have been used for all the samples. Additionally, human primers were also used for the uveal melanoma model. The represented data show the $2^{-\Delta\Delta Ct}$ value. t-student test performed and SEM are represented, n = 6 tumour samples. (*p value < 0,05, **p value < 0,01, ***p value < 0,001, ****p value < 0,0001)

At this point we presented the results of ADAMTS1 substrates, that should be also considered for our protein studies showed later. *Nidogen 1* is significantly upregulated in B16F1 tumours of *Adamts1* KO mice, correlating with tumour and vasculature impairments described above. On the contrary, *Nidogen 1* is downregulated in the uveal melanoma model, recalling again the previously observed alterations. For *Nidogen 2*, we observed a significant downregulation in the breast cancer and LLC models. Finally, *Versican* expression was not significantly altered in any of the models (**Figure 20B**).

Our final set included endothelial-related molecules: *Cd31* and *Ng2*. *Cd31* analyses showed a significant upregulation just in *Adamts1* KO B16F1 tumours, in agreement with the already described increase in vascular density (Fernández-Rodríguez et al., 2016). *Ng2* was selected given its specificity to pericytes, so to approach the maturation of tumour vasculature. In this case, all tumour models showed alterations between tumours in WT and *Adamts1* KO mice, downregulated in the breast cancer model, and upregulated in the rest. These specific findings require a deeper research to validate their significance, although it supports the action of ADAMTS1 affecting vasculature maturation mechanisms (**Figure 20C**).

In general, our gene expression data suggested the need of additional characterisations. At this point we decided to investigate Nidogens and Versican according to their contribution in the vBM.

1.4 CHARACTERISATION OF NIDOGENS AND VERSICAN DEPOSITION IN TUMOUR PERIVASCULAR AREAS

As introduced, the composition of the vBM is well known and it varies among different tissues and organs. More precisely, the vBM in tumour vasculature has been studied but Nidogens have not been specially considered. Importantly, previous sections of these results already showed the study of some vascular parameters and genes of interest for the final interpretation of our results.

Tumour sections of every group were subjected to immunoanalysis. In order to identify tumour vessels, we used CD31 together with our main candidates; NID1, NID2 or VCAN.

In all cases, confocal microscopy was used to identify the different molecules, assigning specific fluorescent signal parameters for every marker and then analysing and comparing intensity between samples (more details in materials and methodology section 9).

For Nidogens, our first and general observation was the increased deposition of NID1 (red signal) in all tumour models with lower ADAMTS1 (**Figure 21**).
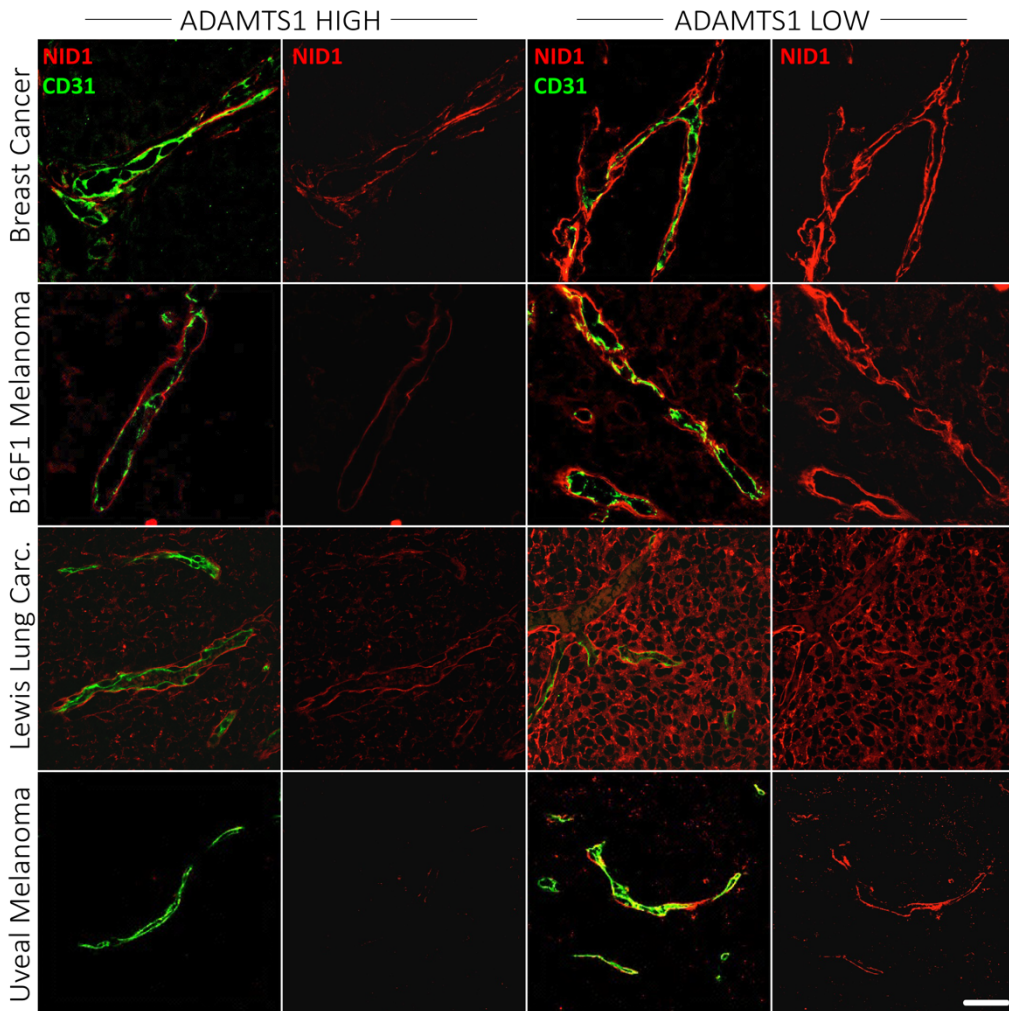
Figure 21. Immunofluorescence evaluation of NID1 in the tumour perivascular niche. Tumour sections from the different *Adamts1* dependent models (ADAMTS1 High or low, include the WT and *Adamts1* KO models and the KD for the uveal melanoma). α-NID1 (red) and α-CD31 (green) were used in all the samples. 63X magnification pictures were obtained by confocal imaging. No colocalisation is expected, NID1 (red) lay in the outer layer of CD31 (green). White bar = 20 μm.

NID1 deposition was commonly identified around the vasculature, recognized with CD31 (green signal). Significantly, LLC model was unique displaying a strong and widespread NID1 signal throughout the tumour stroma (**Figure 21**). For NID2, although our results were not as clear due to the lower abundance of the protein, we also detected an increased deposition in *Adamts1* KO mice, more evident in the LLC and uveal melanoma models (**Figure 22**).
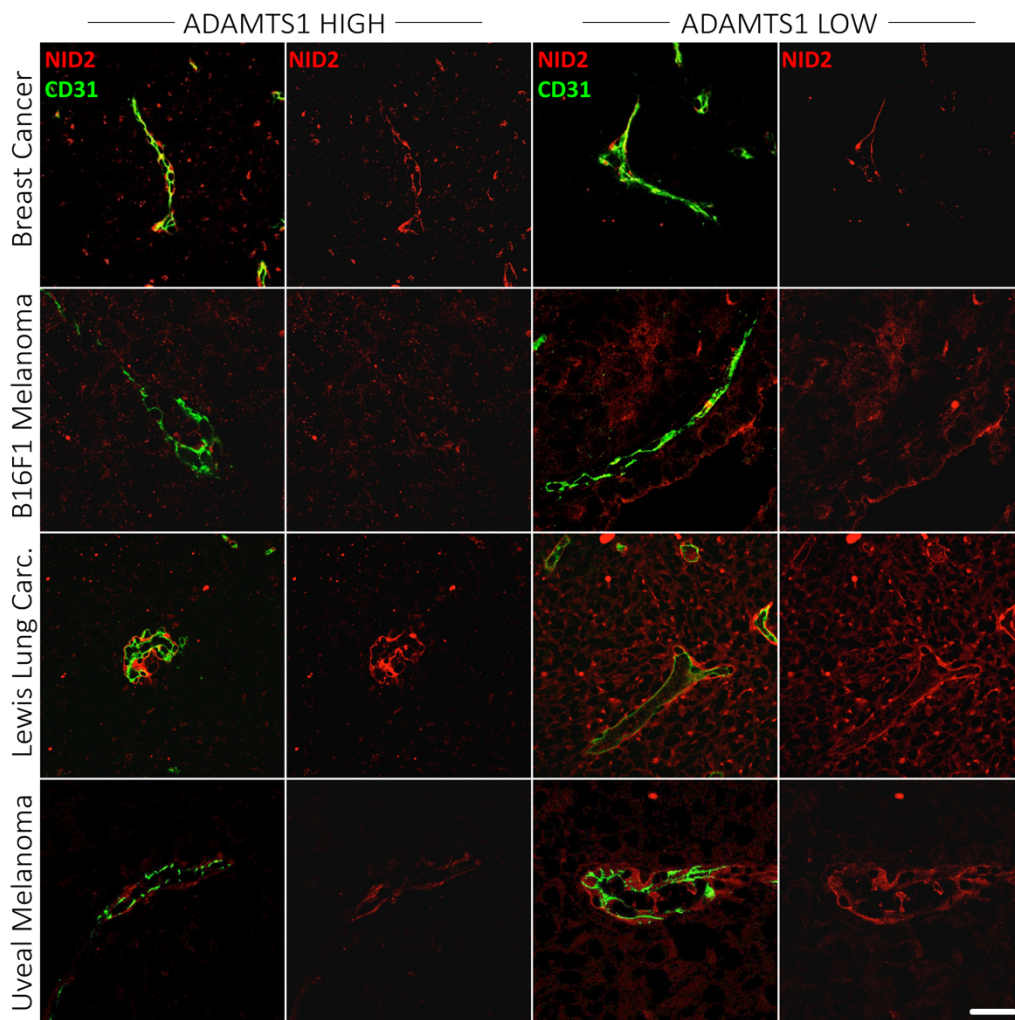
Figure 22. Immunofluorescence evaluation of NID2 in the tumour perivascular niche. Tumour sections from the different *Adamts1* dependent models (ADAMTS1 High or low, include the WT and *Adamts1* KO models and the KD for the uveal melanoma). α-NID2 (red) and α-CD31 (green) were used in all the samples. 63X magnification pictures were obtained by confocal imaging. No colocalisation is expected, NID2 (red) lay in the outer layer of CD31 (green). White bar = 20 μm.

Is of note to mention that NID2 general deposition in tissues, including tumours, is lower than NID1, so its deposition might not be as relevant (**Figure 22**). Nevertheless, this is

tumour-model-dependent as the literature shows how both molecules can be differently expressed and deposited among tissues and tumours (Oivula et al., 1999; Paulsson, 1992).

The differences found in the deposition of both molecules in the vBM, in an *Adamts1*-dependent manner, strength the importance of checking their integrity by western blot analyses. Accordingly, we evaluated the status of NID1 in the different tumour samples. With the exception of LLC-derived tumours, the increased deposition found by immunofluorescence with downregulated *Adamts1*, was positively correlated by a protein increase in the western blot. Nevertheless, NID1 cleavage occurred in all models, independently of the presence or lack of *Adamts1* in tumour and/or stromal cells, confirming the existence of other proteases that may act in compensation of the lack of ADAMTS1 (**Figure 23A-B**).
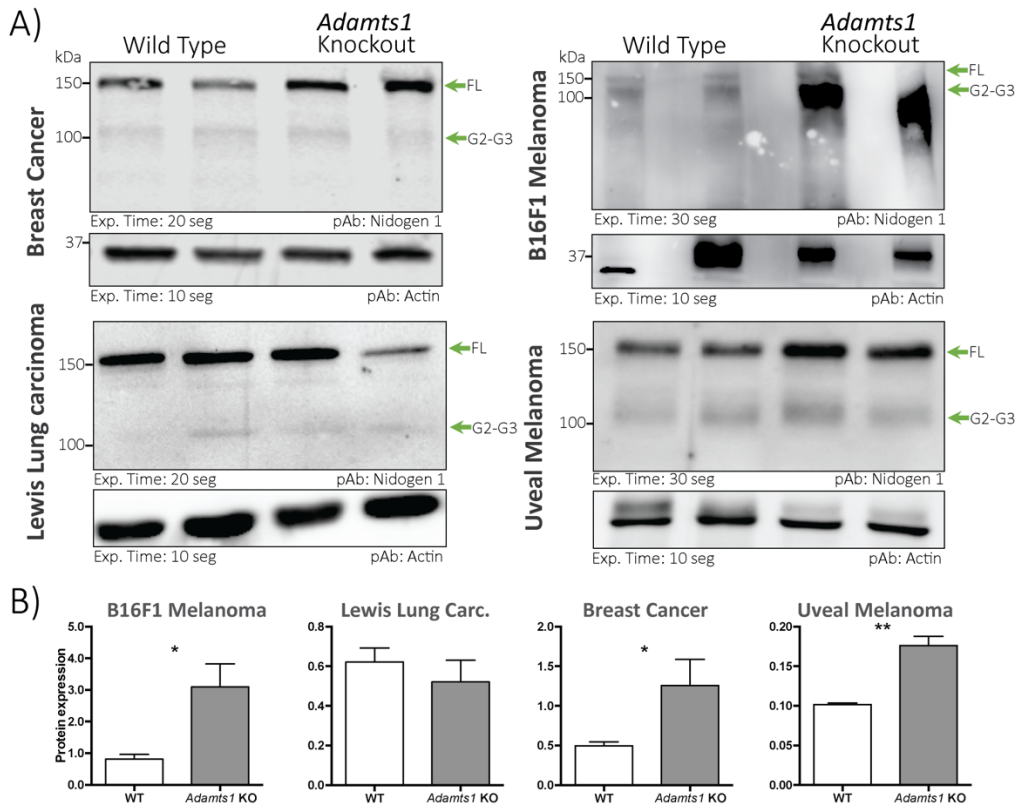
Figure 23. Analysis of NID1 by Western blot and protein quantification of different tumour models. A) Western blot of tumour protein lysate (50 µg of protein per lane). Below every image, the antibody (pAb – polyclonal or mAb – monoclonal) used is located in the right corner and the membrane exposure time in the left corner. For NID1, the full length (FL) and cleavage (G2-G3) fragments are indicated (green arrows). Protein lanes are indicated by its molecular weight (kDa). B) Protein densitometry measurements were

taken using Image J. The total protein lanes signals were normalised with Actin housekeeping signal. t-student test performed and SEM are represented, n < 4 samples/lanes. (*p value < 0,05, **p value < 0,01).

Next we studied Versican (VCAN). For this evaluation we used specific antibodies for the full length protein (identified as VCAN in general) and another one that recognizes the cleavage product of ADAMTSs, named Versikine (VKIN) (Nandadasa et al., 2014). In general, VCAN, although found in the perivascular area, its association with the vasculature is not as predominant as for Nidogens. Nevertheless, we used the endothelium as a guide to compare among the groups (**Figure 24-25**).
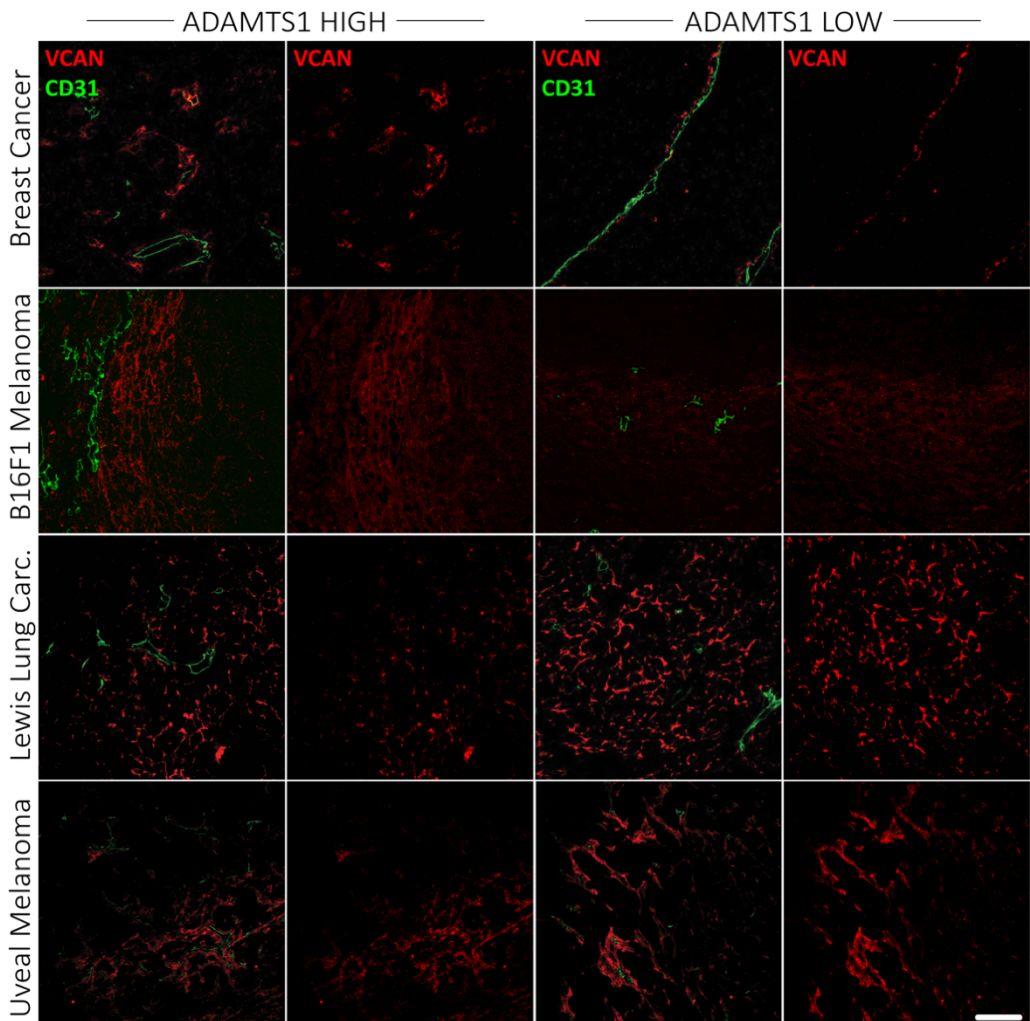
Figure 24. Immunofluorescence evaluation of VCAN in the tumour perivascular niche. Tumour sections from the different *Adamts1* dependent models (ADAMTS1 High or low, include the WT and *Adamts1* KO models and the KD for the uveal melanoma). α-VCAN (red) and α-CD31 (green) were used in all the samples. 63X magnification pictures were obtained by confocal imaging. No colocalisation is expected, VCAN (red) is found in the tumour stroma and CD31 (green) lays on the tumour vessel niche. White bar = 20 µm.

In the breast cancer and B16F1 models there is an accumulation of VCAN in the stroma WT tumours. Interestingly in the LLC and uveal melanoma models the reduction is found in the wild type tumours, no correlating with the ADAMTS1-dependency (**Figure 24**).

As a complementary information, we have also evaluated the presence of VKIN. In this case, its positive signal seemed to be affected by the presence of *Adamts1*, hence we found a decrease of VKIN in KO tumours of every model except the uveal melanoma. Importantly, in this last model the stromal ADAMTS1 has not been modified (**Figure 25**).
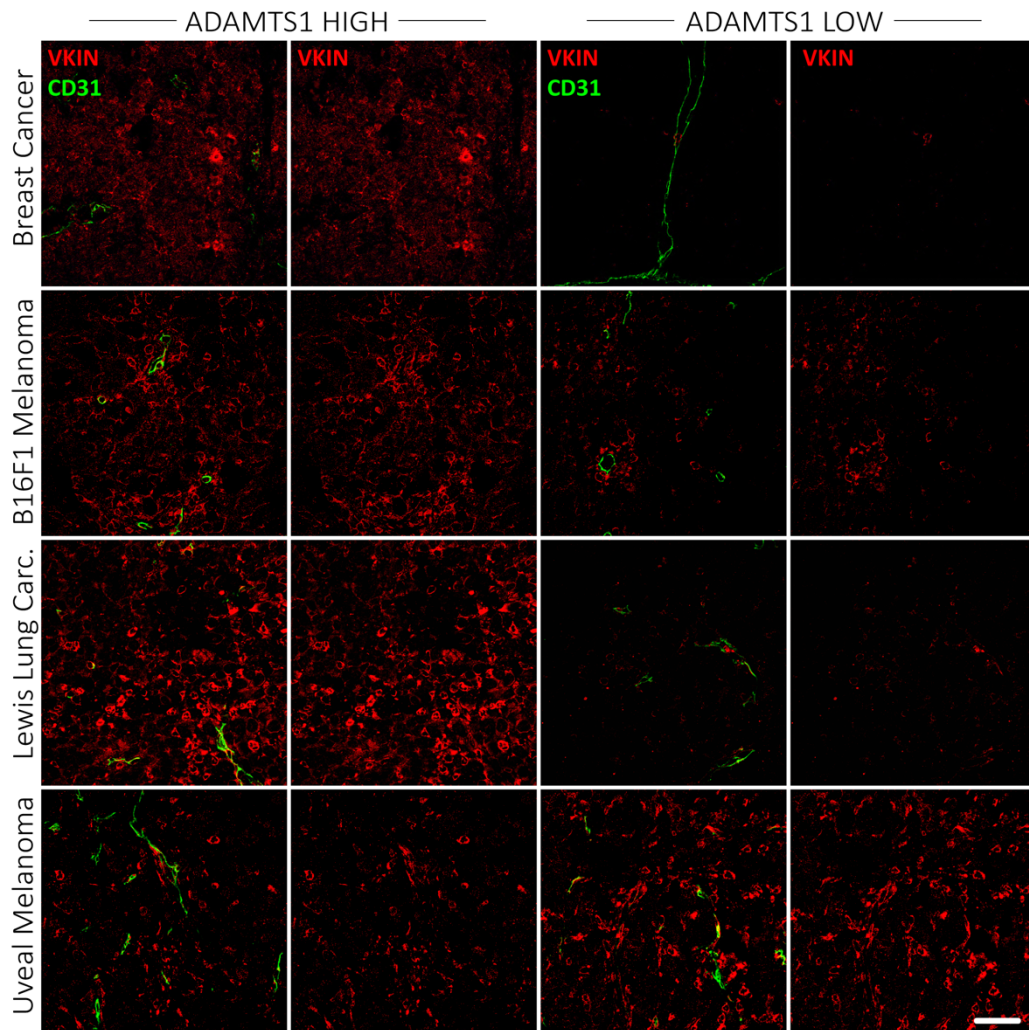
Figure 25. Immunofluorescence evaluation of VKIN in the tumour perivascular niche. Tumour sections from the different *Adamts1* dependent models (ADAMTS1 High or low, include the WT and *Adamts1* KO models and the KD for the uveal melanoma). α-VKIN (red) and α-CD31 (green) were used in all the samples. 63X magnification pictures were obtained by confocal imaging. No colocalisation is expected, VKIN (red) is found in the tumour stroma and CD31 (green) lays on the tumour vessel niche. White bar = 20 μm.

As a summary of the results of this section we can conclude that *Adamts1* expression regulates diversely the tumour progression and vascular patterning. Mainly our protein analyses revealed a different Nidogen, VCAN and VKIN deposition in the tumour perivascular area in an *Adamts1*-dependent manner. Indeed, our more consistent results are the increase of NID1 deposition in *Adamts1* KO tumours and the loss of VKIN deposition (except in the uveal melanoma model). These results led us to keep exploring the functional role of *Nidogens* in tumour biology, as well as the overall relevance of these and other substrates, such as VCAN.

.

2. EFFECTS OF NIDOGEN OVEREXPRESSION IN A B16F1 MELANOMA MODEL

The previous findings indicated a relevant NID1 alteration in the vBM of tumour in an ADAMTS1-dependent manner, so we were entailed to keep investigating this relationship. Indeed, we chose the B16F1 melanoma model, given our extensive experience with it and the interest of our previous data. Accordingly, we approached a gain-of-function of both *Nidogens* independently and the subsequent study of their tumour progression.

As reported before, our gene expression analyses showed a very low expression of both *Nidogens* in the B16F1 cell line (**Figure 19**). Now we compared this expression with two murine organs, lung and liver, and also with mouse lung endothelial cells (MLEC). While these results showed a higher *Adamts1* expression in B16F1, we confirmed the lowest levels of *Nidogens* (**Figure 26**).
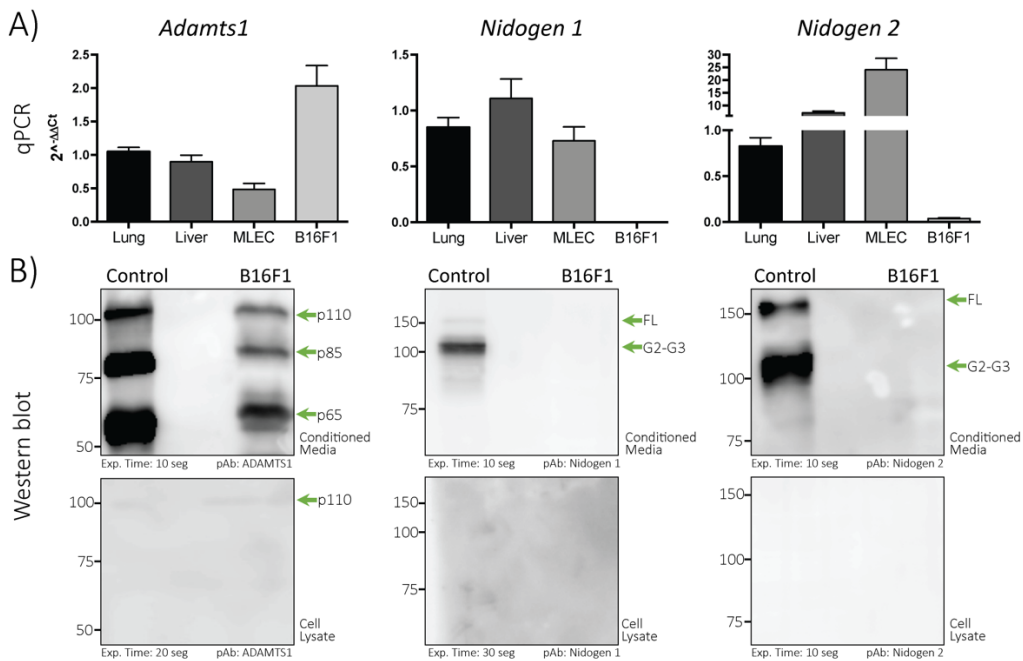
Figure 26. Gene and protein expression analyses of B16F1 cell line. A) A comparative quantitative PCR analysis of *Adamts1*, *Nidogen 1* and *Nidogen 2* genes in murine lung, liver, lung endothelial cells (MLEC) and B16F1 cell line. Represented data show the $2^{-\Delta\Delta Ct}$ value (n = 4 samples). B) Western blot analyses of conditioned media and cell lysates (30 µg) were assessed. Below every image, the antibody (pAb – polyclonal or mAb – monoclonal) used is located in the right corner and the membrane exposure time in the left corner. For ADAMTS1, the different isoforms are represented by its molecular weight (p110, p85 and p65). For NID1 and NID2, the full length (FL) and cleavage (G2-G3) fragments are indicated (green arrows). Molecular weight (kDa) reference is included in the left side of every blot.

Meanwhile, conditioned media (CM) and the cell lysate (CL) were evaluated by western blot using a positive control (HEK-293T overexpressing human *Adamts1*) (Rodriguez-Manzaneque et al., 2000). For ADAMTS1, we observe a similar expression pattern that our control (notice that the antibody recognises both human and mouse isoforms) with the three main isoforms. For NID1 and NID2 there is little to none expression neither in CM or CL (**Figure 26**). These biochemical analyses of the B16F1 cell line confirmed that this model would be suitable for a gain-of-function approach of both *Nidogens* independently. The absence of these molecules would allow us to study and compare cellular morphology and *in-vitro* behaviour and thus contribute to the knowledge of the biological functions of *Nidogens*.

2.1 ENGINEERING THE OVEREXPRESSION OF NIDOGENS IN B16F1 MOUSE MELANOMA CELLS

B16F1 parental cells were transduced with Zs-green backbone vectors including mouse *Nidogen 1* or *Nidogen 2* cDNAs (cloning strategy in materials and methodology section 4). We created stable cell lines and sorted by fluorescence in order to enrich the population in Nidogen-producing cells. We confirmed that *Nidogens* were overexpressed and that the expression of *Adamts1* was not significantly altered (**Figure 26**).
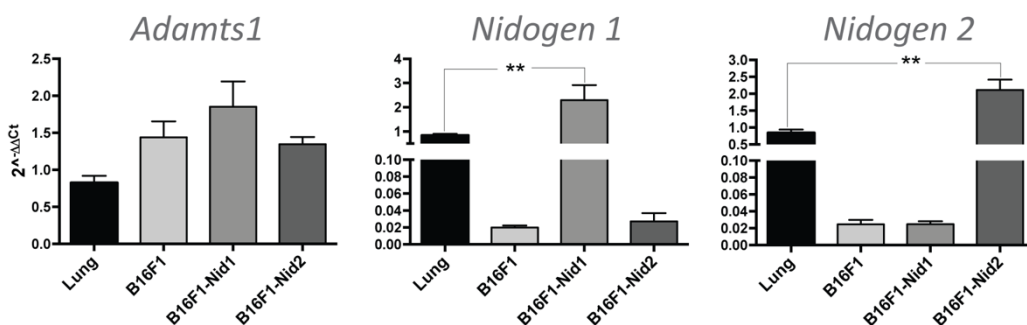
Figure 27. Gene expression analysis of B16F1 *Nidogen*-overexpressing cell lines. A comparative quantitative PCR analysis of the B16F1 cell line engineered to overexpress *Nidogens* with its B16F1 control and a C57BL/6 WT lung for *Adamts1*, *Nidogen 1* and *Nidogen 2* genes. The represented data show the $2^{-\Delta\Delta Ct}$ value. t-student test performed and SEM are represented, n = 4 samples. (*p value < 0,05, **p value < 0,01)

Protein was evaluated in the CM of the different cell lines showing a significant increase of both Nidogens in comparison with parental cells. We also confirmed that cleavage of both Nidogens is occurring in the CM of our engineered cells. Furthermore, ADAMTS1

levels were not altered in relation with the Nidogen overexpression (**Figure 28**). These results led us to follow studying the in-vitro and in-vivo characteristics of these cell lines.
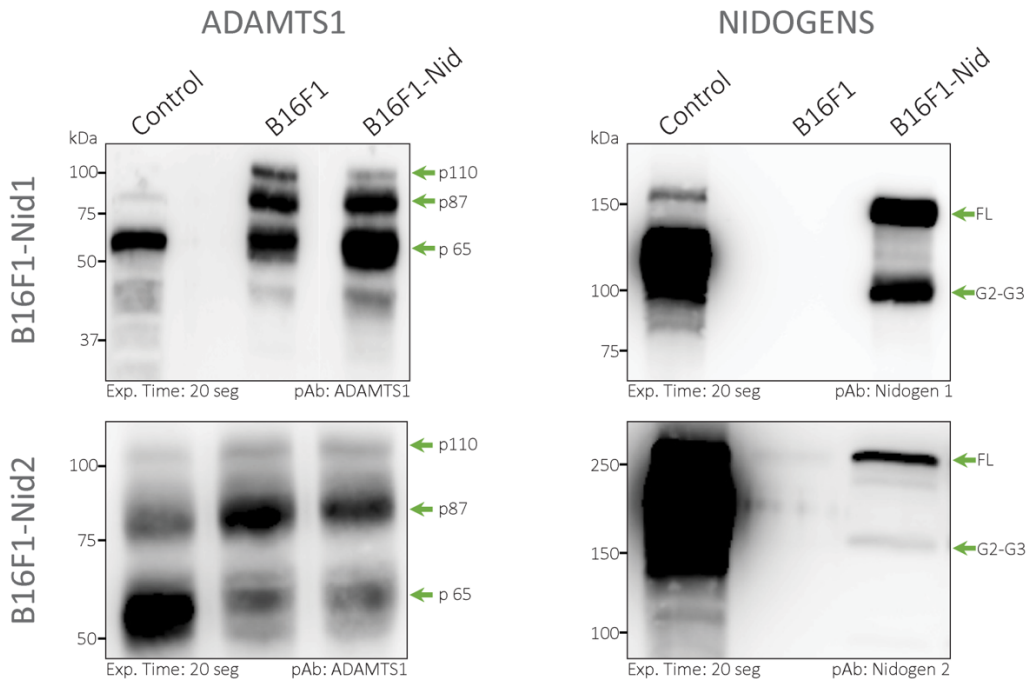
Figure 28. Protein expression analysis of the B16F1 *Nidogen*-overexpressing cell lines. Western blot of conditioned media was performed under reducing conditions. Below every image, the antibody (pAb – polyclonal or mAb – monoclonal) used is located in the right corner and the membrane exposure time in the left corner. For NID1 and NID2, the full length (FL) and fragments (G2-G3 and G1) are indicated (green arrows). Protein lanes are indicated by its molecular weight (kDa).

2.2 *IN-VITRO* CHARACTERIZATION OF NIDOGEN-OVEREXPRESSING CELLS

The engineered cell lines were studied regarding the *in-vitro* adhesion, proliferation and migration properties. First, adhesion was assessed on differently coated culture plates (described in materials and methodology section 3). Three coatings were used: Collagen type I, Fibronectin and Poly-L-Lysine. Collagen I is known to bind nidogens directly, and Fibronectin is a mediator for adhesion to Integrins via the RGD domain. Poly-L-lysine is a recognized agent for cell attachment due to the creation of positively charged sites on the surface available for cell binding. Adhesion is generally impaired for the NID1 overexpressing cell line since its ability to adhere to all coated and non-coated surfaces is equally reduced. In the case of NID2 overexpressing cell line we observed the opposite (**Figure 29**).

Proliferation and migration were assessed using a xCELLigence device, a bioimpendance-dependent platform (described in materials and methodology section 3). For both cell lines, both proliferation and migration capacities did not differ in comparison with parental cells (**Figure 29**).
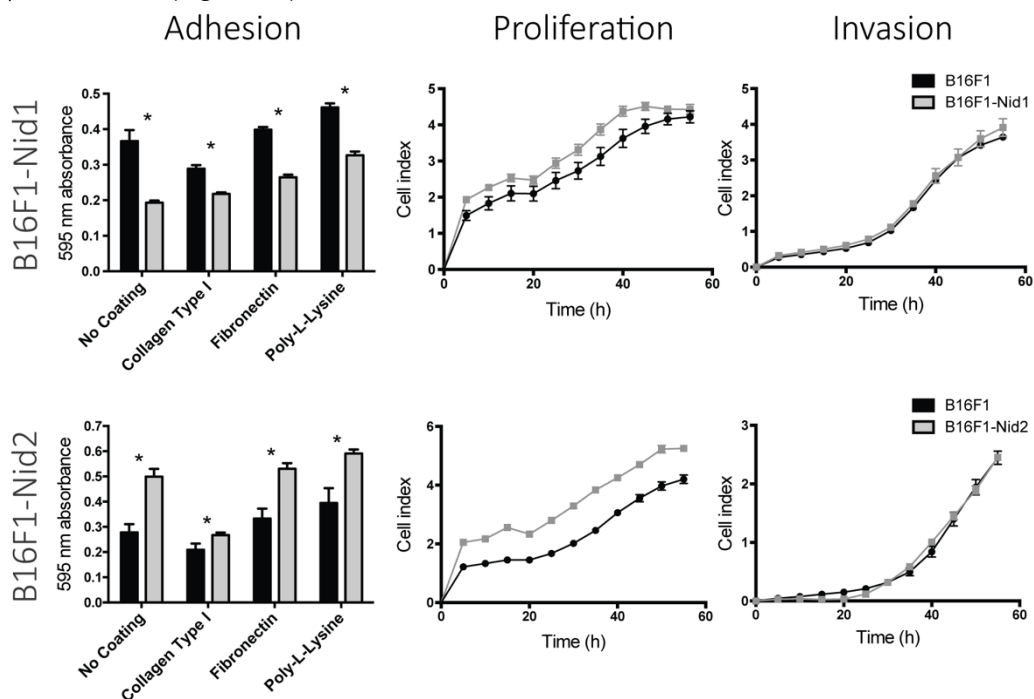
Figure 29. Adhesion, proliferation and invasion properties of B16F1 *Nidogen*-overexpressing cell lines. Adhesion experiments were performed in 96 plates coated with the indicated molecules. Graph represents the colorimetric Toulidin-blue-based quantification. Proliferation and invasion assays were performed with a total of $4 \cdot 10^4$ cells per well using the xCELLigence platform.

The changes observed in the adhesion of the *Nidogen* overexpressing cell lines are interesting and need to be further considered. These alterations can influence the tumour cell abilities in more complex scenarios as it is the *in-vivo* generation of tumours. Such findings are also interesting given the small differences of structure of both molecules.

2.3 ASSESSING THE CAPILLARY-LIKE PROPERTIES OF NIDOGEN-OVEREXPRESSING CELLS

According to the capillary-like behaviour properties of parental B16F1 cells in Matrigel, we approached this assay (further described in materials and methodology section 2) with our Nidogen-overexpressing cells (**Figure 30**).
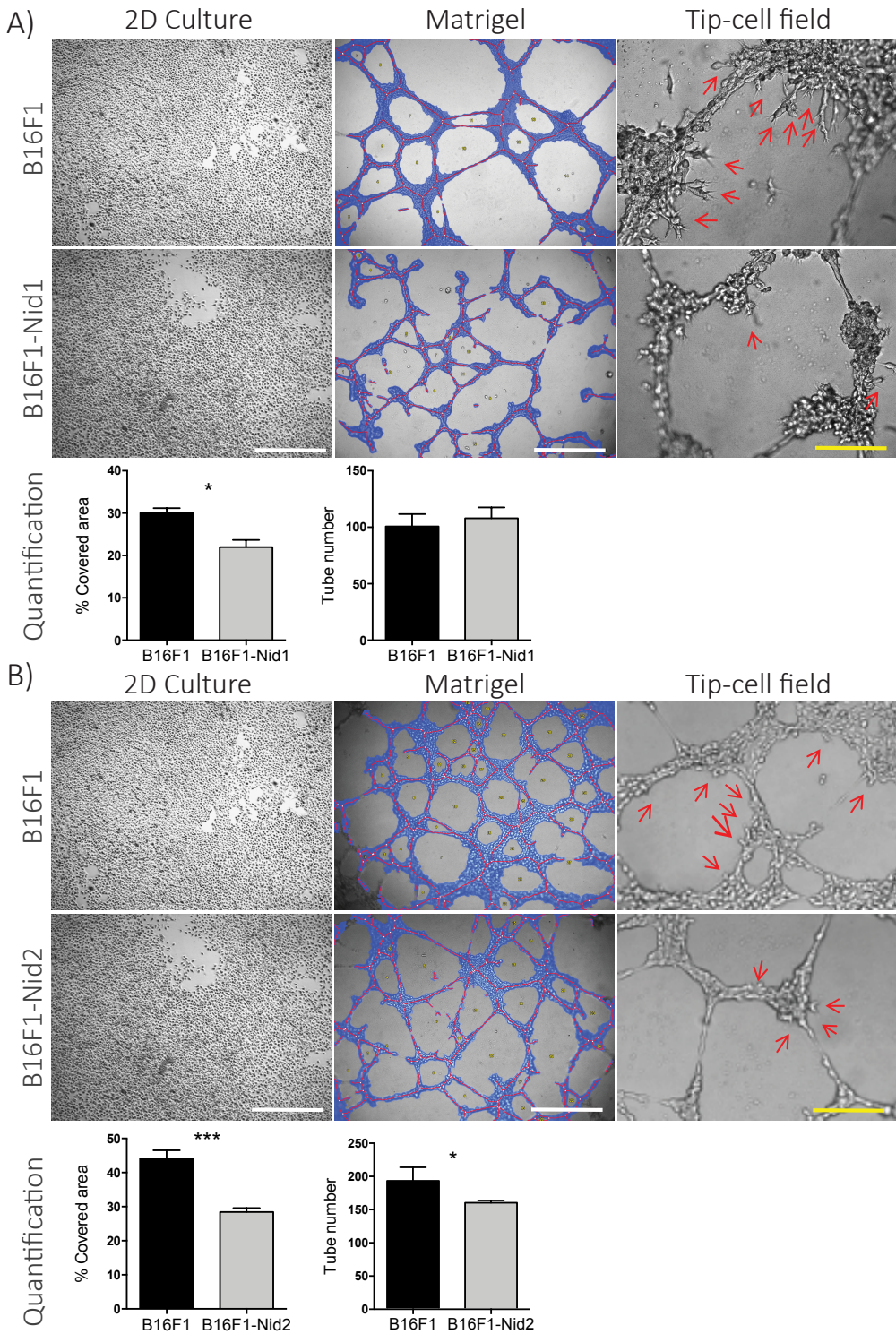
Figure 30. Culture of B16F1 *Nidogen* overexpressors in Matrigel to assess their capillary-like abilities. B16F1-Nid1 (A) and B16F1-Nid2 (B) representative 2D cultures are showed in comparison to the cells growing in Matrigel. 3·10^4 cells/well are grown in 96 well plates, with and without Matrigel. Showed images correspond

to a 24-hour time point, acquired with an inverted light microscope (10X magnification). Higher magnification images (40X) are also displayed to show the tip-cell abundance per field (red arrows). White bars scale = 200 µm, yellow bars scale = 60 µm. Graphs represent Tube Number and % Covered Area, according to the WIMASIS-based quantification. t-student test performed and SEM are represented, n = 12 images per group, 4 replicates per 3 different experiments. (*p value < 0,05, ***p value < 0,001)

We found that the capillary-like pattern of B16F1 parental cells was modified when *Nid1* or *Nid2* were overexpressed. The cellular network created by both overexpressors is less stable in general, the number of tubes and the percentage of the covered area is reduced in both cases. To obtain a non-bias quantitave measure, acquired images (10X magnification) were analysed by the Wimasis® software (explained in detail in the materials and methodology section 2).

The data show that the total covered area by the cell network is reduced in both models and also the numbers of tubes decreased in the NID2 model (**Figure 30**). Higher magnification images (40X magnification) allowed a deeper exploration of cell-cell connections with interesting findings. As showed, the number of tip endothelial-like cells decreased in both Nidogen-overexpressing cell lines, even more significantly for B16F1-Nid1 cells, suggesting that the plasticity of these cells is compromised probably due to the increased amounts of Nidogens (**Figure 30**). In general, it would be important to recall all these *in-vitro* observations in order to understand the results obtained in the *in-vivo* experiments.

2.4 ASSESSING TUMOUR PROGRESSION IN THE NIDOGEN-OVEREXPRESSING B16F1 MELANOMA MODEL

After the *in-vitro* studies, and according to our extensive expertise with the B16F1 syngeneic model (as reported in the results section 1.3), we proceeded to investigate the tumour progression properties of the engineered cell lines in our C57BL/6 WT and *Adamts1* null mice model. The following cells were included: B16F1 parental, B16F1-Nid1 and B16F1-Nid2, all of them implanted subcutaneously in WT and *Adamts1* KO animals. Our main aim is the comparison of the tumour growing capacities and final morphological characteristics of each overexpressing cell line in comparison with the parental control, including a deep characterisation of the tumour vasculature and its vBM. As detailed in materials and methodology section 6, tumour bearing mice were kept under observation until day 21 since the cell injection. At this end point, tumours were dissected and properly processed for various studies. First, a macroscopic characterisation was outlined.

Regarding the overexpression of *Nidogen 1,* in a wild type background, we observed a clear reduction of both tumour weight and volume in comparison with the B16F1 parental tumours. The results in the *Adamts1* KO mice confirmed a reduced tumour progression, already reported by ourselves (Fernández-Rodríguez et al., 2016), but not additive effects where associated to the *Nidogen 1* overexpression, at least at this macroscopic level (**Figure 31**).
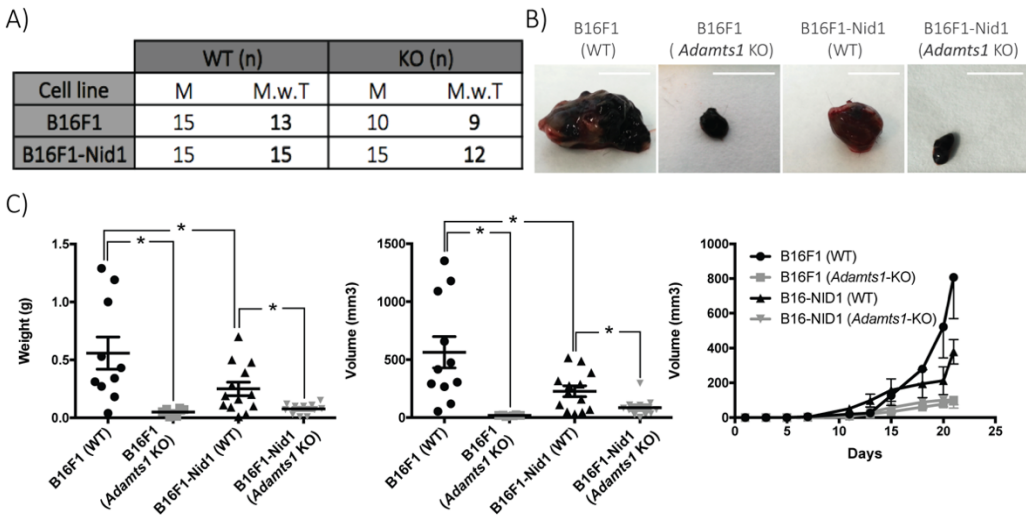
Figure 31. Tumour progression of B16F1-Nid1 tumours. A) Table including the number of mice used for tumour experiments (M) and the number of mice with tumour (M.w.T). B) Representative pictures of every tumour group, white bar scales = 1 cm. C) Graphs representing tumour weight (grams) and volume (mm^3) at end point, and progression of tumour volume during the experiment (measurements were taken according to materials and methodology section 7).
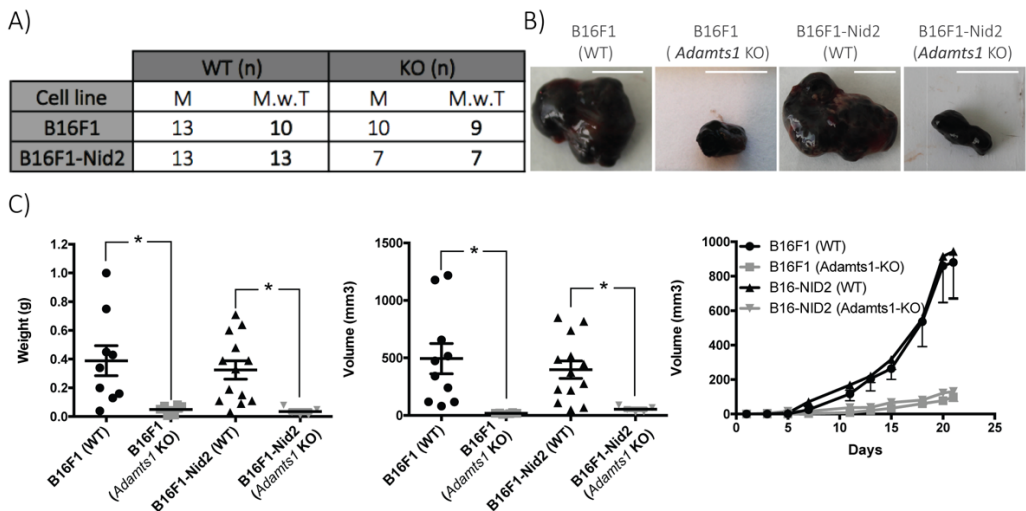
Figure 32. Tumour progression of B16F1-Nid2 tumours. A) Table including the number of mice used for tumour experiments (M) and the number of mice with tumour (M.w.T). B) Representative pictures of every

tumour group, white bar scales = 1 cm. C) Graphs representing tumour weight (grams) and volume (mm^3) at end point, and progression of tumour volume during the experiment (measurements were taken according to materials and methodology section 7).

However, the overexpression of *Nidogen 2* did not have a similar outcome. We did not find significant differences in tumour size and volume in comparison with the B16F1 parental group, neither in wild type or *Adamts1* KO backgrounds, apart from the well-known reduction in *Adamts1* KO mice (Fernández-Rodríguez et al., 2016) (**Figure 32**).

In general, the phenotypical tumour alterations given by the overexpression of *Nidogen 1* encouraged additional studies that could explain these differences. Although the overexpression of *Nidogen 2* did not supposed such changes, we also proceed with a deeper characterization that could provide relevant information.

2.5 EVALUATION OF TUMOUR VASCULATURE AND RELEVANT ECM COMPONENTS IN NIDOGEN-OVEREXPRESSING TUMOURS

As showed above, the over-expression of *Nidogens* in the B16F1 cell line implied behavioural and phenotypical changes with different impacts in tumour progression. In accordance to our own studies and the importance of Nidogens as components of the vBM we explored main vascular parameters including the deposition of relevant molecules in the tumour vascular niche, together with global gene and protein expression analyses. To clarify, we have compared independently tumours obtained from each overexpressor and the parental cell line, so the results will be displayed for each group.

First, a vasculature analysis was performed in the different tumour groups. The comparison of parental B16F1 and B16F1-Nid1 tumours did not reveal evident changes in WT animals. However, in the *Adamts1* KO background we observed that the overexpression of *Nidogen 1* showed an increased vessel density without altering the vessel perimeter (**Figure 33A**). We also analysed the NID1 deposition in the tumour perivascular area. We hypothesised that the increase of molecules in the vBM or ECM, as NID1 in our case, may induce changes in the vascular phenotype contributing to or impeding tumour progression. In accordance with the use of B16F1-Nid1 cells, we found a significant increase of NID1 surrounding the endothelium in comparison to B16F1 parental tumours (**Figure 33B**). However, no clear differences were found between the B16F1-Nid1 in WT and *Adamts1* KO, although we need to highlight our former results that *Adamts1* KO mice already showed an increased deposition of NID1 (**Figure 21**).
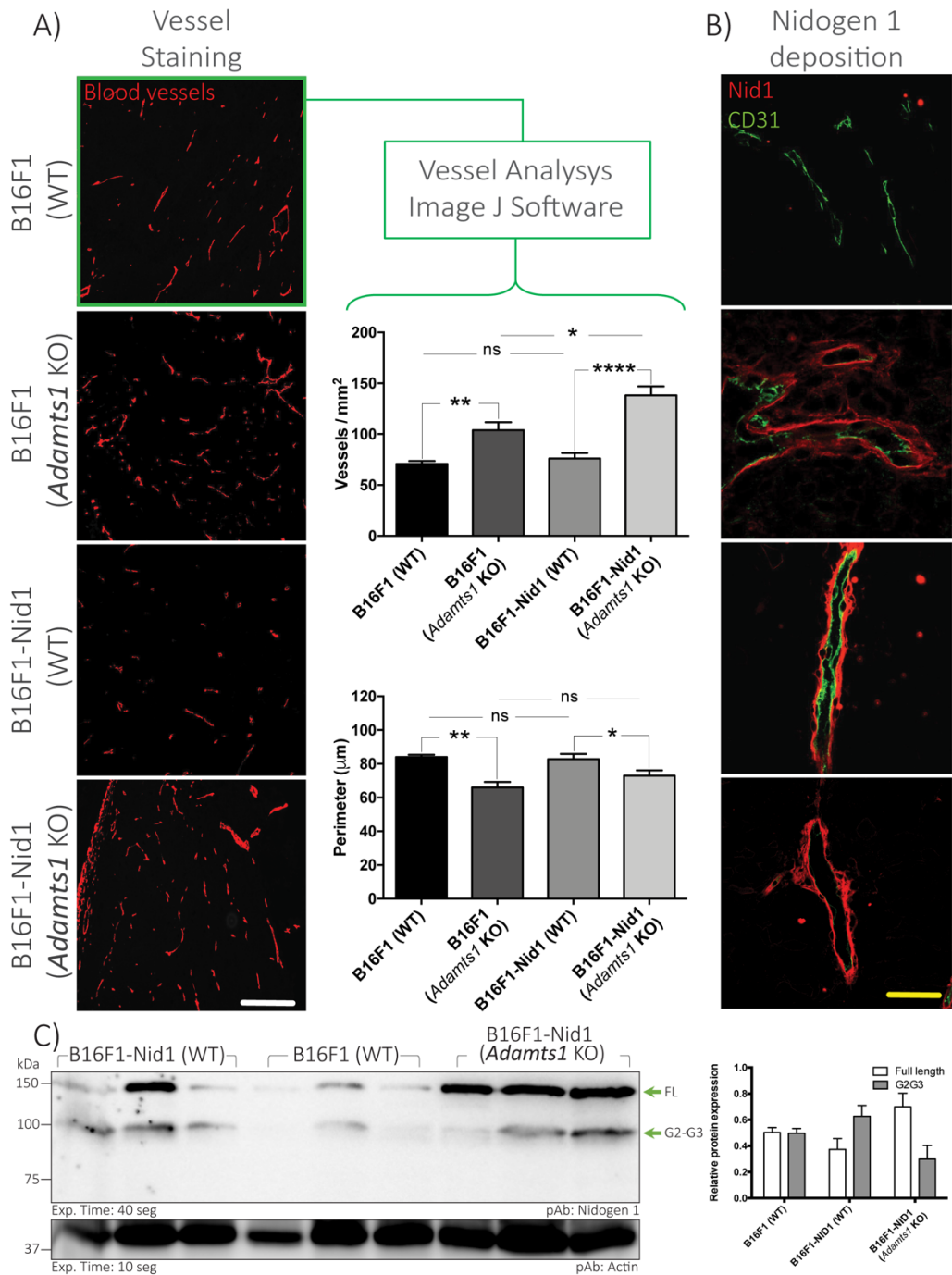
Figure 33. Tumour vasculature characterisation and NID1 deposition of the B16F1-Nid1 tumours. A) Representative images (10x magnification) of immunofluorescences with α-CD31 antibody (red signal). Graphs on the right show quantification of vessel density (vessels/mm^3) and perimeter (µm) as detailed in materials and methodology section 10 (n = 8 tumour samples). White bar = 200 µm. B) Representative images of immunofluorescences with α-CD31 (green) and α-NID1 (red) antibodies to assess NID1 deposition in the perivascular niche. Yellow bar = 20 µm. C) Western blot of tumour protein lysate (50 µg). Below every

image, the antibody used is located in the right corner and the membrane exposure time in the left corner. For NID1, the full length (FL) and fragments (G2-G3 and G1) are indicated (green arrows). Graph on the right show densitometry measurements of indicated isoforms signal intensity normalised with the housekeeping.
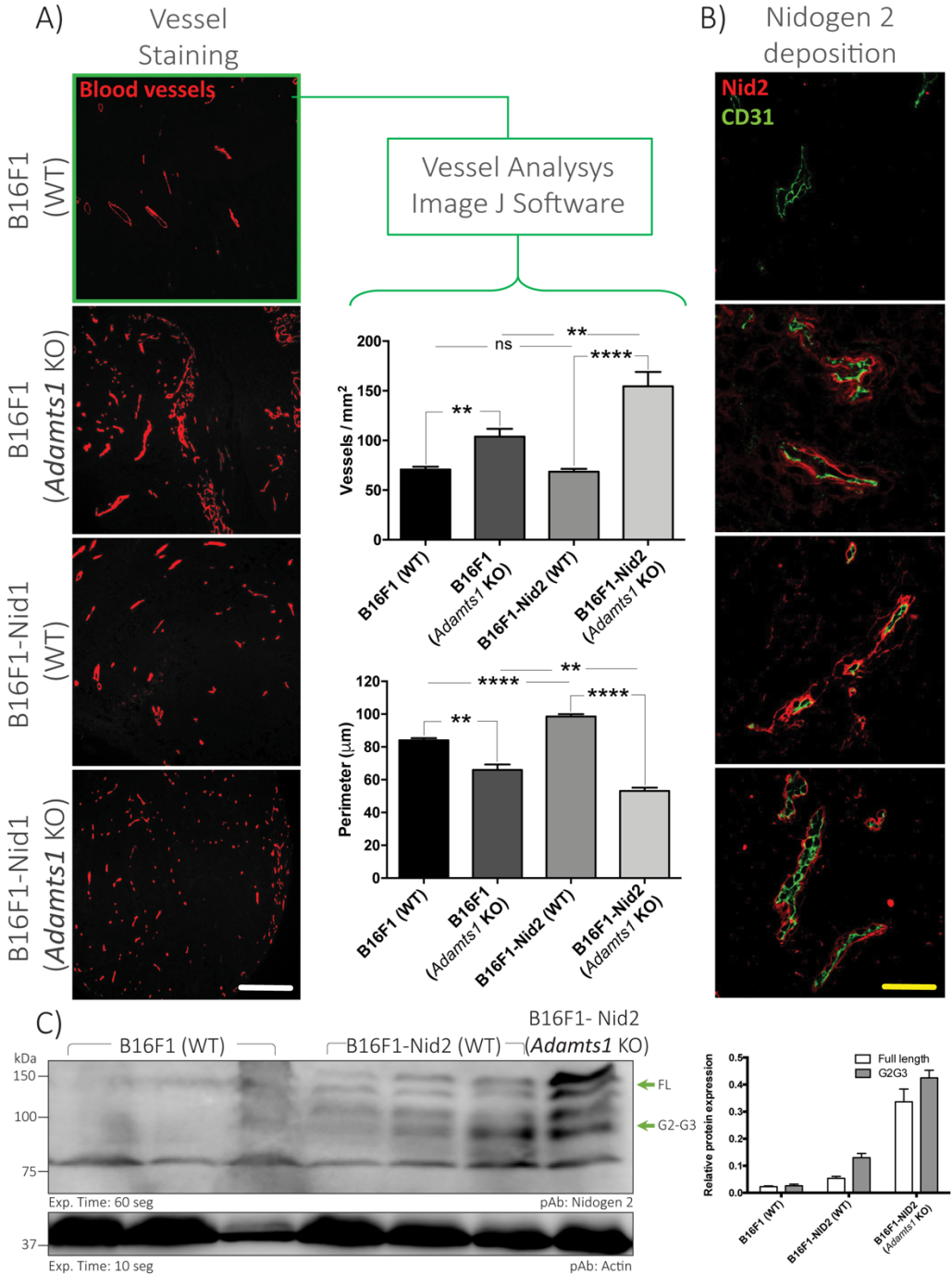
Figure 34. Tumour vasculature characterisation and NID2 deposition of the B16F1-Nid2 tumours. A) Representative images (10x magnification) of immunofluorescences with α-CD31 antibody (red signal).

Graphs on the right show quantification of vessel density (vessels/mm^3) and perimeter (μm) as detailed in materials and methodology section 10 (n = 8 tumour samples). White bar = 200 μm. B) Representative images of immunofluorescences with α-CD31 (green) and α-NID2 (red) antibodies to assess NID2 deposition in the perivascular niche. Yellow bar = 20 μm. C) Western blot of tumour protein lysate (50 μg). Below every image, the antibody used is located in the right corner and the membrane exposure time in the left corner. For NID2, the full length (FL) and fragments (G2-G3 and G1) are indicated (green arrows). Graph on the right show densitometry measurements of indicated isoforms signal intensitiy normalised with the housekeeping.

Finally, we also assessed NID1 protein by western blot in order to know its status. The quantification of the full length and the G2-G3 fragment forms did not reveal differences between the tumour groups but it confirmed the higher expression in the B16F1-Nid1 model (**Figure 33C**).

In the comparison of parental B16F1 and B16F1-Nid2 tumours in WT animals we observed a significant vessel perimeter increase without vascular density modification. In addition to the known changes within the *Adamts1* KO mouse, the overexpression of *Nidogen 2* also entailed an increase of the vessel density and perimeter reduction (**Figure 34A**). Our studies of the deposition of NID2 in tumour vessels confirmed its increase in the overexpressor models (**Figure 34B**). Finally, the western blot analysis of NID2 also confirmed an increase of NID2 in both overexpressing WT and *Adamts1* KO tumours, with low or very little expression in the B16F1 parental tumours. The cleavage of this molecule was evident but without quantifiable differences (**Figure 34C**).

Additional analyses of the vasculature were performed. First, the identification of SMA positive vascular supporting cells, that would assess vessel maturity, did not show any differences between B16F1 controls and *Nidogen* overexpressors (**Figure 35A**). Furthermore, we assessed Collagen IV (COL IV), as a relevant molecule in the vasculature and because it is known to interact directly with both Nidogens. Interestingly, in this case we found an increase in COL IV accompanying the *Nidogen* overexpression in both, WT and *Adamts1* KO tumours (**Figure 35B**).

The change in vBM components of a tumour vessel can also impede the diffusion capacities to the surrounding niche, thus becoming more hypoxic. Hence, we decided to check if the accumulation of Nidogens in the vBM of the tumour vasculature its viability by measuring the hypoxic areas (**Figure 36**). For these evaluations, we only used WT mice implanted with B16F1 parental and B16-NIDs overespressing cells. Significantly, the accumulation of NID1, but not NID2, was accompanied by an increased hypoxia confirming the deficient functionality of some vessels (**Figure 36**), in direct agreement with the strong impairment of B16F1-Nid1 tumours showed above.
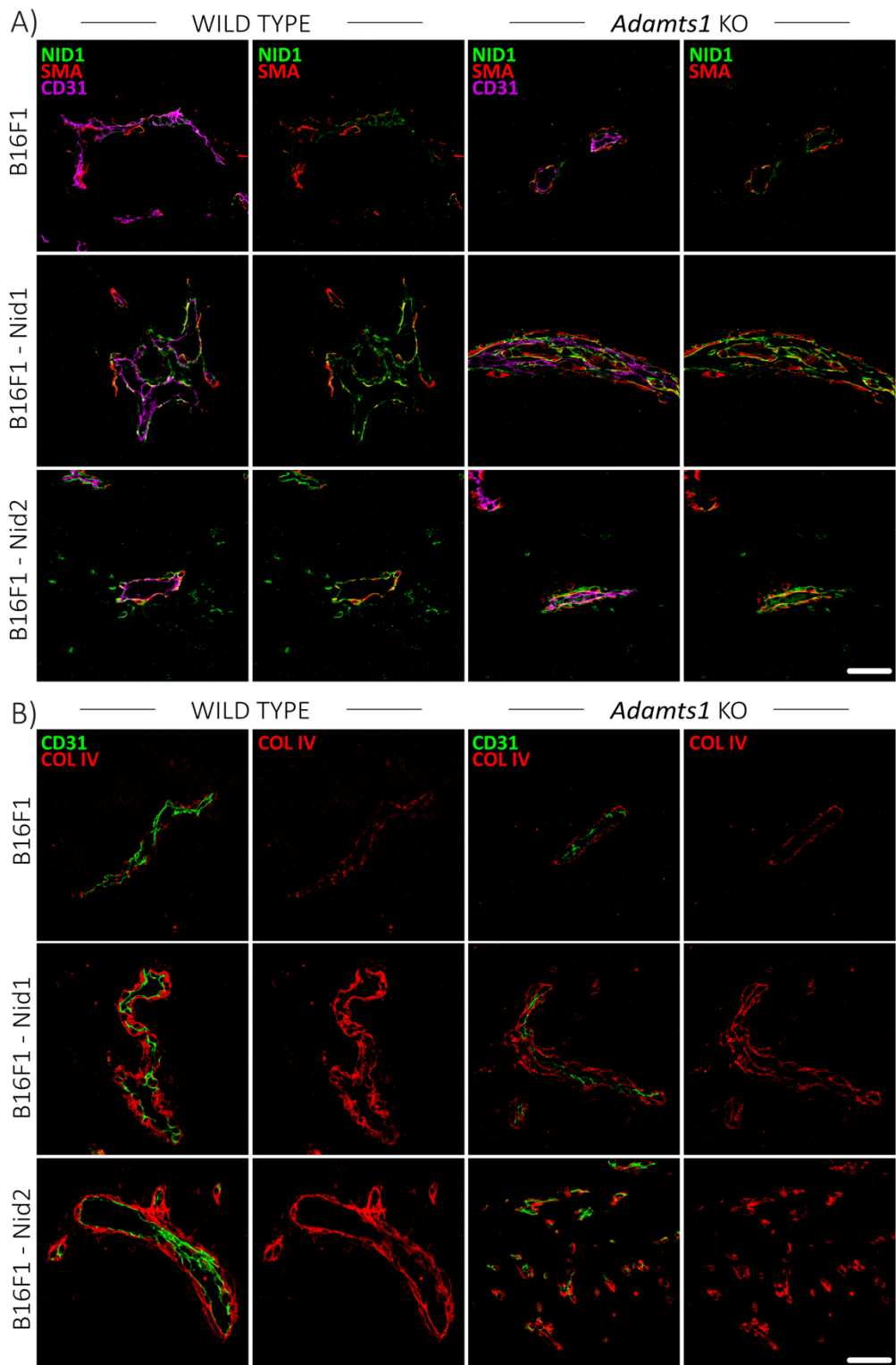
Figure 35. Identification of vascular supporting cells and Collagen IV deposition in parental and *Nidogen*-overexpressing B16F1 tumours. Tumour sections from B16F1 control and Nidogen overexpressors WT and

Adamts1 KO tumours were evaluated for: A) α-CD31 (purple), α-NID1 (green) and α-SMA (red). No colocalisation is expected, CD31 (purple) is labelling the endothelium while NID1 (green) lays on the surface of it and SMA (red) covers the vessel structures. B) α-CD31 (green), α-COLIV (red). 63X magnification pictures were obtained by confocal imaging. White bar = 20 μm. No colocalisation is expected, CD31 (green) is labelling the endothelium and COL IV (red) lays in the outer layer of CD31.
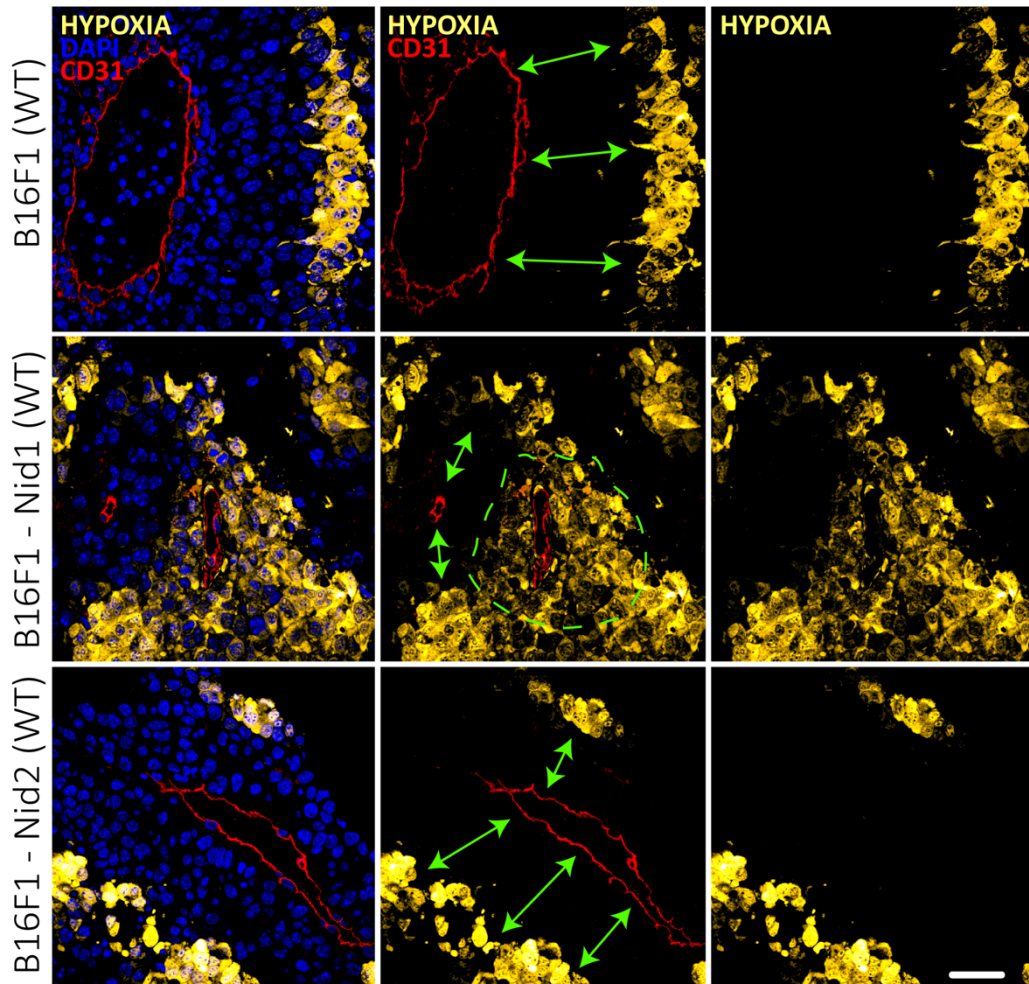
Figure 36. Immunofluorescence evaluation for hypoxia in B16F1 *Nidogen* overexpressing tumours. Tumour sections from B16F1 control and *Nidogen* overexpressors WT and *Adamts1* KO tumours were evaluated for hypoxic areas. The immunofluorescence evaluation consisted in α-CD31 (red) and α-PIM-FITC, which binds protein adducts of pimonidazole in hypoxic areas (FITC — coloured in yellow). Green arrows indicate the distance between the vessel and hypoxic areas. The dashed lines indicate a hypoxia area in a blood vessel field. White bars = 20 μm.

An overview of these results about the effects of the overexpression of *Nidogens* on tumour vasculature supports a change in the vascular patterning, that in the case of *Nidogen 1* appears closely associated to the effect of the loss of stromal ADAMTS1, showed in our first section of results. Also in this line, the overexpression of *Nidogen 1*,

but not *Nidogen 2,* entailed a prone hypoxic niche, which correlates with the tumour growing deficiencies of the B16F1-Nid1 model. Importantly, it was common the finding that the overexpression of both *Nidogens* gave rise to an accumulation of COL IV in the tumour vBM.

2.6 GENE EXPRESSION ANALYSES OF NIDOGEN-OVEREXPRESSING TUMOURS

The characterization of these tumours was followed by a comprehensive gene expression analysis. We approached two comparisons: first, between tumours derived from parental B16F1 cells and both *Nidogen*-overexpressors; and second, between tumours obtained in WT and ADAMTS1 KO groups.

The genes evaluated were categorised in four groups: i) *Adamts1* and related genes (*Timp3* and *Hif1α*); ii) *Adamts1* substrates; iii) endothelium-related genes; and iv) immune-related genes.
In the first category, the most noticeable change was *Adamts1* itself, significantly downregulated in WT tumours when both *Nidogens* are overexpressed (**Figure 37A**). The main *Adamts1* inhibitor, *Timp3*, is highly upregulated in both B16F1-Nid models in WT and *Adamts1* KO tumours.

Finally, the hypoxia-related gene *Hif1α* was included because of the relationship with *Adamts1* expression and also because a change of it could be an indicator of a deficient tumour vasculature (Hatipoglu et al., 2009). Interestingly, the B16F1-Nid2 model displayed a downregulation in the WT animals in comparison B16F1 parental tumours. Also, comparing B16F1-Nid2 in WT and *Adamts1* tumours, this difference is seen again. This could be an indicator of the good vasculature status in this model. Nevertheless, the B16F1-Nid1 WT tumours indicated an increased tendency in comparison with B16F1 parental, something that needs further assessment (**Figure 37A**).

The following set includes *Adamts1* substrates. The overexpression of each *Nidogen* was properly confirmed, without additional alterations (**Figure 37B**). Regardless, to notice that both *Nidogens* are also upregulated in the B16F1 tumours in *Adamts1* KO vs. WT mice (Fernández-Rodríguez et al., 2016). Finally, our analyses of *Versican* did not show major changes, with the exception of a downregulation in B16F1-Nid1 tumours in comparison with parental B16F1, all in the *Adamts1* KO background (**Figure 37A**), supporting once more the high heterogeneity of every group.
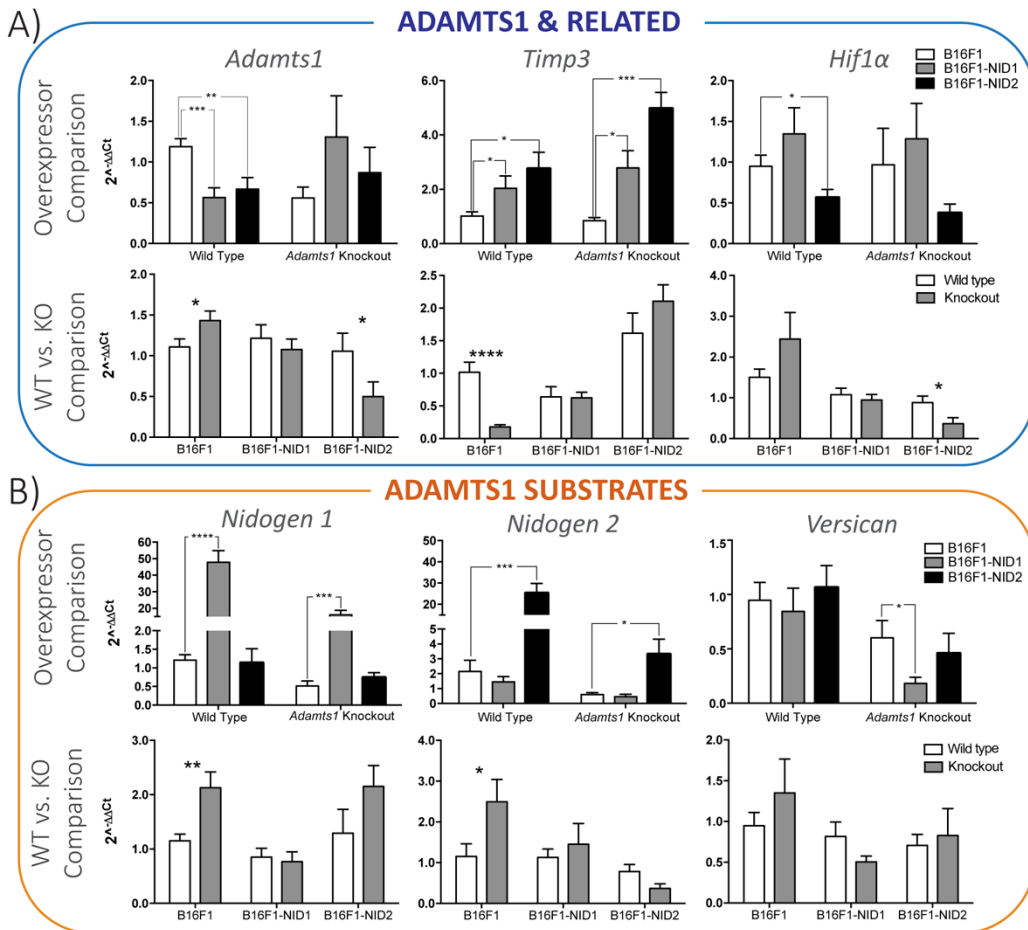
Figure 37. Gene expression analysis of B16F1 control and *Nidogen* overexpressing tumours for *Adamts1*, related molecules and its substrates. A quantitative PCR analysis for; A) *Adamts1*, *Timp3*, and *Hif1α* B) *Nidogen 1*, *Nidogen 2* and *Versican*. In every panel, two comparative analyses have been included; in the upper panel, control WT or *Adamts1* KO tumours are compared with the *Nid1* or *Nid2* overexpressors. In the bottom panel, groups; control, *Nid1* or *Nid2* are compared between WT and *Adamts1* KO. The represented data show the $2^{-\Delta\Delta Ct}$ value. t-student test performed and SEM are represented, n = 6 samples. (*p value < 0,05, **p value < 0,01, ***p value < 0,001, ****p value < 0,0001).

In accordance with the vascular phenotype that we observed in some cases, a third set of genes included endothelial-related molecules. For example, we evaluated: *Cd31*, *Vegfr2*, *Endoglin* and *Tie1*, to directly assess the endothelium, and *Smooth muscle actin* and *Ng2*, as recognized markers of vascular supporting cells. However, we presented here just *Cd31*, *Sma* and *Ng2*, as the most significant (**Figure 38**).

Among these data we should highlight that the described upregulation of *Cd31* and *Ng2* in *Adamts1* KO mice (Fernández-Rodríguez et al., 2016) (**Figure 38**) was attenuated with our *Nidogen* overexpressing cells, probably due to the overall alteration of the

vasculature in these tumours. On top of that observation, it was surprising the general downregulation of *Sma* in both B16F1-Nid models in WT and *Adamts1* KO tumours, more relevant with the Nid2 group (**Figure 38**).
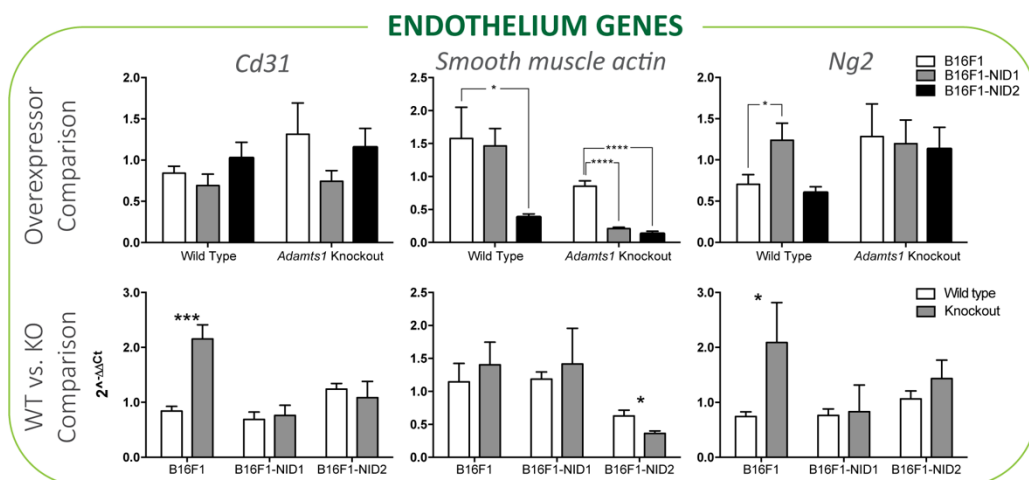
Figure 38. Gene expression analysis of B16F1 control and *Nidogen* overexpressing tumours for endothelium genes. A quantitative PCR analysis for *Cd31, Sma* and *Ng2*. In every panel, two comparative analyses have been included; in the upper panel, control WT or *Adamts1* KO tumours are compared with the *Nid1* or *Nid2* overexpressors. In the bottom panel, groups; control, *Nid1* or *Nid2* are compared between WT and *Adamts1* KO. The represented data show the $2^{-\Delta\Delta Ct}$ value. t-student test performed and SEM are represented, n = 6 samples. (*p value < 0,05, **p value < 0,01, ***p value < 0,001, ****p value < 0,0001).

Finally, a fourth gene set includes immune-related molecules. In addition to the close relationship of this field with tumour vascularization, we were also encouraged by our own preliminary results with B16F1 tumours in the *Adamts1* KO (Fernández-Rodríguez et al., 2016). Markers as *Cd11b, Tnfα* and *Tgfβ* were assessed (**Figure 39**). As reported, B16F1 parental tumours in the *Adamts1* KO mice displayed a significant downregulation of *Cd11b*. Indeed, this decrease correlated with tumour growth impairment (Fernández-Rodríguez et al., 2016). However, this alteration was lost in tumours derived from *Nidogen*-overexpressors, in a similar manner as occurred with vascular-related genes *Cd31* and *Ng2* (**Figure 39**).

The cytokine *Tnfα* displayed a downregulation tendency in B16F1 *Nidogen* overexpressing tumours in both backgrounds. As for *Tgfβ*, its unique significant alteration was the upregulation showed in B16F1-Nid2 tumours in *Adamts1* KO mice. In general, these changes in immune-related genes may be attributed to the vascular phenotype and thus by an alteration in the vBM provoked by an increase of Nidogens in their structure (**Figure 39**).
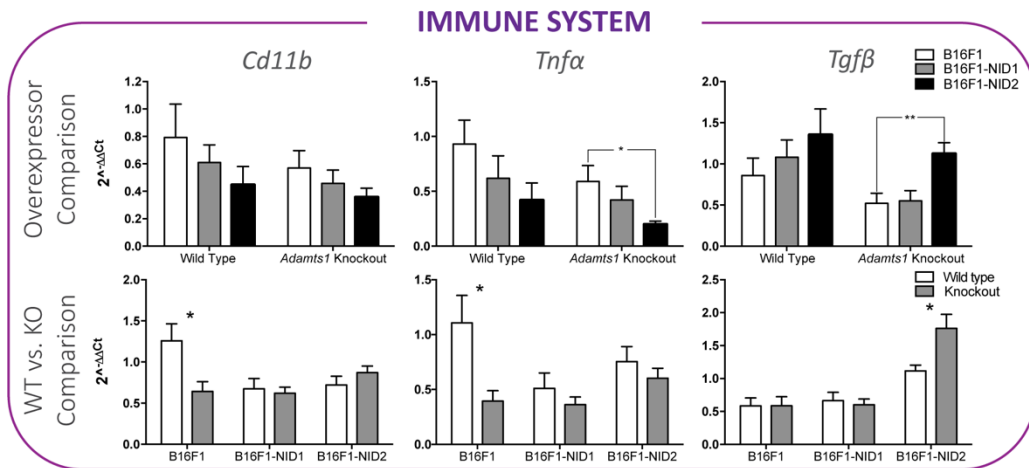
Figure 39. Gene expression analysis of B16F1 control and *Nidogen* overexpressing tumours for immune system genes. A quantitative PCR analysis for *Cd11b, Tnfα*, and *Tgfβ*. In every panel, two comparative analyses have been included; in the upper panel, control WT or *Adamts1* KO tumours are compared with the *Nid1* or *Nid2* overexpressors. In the bottom panel, groups; control, *Nid1* or *Nid2* are compared between WT and *Adamts1* KO. The represented data show the $2^{-\Delta\Delta Ct}$ value. t-student test performed and SEM are represented, n = 6 samples (*p value < 0,05, **p value < 0,01).

3. ASSESSING THE IMPACT OF THE LACK OF ADAMTS1 IN DIFFERENT MOUSE ORGANS

As already introduced, the genetic deletion of murine *Adamts1* has severe consequences for the animal biology. Of note, 40% of the homozygous animals do not birth, which makes difficult the study of this colony. Among the identified alterations the most conspicuous are: a reduced body weight, fat-tissue diminish, kidney malformation and ovulation deficiencies in heterozygous females and sterility in homozygous ones (Mittaz et al., 2004; Shindo et al., 2000). To date, not much is known about the genetic and protein profile of *Adamts1* substrates in different organs of the *Adamts1* null mice. Given our expertise, we thought this information could shed light over the multiple roles of the protease during development and adult life. At this point, our main aim was to continue unveiling the relationship of ADAMTS1 and its substrates Nidogens and Versican in a variety of organs, including a deeper look at their vasculature. In this study we included the following: brain, lung, kidney, heart, spleen, ovary and bone marrow.

3.1 GENE EXPRESSION ANALYSIS OF ADAMTS1 AND RELATED GENES

The expression of *Adamts1* is generally low in a mature individual, decreasing along development (Thai and Iruela-Arispe, 2002). According to our interests we screened a panel of genes comprising *Adamts1* and substrates as *Nidogens* and *Versican*, vascular-related genes as *Cd31, Sma* and *Ng2,* and finally immune-related genes as *Cd11b*. In line with the advance of this thesis, our interest in immune-related processes has become constant in our research.

Looking at *Adamts1* expression, we found a strongest expression in kidney and lung, with Ct values slightly under 30. Following: brain, heart, ovary, spleen and liver with Ct values over 30, being the bone marrow the lowest-expressing among all the analysed samples, Ct values around 34 (**Figure 40**).

As ADAMTS1 substrates we analysed Nidogens and Versican, according to their contribution for specialized ECM and the immune system, respectively. *Nidogen 1* was found to be downregulated in *Adamts1* KO spleen and bone marrow. Interestingly, both *Nidogen 1* and *Nidogen 2* were downregulated in *Adamts1* null hearts, although this organ has not been associated with the main defects of these animals. Meanwhile, *Versican* appeared significantly upregulated just in the bone marrow of *Adamts1* null mice.
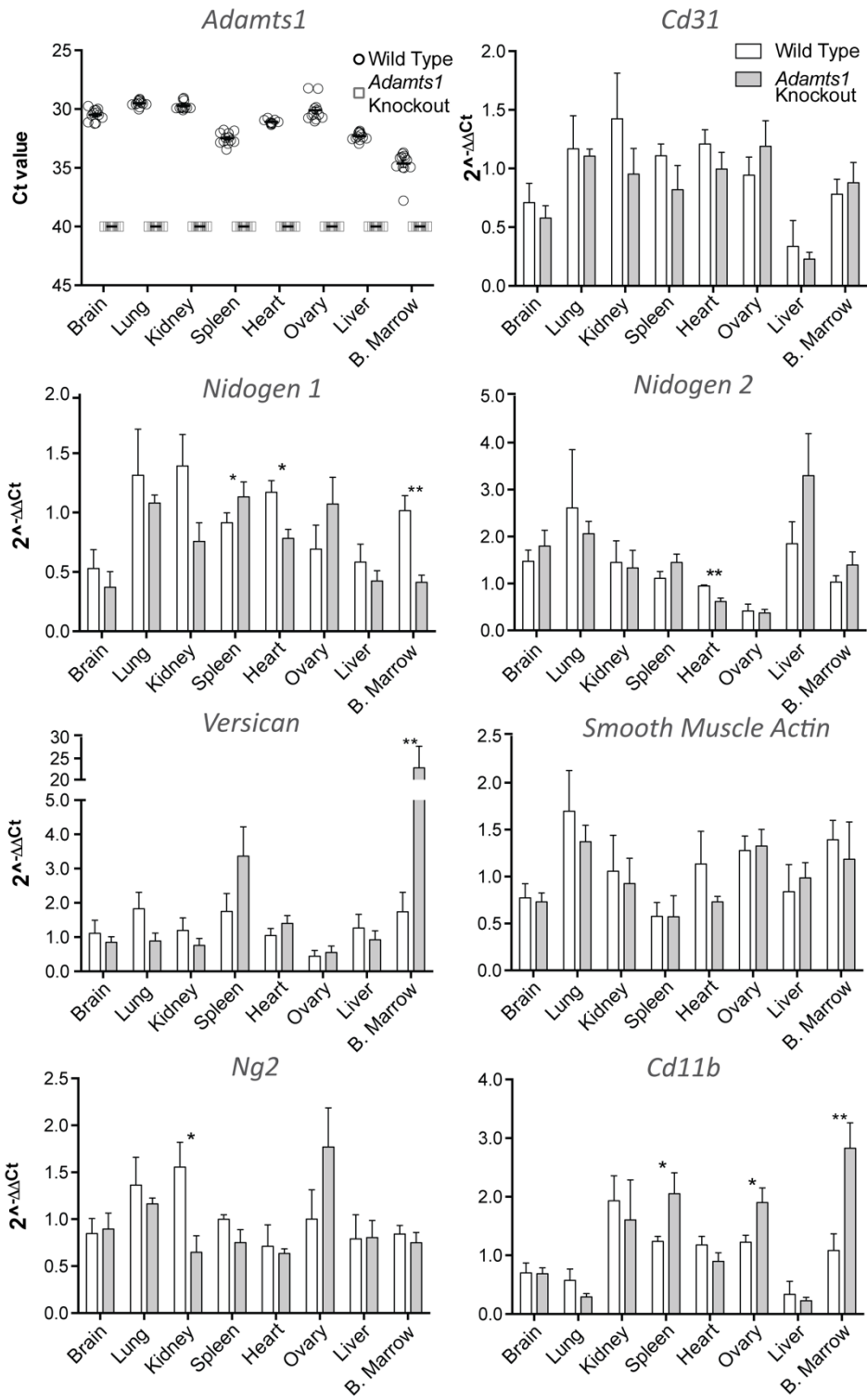
Figure 40. Gene expression analysis of the WT and *Adamts1* KO tissues. A quantitative PCR analysis for *Adamts1, Cd31, Nidogen 1, Nidogen 2, Sma, Ng2, Cd11b* and *Versican* genes. A general comparison between

WT and *Adamts1* KO organs have been performed, being the one of the WT samples the plate calibrator and the reference sample to normalise the rest. The represented data show the Ct values for *Adamts1* and the $2^{-\Delta\Delta Ct}$ value for the rest of the genes. t-student test performed and SEM are represented, n = 5 samples. (*p value < 0,05, **p value < 0,01).

The information of vasculature-related genes, based in the recognized actions of *Adamts1* on angiogenesis and vasculature in general, did not show significant alterations in the analysed adult organs, with the exception of *Ng2* that appeared downregulated in *Adamts1* null kidneys. Kidney malfunction in *Adamts1* knockout mice has been recognized, so this result may be related although further studies are required (**Figure 40**).

Finally, the evaluation of the selected immune-related genes as *CD11b* also showed its upregulation in spleen, ovary and bone marrow of *Adamts1* null mice (**Figure 39**). This last piece of data resulted very encouraging for us. However, the upregulation in the ovary could be related with the reported malfunction of this organ in *Adamts1* deficient mice.

3.2 A VASCULATURE ANALYSIS OF THE DIFFERENT ORGANS

In line with our research in tumour scenarios (results section 1.1.), we evaluated by immunofluorescence the vasculature of selected organs from wild type and *Adamts1* KO mice: brain, lung, kidney, spleen, heart and ovary. Sections were incubated with CD31 antibody and vessel density and perimeter were evaluated as detailed in materials and methodology section 10. In general, and in accordance with our previous gene expression studies, these analyses did not show significant changes in the vasculature of the selected organs, at least regarding vessel density and perimeter (**Figure 41**).

Although our evaluations did not reveal relevant changes in the vascular network correlating with the loss of *Adamts1,* we proceeded with further studies to explore the vBM of the different organs.
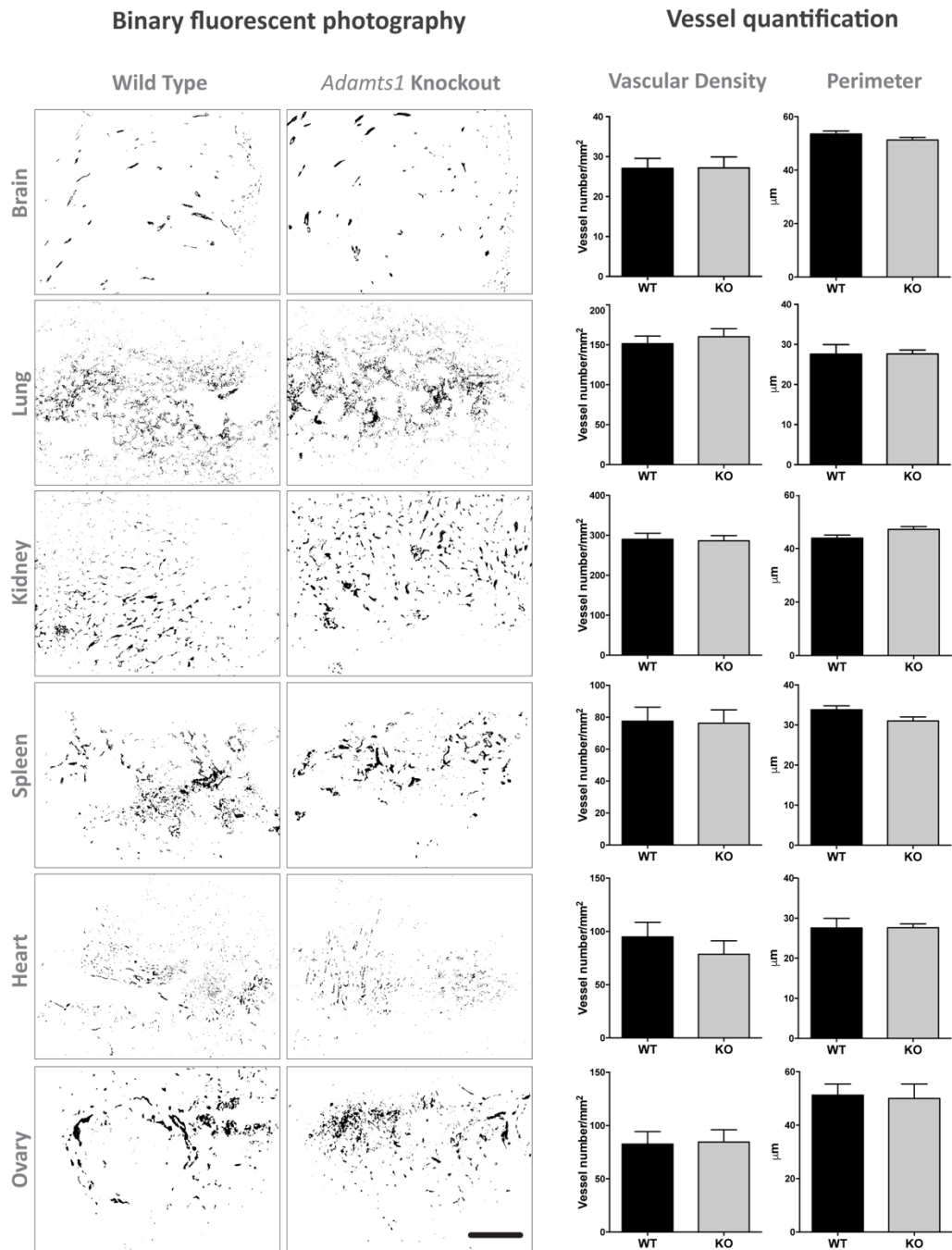
Figure 41. Analysis of vasculature of WT and *Adamts1* KO organs. Tissue sections of WT and *Adamts1* KO tissues were assessed by immunofluorescence with α-CD31 to visualize the vasculature. On the left, there are representative images (10x) captured with an epi-fluorescence microscope and converted to a binary image for proper analysis, as detailed in materials and methodology section 10 (black bar = 200 µm). Graphs on the right represent the quantification of vascular density (vessels per mm^2) and vessel perimeter (µm) for every organ (n = 5 tissue samples).

3.3 PROTEIN DEPOSITION AND CLEAVAGE OF RELEVANT ADAMTS1 SUBSTRATES

Here we approached the study of specific ECM components as NIDOGENS and Versican. Although vasculature in general did not appear affected by the absence of ADAMTS1, the location and/or deposition of these substrates may differ in these mature organs. In general, we keep performing CD31 immunofluorescence to identify perivascular areas.

Regarding Nidogens, while the overall deposition of NID1 is high enough to acquire good images for analyses, the NID2 signal was very low and its evaluation did not reveal significant findings to constitute a figure. Our studies with NID1 showed no differences between wild type and *Adamts1* KO organs, with the exception of spleen and kidney. Unexpectedly, we found a clear decrease of NID1 deposition in these organs of the *Adamts1* null mice, suggesting the existence of compensatory mechanisms. Indeed, in heart, which gene expression data indicated a downregulation of both *Nidogens* in *Adamts1* KO mice, no important changes were appreciated (**Figure 42**).

To complete these evaluations, we performed western blot for some of the tissues that have been under study (not all are represented here). Both NIDs were assessed but only NID1 is showed. We decided to represent two tissues that revealed clear changes and two other that did not differ at all (**Figure 43A-B**).

In general, these analyses showed a tremendous heterogeneity, quite evident between organs, but also noticed between samples. For instance, heart and ovary presented no differences in the protein expression between WT and *Adamts1* KO, but showed completely different patterns of cleavage (**Figure 43**), being NID1 FL predominant in heart, and G1 and G2-G3 forms in the ovary. In spleen, NID1 was mainly represented by the G1 fragment, however, the FL and G2-G3, despite its low expression, showed an increase in the *Adamts1* null spleens, as reported the western blot quantification (**Figure 43B**). Finally, kidney presents all three forms although G1 is the most abundant and appeared significantly induced in *Adamts1* KO samples (**Figure 43A**).

These findings confirm that NID1 is differently cleaved along the tissues and also that the lack of ADAMTS1 may be accompanied by a differential deposition and cleavage. Nevertheless, we did not find a consistent correlation between the absence of ADAMTS1 and the cleavage pattern of NID1, suggesting the existence of alternative proteases which activity is probably affected by overlapping mechanisms.
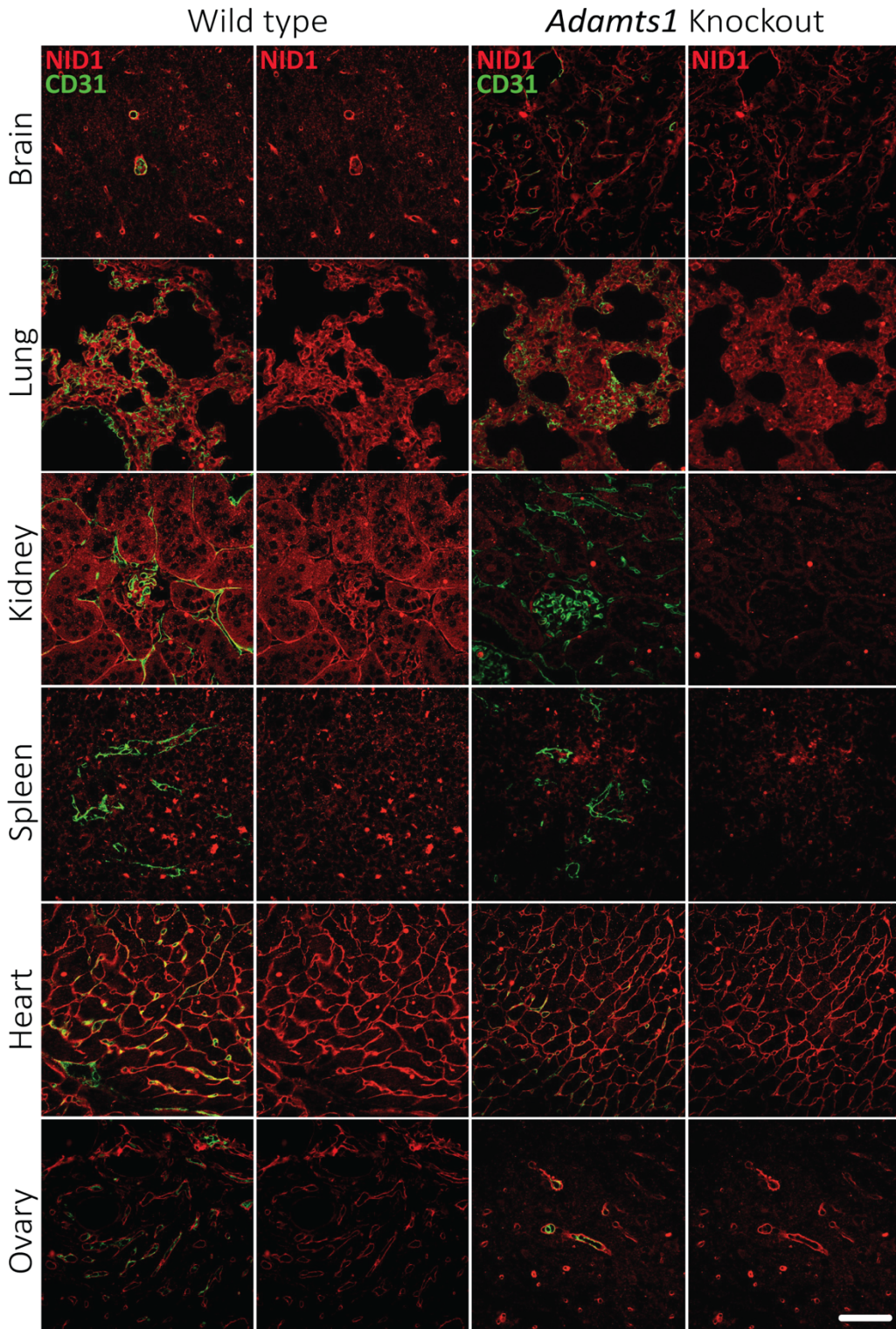
Figure 42. Evaluation of NID1 in the perivascular niche of WT and *Adamts1* KO organs. Representative images (63X) of WT and *Adamts1* KO organs, previously subjected to immunofluorescence with α-NID1 (red)

and α-CD31 (green). 63X magnification pictures were obtained by confocal imaging. No colocalisation is expected, NID1 (red) is found in the tissue stroma and CD31 (green) lays on the vessel niche. White bar = 20 μm.
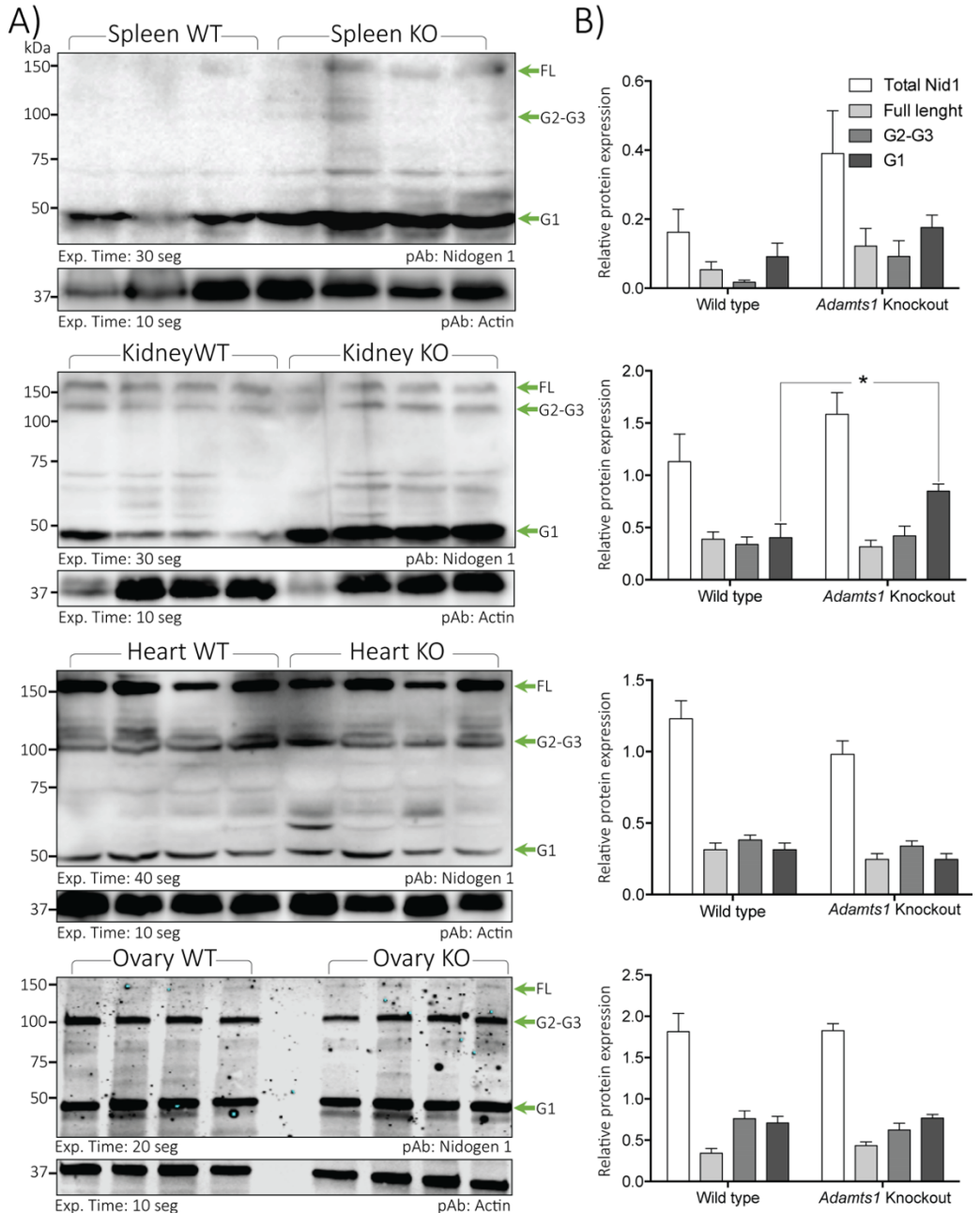
Figure 43. Protein expression and quantification analysis of the WT and *Adamts1* KO organs. A) Western blot of tissue protein lysate were performed with a total of 50 μg of protein per lane of WT and *Adamsts1* KO tissues. Below every image, the antibody (pAb – polyclonal or mAb – monoclonal) used is located in the right corner and the membrane exposure time in the left corner. For NID1, the full length (FL) and fragments (G2-G3 and G1) are indicated (green arrows). Protein lanes are indicated by its molecular weight (kDa). B)

Protein densitometry measurements were taken using Image J, normalised with every Actin housekeeping signal. t-student test performed and SEM are represented, n = 4 samples. (*p value < 0,05).

We extended our evaluations to VCAN and its fragment VKIN in the different organs. We observed that VCAN was also affected in some organs in consonance with the absence of the protease. Our collaborators already described alterations of the VCAN in the *Adamts1* null ovaries during ovulation and this was one of the clues that led us to perform this study (Brown et al., 2010).

The expression of VCAN is especially high in tissues as cycling ovaries and its deposition is not always linked to the vasculature, it can be also found in specific isolated cells, an example of what happen in the spleen (**Figure 44**). Our studies showed no differences between WT and *Adamts1* KO in brain, lung, kidney and heart. However, spleen and ovary display a higher deposition of VCAN in *Adamts1* KO organs (**Figure 44**).

The recognized fragment VKIN also displays a heterogeneous deposition among the organs. With the exception of lung and spleen, we observed a lower deposition in *Adamts1* KO brain, kidney, heart and ovary, more evident in these two last organs given its higher levels (**Figure 45**). In general, there is a tendency of VKIN reduction in the *Adamts1* KO organs, however, the lack of correlation in spleen and lung might be mediated by the compensatory action of other proteases in the ECM.

Concluding, we observe that the loss of *Adamts1* does not clearly affect the formation of a vessel network in mature organs but it affects the composition of specialized ECMs. Comprehensive studies at early stages of development would instruct us about the role of *Adamts1* during organ development.
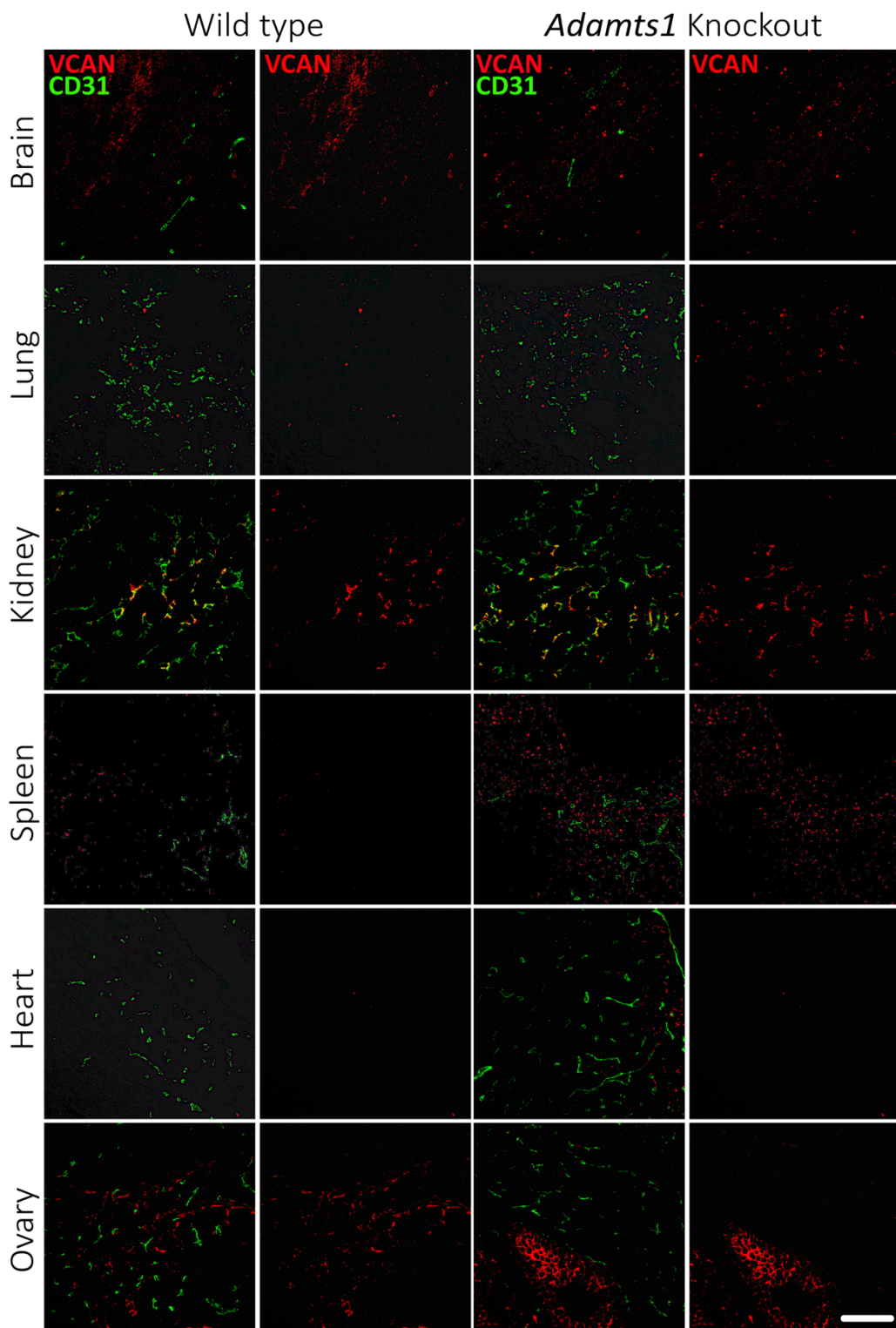
Figure 44. Evaluation of VCAN in the perivascular niche of WT and *Adamts1* KO organs. *Adamts1* WT and KO tissues were subjected to immunofluorescence. α-VCAN (red) and α-CD31 (green). 63X magnification

pictures were obtained by confocal imaging. No colocalisation is expected, VCAN (red) is found in the tissue stroma and CD31 (green) lays on the vasculature. White bars = 20 µm.
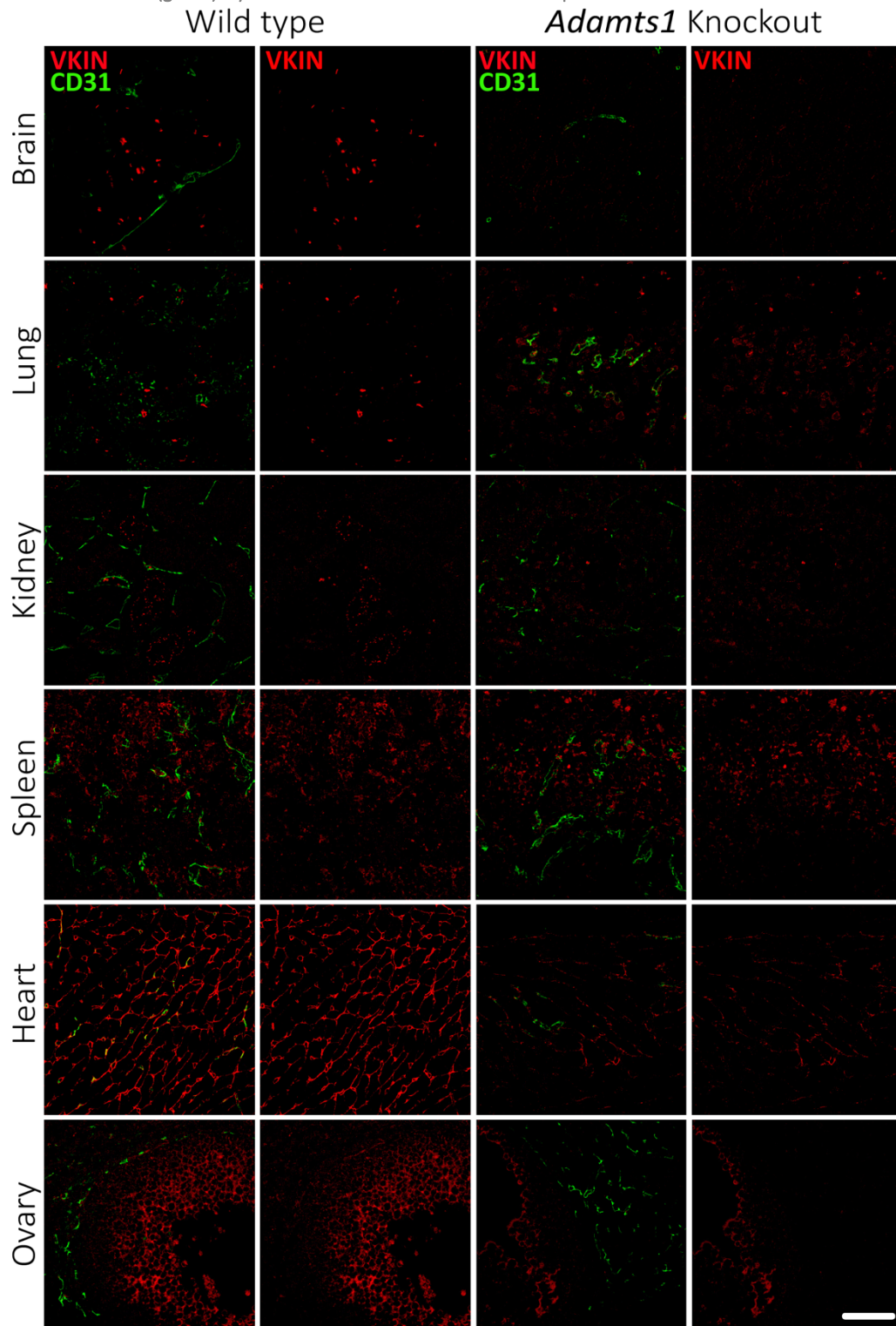
Figure 45. Evaluation of VKIN in the perivascular niche of WT and *Adamts1* KO organs. *Adamts1* WT and KO tissues were subjected to immunofluorescence. α-VKIN (red) and α-CD31 (green). 63X magnification pictures were obtained by confocal imaging. No colocalisation is expected, VKIN (red) is found in the tissue stroma and CD31 (green) lays on the vasculature. White bars = 20 µm.

3.4 STUDY OF IMMUNE-RELATED ORGANS

In regard to previous results, the gene expression data entailed us to delve into the immune field. The fact that some genes as the myeloid marker *Cd11b* were altered in organs as spleen, bone marrow and ovary, were in agreement with defects found in *Adamts1* KO organs. Still, the relationship of *Adamts1* and the immune system is vague and need a deep characterization. Hence, we analysed certain immune cell populations of the spleen and the bone marrow, as principal contributors of the immune system. With this purpose, we performed flow cytometry, gene expression and *ex-vivo* analyses with wild type and *Adamts1* KO organs.

Starting with the spleen, a splenomegaly effect was first appreciated in *Adamts1* KO animals in comparison with their WT littermates. According to the body mass reduction described for the *Adamts1* null animals (Shindo et al., 2000), the results were normalised with body weight (**Figure 46A**). Next, we performed flow cytometry determinations from these spleens. Although not all populations were altered, we remark next our more significant data. In one side we found that *Adamts1* KO spleens have increased CD3$^+$ T-cell population, and oppositely, we detected less CD11b$^+$ and F4/80$^+$ cells (**Figure 46B**).
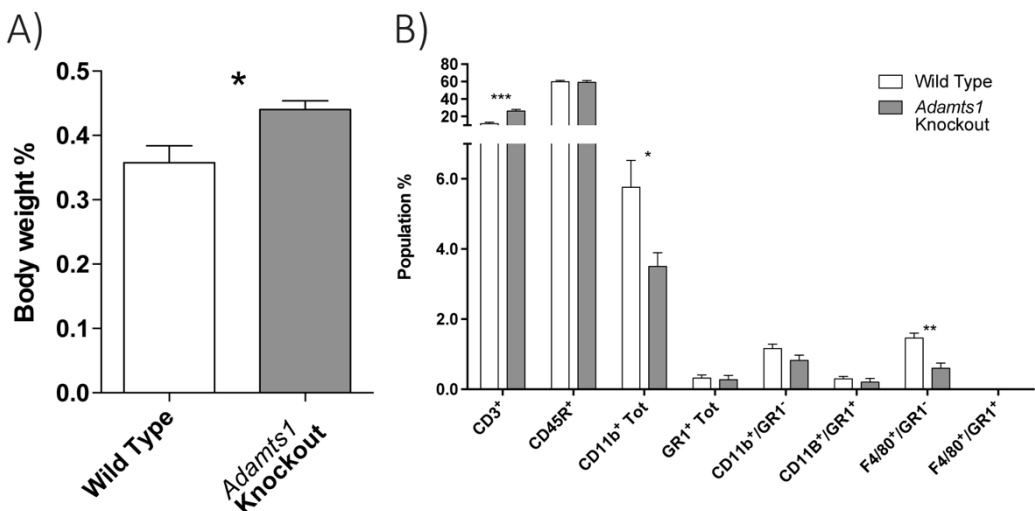
Figure 46. Macroscopic and flow cytometry analysis of WT and *Adamts1* KO spleens. A) The graph represents the spleen percentage in relation to the animal body weight. B) Flow cytometry analyses of certain immune

populations in the spleen. The analysed subsets are; CD3 T-lymphocytes, CD45 B-lymphocytes, CD11b myeloid cells, GR1$^+$ cells, CD11b$^+$/GR1$^+$ MDSC, F4/80$^+$ macrophages and F4/80$^+$/GR1$^+$ macrophages. The percentages are relativized to the total living cells within the spleen. t-student test performed and SEM are represented, n = 5 samples. (*p value < 0,05, **p value < 0,01).

Our previous gene expression analyses revealed an increment of *Nidogen 1* in *Adamts1* KO spleens (**Figure 39**) but the protein deposition indicated the opposite (**Figure 42-43**). In an attempt to complete this characterization, we added further gene expression studies, including lymphocyte and macrophage markers and some cytokines of particular interest.

Lymphocytes markers *Cd3*, *Cd4*, *Cd8* and *Cd45* were selected as a good representation of the T-lymphocyte population (**Figure 47A**). Accordingly, all of them were upregulated in *Adamts1* KO spleens in correlation with the flow cytometry data (**Figure 47A**). Related to myeloid-macrophage and polarised populations we assessed: *Nos2*, *Arg1*, *Cd163* and *Tnfα*. These genes did not show relevant changes in this scenario (**Figure 47A**), revealing a limited significance of the CD11b$^+$ decrease found by flow cytometry in *Adamts1* KO spleens.
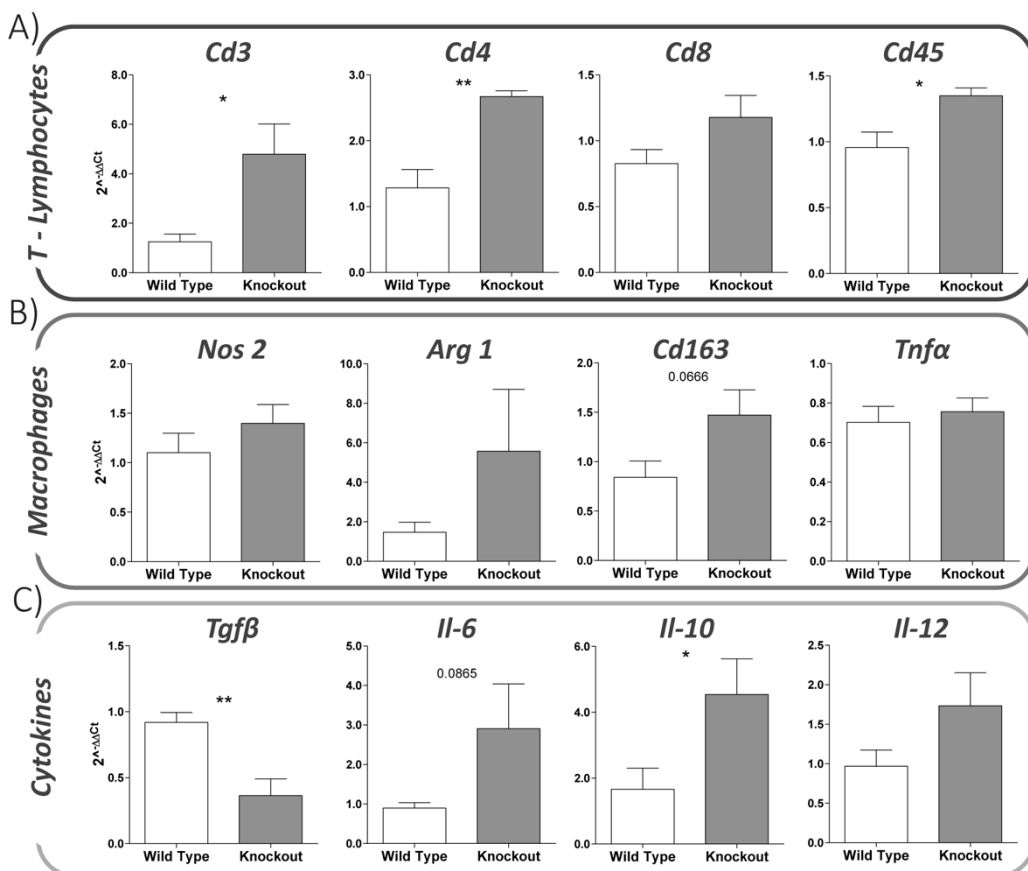
Figure 47. Gene expression analysis of the WT and *Adamts1* KO spleens. A quantitative PCR analysis have been performed for the following groups; A) T-lymphocyte genes (*Cd3*, *Cd4*, *Cd8*, *Cd45*), B) macrophage-related genes (*Nos2*, *Arg1*, *Cd163* and *Tnfα*) and C) cytokines (*Tgfβ*, *Il-6*, *Il-10* and *Il-12*). A general comparison between WT and *Adamts1* KO spleens have been performed. The represented data show the $2^{-\Delta\Delta Ct}$ value. t-student test performed and SEM are represented, n = 6 samples. (*p value < 0,05, **p value < 0,01).

Finally, a series of cytokines were evaluated to study possible differences in the inflammatory status of the spleen. The results show how *Tgfβ*, an important immunosuppressive cytokine, is reduced in the *Adamts1* KO spleens. This correlates also with the decrease of CD11b$^+$ cells. The expression of *Il-6* also seems upregulated; this is a pro-inflammatory interleukin but at higher levels it can also act as immunosuppressive. Unlike the previous cytokines, *Il-10* a molecule that promotes an immunosuppressive environment, is upregulated as well (**Figure 47C**).

In general, our findings with *Adamts1* KO spleens correlated with the creation of a pro-inflammatory scenario in the absence of the protease, corroborated by both flow cytometry and gene expression analyses. However, although the flow cytometry analysis showed an alteration in the myeloid population, our gene expression data does not fully match this result, thus denoting the minor importance of this population within the spleen.

Next, we performed the same assays with the bone marrow, the main source of hematopoietic precursors and myeloid cells. As found in spleen, flow cytometry revealed an increase of the CD3$^+$ lymphocytes of *Adamts1* KO bone marrow, but this population is very low and its significance in the bone marrow is still not clear (Zhao et al., 2012). The most remarkable finding was the significant accumulation of myeloid-derived suppressor cells (MDSC) cells: CD11b$^+$, CD11b$^+$/GR1$^+$ and F4/80$^+$/GR1$^+$, in *Adamts1* KO bone marrow, associated with an immunosuppressive environment (**Figure 48**).
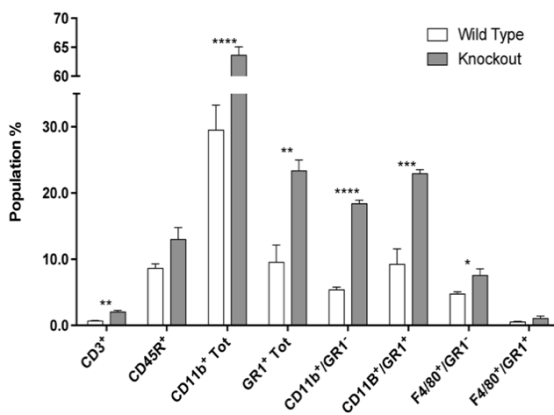
Figure 48. Characterisation of immune populations of WT and *Adamts1* KO bone marrow by flow cytometry. Flow cytometry analyses of certain immune populations in the spleen. The analysed subsets are; CD3$^+$ T-lymphocytes, CD45$^+$ B-lymphocytes, CD11b myeloid cells, GR1$^+$ cells, CD11b$^+$/GR1$^+$ MDSC, F4/80$^+$ macrophages and F4/80$^+$/GR1$^+$ macrophages. The percentages are relativized to the total living cells within the bone marrow. t-student test performed and SEM are represented, n = 5 samples. (*p value < 0,05, **p value < 0,01).

Looking back at our previous gene expression data in organs, we should recall that *Adamts1* KO bone marrow showed increased *Cd11b* and also *Versican* (**Figure 40**), somehow correlating with the increase of the immunosuppressive population of CD11b$^+$GR1$^+$ MDSC. Again, we extended our gene expression studies in order to unveil the changes given in this scenario.

Our results with the T-cell lymphocytes-related genes *Cd3*, *Cd8* and *Cd45,* also support the flow cytometry evidence of the CD3$^+$ population increase (**Figure 49A**). Interestingly, we observed an upregulation of macrophage markers as *Arg1* and *Cd163,* supporting in this case an alternatively activated macrophage shift, in line with the immunosuppressive scenario (**Figure 49B**). Further support comes with our data, showing upregulation of *Tgfβ* and downregulation of *Il-6* (**Figure 49C**). As an overall, we observed that in the case of the bone marrow, the loss of *Adamts1* favours an enrichment of CD11b$^+$ and other myeloid populations related with immunosuppression.
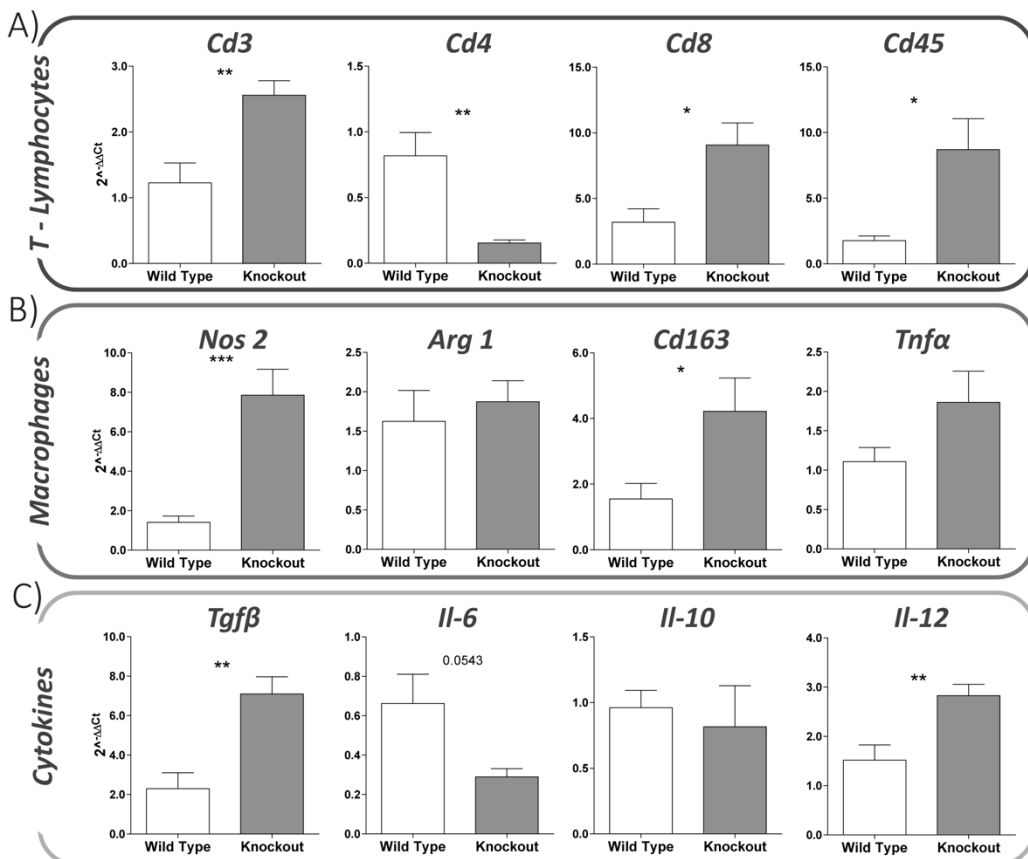
Figure 49. Gene expression analysis of the WT and *Adamts1* KO bone marrow. A quantitative PCR analysis have been performed for the following groups: A) T-lymphocyte genes (*Cd3*, *Cd4*, *Cd8*, *Cd45*), B) macrophage genes (*Nos2*, *Arg1*, *Cd163* and *Tnfα*) and C) cytokines (*Tgfβ*, *Il-6*, *Il-10* and *Il-12*). A general

comparison between WT and *Adamts1* KO bone marrow have been performed. The represented data show the $2^{-\Delta\Delta Ct}$ value. t-student test performed and SEM are represented, n = 6 samples. (*p value < 0,05, **p value < 0,01).

In fact, given these relevant findings with the myeloid CD11b^{+} population, we decided to isolate the bone marrow and stimulate towards CD11b and classical or alternatively activated macrophages in order to study further cell characteristics.

3.4.1 STUDY OF POLARISATION OF BONE MARROW-DERIVED MACROPHAGES FROM WT AND ADAMTS1 KO MICE

Since our first observations of immune-related infiltrates in B16F1-derived tumours, the study of macrophages became a priority to us. Furthermore, the changes observed in the bone marrow niche of our *Adamts1* KO mouse model also stand out their importance in relationship to *Adamts1* but the role of this protease within this niche remains unknown. Therefore, we aimed to study *ex*-vivo the bone marrow-derived macrophages (BMDM) as a further step that could shed light in this scenario.

Accordingly, we isolated BM from WT and *Adamts1* KO healthy mice and induced their differentiation towards a CD11b^{+} myeloid population. A first assessment of their adhesive properties *in-vitro* (as detailed in materials and methodology section 3) showed no differences (**Figure 50A**).

Hence, we polarised these BMDM towards classically or alternatively activated macrophages to unveil if this differentiation process is affected in *Adamts1 KO* derived cells. We observed phenotypic changes between the parental and classical or alternatively activated BMDM, validating our assay (**Figure 50B**). In one side, classically activated macrophages change its morphology from elongated and spindle to a rounded shape with a marked and big nucleus. Alternatively activated macrophages morphology differ less from parental cells, showing a more elongated shape and with characteristic ruffled prolongations at one cell end. This polarisation did not reveal significant changes between WT and *Adamts1* KO derived cells under the light microscope (**Figure 50B**). Unfortunately, the lack of differences was confirmed by confocal microscopy analysis of the cytoskeleton, after the incubation with phalloidin and Tubulin (**Figure 50B).**

Finally, gene expression was also assessed and two different comparisons were performed (**Figure 50**). First, we analysed if the polarisation underwent accordingly in the *Adamts1* null BMDM in comparison with WT. The assessment of *Nos2*, for classically

activated macrophages, and *Arg1* and *Tnfα,* for alternatively activated macrophages, revealed correct polarisation process in both WT and *Adamts1* KO BMDM.

A)

B)
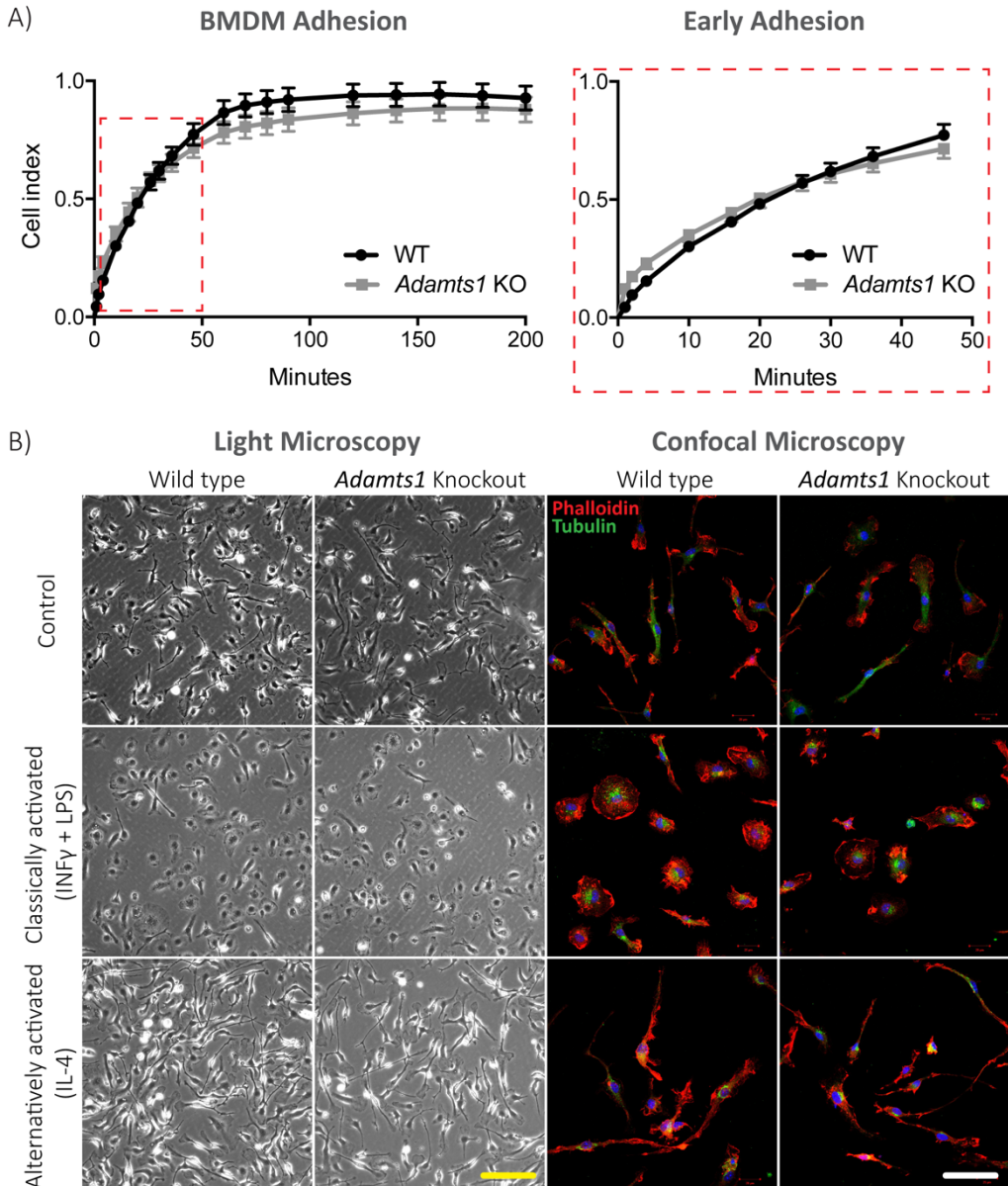
Figure 50. Characterization of adhesive properties of BMDM and polarisation morphology from WT and *Adamts1 KO* mice. A) Adhesion assays were performed with xCELLigence using control and non-polarised BMDM with a fibronectin coating. The cell index measured by bio-impedance represent the cell adhesion until 200 minutes. The red dashed box represents the early adhesion, the first 50 minutes of the experiment (right panel). B) BMDM control and polarised were studied under light microscopy to assess morphological changes at a 24-hour point after seeding. Images were taken at a 40X magnification. Immunofluorescence with phalloidin-TRITC (red) to label α-actin and α-Tubulin-FITC (green) was performed with BMDM onto

coverslips coated with fibronectin at a 24-hour point after seeding. Confocal images were taken at a 63C magnification. Yellow scale bar = 40 µm, white scale bar = 20 µm.

The expression of *Adamts1* does not change during the polarisation of WT cells. It is interesting thought that the expression of *Nidogen 1* increases just in the classically activated BMDM in WT mice, while for the alternative pathway appeared upregulated in both WT and *Adamts1* KO derived BMDM. For *Versican*, the expression increases drastically only in the classically activated BMDM, thus it can be considered a marker for this population as some publications suggests (Chang et al., 2014) (**Figure 51A**). The increase of both *Nidogen 1* and *Versican* in the classically activated BMDM suggest a role for these ECM molecules in the *ex-vivo* differentiation process of these BMDM.
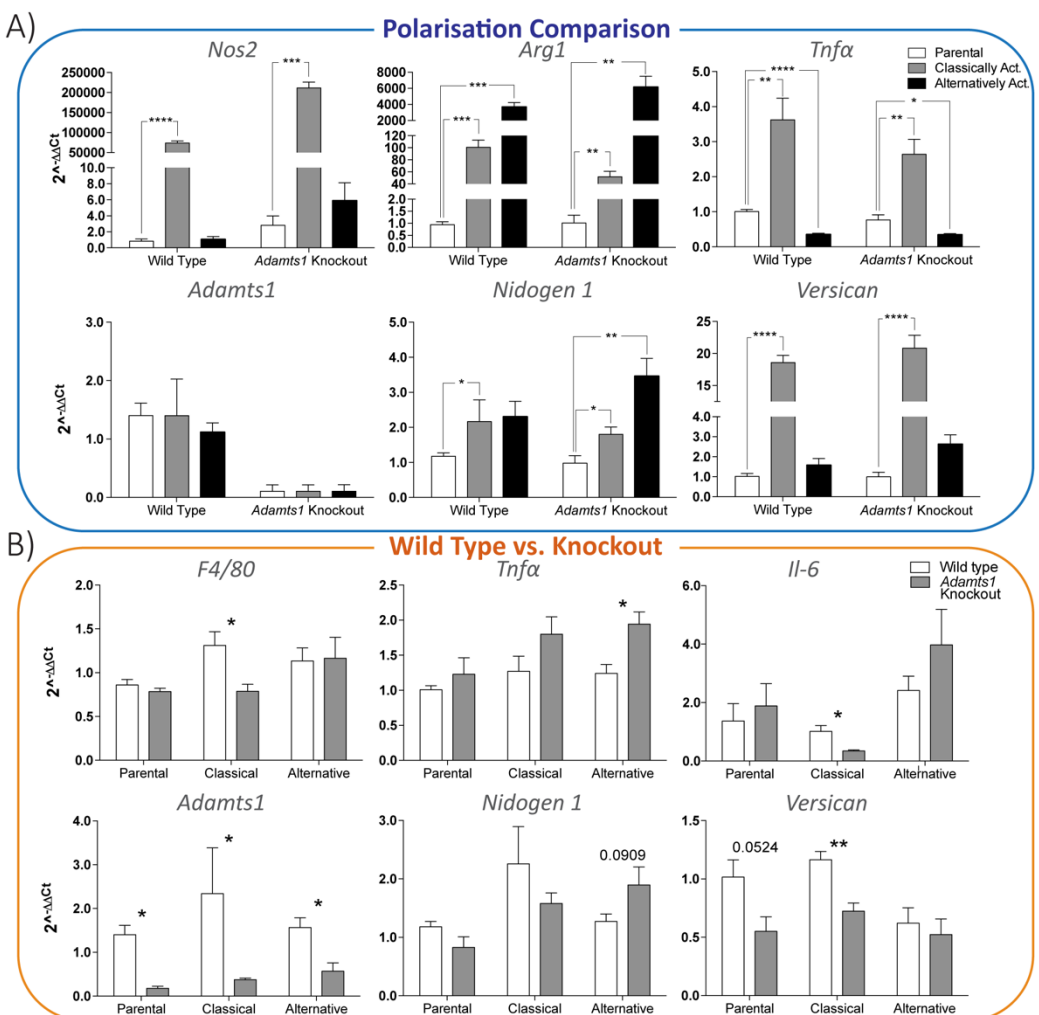
Figure 51. Gene expression analysis of WT and *Adamts1* KO BMDM and its polarisation. A) A quantitative PCR analysis comparison to assess the performance of the polarisation (*Nos2*, *Arg1*, and *Tnfα*) and further genes of interest (*Adamts1, Nidogen 1*, and *Versican*) B) A comparison between WT and *Adamts1* KO BMDM

for the following genes: *F4/80*, *Tnfα*, *Il-6*, *Adamts1*, *Nidogen 1* and *Versican*. The represented data show the $2^{-\Delta\Delta Ct}$ value. t-student test performed and SEM are represented, n = 4 samples. (*p value < 0,05, **p value < 0,01, ***p value < 0,001, ****p value < 0,0001).

Secondly, we compared every BMDM WT group with *Adamts1* KO to assess possible differences in each independent population, due to the loss of *Adamts1*. The macrophage markers *F4/80* and *Il-6* outlined a downregulation in *Adamts1* KO BMDM and the *Tnfα* cytokine is upregulated in alternatively activated *Adamts1* KO BMDM. These gene expression switches suggested a different differentiation process that does not induce phenotypical changes but it may affect to the cell functionality *in-vivo* by the loss of *Adamts1* (**Figure 51B**).

As for the substrate *Nidogen 1*, no significant changes were detected in general, but a consistent upregulation of this gene was observed in the alternatively activated *Adamts1* KO BMDM. *Versican,* according to its recognized induction in the classically activated BMDM, appears significantly downregulated in classically activated *Adamts1* BMDM, in a similar manner to *F4/80* and *Il-6*, showed above. Again, these changes suggest that the loss of *Adamts1* may affect cell functionality with consequences in real *in-vivo* scenarios (**Figure 51B**).

4. ASSESSING THE CONTRIBUTION OF ADAMTS1 IN THE TUMOUR IMMUNE RESPONSE IN B16F1 AND LLC TUMOUR MODELS

Our very first findings about changes in the tumour immune infiltration where found in the development of the B16F1 melanoma model in the WT and *Adamts1* KO mouse model. Further investigation on healthy *Adamts1* KO animals shed important information about the modulation of immune populations in spleen and bone marrow, thus, revealing a modified immune landscape. Such alterations could finally impede or enhance the growing properties of a determined tumour population. To this extent, we evaluated this question using two different *Adamts1*-responding models.

According to our previous results with B16F1 melanoma and Lewis lung carcinoma mouse models (results section 1), B16F1 tumour growth was significantly blocked in *Adamts1* KO mice but LLC tumour growth was not affected (**Figure 15-16**). Hence we chose these two models to study some immune-related parameters.

With this purpose we generated B16F1 and LLC tumours in WT and *Adamts1* KO animals, as indicated above and detailed in materials and methodology section 7. At final point, spleens, bone marrow and tumours were dissected and processed for a closer evaluation. In parallel we included healthy mice to approach proper comparisons. In general, these analyses included:

- Flow cytometry:
    - Myeloid derived suppressor cells (MDSC) CD11b$^+$GR1$^+$.
    - F4/80$^+$ Macrophages.
    - CD3$^+$ T-lymphocytes.
    - CD45R$^+$ B-lymphocytes.

- Gene expression:
    - *Adamts1*, *Nidogen 1*, *Versican* and *Tgfβ,* for spleen, bone marrow and tumour samples.
    - Other immune-related genes: *Cd4*, *Arg1*, *Nos2* and *Cd163*, only for tumour samples.

4.1 SPLEEN CHARACTERISATION

In agreement with our previous results, spleens of *Adamts1* KO mice displayed a modest splenomegaly in comparison with WT animals, in the absence and/or presence of tumours, showing highest differences with LLC tumours in the *Adamts1* KO background (**Figure 52A**).

Then we analysed these spleens by flow cytometry. Common to both tumour models in WT and *Adamts1* KO, spleens from tumour-bearing mice showed a reduction of CD45R$^+$ B-lymphocytes (**Figure 52B**). CD3$^+$ T-lymphocytes were clearly impaired in *Adamts1* KO spleens, in agreement with our previous results (**Figure 46B**) that showed their increase in healthy *Adamts1* KO spleens. Now, the presence of tumours significantly reduced this population, even to similar levels of healthy spleens in the case of LLC-bearing mice (**Figure 51B**). Regarding the myeloid and macrophage populations, although very low in this organ, we just detected a significant increase of F4/80$^+$ macrophages in spleens of B16F1-bearing *Adamts1* KO mice (**Figure 52C**).
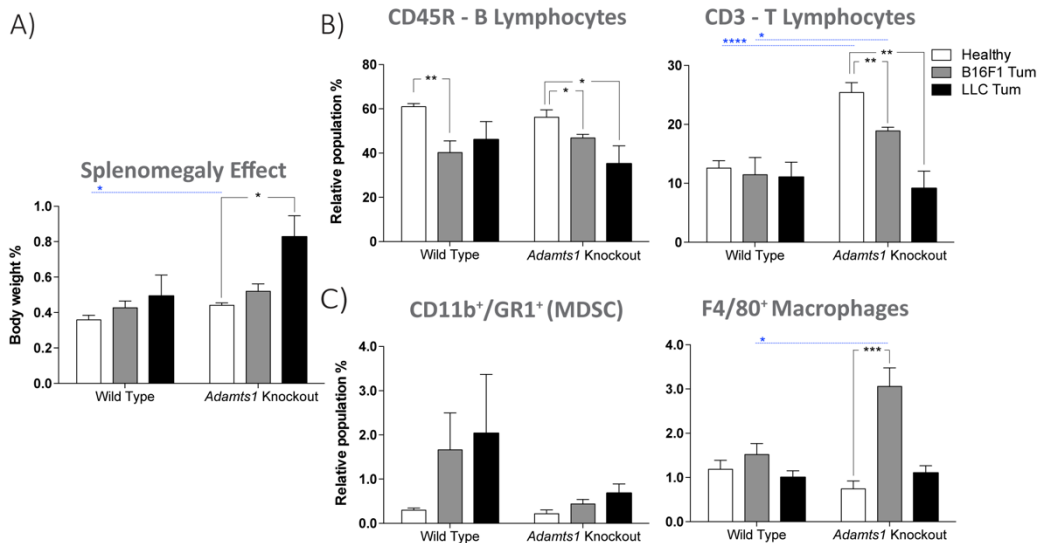
Figure 52. Macroscopic and flow cytometry analysis of WT and *Adamts1* KO spleens of healthy and tumour-bearing mice. A) Graph representing body weight percentage of spleens from healthy and tumour-bearing (B16F1, LLC) WT and *Adamts1* KO animals. B-C) Graphs representing results from flow cytometry analyses of immune populations in the spleen, including: CD45R$^+$ B-lymphocytes, CD3$^+$ T-lymphocytes, CD11b$^+$GR1$^+$ MDSC and F4/80$^+$ macrophages. Percentages are relativized to the total living cells from spleen homogenates. For statistical purposes, two comparisons have been performed. First, between spleens of healthy and tumour-bearing animals for each WT and *Adamts1* KO background (when significant, grey bars are included). Second, between spleens of WT and *Adamts1* KO for each healthy or tumour-bearing group (when significant, a dashed blue bar above the graphs is included). t-student test and SEM are represented, n = 5 samples. (*p < 0,05, **p < 0,01, ***p < 0,001).

We completed this characterization with specific gene expression analyses. For the correct interpretation of the data represented onwards is necessary to explain the two comparisons performed between the experimental groups:

- Wild type / *Adamts1* KO comparison: To evaluate differences between spleens of WT and *Adamts1* KO mice, from healthy and tumour bearing animals (B16F1 and/or LLC).

- Healthy / tumour-bearing animals: To evaluate differences between spleens of healthy and tumour-bearing mouse, from WT and *Adamts1* KO backgrounds.

Comparing healthy and tumour-bearing groups we first found a common *Adamts1* downregulation in the spleen of both tumour models, that corroborates the alteration of this organ due to the tumour growth (**Figure 53A**). As regards to the substrate *Nid1*, also a significant downregulation was observed in tumour-bearing mice. When we compared WT and *Adamts1* KO, we confirmed its upregulation in healthy *Adamts1* KO spleens (already reported in **Figure 40**), that was slightly attenuated in the tumour groups (**Figure 53A-B**). *Versican* expression displayed a different pattern for each tumour model, suggesting again the distinct "education" of distant organs depending of the primary tumour. While spleens of B16F1-bearing mice showed a clear downregulation in comparison with the healthy animal, in both WT and *Adamts1* KO backgrounds, LLC group displayed an increase, quite significant in the WT group (**Figure 53A-B**)
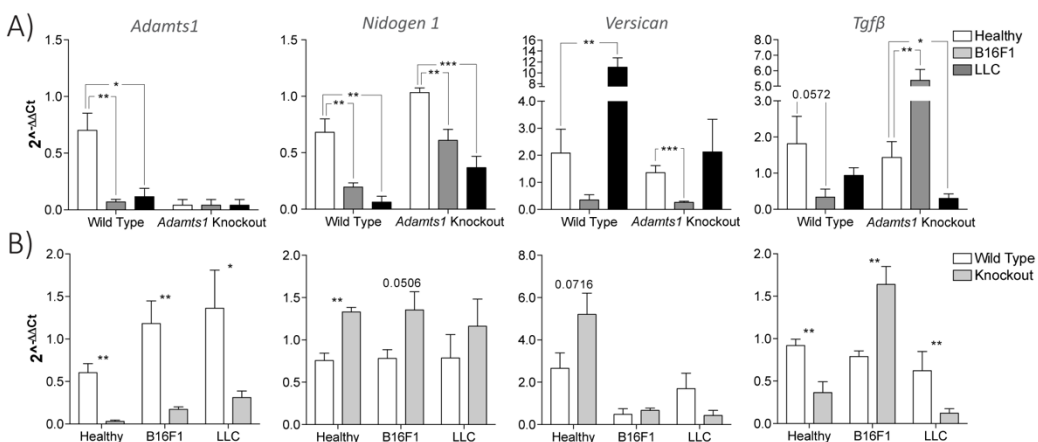
Figure 53. Gene expression analysis of WT and *Adamts1* KO spleens of healthy and tumour-bearing mice. Two comparative analyses are represented. A) Graphs represent comparison between spleens of healthy and tumour-bearing mice for each genetic background (WT and *Adamts1* KO). B) Graphs represent comparison between spleens of WT and *Adamts1* KO mice for each experimental group (healthy, B16F1-, and LLC-tumour bearing). Represented data show the $2^{-\Delta\Delta Ct}$ value. t-student test performed and SEM are represented, n = 6 samples (*p value < 0,05, **p value < 0,01, ***p value < 0,001).

Finally, *Tgfβ* gene expression was also differently regulated, evocative of its significant downregulation in healthy *Adamts1* KO spleens (**Figure 53A-B**). In this *Adamts1* KO background, the presence of B16F1 tumours provoked a significant induction in an opposite manner that LLC tumours.

As an overall of the spleen data, the accumulation of CD3$^+$ in *Adamts1* KO spleens is reduced in the presence of B16F1 tumours, more importantly in the LLC model, restoring it to WT spleen levels. We can depict a role for *Adamts1* in this organ during tumorigenesis. *Adamts1* itself is downregulated in both tumours-bearing models, but probably more important is the differential regulation of *Versican* and *Tgfβ* in response to different tumour growth.

4.2 BONE MARROW CHARACTERISATION

Our last results with the spleen demonstrated that tumour growth can alter the immune populations of a distant organ. In this line we proceeded with the analysis of bone marrow as another main immune-regulatory organ (**Figure 54**).
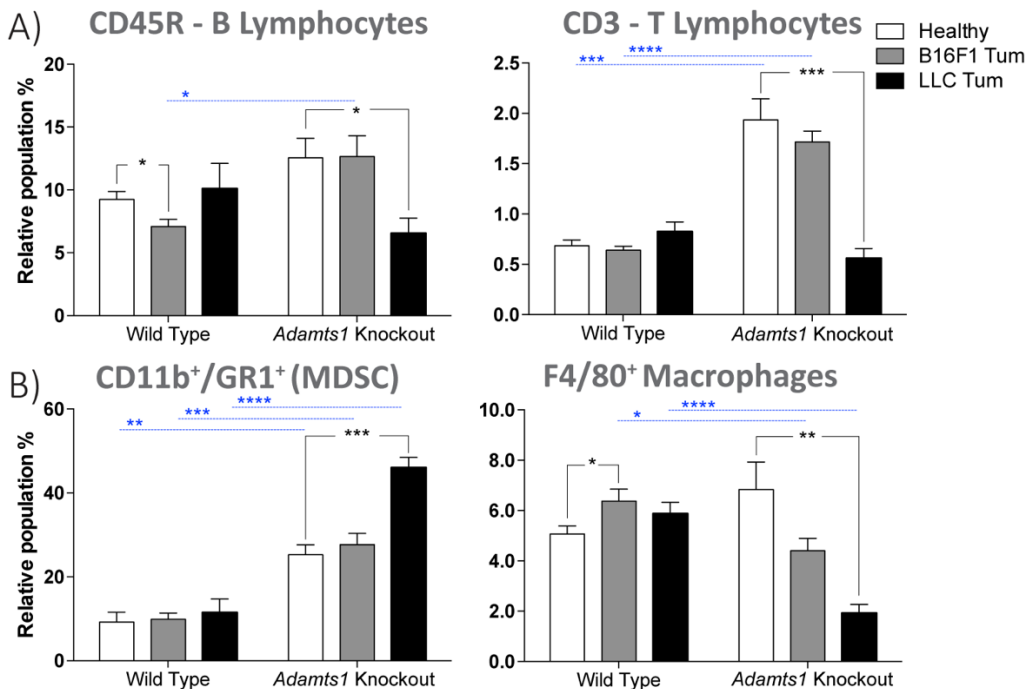
Figure 54. Flow cytometry analysis of WT and *Adamts1* KO bone marrow of healthy and tumour-bearing mice. Graphs represent immune populations in the bone marrow, including: A) CD45R+ B-lymphocytes, CD3+ T-lymphocytes, and B) CD11b/GR1 MDSC and F4/80 macrophages. Percentages are relativized to the

total living cells from bone marrow homogenates. For statistical purposes, two comparisons have been performed. First, between spleens of healthy and tumour-bearing animals for each WT and *Adamts1* KO background (when significant, grey bars are included). Second, between bone marrow of WT and *Adamts1* KO for each healthy or tumour-bearing group (when significant, a dashed blue bar above the graphs is included). t-student test and SEM are represented, n = 5 samples. (*p value < 0,05, **p value < 0,01, ***p value < 0,001, ****p value <0,0001).

Now, flow cytometry analyses of CD45R$^+$ B-lymphocytes, although slightly affected, do not display a clear pattern in relation to the loss of *Adamts1* or the progression of different tumours. However, CD3$^+$ T-lymphocytes, which increase was already indicated in *Adamts1* KO healthy bone marrows (**Figure 48**), were significantly downregulated in LLC-bearing mice in this KO background (**Figure 54A**).

Also, as previously described for healthy mice, our data already suggested an immunosuppressive shift in the bone marrow of *Adamts1* KO mice in comparison with WT (**Figure 47**). Very importantly, the presence of LLC tumours magnified such differences in the *Adamts1* KO background (**Figure 54B**). However, F4/80$^+$ macrophages were altered in an opposite direction (**Figure 54B**).

Again, this characterization was completed by gene expression analyses, including similar comparisons as indicated for spleens. Importantly, *Adamts1* showed a similar downregulation in tumour-bearing groups (**Figure 55A**). For *Nidogen 1* we observed an interesting normalization of its expression in bone marrow of WT and *Adamts1* KO B16F1-bearing mice (**Figure 55A**), in comparison with the described downregulation that occurred in *Adamts1* KO healthy mice (**Figure 40 and 55B**), and confirmed in the LLC model (**Figure 55A**).
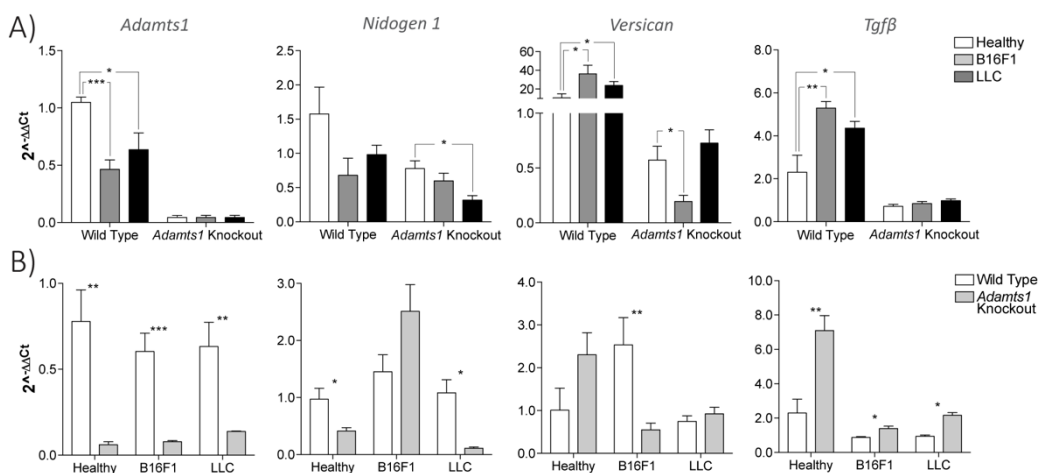
Figure 55. Gene expression analysis of WT and *Adamts1* KO bone marrow of healthy and tumour-bearing mice. Two comparative analyses are represented. A) Graphs represent comparison between bone marrows of healthy and tumour-bearing mice for each genetic background (WT and *Adamts1* KO). B) Graphs represent comparison between bone marrow of WT and *Adamts1* KO mice for each experimental group

(healthy, B16F1-, and LLC-tumour bearing). Represented data show the $2^{-\Delta\Delta Ct}$ value. t-student test performed and SEM are represented, n = 6 samples. (*p value < 0,05, **p value < 0,01, ***p value < 0,001).

Once more, *Versican* expression revealed significant differences between healthy and each tumour model, more striking for B16F1-bearing mice. While this substrate is upregulated in the bone marrow of WT mice, the *Adamts1* KO bone marrow displayed an opposite and significant downregulation when B16F1 tumours are present (**Figure 55A-B**). Finally, the expression of *Tgfβ* was positively regulated in tumour-bearing models in comparison with bone marrow of healthy mice just in a WT background (**Figure 55A-B**).

The overview of our bone marrow data supports the relevant shift towards an immunosuppressive scenario in the LLC tumour model, mostly in *Adamts1* KO mice, showed by the increase of a MDSC but also magnified by the decrease of CD3$^+$ T-lymphocytes. The downregulation of *Adamts1* and upregulation of *Versican* and *Tgfβ* could also support this immunosuppressive environment.

4.3 TUMOUR CHARACTERISATION

In addition to the previous sections, that provided a relevant input regarding the distinct "educational" contributions of each tumour model in distant organs as spleen and bone marrow, we finally analysed the immune infiltration differences in B16F1 and LLC tumours, also concerning their genetic background, WT or *Adamts1* KO.

Our first flow cytometry data already indicated very interesting differences. Although CD45$^+$ B-lymphocytes showed no differences (in fact its low abundance was near irrelevant), CD3$^+$ T-lymphocytes were significantly more infiltrated in B16F1 tumours, even more in the *Adamts1* KO scenario (**Figure 56A**). In the other side, LLC tumours displayed a significantly higher infiltration of CD11b$^+$GR1$^+$ MDSC in both WT and *Adamts1* KO backgrounds. Finally, F4/80$^+$ macrophages, also very importantly infiltrated in LLC tumours, were diminished in *Adamts1* KO mice (**Figure 56B**). In general, these results would support the differences in tumour growth that we observed in these two models, but our final gene expression analysis could help us.
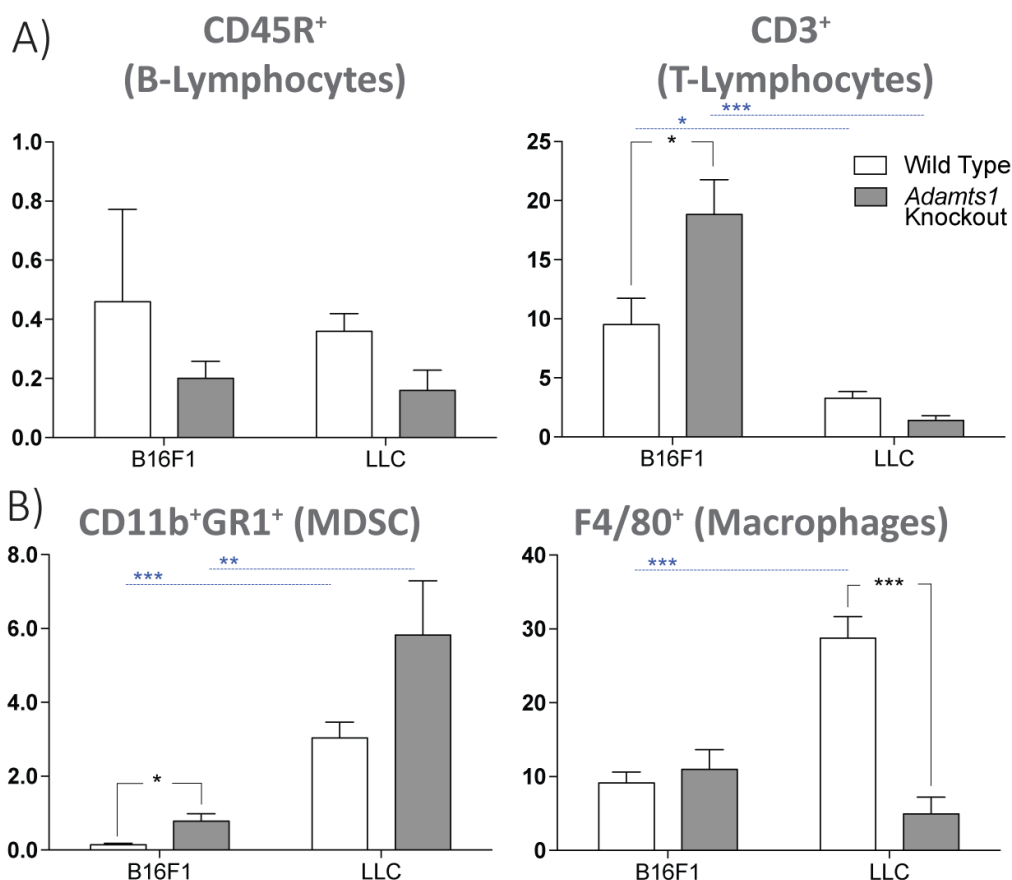
Figure 56. Flow cytometry analysis of WT and *Adamts1* KO tumours. Graphs representing results of immune populations in tumours, including: A) CD45R+ B-lymphocytes and CD3+ T-lymphocytes, and B) CD11b/GR1+ MDSC and F4/80+ macrophages. Percentages are relativized to the total living cells from tumour homogenates. For statistical purposes, two comparisons have been performed. First, between tumours of WT and *Adamts1* KO mice for each model (B16F1, LLC). Second, between B16F1 and LLC tumours for each WT and *Adamts1* KO background (when significant, a horizontal-dashed blue bar above the graphs is included). t-student test performed and SEM are represented, n = 5 samples (*p value < 0,05, **p value < 0,01, ***p value < 0,001).

Then, in an attempt to complement these valuable findings, we approached the evaluation of several immune-related molecules by gene expression analysis. The evaluation of *Cd4*, according to its relevance in T-regulatory cells and the recruitment of cytotoxic T-cells, showed a significant upregulation in B16F1 tumours in *Adamts1* KO mice (**Figure 57A**), in full agreement with flow cytometry data with CD3 marker. Related to classically-activated macrophages, we analysed *Nos2*, but it did not reveal major changes (**Figure 57A**). As for alternatively-activated macrophages, we considered both *Arg1* and *Cd163*. Significantly, both genes were upregulated in LLC tumours, but just in a WT background, although a similar tendency was observed for *Cd163* in *Adamts1* KO

mice (**Figure 56A**). These last two genes were in agreement with a pro-tumorigenic environment suggested in the LLC model.
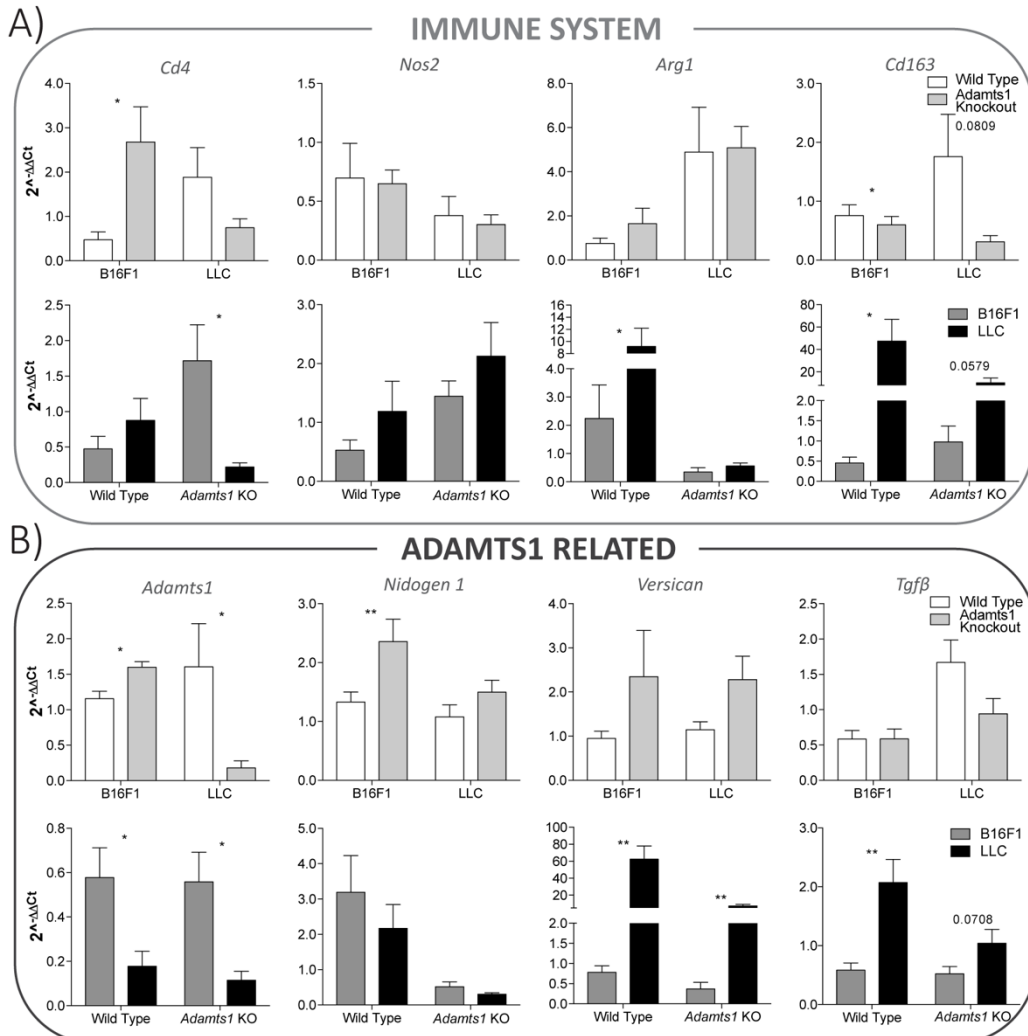
Figure 57. Gene expression analysis of B16F1 and LLC-derived tumours in WT and *Adamts1* KO mice. A quantitative PCR analysis for two panels of genes: A) *Cd4*, *Arg1*, *Nos2* and *Cd163*. B) *Adamts1, Nidogen 1*, *Versican* and *Tgfβ*. Two comparisons have been performed. Upper panels show comparison between WT and *Adamts1* KO mice for each tumour group. Lower panels show comparison between B16F1 and LLC tumours for each WT and *Adamts1* KO background. The represented data show the $2^{-\Delta\Delta Ct}$ value. t-student test performed and SEM are represented, n = 6 samples (*p value < 0,05, **p value < 0,01).

Our final studies included the gene expression of *Adamts1* and related genes, as approached for spleen and bone marrow. Although it is also included here, we previously reported the upregulation of *Adamts1* expression in B16F1 tumours in the *Adamts1* KO mice, suggesting its induction in B16F1 tumour cells, probably by hypoxia (**Figure 20 and 57B**). On the contrary LLC tumours showed the expected downregulation in the *Adamts1*

KO background (**Figure 57B**). As for the expression of substrates, Nidogen 1 and versican, at this point we just wanted to highlight the more important expression of versican in LLC tumours, a similar finding to the highest relevance of *Tgfβ* in this same tumour model (**Figure 57B**).

A final compilation of the immune infiltration and gene expression data supports in general a prone-immunosuppressive scenario in the LLC model, importantly corroborated with the increasing amount of versican. On the contrary, a pro-inflammatory landscape is associated with B16F1 tumours, significantly induced in *Adamts1* KO mice, so supporting the relevant reduction of tumour size and volume. Furthermore, the F4/80[+] population in the LLC model could exert a immunosuppressive features (Bronte et al., 2000) but without further characterisation (identification by MHC II or CD163 markers) they cannot be identified as TAMs.

DISCUSSION

The current research in tumour biology has demonstrated the rising relevance of the tumour microenvironment (TME). This is a highly dynamic constituent which participates during numerous processes as angiogenesis, inflammation, migration, invasion and differentiation (Hanahan et al., 2011). In addition to tumour cells, the TME is composed by stromal cells of different nature and non-cellular components provided by both tumour and stroma. Within the non-cellular compartment of the TME we find multiple extracellular matrix (ECM) components, forming a network that serves as a multifunctional scaffold for the surrounding cells, but also includes extracellular proteases, which actively contribute to the dynamism of this environment. Within the extracellular proteases there are several families of remarkable interest: MMPs, ADAMs and ADAMTSs. Our research group has focused in the study of the first discovered member of this last group, A Disintegrin And Metalloprotease with ThromboSpondin motif 1 (ADAMTS1), which contributions comprise angiogenic modulation and tumour progression (Rodríguez-Manzaneque et al., 2015).

With the eagerness to reveal the functions and biological relevance of proteases, the "Degradome Project" started more than 15 years ago (López-Otín and Overall, 2002). This ambitious venture tried to recapitulate every protease substrate, that includes its processing in a biological context. Regarding the proteolytic activity of ADAMTS1 and its role within the TME, it has not been fully characterised. Therefore, we aimed to study the activity of ADAMTS1 on various substrates and their deposition in the tumour perivascular area, including the understanding of their contribution during tumour progression. More precisely, this thesis has focused in Nidogen 1, Nidogen 2 and Versican. Both Nidogens are part of the vascular basement membrane (vBM) but are also found in the tumour stroma (Ho et al., 2008), and Versican has been reported by its significance in various ECMs with implications in cancer and inflammation (Gorter et al., 2010; Ricciardelli et al., 2009). Although their relationship with the perivascular environment have been reported, the consequences of their cleavage by proteases as ADAMTS1 remain unknown.

The *Adamts1* knockout mice has become a very useful tool since the first model was developed (Shindo et al., 2000). A deep characterisation of these animals was assessed by several research groups, and severe defects were described. The most conspicuous were related to the ovarian function, revealing that *Adamts1* null females are infertile, and also they present complications in the renal-urogenital system (Lee et al., 2005; Mittaz et al., 2004). Indeed, its contribution to the cleavage of certain molecules in the stroma of different organs has not been evaluated so it turns out to be one of the principal aims of our research group.

Since the discovery of ADAMTS1, this protease has been linked to inflammation processes (Kuno et al., 1997a). The human orthologue was reported as a potent anti-angiogenic molecule (Luque et al., 2003; Vázquez et al., 1999) and its role during endothelial sprouting initiation was also described (Su et al., 2008). Additionally, various reports showed its dual role in the promotion of tumorigenesis (Fernández-Rodríguez et al., 2016; Lee et al., 2006b; Martino-Echarri et al., 2013) and its genetic regulation by several interleukins and the interaction with other cytokines already pave the way to keep investigating the functional role of this protease within the immune landscape (Bourd-Boittin et al., 2011).

Importantly, our own studies showed alterations of the vasculature, but also in tumour immune infiltration, in a syngeneic tumour model with wild-type and *Adamts1* knockout mice (Fernández-Rodríguez et al., 2016). With these precedents, this thesis followed studies in *Adamts1* deficient scenarios including different tumour models and approaches to examine the immune cell landscape of healthy animals.

1. ACTIONS OF ADAMTS1 IN THE VASCULATURE OF DIFFERENT TUMOUR MODELS

The contribution of ADAMTS1 to angiogenesis has been studied for a long time. This protease was first described to be an antiangiogenic molecule by its VEGF binding and sequestering properties, with stronger effects than recognised inhibitors as Thrombospondin-1 and Endostatin (Luque et al., 2003). Interestingly, knocking down the expression of *Adamts1* blocked the *in-vitro* sprouting activity of ECs. These authors reported a peak expression at short times when the EC tip cell was invading the tissue (Su et al., 2008). Such findings are just representative of the dual role of this protease during angiogenesis.

In a tumour context, the expression of *Adamts1* and its relationship with the vascular network have been evaluated in several settings. In a prostate cancer model, the low expression of the protease were associated with small diameter blood vessels, and inversely correlated with an upregulation of *Tsp1* (Gustavsson et al., 2010). In another model -included in this thesis-, tumour progression in the MMTV-PyMT murine breast cancer model was decreased in *Adamts1* KO animals but without vascular differences (Ricciardelli et al., 2011). Our own studies with this model confirmed the absence or relevant changes in vascular related parameters. In addition, this thesis included two syngeneic models, B16F1 melanoma and Lewis lung carcinoma (LLC), that allowed the evaluation of tumour progression in an *Adamts1*-free environment. Interestingly, only B16F1-derived tumours in *Adamts1* KO mice portrayed a significant reduction in the tumour size and volume, accompanied by an increase of tumour vessel density but with reduced vessel perimeter. On the other hand, tumour progression of LLC model was not compromised in *Adamts1* KO animals but, also opposite to B16F1 tumours, their vascular density was reduced in such *Adamts1* deficient scenario. Comparing the differences between our B16F1 and LLC models, we should highlight that LLC cells and derived-tumours have a lower tumour *Adamts1* expression and this could be one of the multiple drivers of its distinct tumour growth performance. Highlighting such heterogeneity, our results also confirmed that *Versican* expression and deposition within the TME is much higher in the LLC model, together with meaningful shifts in their respective immune-related landscapes that will be discussed below. Surely further gain- and loss-of-function experiments with *Adamts1* itself and its substrates within the tumour models would help to unveil these differences. Finally, our human uveal melanoma xenograft model supported an anti-tumour and antiangiogenic role for ADAMTS1 in this specific context, taking into consideration that the downregulation of *Adamts1* was managed exclusively in tumour cells.

In addition to these studies about vascular patterning in our *Adamts1*-dependent tumour models, we also approached the vasculogenic mimicry (VM) phenomena. These events were first described for human melanoma tumours (Hendrix et al., 2003; Maniotis et al., 1999; Seftor et al., 2001), reporting the ability of melanoma cells to form *de-novo* pseudovascular structures connected to the normal vasculature and thus contributing to tumour perfusion (Goel et al., 2011). Parallel studies revealed the plastic properties of tumour cells *in-vitro*. Indeed, certain tumour cells have the ability to mimic the formation of capillary-like networks *in-vitro* (Maniotis et al., 1999). Regarding our tumour models, the endothelial-like plasticity of human uveal melanoma MUM2B cells was already demonstrated (Maniotis et al., 1999), and we confirmed here such ability for murine B16F1 melanoma. In our hands, LLC and PyMT cell lines did not display the mentioned capillary-like plasticity.

All our tumour models were assessed for gene expression of markers related to VM, such as *EphA2* and *LamC2* (Hess et al., 2001), finding a significant induction just in B16F1-derived tumours in *Adamts1* KO mice. As another approach, we generated tumours in WT and *Adamts1* KO mice with B16F1-GFP[+] and LLC-GFP^{+} cells. According to our rationale, we expected to identify vascular structures, using endothelial markers as CD31 and/or VE-CAD, co-localised with the GFP tumour signal. Indeed, we observed such VM events within both tumour models, much more frequent in B16F1-derived tumours, in agreement with its capillary-like abilities *in-vitro*. The existence of this phenomenon was also confirmed by flow cytometry analyses of B16F1 tumours, and in fact we detected a slight increase of double CD31^{+}/GFP^{+} signals in tumours from *Adamts1* KO mice. As introduced above, the absence of stromal *Adamts1* in the B16F1 model increased vessel density and also induced the expression of tumour *Adamts1* (Fernández-Rodríguez et al., 2016) that, somehow, correlates now with the slight increment of the VM[+] cases. Although the contribution of *Adamts1* to tumour cell plasticity was already reported by this same research group (Casal et al., 2010), its specific role depending of its stromal and/or tumour origin still requires further research.

Nevertheless, the identification of VM positive vessels has been debated since its discovery (Maniotis et al., 1999) and continues being a fascinating field of exploration to improve current antiangiogenic therapies (Dunleavey et al., 2014; Hendrix et al., 2016; Lai et al., 2012).

2. THE TUMOUR PERIVASCULAR NICHE

Within the study of the tumour stroma, recent research reported a different TME composition between the primary tumour and invading tissue. Indeed, ECM components of the metastatic niche were more similar to the primary tumour rather than the host tissue (Naba et al., 2014). The status of the ECM regulates functions as proliferation, invasiveness, sustained angiogenesis, etc. (Pickup et al., 2014). Within the ECM, the vBM is a very specialised matrix that lays on the surface of blood vessels, and it is mainly created by endothelial and vascular supporting cells (Bhowmick et al., 2004). In a tumour context, cancer cells have the ability to modify the behaviour and secretome of stromal cell as fibroblasts, macrophages and endothelial cells, which stands the importance of their continuous cross-talk (Bissell and Hines, 2011; Lu et al., 2011). As a consequence, alterations in the vBM would affect its properties as a physical barrier but also its contribution as modulator of cell behaviour and recruitment (Kalluri, 2003).

Extracellular proteases as ADAMTS1 have important roles in the modification of vBM components and the regulation of these proteases are also under a tight control during tumorigenesis. In this scenario, the remodelling and deposition of ECM components, as Nidogens and Versican, have not been a major focus. In fact, our characterisation of the different tumour models included a deeper insight of these molecules.
Significantly, the downregulation of *Adamts1* in all tumour models showed an increased deposition of Nidogen 1 in the vBM. However, we did not find differences in its cleavage, suggesting the participation of additional proteases. On the contrary, the assessment of Nidogen 2 deposition within the vBM did not show relevant results, although its low abundance probably influenced these evaluations.

Another important ECM component with differential deposition in perivascular areas is Versican. Directly related with the absence of stromal *Adamts1*, we observed an unexpected Versican decreased deposition in the TME, and also for its fragment Versikine, in both the breast cancer (already described by Ricciardelli et al.,2011) and the B16F1 model. Although the lower presence of the fragment Versikine could be associated with the lack of *Adamts1*, the finding that the intact Versican is also diminished could be associated to the existence of alternative mechanisms of degradation. With a different output, our uveal melanoma model displayed a higher deposition of Versican, but also Versikine, when tumour *Adamts1* is downregulated. Indeed, this case suggests the participation of additional proteases, but with a similar cleavage specificity. These observations may also relate with the fact that stromal *Adamts1* is not modified in this scenario. Finally, the unique setting that showed an

increased deposition of Versican together with a decrease of the fragment Versikine is the LLC model in the *Adamts1* KO mice, supporting a direct and unique activity of ADAMTS1. Looking at the literature, *Versican* upregulation has been demonstrated in lung cancer, melanoma and gliomas. These studies demonstrate the correlation between the higher accumulation of Versican in the stroma with tumour recurrence and a more advanced disease, also in line with our results found in the breast cancer and the B16F1 models (Onken et al., 2014; Pirinen et al., 2005; Touab et al., 2002).

Trying to elucidate the role of vBM components as Nidogens in tumour biology, we performed a gain-of-function approach by overexpressing these molecules in B16F1 cells, which lack expression. Although proliferation and migration properties were not altered in general, we observed that *Nidogen 1* overexpression decreased *in-vitro* adhesion to Fibronectin, Collagen I and Poly-L-lysine, whereas *Nidogen 2* overexpression enhanced these characteristics. According to the literature, both molecules differ in their abilities to bind certain components of the ECM. For example Nidogen 1 binds Fibulins whereas Nidogen 2 cannot (Kohfeldt et al., 1998; Salmivirta et al., 2002). Interestingly, when the *in-vitro* capillary-like forming abilities were assessed, both *Nidogen* overexpressing cell lines altered the capacities to form capillaries in comparison with controls, observing a relevant inhibition of tip-like cells. A previous work using *Dll4*$^{+/-}$ mutants demonstrated a common overexpression of *Adamts1* and *Nidogens* in tip cells, (del Toro et al., 2010), suggesting that a balance of Nidogen deposition is necessary to keep the tip-endothelial cell migratory properties.

In line with the *in-vitro* findings, the analysis of our *Nidogen 1* overexpressing tumour model showed a severe tumour reduction, while *Nidogen 2* overexpression did not differ from the controls. Interestingly, this effect observed with the *Nidogen 1* overexpressor directly relates with tumour and vasculature impairment previously observed in B16F1-derived tumours in *Adamts1* KO mice. At this point we should recall the accumulation of endogenous Nidogen 1 found in their tumour vessels. In addition, the analyses of tumour vasculature showed similar vascular density increases in the *Adamts1* KO groups in comparison with WT, in agreement with our published results (Fernández-Rodríguez et al., 2016).

The increase of Nidogens in the vBM also was accompanied by an accumulation of Collagen IV in both WT and *Adamts1* KO tumours (**Figure 57**), probably due to their crosslinking properties. This kind of alterations could affect vessel integrity, but in our studies, the increased deposition of Collagen IV correlated with a deficient vasculature just in conjunction with Nidogen 1, but not with Nidogen 2. Therefore, although collagen

IV has been recognized as a double-edged ECM component, driving tumour progression in some cases (Fang et al., 2014), our findings highlight the likely contribution of further ECM components, as Nidogen 1 here. Accordingly, additional investigations are required.
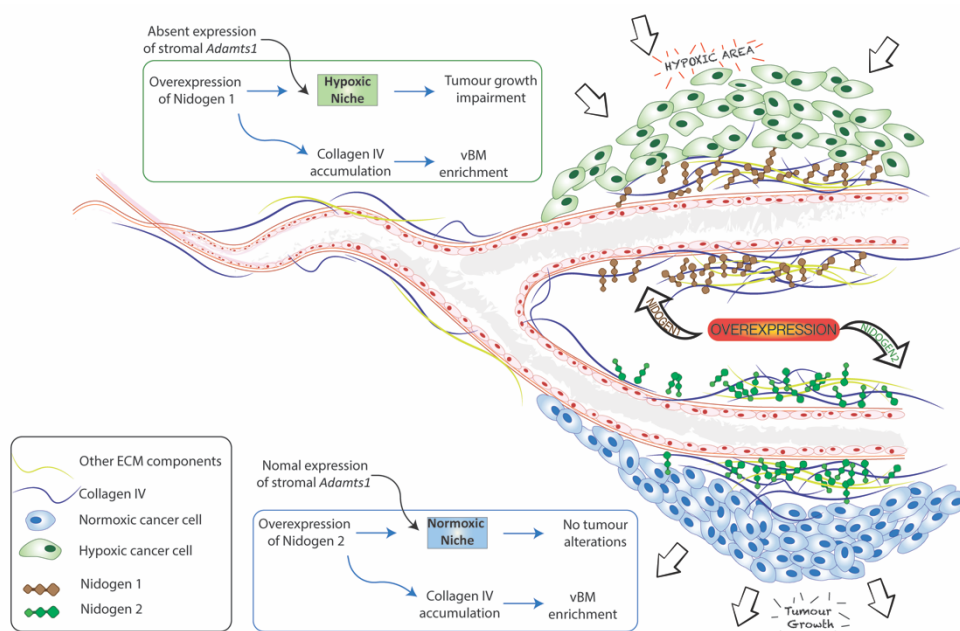
Figure 58. Representation of the Nidogen increase in the tumour perivascular niche and its consequences. The overexpression of *Nidogens* in a B16F1 mouse melanoma was associated with an accumulation of Collagen IV in the tumour vBM but this effect was not linked with changes in tumour vascular parameters in both *Nidogen* overexpressors. However, the increased deposition of NID1, but not NID2, corresponded with a hypoxic niche and also with an impaired tumour growth.

In recent studies of colorectal cancer, authors report an increase of some vBM components after antiangiogenic treatments in human patients and mouse models. They proposed that tumour hypoxia appeared to be the driving force of these changes, in relation to the acquisition of resistance-episodes (Rahbari et al., 2016; Stylianopoulos et al., 2013). In consonance with our findings we finally evaluated hypoxia on our *Nidogens* overexpressing tumours, to assess the functionality of their vasculature. *Nidogen 1* overexpressing tumours showed increased levels of hypoxia in the bulk of the tumour and, particularly blood vessels were closely surrounded by hypoxic areas (**Figure 58**). This last finding clearly supports the reduction of the tumour size observed in the *Nidogen 1* overexpressor in WT animals, indeed correlating with our findings in the *Adamts1* KO mice. Also it contributes to the idea of Nidogens as molecules involved in the development of a proper vascular network.

Former reports by our group also showed the importance of the deposition of Nidogens in the tumour vBM in an *Adamts1* overexpressor model (Martino-Echarri et al., 2013). This approach showed a loss of Nidogen deposition in the tumour vBM when *Adamts1* was overexpressed, also reducing vascular density and affecting size and vessel diameter in this case. All our findings together suggest the relevance of maintaining a tight equilibrium of these molecules, Nidogens and ADAMTS1, for the correct formation of vascular structures. Moreover relevant for us, it was reported that the ablation of *Nidogen 2,* but not *Nidogen 1,* in a mouse model, ended in a reduction of metastasis with a B16F1 mouse melanoma model, supporting a tumour protective role for these vBM components (Mokkapati et al., 2012). Unfortunately, this work does not look closely at the vasculature.

3. ADAMTS1 RELEVANCE IN THE MOUSE PHYSIOLOGY

The *Adamts1* null mouse has been investigated for almost two decades now. Although the four known models were developed independently, the most relevant phenotypic changes have been confirmed in all of them. The first observations incurred in the urogenital system, focusing in the ovarian function and also the kidney physiology (Shindo et al., 2000).

With the exception of the ovary (Brown et al., 2010), the mechanisms underlying the defects found in the *Adamts1* KO mouse model have not been deeply investigated. Hence, we wanted to assess the overall contribution of *Adamts1* by analysing adult organs, focusing now in the evaluation of the vasculature and the study of specific substrates mostly related with the vBM. For this we collected a series of organs: brain, lung, kidney, heart, ovary, spleen and bone marrow, properly processed for our goals. Our first studies did not show significant changes in the vascular density or further vascular-related parameters. Still, in agreement with a report that shows a reduction of the size of large blood vessels in the ovary of *Adamts1* KO mice (Shozu et al., 2005), we observed something similar but without statistical significance.

A brief discussion about our gene and protein analyses from WT and *Adamts1* KO tissues follows next. For example, *Adamts1* KO kidneys, which dysfunction has been already recognized (Shindo et al., 2000), discloses a delocalisation of Nidogen 1 from the ECM in comparison with the WT organ. Moreover, WB analysis indicates a higher processing of the protein, being the G1 fragment highly accumulated in *Adamts1* KO, suggesting the contribution of additional proteases, maybe as a compensatory mechanism. Likewise, these alterations could be a consequence of the abnormal development of this organ. It is important to remark the highly specialised vBM found in the kidney glomerulus (Tanjore and Kalluri, 2006). In fact, *Adamts1* and its endogenous inhibitor *Timp3*, have been found to play a relevant role for the development of a correct BM in kidney (Schrimpf et al., 2012). In line with our results, the control of the proteolytic balance of Nidogens in the *Adamts1* KO animal is therefore altered, with major consequences for the functionality of organs, as showed here for kidney.

In relation to spleens, we found a relevant upregulation of *Nidogen 1* in *Adamts1* KO mice, but not corroborated by its immunoanalysis. In fact, *Adamts1* KO spleens showed an increase of the G2-G3 and G1 cleavage, denoting a relevant (and unknown so far) alteration of this organ. Indeed, there is a higher accumulation of Versican in *Adamts1*

KO spleens. Importantly, our results within this organ deserved further discussion in next section.

Finally, hearts from *Adamts1* KO mice showed a decreased expression of both *Nidogens*, but again, we did not find a corroboration with protein studies. Although the basal expression of Versican is very low in this organ, we detected a relevant increase of its fragment Versikine in WT mice, encouraging deeper studies. In this context, it is necessary to mention that *Adamts1* has already been implicated during heart morphogenesis (Stankunas et al., 2008) but not in the adult life.

4. ADAMTS1 AS A MODULATOR IN THE IMMUNE SYSTEM

Since the discovery of *Adamts1* in a cachexia model, several reports keep a constant link of this protease with the immune system. For instance, *Adamts1* is found to be under the regulation of interleukins as *Il-1β* (Kuno et al., 1997a) and *Tgfβ* (Bourd-Boittin et al., 2011). We also reported its downregulation associated to a different tumour immune infiltration in a B16F1 melanoma model (Fernández-Rodríguez et al., 2016). Indeed, we showed here studies with adult mice that reveal preliminary but very interesting data. To illustrate, gene expression analyses showed a relevant upregulation of myeloid macrophage markers (*Cd11b* and *F4/80*) in *Adamts1* KO ovary, spleen and bone marrow. The fact that these two last organs are important immune regulators strongly denotes the importance of *Adamts1* in this new scenario for us. Another interesting work reported significant levels of ADAMTS1 in interstitial fluid of spleens, lymph nodes and plasma after a systemic lipopolysaccharide-induced inflammation (Oveland et al., 2012).

All these findings led us to a deep evaluation of the wild type and *Adamts1* KO mouse spleens. First, we observed a modest splenomegaly in *Adamts1* KO animals in relation to its body weight. Splenomegaly is normally caused by diseases and malignancies such as cirrhosis, viral or bacterial infections, or the existence of tumours. At a cellular level, our studies revealed a significant increase of CD3$^+$ T-lymphocytes in such *Adamts1* KO spleens, although it could be associated to the splenomegaly. Furthermore, our gene expression data support the increase of the T-lymphocyte population, as *Cd4*, *Cd8* and *Cd45* genes are upregulated. Interestingly, this accumulation is accompanied by a reduction of CD11b$^+$ cells, but the importance and abundance of this myeloid macrophage-related population in the spleen is minor. Indeed, the downregulation of *Tgfβ* in the spleen niche, and the deregulation of some other cytokines as *Il-6* and *Il-10*, illustrated in general an altered landscape in the *Adamts1* KO spleen, more prone to inflammation. It is also relevant to mention that TGFβ has a dual role in driving inflammation depending of the niche or environment (Han et al., 2012; Meulmeester and ten Dijke, 2011).

As showed, we approached a parallel evaluation of the bone marrow. In this case we found a clear enrichment of immunosuppressive-related CD11b$^+$ and CD11b$^+$GR1$^+$ cells, addressed as myeloid derived suppressor cells (MDSC), in *Adamts1* KO mice (Bronte et al., 2000). The differentiation and enrichment of MDSC has been attributed to a high presence of granulocyte macrophage colony-stimulating factor (GM-CSF) (Gargett et al., 2016), but we did not measure its levels in our models. Very interestingly, GM-CSF expression is associated to fibroblasts and endothelial cells (Boettcher et al., 2014), cell

types that could be targeted by the loss of *Adamts1* in the bone marrow niche. In addition, our gene expression profile shows an upregulation of *Tgfβ* and a downregulation of the inflammatory cytokine *Il-6* in *Adamts1* KO bone marrows, supporting again the shift to an immunosuppressive niche (**Figure 59**). Finally, we detected a *Nos2* gene upregulation in this same scenario, relevant to induce a macrophage polarisation towards the classical activation pathway that also correlates with the MDSC accumulation.

As reported, we also approached the *in-vitro* polarisation of bone marrow-derived macrophages from WT and *Adamts1* KO mice. While no relevant changes were observed in adhesive properties, cytoskeleton distribution, neither in the efficiency of the polarisation process, our gene expression analyses found an upregulation of *Nidogen 1* in both classical and alternatively polarisation. As for *Versican*, we confirmed its upregulation in the classically activated pathway, as already described (Chang et al., 2014). Furthermore, the comparison of WT and *Adamts1* KO classically activated macrophages shows a gene expression downregulation of *Versican*, *Il-6* and *F4/80*, indicating a differential potential of these cells in a real scenario, finding that is being currently studied in our group.

Interestingly, we described for the first time that the loss of *Adamts1* affects the functionality of immune organs as spleen and bone marrow. Particularly motivating appears the increase of the MDSC population with immunosuppressive activities, which consequences are still to be evaluated. For instance, the connection of these data with our tumour studies is appealing, so it is discussed in next section. Indeed, the increase of this MDSC population is known to be stimulated by VEGF (Voron et al., 2014, 2015), so we need to recall the VEGF-sequestering properties of *Adamts1* (Luque et al., 2003) (**Figure 59**).

5. ADAMTS1 AND THE TUMOUR IMMUNE INFILTRATION

The role of extracellular proteases as MMPs, ADAMs and ADAMTSs in the TME has been widely studied. Their multiple roles, including proteolytic and non-proteolytic functions, are becoming an important concern when researchers want to look at the tumour immune infiltration. In this scenario, the activity of extracellular proteases on ECM components can modulate a relevant niche for immune responses or have an effect on the differentiation and maturation of different immune subpopulations. For example, recent findings support the existence of functional fragments of ECM molecules (also referred as Matrikines) (Maquart et al., 2004), with a wide variety of biological functions, including modulation of the immune system and angiogenesis (Arroyo and Iruela-Arispe, 2010).

As described in previous sections, we unexpectedly observed an altered immune profile in the absence of *Adamts1* in a healthy murine model, highlighting already the immunosuppressive-like landscape in the bone marrow. Such immunosuppressive setting can trigger different mechanisms that would affect the tumour immune infiltration with consequences for tumour progression. It has been shown by other researchers that there is an accumulation of MDSC in the bone marrow of tumour-bearing mice in comparison with healthy individuals (Shojaei et al., 2007; Srivastava et al., 2012). Our results suggest that the downregulation of *Adamts1* in immune-related distant organs, provoked by the presence of tumours, would have major consequences, including the generation of a pro-inflammatory microenvironment in spleen and an immunosuppressive in the bone marrow. However, the different nature of our tumour models would imply a distinct regulation of *Adamts1*, within the TME but also in distant organs, mechanisms which could favour or impede immune infiltration.

For these studies we selected two tumour models, B16F1 and LLC, which progression in *Adamts1* KO mice was completely different. While B16F1 tumour growth was clearly impaired in the absence of stromal *Adamts1*, LLC tumours appeared normal, progressing in a similar manner in WT and *Adamts1* KO mice. Therefore, this parallel study could unveil mechanistic insights about *Adamts1* actions. According to our findings, we hypothesized that B16F1 tumour impairment in *Adamts1* KO mice is driven by their vascular phenotype (Fernández-Rodríguez et al., 2016), together with its differential immune infiltration. In fact, we detected an increase of CD3$^+$ T-cells in these *Adamts1* KO tumours, favouring the development of a pro-inflammatory environment that probably contributes to a tumour blockade. On the other hand, in the LLC model we find

a different immune scenario, more prone to an immunosuppressive landscape, thus, favouring tumour progression.
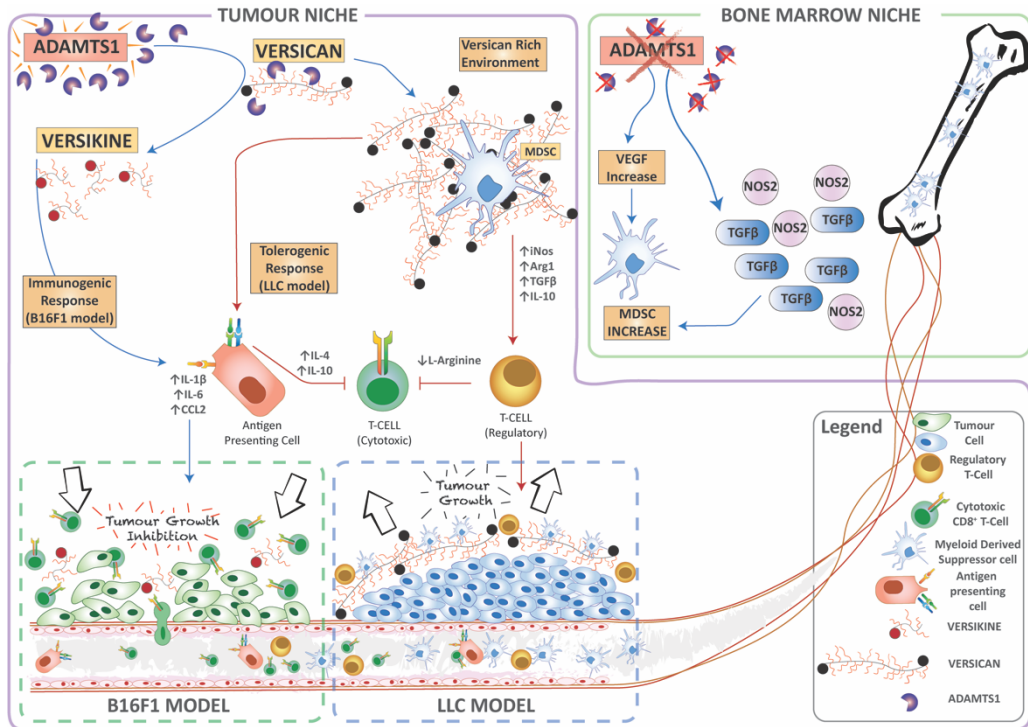
Figure 59. Representation of the bone marrow *Adamts1* KO niche and the tumour microenvironment. The absence of *Adamts1* in the bone marrow niche can increase the availability of VEGF which can drive the increase of MDSC. Also an upregulation of *iNos/Nos2* and *Tgfβ* are found in this environment. In the tumour niche ADAMTS1 can cleave VCAN and generate VKIN, which activate APCs via TLR2 and MAP receptors, provoking a production of IL-1β, IL-6 and CCL2 and would end up attracting CD8^{+} T-cells that would generate an immunogenic response against the tumour. The VCAN full length serve as an immune bed for infiltrating MDSC, a population that can control T-regs and thus inhibit the T-cell response in the tumour. Also, VCAN is known to interact with APCs via TLR2, provoking a switch in the interleukin production (IL-4 and IL-10), controlling also the cytotoxic T-cell subset.

The gene expression profile also reflects a higher *Adamts1* expression in B16F1 tumours, even in the absence of stromal *Adamts1*, which could finally modify the cleavage of Versican to produce Versikine in this microenvironment. The immunogenic competences of this fragment would relate with the attraction of CD8^{+} T-cytotoxic cells that would stop tumour progression (Hope et al., 2016). However, LLC tumours seem to be enriched in VCAN, in agreement with the lower *Adamts1* expression. Here, VCAN serves as an immune bed for MDSC, as already reported (Gao et al., 2012) (**Figure 59**).

Last, the gene expression also showed an upregulation of *Tgfβ* in the LLC model in comparison with the B16F1 in both WT and *Adamts1* KO scenarios, corroborating the

immunosuppressive niche again of the LLC model. Also the increase in markers as *Arg1* and the TAM marker *Cd163* added strength to the hypothesis of the immune tolerance exerted by LLC tumours in the *Adamts1* deficient environment, thus being its tumour progression not impaired.

As a final picture, comparing between B16F1 and LLC models, we can certainly state that the loss of stromal *Adamts1* drives changes in the immune infiltration. Nevertheless, the higher tumour *Adamts1* expression of the B16F1 (even more important in the *Adamts1* KO tumours) may influence the populations that are infiltrating within the TME. While the growth of B16F1 tumours in an *Adamts1* deficient scenario are clearly compromised, by the creation of a pro-inflammatory environment, with increased CD3$^+$ T-Lymphocytes, LLC tumours are favoured by an immunosuppressive niche. In line with the blockade of B16F1 tumours in *Adamts1* KO mice, a recent publication suggests that the proteolysis of Versican by ADAMTS proteases can induce a general immunogenic response in the TME, involving antigen presenting cells (APCs) via TLR2, MAP receptors, and various interleukins (**Figure 59**). On the contrary, the interaction of full length Versican with APCs via TLR2 exerts an opposite role inhibiting T-cell function and thus, favouring tumour progression (Hope et al., 2016; Schmitt et al., 2016) (**Figure 59**).

CONCLUSIONS AND FUTURE PERSPECTIVES

CONCLUSIONES Y PERSPECTIVAS FUTURAS

CONCLUSIONS

α   Downregulation of stromal and/or tumour *Adamts1* correlated with the deposition of Nidogen 1 in the tumour perivascular niche and reduces the amount of generated Versikine in variety of tumours, with consequences for vascular functionality.

α   Alternative mechanisms of vascularization differences have been identified in *Adamts1* knockout B16F1-derived tumours.

α   The overexpression of *Nidogens* in B16F1 murine melanoma cells alters differently their adhesion properties, and impairs capillary-like phenotype in Matrigel culture.

α   The overexpression of *Nidogen 1*, but not *Nidogen 2*, impaired tumour progression in a B16F1 melanoma syngeneic model, directly associated with a strong induction of hypoxia.

α   The overexpression of both *Nidogens* in a B16F1 melanoma syngeneic model entails relevant vascular alterations as the accumulation of Collagen IV. Importantly, in the *Adamts1* knockout animals, tumour vascular density was increased.

α   The *Adamts1* Knockout mouse displays changes in the deposition of Nidogen 1 in the vBM of adult kidney and spleen, but without relevant alterations in the vasculature of these organs.

α   The spleen of *Adamts1* Knockout mouse exhibits a pro-inflammatory environment, supported by the increase of CD3^{+} T-lymphocytes and specific regulation of cytokines.

α   The bone marrow of *Adamts1* Knockout mouse exhibits an immunosuppressive niche, supported by the rise of CD11b^{+}/GR1^{+} myeloid derived suppressor cells and the upregulation of *Tgfβ* and *Versican*.

α   Tumour growth impairment of B16F1 tumours in *Adamts1* Knockout mice correlates with a predominant pro-inflammatory immune infiltration.

α   Normal tumour growth of LLC tumours in *Adamts1* Knockout mice correlates with a predominant immunosuppressive immune infiltration.

CONCLUSIONES

α   La disminución de *Adamts1* estromal y/o tumoral correlaciona con un incremento de la deposición de NIDÓGENO 1 en el área perivascular del tumor y también con la reducción de VKIN en una variedad de tumores, con consecuencias para la funcionalidad vascular.

α   Se han identificado mecanismos alternativos de vascularización principalmente en tumores derivados de la línea celular B16F1.

α   La sobreexpresión de *Nidógenos* en la línea de melanoma murino B16F1 modifica de manera diferente sus propiedades adhesivas, y altera la capacidad de generar estructuras similares a capilares *in-vitro*.

α   La sobreexpresión de *Nidógeno 1* pero no de *Nidógeno 2* bloquea la progresión tumoral del modelo singeneico B16F1, directamente asociado al aumento de hipoxia.

α   La sobreexpresión de ambos Nidógenos en el modelo singeneico B16F1 conlleva importantes cambios en la vasculatura como el incremento en la acumulación de COLÁGENO IV. De manera relevante, en el ratón deficiente en *Adamts1*, los tumores muestran mayor densidad vascular.

α   El ratón deficiente en *Adamts1* muestra cambios en la deposición de NIDÓGENO 1 en la membrana basal vascular del riñón y el bazo, pero sin alteraciones aparentes en su vasculatura.

α   El bazo de ratones deficientes en *Adamts1* presenta un ambiente pro-inflamatorio, corroborado por el incremento de linfocitos T $CD3^+$ y la regulación específica de citoquinas.

α   La médula ósea de ratones deficientes en *Adamts1* presenta un ambiente inmunosupresivo, corroborados por el aumento de células mieloides supresoras $CD11b^+/GR1^+$ y la regulación positiva de *Tgfβ* and *Versicano.*

α   El desarrollo inferior de tumores B16F1 en ratones deficientes en *Adamts1* se corresponde con el predominio de una infiltración pro-inflamatoria en el tumor.

α   El crecimiento normal de tumores LLC en ratones deficientes en *Adamts1* se corresponde con el predominio de una infiltración inmunosupresora en el tumor.

FUTURE PERSPECTIVES

⊕ To expand the studies of Nidogen deposition within the perivascular area to other tumour models with different aggressiveness and metastatic behaviour.

⊕ To overexpress Nidogen proteolytic fragments instead of the full length protein to unveil their specific contributions during tumour progression, according to the different binding to other ECM components.

⊕ To expand the analyses of *Nidogens* and *Adamts1* to human tumour samples to depict their functional relationship during tumorigenesis.

⊕ To develop additional studies to unveil the role of *Adamts1* in the regulation of immune populations:
  ≥ Investigating the peripheral blood and lymph nodes in *Adamts1* knockout mice.
  ≥ Assessing *in-vitro* functional assays with MDSC from WT and *Adamts1* knockout mice
  ≥ Working with a systemic inflammation model to analyse the response of the *Adamts1* knockout mouse model.

⊕ To expand the analysis of tumour immune infiltration to CD4$^+$, CD8$^+$, FOXP3 cytotoxic lymphocytes and Tumour Associated Macrophages (TAMs), in parallel to the evaluation of spleen, bone marrow, lymph nodes and peripheral blood.

⊕ To study the functional interaction between tumour immune infiltration and vascular basement membrane molecules, including the use of anti-angiogenic therapies to challenge the vasculature.

PERSPECTIVAS FUTURAS

- ⊕ Ampliar los estudios de la deposición de NIDÓGENO en el área perivascular a otros modelos tumorales con distinta agresividad y capacidad metastásica.

- ⊕ Sobre-expresar los fragmentos proteolíticos de NIDÓGENO en lugar de la proteína completa para estudiar sus contribuciones específicas durante la progresión tumoral, de acuerdo a sus distintas capacidades de unión a otras moléculas de la matriz extracelular.

- ⊕ Ampliar el análisis de *Nidógenos* y *Adamts1* a muestras tumorales humanas para descifrar su relación funcional durante la progresión tumoral.

- ⊕ Desarrollar nuevos ensayos para estudiar el papel de *Adamts1* en la regulación de las poblaciones inmunes:
  - ⩾ Evaluar la sangre periférica y los nódulos linfáticos en ratones deficientes para *Adamts1*.
  - ⩾ Estudiar la funcionalidad *in-vitro* de células MDSC de animales salvajes y deficientes para *Adamts1*.
  - ⩾ Trabajar con un modelo de inflamación sistémica para analizar la respuesta de los ratones deficientes en *Adamts1*.

- ⊕ Ampliar los estudios de la infiltración tumoral a linfocitos citotóxicos CD4$^+$, CD8$^+$, y FOXP3, así como a macrófagos asociados a tumores (TAMs), tanto en nuestros modelos tumorales, como en bazo, médula ósea, nódulos linfáticos y sangre periférica.
- ⊕ Estudiar la interacción funcional entre el infiltrado inmune en tumores y las moléculas de la membrana basal vascular, incluyendo el uso de terapias anti-angiogénicas que provocan cambios en la vasculatura.

MATERIALS AND METHODOLOGY

1. CELL CULTURE

Murine melanoma cells B16F1, B16F10 and Lewis Lung Carcinoma (LLC) have been cultured in DMEM supplemented with 10% of FCS (*fetal calf serum*) and 1% of penicillin/streptomycin. Mouse Lung Endothelial Cells (MLEC) were cultured in M199 medium (Sigma-Aldrich, USA) supplemented with 10% FCS and 1% of penicillin/streptomycin. Mouse bone marrow derived macrophages (BMDM) are culture in DMEM low glucose, 10% FCS (heat-inactivated), 1% penicillin/streptomycin and 20ng/ml murine m-CSF (Peprotech, USA). Mouse PYMT WT and *Adamts1* KO primary cell line (obtained from A/Prof. Darryl L. Russell) was cultured in α-MEM with 10% FCS and 1% penicillin/streptomycin. Human Embryonic Kidney 293T (HEK293T) cells were cultured with DMEM 10% FCS, 1% penicillin/streptomycin, 2mM L-glutamine and 1% NEAA (non-essential-amino acids). Human umbilical vein endothelial cells (HUVECs) (Lonza, Switzerland) were cultured in EGM-2 (Lonza, Switzerland), special media containing hEGF, VEGF, R3-IGF-1, ascorbic acid, hydrocortisone and hFGF-β, FBS (*fetal bovine serum*) and gentamicin/amphotericin-B. A prior coating in 0,1% gelatine (1 hour, 37°) is necessary for the seeding of these cells. All cells were cultured at 37°C and 5% CO_2 and 95% relative humidity.

2. MATRIGEL CAPILLARY-LIKE ASSAY

The study of the vasculogenic mimicry properties *in-vitro* has been a very useful technique since its discovery. Certain cell lines in culture can mimic capillary-like structures when growth in special matrices and conditions that can resemble a similar scenario of an *in-vivo* ECM (Maniotis et al., 1999). There is a controversy in the literature about the 3-dimensional category of these approaches. What is clear is that they differ from 2-Dimensional classical plastic culture because the behaviour of the seeded cells changes, so it often referred as 2,5D (Shamir and Ewald, 2014). When growth in Matrigel (BD, USA) endothelial cells form a recognized capillary-like organization. Accordingly, melanoma B16F1 and derived cell lines, as well as HUVECs, were subjected to a growth in a 2,5D culture in order to study their *in-vitro* capillary-like properties(Shamir and Ewald, 2014). For this assay, $3 \cdot 10^4$ cells/well (B16F1 and derived) or $5 \cdot 10^4$ cells/well (HUVECs) were used in a 96 well plate. Previously, 30 µl of Matrigel was plated and incubated for 30 minutes at 37°C to create a semi-solid gel matrix. Finally, wells are filled up until 200 µl of DMEM without FCS (B16F1 and derived) or EGM-2 without FBS (HUVECs). These studies were performed up to 48 hours and images were taken at defined time points of 0, 2, 8, 24, 36 and 48 hours with a light microscope (Zeiss axiovert, Germany). Morphometric analysis was performed using a virtual platform, WimTube

(Wimasis, Germany), that provides parameters such as: number and length of tubes, number of loops, covered area and mean size.

3. PROLIFERATION, MIGRATION AND ADHESION ASSAYS.

Cell proliferation, migration and adhesion properties were assessed using the xCelligence system (ACEA Biosciences, California, USA). xCelligence device provides a real-time proliferative, adherent and migration behaviour of cells using specialized 16-well plates known as the E-plate (for proliferation and adhesion) and CIM plates (migration). These plates consist of an underlying sheet of microelectrodes that detect cell interaction upon contact. When cells interact with the underlying electrode surface, it impedes the ability of the electrodes to sense the surrounding conductive culture media, reported as cell impedance, and it corresponds to cell number and strength of the interaction.

According to manufacturer's advice, most of proliferation and adhesion experiments were performed with $4 \cdot 10^4$ cells/well. Early time-points (up to 8 h depending on the cell type) were considered as an adhesion measure while the rest determines proliferation. For migration assays, the wells were uncoated or a Matrigel (BD, USA) (1:20) layer was created during 4 hours at 37 °C. Always a difference in the upper and bottom well media must be acquainted for the cells to have a migratory stimulus.

An alternative adhesion assay was also performed. For it, we coated plates (2 h at 37 ºC, or 4°C overnight) with different substrates such as: purecol 1:30 (a bovine type I collagen solution, Advanced biomatrix, USA), Matrigel 1:10 (BD, USA), rat collagen type 1 (BD, USA), BSA 2mg/ml, and DMEM 10% FCS. Coated plates were washed and rinsed twice with PBS and dried in the tissue culture hood. A total of $5 \cdot 10^4$ cells per well were added and incubated during 1 hour. Then, non-adherent cells were discarded by washes in a warm PBS containing beaker. Attached cells were fixed with 4% PFA during 5 minutes and stained with Toluidin blue 0,5% in 4% PFA, 5 minutes. The culture plates are finally rinsed with tap water and let until dry. 100 µl of 10% SDS in H_2O is added to every well and shaken for 10 minutes. A colorimetric read was obtained using the Infinite 200 Pro NanoQuant (Tecan, Switzerland) at 595 nm.

4. CLONING STRATEGY AND LENTIVIRAL VECTORS

The pLVX-IRES-ZsGreen vector (kindly donated by Dr JL García-Pérez, GENyO, Granada) has been used to construct our expression vectors with murine *Nidogen 1* and *Nidogen 2*. The backbone contains a CMV (cytomegalovirus) promoter followed by a MCS

(Multicloning site). This is followed by an IRES (internal-ribosomal-entry-site) positioned and ZsGreen1 sequence, facilitating cap-independent translation of ZsGreen1 (Jang et al., 1989). The ZsGreen molecule allows the tracking of cells in-vitro or in-vivo experiments as well as the selection of populations of transduced cells. In addition the vector contains a WPRE (woodchuck hepatitis post-transcriptional regulatory element), a cis-acting RNA element that substantially increases the expression of transgenes delivered by retroviral vectors (Zennou et al., 2000), and a Rev-response element (RRE) (Cochrane et al., 1990), which further increases viral titers by enhancing the transport of unspliced viral RNA out of the nucleus. During target cell infection, this element creates a central DNA flap that increases nuclear import of the viral genome, resulting in improved vector integration and more efficient transduction

For murine *Nidogen 1* construct, cDNA was extracted from pBlue_mNID1 (kindly donated by Dr Takako Sasaki, Oita, Japan) with XhoI and NotI. This fragment was directly cloned into pLVX-IRES-ZsGreen. Murine *Nidogen 2* construct required an additional step prior to the incorporation to the pLVX-IRES-ZsGreen. cDNA was extracted from pCEP-PU_mNID2 vector (kindly donated by Dr Takako Sasaki, Oita, Japan) with XhoI and HindIII. This fragment was cloned into a pBSSK(-) empty vector (kindly donated by Dr JL García-Pérez, GENyO, Granada). mNID2 cDNA is extracted again from the resulting vector using XhoI and EcoRI, and finally is inserted in the pLVX-IRES-ZsGreen vector. All ligations were performed using Rapid DNA Dephos & Ligation Kit (Roche, Switzerland). For further expansion, these constructs (5ng DNA each) were transformed in DH5a supercompetent cells by heat-shock. Bacteria were cultured in LB-Agar plates containing Ampicilin 1mg/ml under a 37°C dry atmosphere. Colonies were isolated and minipreps/maxipreps were performed with NucleoSpin plasmid kits (Macherey Nagel, Germany).

5. LENTIVIRAL TRANSDUCTION

Calcium chloride ($CaCl_2$) transfection method was used for virus production in the human cell line HEK293T. Up to $5 \cdot 10^6$ cells were plated in a 100 mm tissue culture dish the day before the procedure starts to reach an optimal confluence of 40-60%. Then, culture media is replaced at least 1 hour before transfection, to boost cell growth. A mix of 20 µg of the expression vector, 15 µg of a packaging vector (psPAX2, Addgene) and 6 µg of envelope vector (vSVG, Addgene) is incubated with 2M $CaCl_2$ and 2X HBS for 30 minutes and then added drop by drop while swirling the plate. Cells are then incubated and culture media was replaced 9 to 14 h post-transfection. At this point the amount of media added was reduced (up to 5 ml per a 100mm plate) and supernatants were

collected every 24 hours for 2-3 times. Finally, media was concentrated using Amicon Ultra-100 filter units (Merck-Millipore, Germany) and used straight away or stored at -80°C.

Lentiviral transduction procedure varied depending on the target cell line. For B16F1 mouse melanoma, $2 \cdot 10^6$ cells/well were counted, resuspended and incubated with the virus-containing-media for 10 min at RT. Then, the cell suspension with the virus particles were added to a 100 mm plate with 9 ml of growth media and kept for 5 hours in the incubator. Later, media is replaced by fresh growth media. Cells were grown until confluence and then passaged, checking the level of fluorescence. After 2-3 days of culture, cells were sorted by Zsgreen$^+$ events (FACs ARIA II Sorter, BD). For HUVECs, $1 \cdot 10^6$ cells/well were counted, resuspended and incubated with the virus-containing-media for 10 min at RT. Then, cell suspension with the virus particles were added to a single well from a 6-well plate and was incubated for 5 hours in the incubator. Then, cells were plated into a 75 cm^2 flask with EGM-2. Due to high efficiency transduction, no sorting was required for HUVECs cell line.

6. MOUSE COLONY MAINTENANCE AND GENOTYPING

The C57/BL6 Wild Type and ADAMTS1 KO mice colony is kept and maintained in the *Centro de Investigación Biomédica, University of Granada* animal facility under pathogen-free conditions and according to institutional guidelines. Mice were weaned fourth weeks after birth. For genotyping purposes, genomic DNA is isolated from ear samples using the Nucleospin tissue kit (Macherey Nagel, Germany). qPCR is performed using iQ SYBR green Supermix (Biorad, USA), keeping the annealing temperature up to 60°C during 37 cycles. The WT gene was amplified using primers covering exons 5-6 of the mouse *Adamts1* gene. The KO allele was amplified with primers of the PGK-Neo cassette which is present in the *Adamts1* KO animals (Lee et al., 2005). Primer sequences are shown in the table contained in this section (Pag. 155).

7. SYNGENEIC TUMOUR ASSAYS

For the generation of syngeneic tumours, $1 \cdot 10^6$ cells (B16F1 and LLC) in 100 μl of PBS were subcutaneously injected in the right flank of wild type and *Adamts1* KO C57Bl/6 mice. Mouse weight and tumour size were monitored every 3 days after cell injection. These assays were performed up to 21 days or until the tumour reached 1 cm in length. All animals were sacrificed following proper guidelines, and tumours were dissected and processed for further analysis, as indicated in next sections. The tumour growth was measured using a digital calliper and the tumour volume was calculated taking two

different measures. The final volume was calculated using three measurements: length (L), width (W) and height (H). For the tumour volume progression, length and width were taken and one of the values were repeated to complete the formula given the difficulty to obtain the height of the tumour in a tumour-bearing animal. The following formula was used:

$$Tumour\ weight = \frac{Pi}{(6 \cdot L \cdot W \cdot H)}$$

8. BONE MARROW ISOLATION AND MACROPHAGE POLARISATION.

Wild type and *Adamts1* KO C57BL/6 mice aged between 8 and 12 weeks were sacrificed following the proper ethic guidelines. Their femur and tibia were dissected from both legs followed by the cut of the boneheads, to open the bone cane. A 23G syringe with PBS was used to flush the bone marrow out of the bone to continue with the disaggregation into single cells. The resulting homogenate was filtered using a 100 μm cell strainer followed by a 300 g spin during 5 minutes, RT. The resulting cell suspension was counted and seeded at a concentration of $4 \cdot 10^5$ cells/ml in a 10 cm non-treated tissue-culture plate, containing DMEM low glucose 10 % FCS, 1 % P/S and 10 ng/ml mCSF (Peprotech 300-25, USA). Culture was maintained a total of 7 days with a change of media every 3 days for the enrichment of the BMDM population. Flow cytometry with CD11b Antibody was performed at day 7 to check the enrichment in macrophage populations. At different stages, bone marrow and macrophage were obtained for RNA or protein extraction.

For polarisation assays, bone marrow derived macrophages (BMDM) were dettached with 2mM EDTA during 10 minutes, together with plate agitation and shaking is necessary, in order to obtain a good cell suspension. Cells were centrifuged at 300 g during 5 min at RT and counted. A total of $1 \cdot 10^6$ BMDM per well were seeded in 6-well tissue-culture plates with the following media: (i) for BMDM control, DMEM low glucose 10 % FCS, 1 % P/S and 10 ng/ml mCSF; (ii) for classically activated macrophages, same media, adding 20 ng/ml murine gamma interferon (IFN-γ) (315-05, Peprotech, USA) and 100ng/ml of lipopolysaccharide (LPS); (iii) for alternatively activated macrophages, the same control media adding 20 ng/ml of murine interleukin 4 (IL-4) (214-14, Peprotech, USA). All cells were incubated during 24 hours and then used for various purposes.

9. IMMUNOFLUORESCENSE

Cells in culture, these were cultured in glass coverslips in tissue-culture plates, coated with poly-L-lysine (P4707, Sigma-Aldrich, USA). Cells were fixed with 4% paraformaldehyde (PFA) in PBS for 10 minutes at RT followed by 2 washes of PBS-Tween-20 0,5% (PBSt). For tumour and tissue specimens, these are collected and treated with 4% formaldehyde in PBS overnight at RT. Samples are dehydrated through a series of graded ethanol baths, and then embedded in paraffin at 58°C. Finally, after 30 minutes of cooling, the tissue is ready for sectioning. In general, 5 µm sections were obtained. Deparaffinization protocol included 5 minutes incubation under gentle shaking with the following solutions: xylene substitute (three times), 100% EtOH (twice), in 95% EtOH (once), in 70% EtOH (once), PBS (once) and ddH$_2$O (once). Heat-based antigen retrieval process was performed, either using Tris-Buffer (10mM Tris Base, 0.05% Tween 20, pH 10) or Sodium Citrate Buffer (10mM Sodium Citrate, 0.05% Tween 20, pH 6.0), during 10 minutes in a microwave at 800 Watts followed by a 30 minutes RT, according to the antibody manufacturer' recommendations. Then, sections were washed with PBSt during 5 minutes prior to immunostaining. For both cells and tumor/tissues, the following procedure was used. A blocking step using a 3% BSA, 1% secondary antibody host serum solution, in PBS for 1 hour RT. Later, two washes of 5 minutes in PBSt, and then samples are incubated overnight at 4°C with the primary antibody solution (1% BSA and 1% of the secondary antibody host serum). Then, the samples are washed three times with PBSt previous to the incubation with the secondary antibody solution (1% BSA and 1% of the secondary antibody host serum), 1 hour RT. Finally, three washes with PBSt were assessed and slides were mounted with Prolong Gold with Dapi (P36930, Thermofisher, USA), left 1 hour RT and then kept at 4°C overnight.

For these assays we used the following antibodies: polyclonal goat anti-human NID1 (AF2570, R&D, USA), polyclonal goat anti-human NID2 (AF3385, R&D, USA), polyclonal rabbit anti-human CD31 (AB28364, Abcam, UK), polyclonal rabbit anti-human laminin (L9393, Sigma-Aldrich, USA), monoclonal mouse anti-SMA (A2547, Sigma-Aldrich, USA), monoclonal rat anti-mouse Endomucin (SC65495, SCBT, USA), polyclonal rabbit anti-mouse Versican DPE (AB19345, Abcam, UK), polyclonal rabbit anti-mouse Versican V1 (2701534, Millipore, USA) and polyclonal rabbit anti-mouse/human α-Tubulin (sc5546, SCBT, USA). In addition, to visualize actin fibers we used Phalloidin–Tetramethylrhodamine B isothiocyanate (P1951, Sigma-aldrich, USA).
Fluorescent images were acquired with an AxioImager A.1 microscope (Zeiss, Germany), and confocal analysis was performed with a LSM710 (Zeiss, Germany) or a TCS SP5 (Leica, Germany). For colocalization analyses, we used ImageJ Software (NIH, USA).

10. VASCULATURE ANALYSIS

Tumour section immunofluorescences were subjected to CD31 to assess the amount of blood vessels present in the preparation (see materials and methodology section 9). From every tumour, the whole section was captured taking into further consideration its area within the analysis. For these evaluations, no further antibodies were included in order to get a better and cleaner signal. Pictures were captured at a low magnification (10X) using the Axioimager A1 (Zeiss, Germany). Using Image J software (NIH, USA), we required 8-bits grey scale images for *in-silico* analysis. We approached the following parameters: vessel count, diameter, perimeter and total area. To distinguish between real and background pixels, a specific threshold was established for every experimental set and it was maintained during the whole analysis. Accordingly, the application identifies positive signals and quantifies the number of positive units (number of vessels), and the area and perimeter of positive units. Simple mathematical functions estimate the average and total area, average and total perimeter, and additional parameters.

11. FLOW CYTOMETRY

Different protocols have been used depending on the nature of the sample. For cells in culture, the plated cells were detached using either Trypsin 0,05% (SH30236, Thermofisher, USA) or Triple Express (12604021, Thermofisher, USA), then spun at 300 g during 5 minutes at RT. For spleens, they were disrupted physically using the plunger of a 5 ml syringe as a pestle and a 70 μm cell strainer in a 100mm plate as a mortar. For B16F1 and LLC tumours we required a previous mechanical disaggregation process. Tumour pieces were cut with curve scissors and fine forceps until a pâté-like consistency was obtained. Cell suspension is incubated with collagenase 0,5% in PBS (C2799, Sigma-Aldrich, USA) for 1 hour at 37°C, shaking from time to time to avoid clump formation. This suspension is centrifuged and suspended in Ammonium-Chloride-Potassium (ACK) buffer pH 7,2 to remove red blood cells, incubating during 4 minutes on ice. Finally, the cells were spun and pellet was resuspended in FACS buffer (PBS 1X, 1% FCS and 2mM EDTA) for cell counting and antibody incubation.

To identify dead cells, we added Blocking solution containing 1% BSA, 1% FCS and 7-Amino-actinomycin D (7-AAD) to the cells suspension and incubated for 10 minutes at RT. Then the conjugated-primary antibody solution was added and incubated for 30 minutes at RT. After the incubation cells were spun at 300g during 5 minutes and finally resuspended in FACS buffer.

The antibodies used for flow cytometry were the following: rat anti-mouse CD11b-APC (553312 BD, USA), rat anti-mouse F4/80-PE (123110, Biolegend, USA), rat anti-mouse/human CD45R/B220-FITC (110452, Thermofisher, USA), hamster monoclonal anti-mouse CD3-PE (12-0031, Thermofisher, USA), rat anti-mouse GR-1-FITC (RB6-8C5, Miltenyi Biotech, Germany), goat anti-mouse/human VE-CAD-PE (SC5468PE, SCBT, USA) and rat anti-mouse CD31-PE (102408, Biolegend, USA). Flow cytometry analyses have been performed using the FACS Canto II (BD, USA).

12. RNA EXTRACTION, cDNA SYNTHESIS and QUANTITATIVE PCR

RNA extraction from mouse and human cells, as well as tumors and tissues, was carried out with the RNAII Nucleospin kit (Macherey-nagel, Germany) or using Trizol (Invitrogen, US). Some delicate tissues, i.e. spleen or brain, were first snap frozen prior to tissue grinding. All tissues and samples that required disaggregation (mouse organs and tumours) were subjected to a physical process using metallic beads and the Tissuelyser LT 1 minute 50 oscillations per second (Qiagen, The Netherlands). RNA quantification was performed with a nanodrop system (Thermo, US) and its quality was evaluated by electrophoresis, loading 200 ng in a 0,7% agarose gel in TAE buffer (tris base, EDTA and acetic acid). cDNA synthesis was performed using the iScript cDNA kit (BioRad, US), starting from 500 to 1000 ng of original RNA. qPCR reactions were carried using Fast SybrGreen in the 7900HT system (Applied Biosystems, US). In every assays, we used 5ng of cDNA per reaction, triplicates and non-template-controls. In general, qPCR representations show the $2^{(\Delta\Delta Ct)}$ value, using a housekeeping gene for endogenous control (actin, GAPDH, 18S and/or β2-microgobulin). However, the Ct value itself could be represented in the case of the lack of normalisation with a proper sample. In this case, the Ct values have been references to the Ct value of the housekeeping gene and then represented. Error bars show the standard error of the mean (SEM). A primer list has been included at the end of this section.

13. WESTERN BLOTTING

To evaluate secreted proteins, serum-free conditioned medium (CM) from cells was clarified and concentrated with StrataClean resin (Stratagene, USA), which binds and concentrates the protein in the sample and removes non-protein impurities. The resin was added to each sample, vortexed for 1 min then incubated at 4°C a minimum of 2 hours, preferably overnight. CM is then centrifuged 10 minutes at 2000 rpm, the supernatant is discarded and the resin resuspended with 1X lamely buffer with 1% of 2-mercaptoetanol. To evaluate proteins from tumour/tissue samples and cell lysates, total

protein was extracted with RIPA buffer containing 1mM PMSF, 1 μg/ml aprotinin and 10 μg/ml leupeptin. All samples were measured using a Pierce BSA protein assay kit (ThermoFisher, USA) at a 455 nm wavelength using the infinite 200Pro nanoquant (Tecan, Switzerland). All the samples are heat-shock treated during 5 to 10 minutes at 100°C. Proteins were resolved by sodium dodecyl sulfate polyacrylamide gel electrophoresis (SDS-PAGE) and transferred to polyvinylidene difluoride membranes (PVDF) (BioRad, USA). Membranes were blocked with 5% low-fat milk (RT during 1 hour) and incubated with the following primary antibodies: monoclonal mouse anti-human ADAMTS1 (AF5867, R&D), polyclonal goat anti-human NID1 (AF2570, R&D, USA), NID2 (AF3385, R&D, USA), α-Actin (A4700, Sigma-Aldrich, USA), β-Tubulin (AB75069, Abcam, UK). All primary antibodies were incubated at 4°C overnight and secondary antibodies RT during 1 hour. Between every incubation step, the membranes are washed with PBSt. After incubation with appropriate secondary peroxidase-conjugated antibodies, signal was detected with the SuperSignal West Dura Chemiluminescence Kit (ThermoFisher, USA). For the image acquisition we used the LAS4000 system (General electric, USA). Membranes are incubated with the supersignal reagent into the dark camera for one minute and the images were acquired every 10 seconds in a sequential burst until the signal was saturated. For signal quantification, WB images were processed with ImageJ software (NIH, USA). A rectangular area was drawn along the signal of all lanes which represented a positive signal. The intensity was measured for each lane. This is normalised with the α-Actin or β-Tubulin for the case of cell lysates and Red Ponceau for conditioned medium loads. The images shown in the western blots correspond to the best signal intensity and thus the exposure time varies among membranes and antibodies. The exposure time is shown in every image.

14. STATISTICAL ANALYSIS

All the statistical analyses have been pursued with the Graphpad Prism 6.0c (Graphpad software Inc., USA). For qPCR, WB quantification and vessel count analyses a *t-student* test was performed in paired groups of samples with known median. The standard error of mean (SEM) is shown with error bars. Studies of the median and outliers by Tukey's test were taken in all the sample cohorts prior to the t-student test.

15. ETHICAL APROVALS

All mice were kept in the Centro de Investigaciones Biomédicas-UGR Animal Facility under pathogen-free conditions and according to institutional guidelines (Animal experimentation ethics committee of CIC-UGR). Indeed, all mice were sacrificed

PCR PRIMER TABLE

Gene	Species	Forward	Reverse	Class
Adamts1	Mouse	CTGGCAGAAACAACACAACAG	TGAATTGGGCCATGTGTTTAAC	Protease related
Adamts1	Human	CCCACAGGAACTGGAAGCATA	CCACTGCCGTGGAATTCTG	
Timp3	Mouse	CAGGACTGTGCAACTTTGTG	AGTAGTAGCAGGACTTGATCTTG	
Timp3	Human	GGTTGTAACTGCAAGCTCAAGTC	GTAGCCAGGGTAACCGAAAT	
Nidogen 1	Mouse	CGGTCTATGTCACCACAAATGGTA	AGGTTCCGGGATGGTATTCTGT	ADAMTS1 substrates
Nidogen 1	Human	GCGCTTACGAGGAGGTCAAG	ACCCATCAGATGCCAAAACTG	
Nidogen 2	Mouse	TTCCTGTCCCTCCTCTGGAA	GCCATTATACGTGAAGACTTGATCAT	
Nidogen 2	Human	CATCATGTAGGCAAGATCAAGTCAA	CGGAAGACCTTGCCCACATA	
Versican	Mouse	CTTTGCTCATCGACGCACAT	TGTCATTGAGGCCGATCCA	
Versican	Human	AGGTGGTCTACTTGGGGTGA	TGGTTGTAGCCTCTTTAGGTTT	
Actin	Mouse	GCGAGCACAGCTTCTTTGC	CGACCAGCGCAGCG	House keeping
Actin	Human	GATGGCCACGGCTGCTT	AGGACTCCATGCCCAGGAA	
β2-microglobulin	Mouse	CATGGCTCGCTCGGTGACC	AATGTGAGGCGGGTGGAACTG	
18S	Mouse	CGGACAGGATTGACAGATTG	CAAATCGCTCCACCAACTAA	
18S	Human	CACGGACAGGATTGACAGATT	GCCAGAGTCTCGTTCGTTATC	
CD31	Mouse	TCCAGGTGTGCGAAATGCT	TGGCAGCTGATGCCTATGG	Endothelium related
CD31	Human	ACCCTTCTGCTCTGTTCAAG	GGGTCAGGTTCTTCCCATTT	
Endoglin	Mouse	CTCGATAGCAGCACTGGATGAC	AGCTTCTGGCAAGCACAAGAA	
Ephrin A2	Mouse	AGCAAAGTGCACGAGTTCCA	CCAGAAGCAAAACAACACCT	
Ephrin A2	Human	TCGGACCGAGAGCGAGAA	AGCAGTACCACTTCCTTGCC	
Ng2	Mouse	GACGGCGCACACACTTCTC	CAGACTCTGGACAGACGGTCAA	
Ng2	Human	CTTTGACCCTGACTATGTTGGC	TGCAGGCGTCCAGAGTAGA	
SMA	Mouse	TCTTTCATTGGGATGGAGTCAG	GACAGGACGTTGTTAGCATAGA	
Tie1	Mouse	GCCTTGGTGTGTATCCGAAGA	TTCACCCGATCCTGACTGGTA	
Tie2	Mouse	GCTGTTGGCGTTTCTGATTATG	CTGGTTCTTCTCTCACGTTCTG	
Ve-Cadherin	Mouse	GCAGCATCGGGTACTCCAT	CAGTTCTTTCTCGTTATAGATGTTTCC	
VEGFc	Mouse	CAAGACATGTCCAACAAACTATGTGT	AATCCATTGGTTGAGTCATCTTCA	
LamC2	Mouse	GTGTTTCTGCTATGGGCATTCA	CCAACCATCCACATCCTGACT	
LamC2	Human	GTGGCTCCTGCCAAATTTCT	ACATCATGGGCAGATGGGTG	
CD11b	Mouse	GCAGCACTGAGATCCTGTTTA	CTCCACTTTGGTCTCTGTCTTAG	Immune related
CD163	Mouse	GAGGAAACTGTAAGTCGCTGAA	ACGGCACTCTTGGTTTGT	
CD45	Mouse	CCCTTCTTCTGCCTCAAAGT	GTGGATAACACACCTGGATGAT	
CX3CR1	Mouse	CTTCCTCTTCTGGACACCATAC	GTCCCTCTTCATGTCACAACT	
F4/80	Mouse	CATAATCGCTGCTGGTTGAATAC	GGCAAGGAGGACAGAGTTTAT	
IL6	Mouse	AGGAGACTTCACAGAGGATACC	GAATTGCCATTGCACAACTCTT	
IL10	Mouse	TCAGCCAGGTGAAGACTTTC	GGCAACCCAAGTAACCCTTA	
IL12	Mouse	GGCAACCCAAGTAACCCTTA	GGCACAGGGTCATCATCAAA	
TGFβ	Mouse	GCAACAATTCCTGGCGTTAC	GTATTCCGTCTCCTTGGTTCAG	
TNFα	Mouse	GAGGAAACTGTAAGTCGCTGAA	ACGGCACTCTTGGTTTGT	
CD3	Mouse	CAGTCAAGAGCTTCAGACAAG	GATGGCTGTACTGGTCATATTC	
CD4	Mouse	GAGTTCCCAGAAGAAGATCAC	AAGGCGAACCTCCTCTAA	
CD8	Mouse	CCATGAGGGACACGAATAATAA	GAGTTCACTTTCTGAAGGACTG	
Arg1	Mouse	CCGATTCACCTGAGCTTTGA	AAAGGAGCCCTGTCTTGTAAAT	
Nos2	Mouse	CTTGGTGAAAGTGGTGTTCTTTG	TCAGACTTCCCGTCTGTCTCAGTAG	
HIF1α	Mouse	GAGAAAAGGGAAAGAACTAAACACACA	GTGCAGTGAAGCACCTTCCA	Hypoxia
HIF2α	Mouse	CCTGGCCATCAGCTTCCTT	GGTCGGCCTCAGCTTCAG	
Adamts1	Mouse	CAAGTGCGTGAACAAGACAGACA	GTATTGAACTCCACCACCACAG	Genotyping
PGK-Neo	-	TGAATGAACTGCAGGACGAG	TGAATGAACTGCAGGACGAG	

ADDITIONAL INFORMATION

ORIGINAL PUBLICATION FROM THIS THESIS

Stroma-derived but not tumor ADAMTS1 is a main driver of tumor growth and metastasis

Rubén Fernández-Rodríguez[1], Francisco Javier Rodríguez-Baena[1], Estefanía Martino-Echarri[1], Carlos Peris-Torres[1], María del Carmen Plaza-Calonge[1], Juan Carlos Rodríguez-Manzaneque[1]

[1]GENYO, Centre for Genomics and Oncological Research: Pfizer/Universidad de Granada/Junta de Andalucía, Granada 18016, Spain

Correspondence to: Juan Carlos Rodríguez-Manzaneque, *e-mail:* juancarlos.rodriguez@genyo.es

ABSTRACT

The matrix metalloprotease ADAMTS1 (*A Disintegrin And Metalloprotease with ThromboSpondin repeats 1*) has been involved in tumorigenesis although its contributions appeared ambiguous. To understand the multifaceted actions of this protease, it is still required a deeper knowledge of its implication in heterogeneous tumor-stroma interactions. Using a syngeneic B16F1 melanoma model in wild type and ADAMTS1 knockout mice we found distinct stroma versus tumor functions for this protease. Genetic deletion of ADAMTS1 in the host microenvironment resulted in a drastic decrease of tumor growth and metastasis. However, the downregulation of tumor ADAMTS1 did not uncover relevant effects. Reduced tumors in ADAMTS1 KO mice displayed a paradoxical increase in vascular density and vascular-related genes; a detailed characterization revealed an impaired vasculature, along with a minor infiltration of macrophages. In addition, ex-vivo assays supported a chief role for ADAMTS1 in vascular sprouting, and melanoma xenografts showed a relevant induction of its expression in stroma compartments. These findings provide the first genetic evidence that supports the pro-tumorigenic role of stromal ADAMTS1.

INTRODUCTION

The impact of the communication between cancer cells and stroma constituents during distinct stages of tumor progression has been an inspiring field of investigation during the last decades. Multiple efforts have highlighted the contribution of stroma cells such as cancer-associated fibroblasts, endothelium, macrophages and other immune-related populations, with major consequences to the design of therapeutic tools. Still, the multitude of factors contributing to this complex scenario of tumor-stroma interactions demands a deeper understanding. For example, studies of extracellular proteases as modifiers of the tumor microenvironment have revealed their participation as oncogenic as well as tumor-protective molecules. In addition to the putative expression of these proteases by both tumor and stromal cells, the presence of specific substrates would further redefine their final effect.

The extracellular protease ADAMTS1 represents a good example of such complexity. Although it was first shown to display anti-angiogenic properties [1], the contribution of ADAMTS1 (and other ADAMTSs) during tumorigenesis is still controversial [2]. Its angiostatic and tumor suppressive properties have been described in distinct models [3–5], but other studies support its relevance in metastasis [6] and tumor growth [7, 8]. As for its catalytic activity it has been observed on various proteoglycans, such as syndecan-4, aggrecan and versican [9–11], and other extracellular components [12–14]. A common finding has been the close connection of ADAMTS1 with neovascularization mechanisms, including its contribution to the acquisition of endothelial-like properties of some tumor cells [5]. Importantly, ADAMTS1 was found to be relevant during endothelial cell sprouting in collagen invasion assays [15], and its expression is induced in endothelial cells under hypoxic conditions and VEGF-treatment [16, 17]. The specific

159

influence of stromal ADAMTS1 has been suggested in some studies of breast cancer [4, 18, 19], and the use of the ADAMTS1 knockout mice, in combination with a spontaneous model of mammary carcinogenesis, revealed its participation in tumor growth and metastasis [7].

Here, to examine the contribution of ADAMTS1 by different cell compartments, we carried out syngeneic tumor experiments in wild type and ADAMTS1 KO mice. Although levels of the protease were still provided by tumor cells, the absence of ADAMTS1 in the host stroma significantly impaired B16F1 tumor growth and metastasis. Our studies also revealed an unexpected effect in the infiltration of macrophage populations. In addition, the downregulation of ADAMTS1 in B16F1 tumor cells was not accompanied by relevant changes in their tumorigenic properties. Finally, a combination of human melanoma xenografts and ex-vivo experiments confirmed the main contribution of the stroma as a supplier of ADAMTS1 and its relevance for vascular functionality.

RESULTS

The absence of ADAMTS1 in the host stroma results in tumor growth delay

To better understand the role of ADAMTS1 during tumor growth and to unveil its matrix-dependent actions, we generated and characterized syngeneic tumors with B16F1 murine melanoma cells in wild type (WT) and *Adamts1* knockout (ATS1-KO) mice. We injected these cells subcutaneously in WT and ATS1-KO mice and followed tumor progression for 18 days. Thereafter, animals were sacrificed and tumors were dissected and thoroughly cleaned of surrounding tissue. The evaluation of tumors revealed a significant reduction of tumor weight in ATS1-KO animals compared to their WT littermates (Figure 1A–1B). According to the endogenous presence of *Adamts1* in B16F1 cells in culture (Supplementary Figure S1), we also evaluated by qPCR its gene expression in the generated tumors. This analysis revealed significant levels of *Adamts1* in the tumor comparing with B16F1 cells in culture; nevertheless no major changes between WT and ATS1-KO mouse tumors were observed (Figure 1C). This result indicates that, although *Adamts1* is relevantly present in the tumor, its absence in the host stroma cells (in the ATS1-KO group) is enough to produce a severe delay in tumor development.

The absence of ADAMTS1 in the host stroma results in the alteration of the vasculature of tumors

As previous tumor studies have shown, the alteration of ADAMTS1 levels is accompanied by changes in the overall tumor structure and consistency, and specifically it has significant effects on the

vasculature [4, 5, 20–23]. Therefore we decided to explore the vascular pattern in our model. To achieve such purpose, we performed an extensive series of histopathological and gene expression analyses. First, we approached single staining of paraffin embedded tumor sections with an antibody against the endothelial marker Endomucin [3] (Figure 2A). Metamorph 7 software was used to quantify and characterize tumor vasculature objectively (more details are included in the Materials and Methods section). These analyses revealed clear differences in certain parameters (Figure 2B). A first assessment showed a significant increase in vessel density (vessels/mm²) in the ATS1-
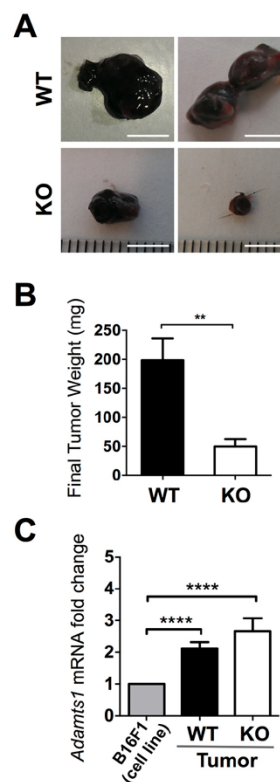
Figure 1: Tumor growth of B16F1 cells in WT and ATS1-KO mice. A. Images of representative tumors obtained in WT and ATS1-KO mice after 18 days post-injection (Scale Bar= 5 mm). **B.** Graph representing mean tumor weight ± SEM after 18 days post-injection (Number of animals in this experiment: WT, n=7; ATS1-KO, n=6). **C.** Graph representing *Adamts1* gene expression in the generated tumors, in comparison with B16F1 cells in culture. Bars show mean values ± SEM. (**, $p < 0.01$; ****, $p < 0.0001$).

160

KO group when both sets of tumors were compared (Figure 2B). This finding correlated negatively with tumor growth rate (Figure 1B). However, additional related parameters, such as average vessel area and average vessel perimeter did correlate positively with tumor size (Figure 2B). Finally, giving the opposite results of vessel density and average vessel area, the measure of the total vessel area displayed no differences (Figure 2B).

According to the changes observed in the vasculature, we completed the study with the expression analysis of endothelial-related genes in tumor lysates, such as CD31 (PECAM1), CD34, and VEGFR2 (KDR) (Figure 2C). Such evaluation indicated that these endothelial genes were also significantly overexpressed in the tumors in ATS1-KO mice, in line with the increased vessel density showed in the previous panel. Yet, this neovasculature does not seem to be properly functional, as tumor size was clearly diminished in ATS1-KO mice (Figure 1B).

Tumors generated in ADAMTS1 KO mice displayed an increased hypoxic response

Consistent with the finding of smaller tumors with increased vessel density in ATS1-KO mice, we approached the evaluation of hypoxia as a measure of functionality of the vasculature. First we evaluated the gene expression of hypoxia players HIF1α and HIF2α by qPCR. A significant upregulation was found just for HIF2α in tumors of the ATS1-KO group compared with WT animals (Figure 3A). To verify the existence of hypoxic regions, a group of mice were i.p. injected with a hypoxia probe, Hypoxyprobe, immediately prior to euthanasia [24–26]. Later on, we visualized hypoxic regions in these tumor sections in combination with the immunolocalization of Endomucin-positive vessels (Figure 3B). This assay revealed that little to no hypoxia was found in tumors from WT animals. In contrast, tumors from ATS1-KO mice displayed multiple hypoxic regions. A closer evaluation showed that these zones did not co-localized necessarily with avascular
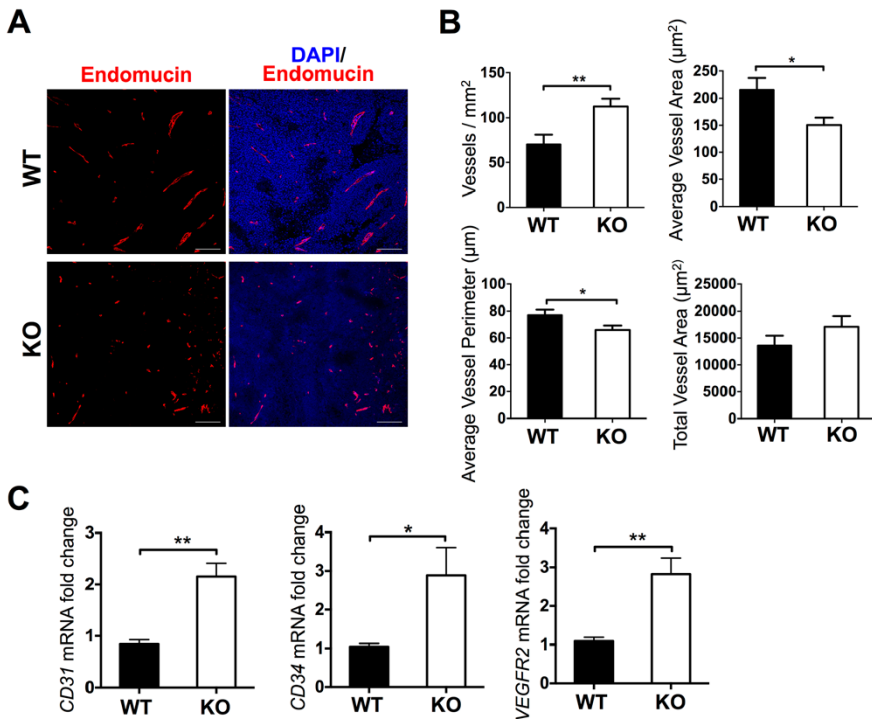
Figure 2: Characterization of vasculature in tumors from WT and ATS1-KO mice. A. Fluorescence microscopy images of representative sections showing Endomucin and DAPI staining. **B.** Graphs representing results from the morphometric analyses of vasculature (Metamorph 7 software). These analyses include vessel density (vessels/mm²), average vessel area (μm²), average vessel perimeter (μm), and total vessel area (μm²). Bars show mean values ± SEM. Statistical analyses show unpaired t test. **C.** Graphs representing gene expression evaluation of vascular-related genes. Bars show mean values ± SEM. (*, $p < 0.05$; **, $p < 0.01$).

161

areas or Endomucin-negative regions (Figure 3B). Quantification of hypoxic-related fluorescence intensity (Figure 3C) confirmed that smaller but more abundant vessels in the ATS1-KO tumors are not fully functional, as the oxygen supply seems to be deficient in these tumors.

Downregulation of ADAMTS1 in tumor cells revealed its minor contribution for tumor progression and angiogenesis

At this point, to uncover the contribution of ADAMTS1 provided by tumor cells, we inhibited the expression of endogenous *Adamts1* in B16F1 melanoma cells and we further evaluated their tumorigenic properties in WT and ATS1-KO mice. To obtain a stable downregulation we used shRNA technology that targeted mouse *Adamts1* gene in B16F1 cells, complemented with the proper control with a vector encoding a scramble sequence. Expression levels of *Adamts1* were severely downregulated upon interference (Supplementary Figure S2A–S2B). The characterization of these cells showed no relevant changes in the proliferation rate (Supplementary Figure S2C) although the migration capacity of interfered cells was increased upon seeding in different matrices (Supplementary Figure S2D). Being aware of this phenotypic characterization, we tested their tumorigenic properties with a similar syngeneic xenograft approach in WT and ATS1-KO mice as indicated in previous
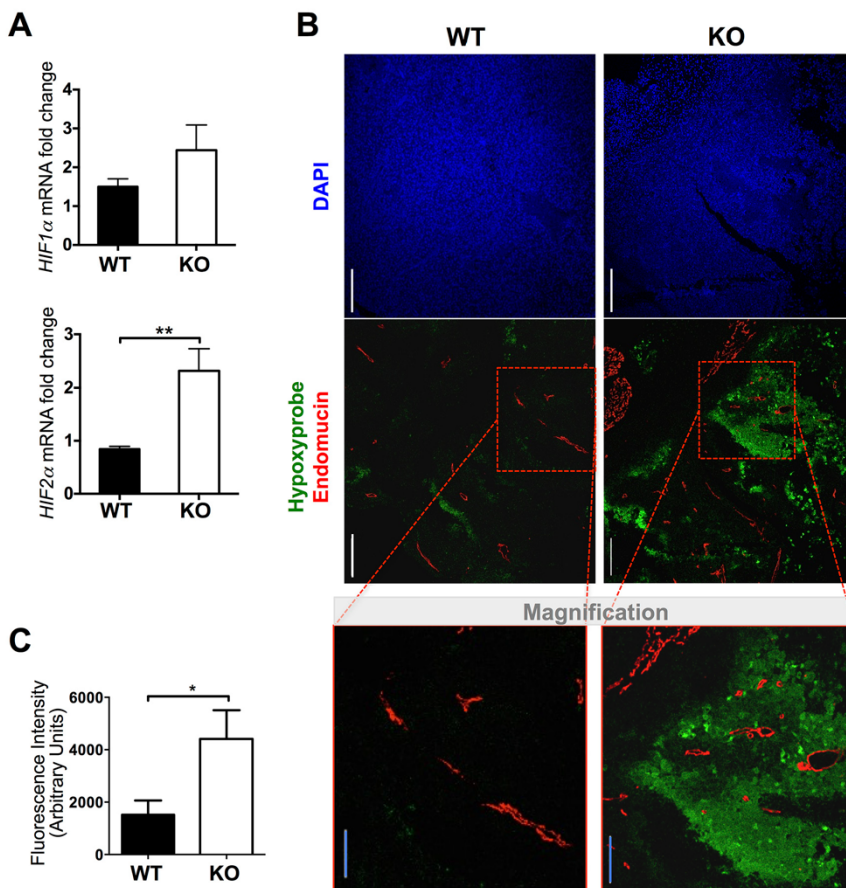
Figure 3: Evaluation of hypoxia in tumors from WT and ATS1-KO mice. A. Graph representing HIF1α and HIF2α gene expression in the generated tumors. Bars show mean values ± SEM. **B.** Representative images and magnification showing DAPI (blue), Hypoxyprobe (green) and Endomucin (red) immunostaining of tumors sections (scale bars = 200 μm (white bar) and 100 μm (blue bar in magnification)). **C.** Graph representing a quantification of fluorescence intensity in tumor sections from both groups (Number of animals in this experiment: WT, n=6; ATS1-KO, n=6). (*, $p < 0.05$; **, $p < 0.01$).

section. Now we included 3 different groups of cells: (i) B16F1 control cells, (ii) B16-shAts1 (with inhibited ADAMTS1), and (iii) B16-shSCR (scramble control). After 18 days all tumors were dissected and processed as previously. The analysis of final tumor weight revealed several findings (Figure 4A–4B). First we confirmed significant differences between tumors in WT and ATS1-KO mice for both control cells (B16F1 and B16-shSCR). Importantly, for tumors generated with inhibited B16-shAts1 cells, although following same tendency, they did not display significant differences between the WT and the ATS1-KO group. These results suggest a partial but minor contribution of ADAMTS1 derived from tumor cells. The evaluation of *Adamts1* gene expression within the tumors showed a similar percentage of inhibition than

that described in the injected cells (approximately 50%) (Figure 4C).

In line with our previous studies, we performed a closer characterization of tumor vasculature by Endomucin staining and a subsequent morphometric evaluation with Metamorph 7 software. In general these analyses confirmed a significant increase in vessel density in tumors of ATS1-KO mice, independently of the type of implanted cells, with *Adamts1* suppression or not (Figure 4D–4E). Also in a similar pattern, an opposite reduction of average vessel perimeter and vessel area was observed (Figure 4E and Supplementary Figure S2E). Total area covered by vessels remained invariable between WT and ATS1-KO mice despite the type of cell injected (Supplementary Figure S2E). Additional gene expression data of endothelial
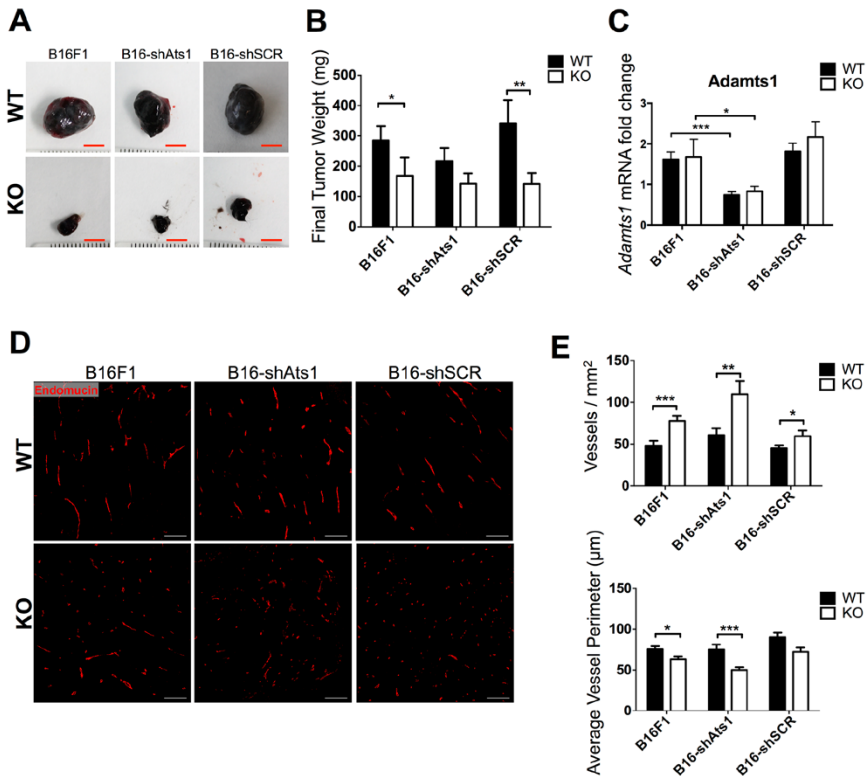
Figure 4: Tumor growth and characterization of vasculature of tumors derived from control and modified B16F1 cells in WT and ATS1-KO mice. A. Images of representative tumors obtained from different mouse groups after 18 days post-injection (Scale bar= 5 mm). **B.** Graph representing mean tumor weight ± SEM after 18 days post-injection. (Number of animals in this experiment: WT/B16F1, n=17; ATS1-KO/B16F1, n=14; WT/B16-shAts1, n=10; ATS1-KO/B16 shAts1, n=10; WT/B16-shSCR, n=7; ATS1-KO/B16-shSCR, n=7). **C.** Graph representing Adamts1 gene expression in the generated tumors. **D.** Fluorescence microscopy images showing Endomucin staining of tumor sections. Scale bar = 200 μm. **E.** Graphs representing results from the morphometric analyses of vasculature showing vessel density and average vessel perimeter. Bars show mean values ± SEM. Statistical analyses show unpaired Student's t test. (*, p < 0.05; **, p < 0.01; ***, p < 0.001).

163

markers from these tumors also confirmed that alterations depend on the nature of the animal (WT versus ATS1-KO mice) and that the downregulation of tumor *Adamts1* did not significantly contribute (Supplementary Figure S2F).

Furthermore, in order to assess vascular functionality, we evaluated gene expression of hypoxia-related genes HIF1a and HIF2a (Supplementary Figure S3A), and tumor hypoxia by the Hypoxyprobe assay, as described above. Again, significant differences were only noted between the animals of different genotypes (WT versus ATS1-KO) but not among those who had altered levels of *Adamts1* in the tumor cells (Supplementary Figure S3B).

In this set of experiments we included a different approach to estimate functionality, as it is the intravenous injection of Bs1 lectin-FITC previous to sacrifice [27]. Subsequent microscopic evaluation of Endomucin-stained tumor sections revealed that a fewer percentage of vessels displayed colocalization of both molecules in tumors from ATS1-KO mice. These results confirmed the dysfunctionality of their vessels, in clear contrast to the WT group (Figure 5A–5B). Nevertheless, and consistently with our previous findings, quantification of fluorescence colocalization between groups of animals implanted with control B16F1 and interfered B16-shAts1 cells showed no significant differences (Figure 5A–5B). All these data together reinforce the notion that stroma-derived but not tumor ADAMTS1 supported tumor development through a vascular-dependent mechanism.

Metastasis assays revealed a relevant contribution of host ADAMTS1 but not of tumor-derived ADAMTS1

Some existing reports claim a pro-metastatic role of ADAMTS1 even with different experimental approaches [6, 7, 22, 28]]. In our study we took advantage of the ATS1-KO mice to determine the contribution of stromal *Adamts1* in the metastatic cascade and, in addition, we included tumor cells with down-regulated *Adamts1*. We performed intravenous tail injection of control B16F1 and modified B16-shAts1 and B16-shSCR melanoma cells used in previous sections. The B16F1 cell model, although metastatic, produces a low number of macrometastasis. This property was positively considered in our research to avoid the potential masking of significant differences if the metastatic process is extremely active, as occurs with other cell models. A first microscopic evaluation of organs allowed us to visualize some metastatic nodules in the liver and lung of WT mice but almost none in the ATS1-KO animals (Supplementary Figure S4A–S4B). Furthermore, to obtain a more objective and quantitative measurement of micrometastasis, we assessed the gene expression of melanoma-related genes (MITF, MLANA, TYR and TYRP) [29] in RNA extracts from lungs and livers of experimental groups (Supplementary Figure 4C). qPCR analyses revealed strong differences between WT

and ATS1-KO animals in both organs (Figure 6A–6B), in accordance with the visualization of metastatic nodules. Importantly, not significant differences were observed when inhibited B16-shAts1 cells were injected in the WT group (Figure 6A–6B). Again, a clear impairment of tumor progression, in this case affecting the metastatic process, appeared dependent of the presence of *Adamts1* in the stroma. However not major relevance was found for tumor-derived *Adamts1*.

Stromal ADAMTS1 is induced in tumors and contributes to vascularization and macrophage infiltration during tumor progression

Given these results, in order to evaluate the contribution of stromal elements during tumor progression, we considered both vascular and inflammatory components in WT and ATS1-KO mice. First, to assess whether the dysfunctional vasculature observed in tumors in the ATS1-KO mice was associated to an anomalous angiogenic activity of their vessels, we performed *ex vivo* VEGF-induced aortic ring assays from WT and ATS1-KO animals. These analyses revealed that aortic ring sprouting was significantly reduced in aortas from ATS1-KO mice in comparison with WT controls (Figure 7A). These observations confirmed the relevance of ADAMTS1 expression during sprouting, in agreement with earlier results in 3D-collagen assays [15]. In addition, our immunocompetent B16F1 tumor model allowed us to investigate macrophage infiltrates, as another recognized and relevant constituent of the host stroma during tumor progression. With this goal we analyzed the gene expression of relevant macrophage-related molecules (F4/80, CD11b, Tie2 and TIMP3) [30, 31] in tumors (Figure 7B). In parallel, to know the basal status of our experimental mice, we tested the expression of these molecules in bone marrow extracts and macrophages derived from bone marrow of non-challenged mice. Whereas our qPCR assays did not display differences between the bone marrow and bone marrow-derived macrophages of WT and ATS1-KO, the analysis of tumor extracts did show a significant decrease in macrophage-related markers in the ATS1-KO group (Figure 7B) revealing an altered infiltration of macrophages probably due to the dysfunctionality of the vasculature.

To explore how stromal *Adamts1* is regulated following tumor induction, we approached the generation of human melanoma xenografts in immunodeficient mice. Importantly, these studies provided us the opportunity to determine the specific gene expression of human and mouse compartments (tumor and stroma, respectively) using species-specific primers. With this purpose we obtained xenografts with two uveal melanoma cell lines, MUM2B and MUM2C, which different endogenous levels of ADAMTS1 were previously revealed [5]. As the levels of mouse *Adamts1* transcripts have been found at low levels

in a wide variety of organs [32] (and our unpublished results), we used lung tissue and the murine LLC cell line to normalize these results. Very significantly, mouse *Adamts1* expression was upregulated in both types of xenografts, independently of the endogenous levels of the protease in the human melanoma cells (Figure 7C). These results also supports a main role of ADAMTS1

provided by the host microenvironment as a relevant player during tumorigenesis.

DISCUSSION

The current report reveals that the loss of ADAMTS1 in the host stroma leads to the impairment of
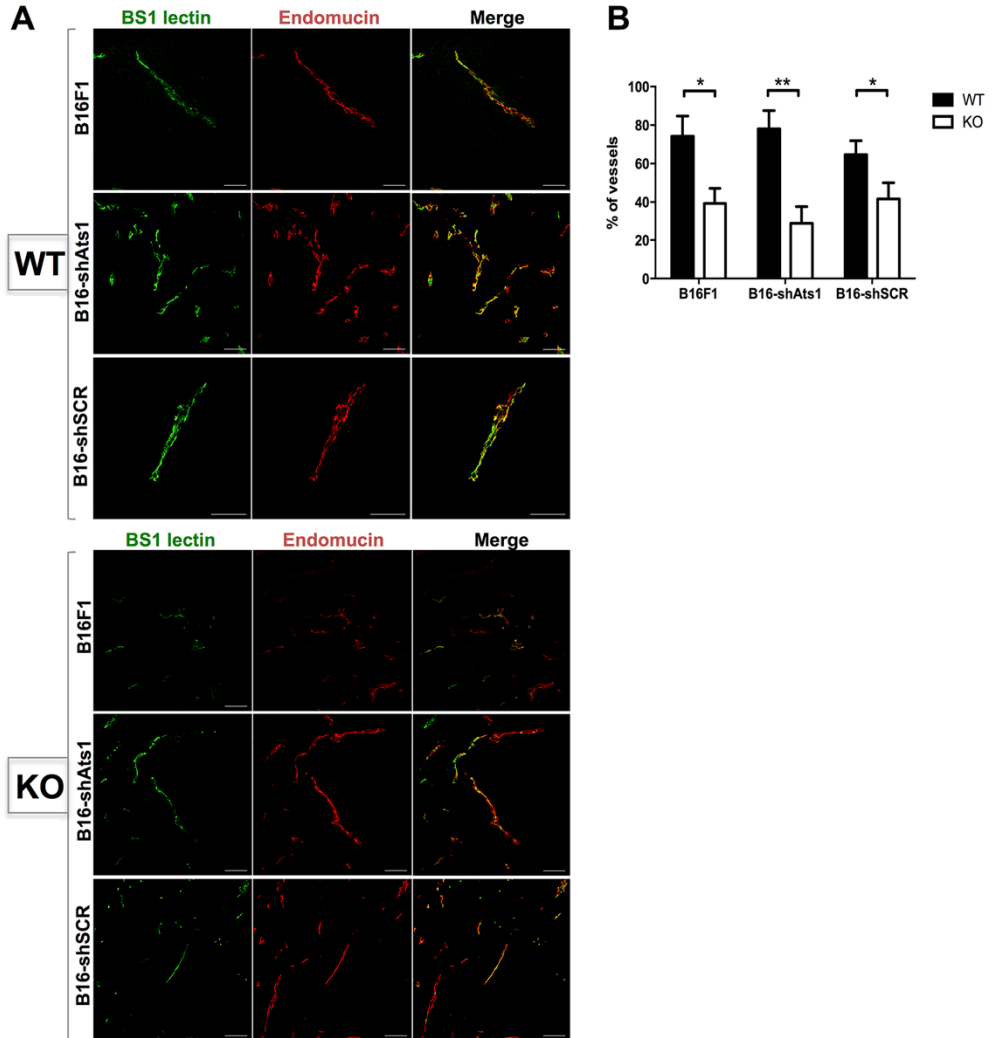
Figure 5: Evaluation of functionality of vasculature of tumors derived from control and modified B16F1 cells in WT and ATS1-KO mice. A. Fluorescence microscopy images of tumor sections from different mouse groups, showing positive signal of Bs1 lectin (green), Endomucin immunostaining (red), and merge. **B.** Graph representing the quantification (in percentage) of the number of vessels that showed a colocalization of Bs1 lectin and Endomucin signals within each tumor sections. (Number of animals in this experiment: WT/B16F1, n=4; ATS1-KO/B16F1, n=4; WT/B16-shAts1, n=7; ATS1-KO/B16 shAts1, n=10; WT/B16-shSCR, n=6; ATS1-KO/B16-shSCR, n=8). Bars show mean values ± SEM. Statistical analyses show unpaired Student's t test. (*, $p < 0.05$; **, $p < 0.01$).

165

tumor progression and development of metastasis. The use of a syngeneic tumor model with the ADAMTS1 KO mice, in combination with human xenografts and ex-vivo studies, allowed us to discriminate between the functional contribution of ADAMTS1 provided by tumor or stromal elements. Our findings also showed that the actions of ADAMTS1 affect functional neovascularization in the developing tumors with consequences for macrophage infiltration. It is likely that various mechanisms underlie these effects of ADAMTS1 according to its enzymatic activity and interaction with extracellular matrix components.

A relevant number of studies already implicated ADAMTS1 in tumor growth and metastasis although with different approaches (recently reviewed in [2]). For example, ADAMTS1 was found to be significantly over-expressed in clonal populations of highly metastatic cells to bone [33], and other authors have shown that its contribution to tumor development involved an induction of stroma remodeling [34] . More recently, the use of a tumor-prone model for mouse mammary carcinoma

reported the requirement of *Adamts1* gene for invasion and progression [7]. Importantly this last report has been the only one, as far as we know, that included an *Adamts1*-deficient mouse [35] in a cancer-related study. The comparison with our model is compulsory and we must remark several distinctions. Firstly, Russell and colleagues [7] used the well recognized MMTV-PyMT transgenic mice [36] to evaluate mammary tumor progression. Since the absence of *Adamts1* occurs in all cells, both neoplasic and stromal, it is not possible to discriminate between the relevance of the protease secreted by tumor cells or by different stromal components. As for our approach, although we need to agree about the caveat that tumors do not develop in a spontaneous manner, the implantation of tumor cells in a genetically modified mouse remains as a powerful tool to unveil the specific contribution of singular compartments, namely tumor versus stroma. Remarkably our results also support a pro-tumorigenic and pro-metastatic activity of ADAMTS1, and we provided for the first time the finding that ADAMTS1 originated in the stroma contributes more significantly than ADAMTS1
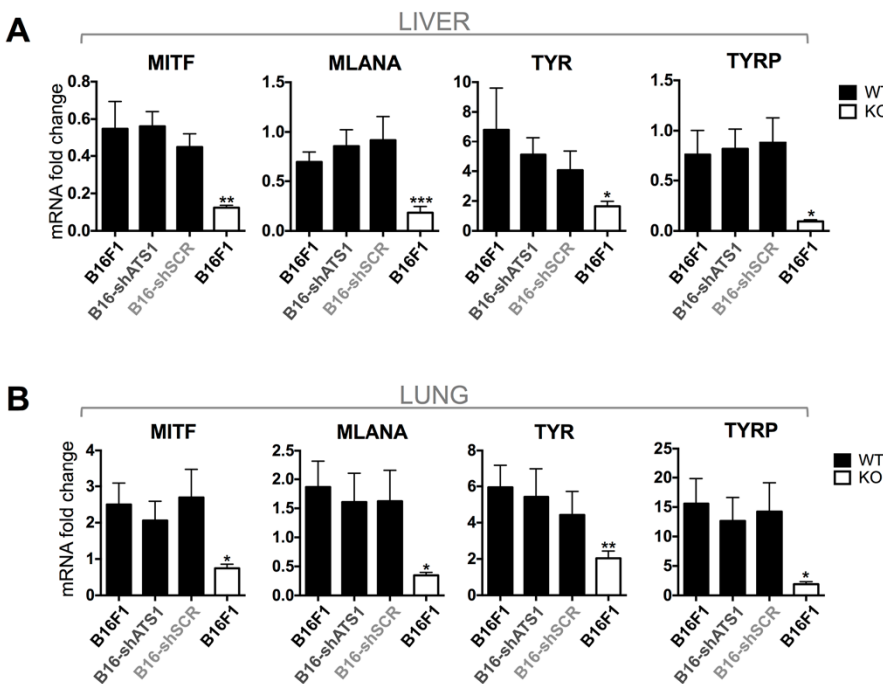
Figure 6: Gene expression analysis of melanoma markers (MITF, MLANA, TYR, TYRP). A. Graphs representing gene expression of the indicated genes in liver of WT and ATS1-KO mice. Animals were previously injected with control and modified B16F1 cells. In the case of WT mice (black bars), they were intravenously injected with non-modified cells (B16F1) (n=6), interfered shATS1 cells (B16-shATS1) (n=7), and scramble control cells (B16-shSCR) (n=5). Additionally, ATS1-KO mice (white bars) were injected with non-modified B16F1 cells (n=6). **B.** Graphs representing gene expression of the indicated genes in lung of WT and ATS1-KO mice. Groups are as specified for panel A. Bars show mean values ± SEM (*, $p < 0.05$; **, $p < 0.01$; ***, $p < 0.001$).

derived from tumor cells. The use of a syngeneic model with genetically-modified animals has been described for a variety of extracellular molecules [37–42]. In this study we added the manipulation of our gene of interest in the implanted tumor cells, revealing its minor contribution, at least in this tumor model.

The evaluation of *Adamts1* gene expression in our different experimental groups also provided a critical observation. We considered very relevant the lack of differences in *Adamts1* expression between tumors generated in WT and in ATS1-KO animals (Figure 1C and 4C), although tumor progression was clearly affected (Figure 1B and 4B). In fact we even detected that *Adamts1* tumor expression suffered an induction in the ATS1-KO

mice, probably related with its regulation by hypoxia. Such findings suggested that currently ongoing expression analyses of whole tumor samples might not provide the proper information to discard or to predict the malignancy of a neoplasia. With a similar perspective, an avalanche of reports on tumor heterogeneity are emphasizing the necessity to implement current clinical strategies [43]. Here we also highlight the importance to discriminate between stroma and tumor components.

Very interestingly, our recent results demonstrate that the basal expression of ADAMTS1 in stromal cells, such as endothelium and macrophage-related population, is induced in a tumor context. Such findings suggest a relevant role for this protease under stressing conditions.
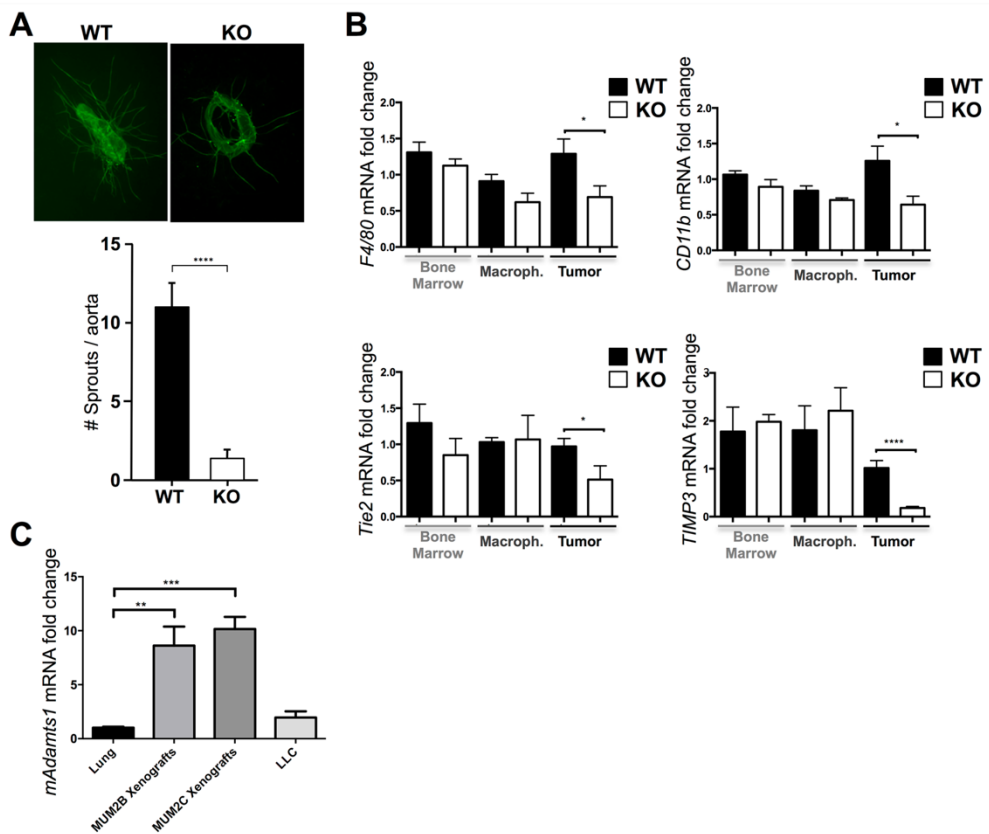
Figure 7: Contribution of ADAMTS1 to vascularization and macrophage infiltration and induction of its expression in stromal compartments. A. Representative images (5x magnification) of *ex vivo* aortic rings (day 6) from WT and ATS1-KO mice, stained for FITC-BS1 Lectin to visualize sprouts. Accompanying graph represents the quantification of sprouts from aortic rings of WT (n=52) and ATS1-KO (n=69) animals. **B.** Graphs representing gene expression analyses of various macrophage-related markers (F4/80, CD11b, Tie2, TIMP3) in bone marrow, macrophages derived from bone marrow, and B16F1 tumors from WT and ATS1-KO mice. **C.** Graph representing gene expression of mouse *Adamts1* in lungs (n=5), MUM2B xenografts (n=8), MUM2C xenografts (n=21), and LLC cells (n=5). All statistical analyses show unpaired Student's t test (*, p < 0.05; ***, p<0.001; ****, p < 0.0001).

The identification of specific substrates in every situation is still a current and required focus on the extracellular matrix field.

The implication of ADAMTS1 (and other ADAMTS members) for various vascular-related phenomena has been a constant finding since the first functional studies, though the results are apparently contradictory, with both pro- and anti-angiogenic features (reviewed in [44]). Still there is necessity to investigate the extracellular components of every cellular model in order to unveil this complex picture. For example, multiple abnormalities have been described in the basement membrane surrounding tumor vessels compared with normal vasculature [45], such as distinct thickness, reduced pericyte coverage, but also altered processing of basic components [4]. In this work we found that the lack of ADAMTS1 precludes endothelial sprouting in the aortic ring assay. Furthermore, tumor vasculature in ATS1-KO mice appeared dysfunctional, showing strong hypoxic areas.

Finally, our finding that infiltration of macrophages is challenged in tumors in the absence of stromal ADAMTS1 provokes a novel perspective for future research. In one side the reciprocal interaction, between the vasculature and the specialization of macrophages, deserves a major effort. Furthermore, the link of this observation with the current and successful advances in immunotherapies to fight cancer definitively emphasizes the importance to get deeper in these studies.

MATERIALS AND METHODS

Vectors, lentiviral production, and transduction

Knockdown vectors containing shRNAs to inhibit ADAMTS1 expression were purchased from Sigma (MISSION, St. Louis, MO, USA). Lentiviral particles pseudotyped with the VSV-G protein were generated on HEK293T cells using a standard calcium-phosphate transfection protocol. Mouse B16F1 melanoma cells were infected overnight. The following day, the viral supernatant was removed and transduced B16F1 cells were washed with media and allowed to expand. Media containing puromycin 1µg/ml was added to cultures and selection was carried out for 2 weeks. ADAMTS1 downregulation was tested by qPCR and western blot analyses (Supplementary Figure S2A–S2B).

Cell culture

Mouse tumor cells B16F0, B16F1, Lewis Lung Carcinoma (LLC), and brain immortalized endothelial cells (BEND), were cultured in DMEM supplemented with 10 % fetal bovine serum (FBS), and 1 % penicillin-streptomycin. Mouse aortic primary endothelial cells (MAEC) from C57BL/6 mice (Cell Biologics Inc,

Chicago, IL) were cultured in complete mouse endothelial cell culture medium (M1168 Kit, Cell Biologics Inc). Human umbilical vein endothelial cells (HUVECs) (Lonza, Switzerland) were cultured in EGM-2 medium. Human embryonic kidney (HEK293T) cells were grown in DMEM supplemented with 10 % FBS, 1 % penicillin-streptomycin and 2 mM L-glutamine. All cells were maintained at 37 °C under 5 % CO_2 atmosphere and 95 % humidity.

Tumor xenograft and metastasis assays

All mice were kept in the Centro de Investigaciones Biomédicas-UGR Animal Facility under pathogen-free conditions and according to institutional guidelines. For the generation of syngeneic tumors, $1x10^6$ cells in 200 µl of PBS were subcutaneously injected in the right flank of C57Bl/6 mice from wild type and *Adamts1* KO (ATS1-KO) genotypes [46]. Tumor growth was monitored up to 18 days. All animals were sacrificed following proper ethical and institutional guidelines. Tumors were dissected and processed for further analysis.

For the metastasis assay, $3x10^5$ cells in 100 µl of PBS were intravenously injected through the tail vein of C57Bl/6 mice, also from wild type and ATS1-KO genotypes. These mice were under observation for 13 days and then they were sacrificed and various organs were properly dissected for further analysis.

Human melanoma xenografts were generated in Swiss Nude mice with human uveal melanoma cells MUM2B and MUM2C [5]. $1x10^6$ cells in 200 µl of PBS were subcutaneously injected in the right flank, and tumor growth was monitored during 18-25 days. Tumors were dissected and processed for gene expression analysis.

Immunohistological analysis and vasculature characterization

A morphometric analysis of vessels was obtained by immunostaining with a monoclonal rat anti-mouse Endomucin antibody (SC-65495, SCBT) in tumor sections, and images were captured with the AxioImager A1 microscope (Zeiss). Depending of the size of the section, up to 10 fields per tumor were captured. All the analyses were done as previously reported [27], in this case using Metamorph 7 software (Molecular Devices, California, USA). Grey scale images of endomucin-stained sections are required. Previous to quantification, the operator establishes an optimal threshold (to discard non-specific signals) that it is maintained through the complete study. Accordingly, the application identifies positive signals and quantifies the number of positive units (number of vessels), and the area and perimeter of positive units. Simple mathematical functions estimate the average and total area, average and total perimeter, and additional parameters.

To measure hypoxia we followed the instructions of the Hypoxyprobe-1 kit (Hypoxyprobe Inc., Burlington, Mass., USA). Accordingly, 60 mg/kg pimonidazole hydrochloride were injected intraperitoneally into tumor-bearing mice that were sacrificed 30 minutes later. Tumor tissues were properly dissected and embedded in paraffin. Immunofluorescence staining using an antipimonidazole monoclonal FITC antibody was performed according to the manufacturer's instructions. Images were captured with a LSM710 (Zeiss) and quantification was done using ZEN 2010B SP1 software (Zeiss).

To assess vascular viability we injected intravenously a group of tumor-bearing mice with 100 μl of FITC-conjugated *Bandeira simplicifolia (Bs1)* lectin (50 μg/ml). 5 minutes later animals were anesthetized with intraperitoneal administration of ketamine (100 mg/kg) and xylazine (10 mg/kg). In sedated mice we administered 500 μl of PFA 4 % intracardially in the left ventricle to fix the lectin.

Aortic ring assay

Aortas from different animal backgrounds were extracted, cleaned from fat and connective tissue and embedded in a matrix of collagen I for 1 h at 37 °C to solidify, as previously described [47]. Optimem media supplemented with 2,5 % FBS and 30 ng/ml VEGF was added to rings and they were maintained at 37 °C and 8 % CO_2. Media was refreshed every three days. After sprouting, the rings were fixed for staining with 4 % PFA for 1 h. Tips from sprouts were counted at day 10.

Bone marrow extraction and macrophage differentiation

Wild type and ATS1-KO C57Bl/6 mice aged between 8 and 12 weeks were sacrificed and dissected following the proper ethic guidelines. Their femur and tibia were extracted from both legs followed by the cut of the boneheads, leaving the bone cane open. A 23G syringe with PBS was used to flush the bone marrow out of the bone to continue with the disaggregation into single cells. The resulting extract was filtered using a 100 μm cell strainer followed by a 300 g spin during 5 minutes at RT. The resulting cell suspension was counted and seeded at a concentration of $4x10^5$ cells/ml in a 10 cm non-treated tissue culture plate, containing DMEM 10 % FCS, 1 % P/S and 10 ng/ml mCSF (Peprotech 300-25). Culture was maintained for 7 days with a media change at day 3. Flow cytometry with CD11b Antibody (553311, BD Pharmigen) was performed at day 7 to check the enrichment in macrophage populations. At different stages, bone marrow and macrophage lysates were obtained for RNA or protein extraction.

Quantitative RT-PCR and statistical analysis

Total RNA was extracted from tumor biopsies and tissues using the NucleoSpin RNAII kit (Macherery-Nagel). cDNA was synthesized with iScript cDNA Synthesis Kit (Bio-Rad). qPCR reaction was performed in a 7900HT PCR machine (Applied Biosystems) using Fast SYBR green master mix (Applied Biosystems). qPCR representations show the $2^{\wedge}(-\Delta\Delta Ct)$ value using actin, β2 microglobulin and 18S RNA as reference genes. A geometric mean of the selected housekeeping genes was used for normalization. Values show mean ± standard error of the mean (SEM). Statistical analyses were performed by unpaired Student's t test using GraphPad Prism software. Differences were considered statistically significant at $p < 0.05$.

Western blot analysis

Conditioned medium from cells was clarified and concentrated with StrataClean resin (Stratagene) as previously described [12]. Total protein from tumor samples and cell lysates was extracted using RIPA buffer containing 1 mM PMSF, 1 μg/ml aprotinin and 10 μg/ml leupeptin. Proteins were resolved by SDS-PAGE and transferred to PVDF membranes (BioRad). Membranes were blocked with 5 % low-fat milk and incubated with the monoclonal mouse anti-human ADAMTS1 antibody (AF5867, R&D Systems). After incubation with the appropriate secondary peroxidase-conjugated antibody, signal was detected with the SuperSignal West Dura Chemiluminescence Kit (Pierce) in an ImageQuant LAS4000 (GE Healthcare Life Sciences).

169

REFERENCES

1. Vázquez F, Hastings G, Ortega MA, Lane TF, Oikemus S, Lombardo M, et al. METH-1, a human ortholog of ADAMTS-1, and METH-2 are members of a new family of proteins with angio-inhibitory activity. J Biol Chem. 1999 Aug 13;274:23349–57.

2. Cal S, López-Otín C. ADAMTS proteases and cancer. Matrix Biol. 2015 Jan;44-46C:77–85.

3. Reynolds LE, Watson AR, Baker M, Jones TA, D'Amico G, Robinson SD, et al. Tumour angiogenesis is reduced in the Tc1 mouse model of Down's syndrome. Nature. 2010 Jun 10;465:813–7.

4. Martino-Echarri E, Fernández-Rodríguez R, Rodríguez-Baena FJ, Barrientos-Durán A, Torres-Collado AX, Plaza-Calonge M del C, et al. Contribution of ADAMTS1 as a tumor suppressor gene in human breast carcinoma. Linking its tumor inhibitory properties to its proteolytic activity on nidogen-1 and nidogen-2. Int J Cancer. 2013 Nov 15;133:2315–24.

5. Casal C, Torres-Collado AX, Plaza-Calonge MC, Martino-Echarri E, Ramon y Cajal S, Rojo F, et al. ADAMTS1 contributes to the acquisition of an endothelial-like phenotype in plastic tumor cells. Cancer Res. 2010;70:4676–86.

6. Lu X, Wang Q, Hu G, Van Poznak C, Fleisher M, Reiss M, et al. ADAMTS1 and MMP1 proteolytically engage EGF-like ligands in an osteolytic signaling cascade for bone metastasis. Genes Dev. 2009;23:1882–94.

7. Ricciardelli C, Frewin KM, Tan I de A, Williams ED, Opeskin K, Pritchard MA, et al. The ADAMTS1 protease gene is required for mammary tumor growth and metastasis. Am J Pathol. 2011 Dec;179:3075–85.

8. Rocks N, Paulissen G, Quesada-Calvo F, Munaut C, Gonzalez ML, Gueders M, et al. ADAMTS-1 metalloproteinase promotes tumor development through the induction of a stromal reaction in vivo. Cancer Res. 2008;68:9541–50.

9. Rodriguez-Manzaneque JC, Carpizo D, Plaza-Calonge Mdel C, Torres-Collado AX, Thai SN, Simons M, et al. Cleavage of syndecan-4 by ADAMTS1 provokes defects in adhesion. Int J Biochem Cell Biol. 2009;41:800–10.

10. Rodríguez-Manzaneque JC, Westling J, Thai SN-M, Luque A, Knauper V, Murphy G, et al. ADAMTS1 cleaves aggrecan at multiple sites and is differentially inhibited by metalloproteinase inhibitors. Biochem Biophys Res Commun. 2002 Apr;293:501–8.

11. Sandy JD, Westling J, Kenagy RD, Iruela-Arispe ML, Verscharen C, Rodriguez-Manzaneque JC, et al. Versican V1 proteolysis in human aorta in vivo occurs at the Glu441-Ala442 bond, a site which is cleaved by recombinant ADAMTS-1 and ADAMTS-4. J Biol Chem. 2001;276:13372–8.

12. Canals F, Colome N, Ferrer C, Plaza-Calonge Mdel C, Rodriguez-Manzaneque JC. Identification of substrates of the extracellular protease ADAMTS1 by DIGE proteomic analysis. Proteomics. 2006;6 Suppl 1:S28–35.

13. Esselens C, Malapeira J, Colome N, Casal C, Rodriguez-Manzaneque JC, Canals F, et al. The cleavage of semaphorin 3C induced by ADAMTS1 promotes cell migration. J Biol Chem. 2010;285:2463–73.

14. Torres-Collado AX, Kisiel W, Iruela-Arispe ML, Rodriguez-Manzaneque JC. ADAMTS1 interacts with, cleaves, and modifies the extracellular location of the matrix inhibitor tissue factor pathway inhibitor-2. J Biol Chem. 2006;281:17827–37.

15. Su S-C, Mendoza EA, Kwak H-I, Bayless KJ. Molecular profile of endothelial invasion of three-dimensional collagen matrices: insights into angiogenic sprout induction in wound healing. Am J Physiol Cell Physiol. 2008 Nov 1;295:C1215–29.

16. Hatipoglu OF, Hirohata S, Cilek MZ, Ogawa H, Miyoshi T, Obika M, et al. ADAMTS1 is a unique hypoxic early response gene expressed by endothelial cells. J Biol Chem. 2009;284:16325–33.

17. Xu Z, Yu Y, Duh EJ. Vascular endothelial growth factor upregulates expression of ADAMTS1 in endothelial cells through protein kinase C signaling. Invest Ophthalmol Vis Sci. 2006;47:4059–66.

18. Tyan S-W, Hsu C-H, Peng K-L, Chen C-C, Kuo W-H, Lee EY-HP, et al. Breast cancer cells induce stromal fibroblasts to secrete ADAMTS1 for cancer invasion through an epigenetic change. PLoS One. 2012 Jan;7:e35128.

19. Porter S, Scott SD, Sassoon EM, Williams MR, Jones JL, Girling AC, et al. Dysregulated expression of adamalysin-thrombospondin genes in human breast carcinoma. Clin Cancer Res. 2004;10:2429–40.

20. Gustavsson H, Tesan T, Jennbacken K, Kuno K, Damber JE, Welen K. ADAMTS1 alters blood vessel morphology and TSP1 levels in LNCaP and LNCaP-19 prostate tumors. BMC Cancer. 2010;10:288.

21. Iruela-Arispe ML, Carpizo D, Luque A. ADAMTS1: a matrix metalloprotease with angioinhibitory properties. Ann N Y Acad Sci. 2003;995:183–90.

22. Liu YJ, Xu Y, Yu Q. Full-length ADAMTS-1 and the ADAMTS-1 fragments display pro- and antimetastatic activity, respectively. Oncogene. 2006;25:2452–67.

23. Obika M, Ogawa H, Takahashi K, Li J, Hatipoglu OF, Cilek MZ, et al. Tumor growth inhibitory effect of ADAMTS1 is accompanied by the inhibition of tumor angiogenesis. Cancer Sci. 2012 Oct;103:1889–97.

24. Carlin S, Pugachev A, Sun X, Burke S, Claus F, O'Donoghue J, et al. In vivo characterization of a reporter gene system for imaging hypoxia-induced gene expression. Nucl Med Biol. 2009 Oct;36:821–31.

25. Gaustad J-V, Simonsen TG, Leinaas MN, Rofstad EK. Sunitinib treatment does not improve blood supply but induces hypoxia in human melanoma xenografts. BMC Cancer. 2012 Jan;12:388.

170

26. Zhou Z, Yu L, Kleinerman ES. EWS-FLI-1 regulates the neuronal repressor gene REST, which controls Ewing sarcoma growth and vascular morphology. Cancer. 2014 Feb 15;120:579–88.

27. Rodriguez-Manzaneque JC, Lane TF, Ortega MA, Hynes RO, Lawler J, Iruela-Arispe ML. Thrombospondin-1 suppresses spontaneous growth and inhibits activation of matrix metalloproteinase-9 and mobilization of vascular endothelial growth factor. Proc Natl Acad Sci USA. 2001;98:12485–90.

28. Lee YJ, Koch M, Karl D, Torres-Collado AX, Fernando NT, Rothrock C, et al. Variable inhibition of thrombospondin 1 against liver and lung metastases through differential activation of metalloproteinase ADAMTS1. Cancer Res. 2010;70:948–56.

29. Hendrix MJ, Seftor EA, Hess AR, Seftor RE. Vasculogenic mimicry and tumour-cell plasticity: lessons from melanoma. Nat Rev Cancer. 2003;3:411–21.

30. Ruffell B, Coussens LM. Macrophages and therapeutic resistance in cancer. Cancer Cell. 2015 Apr 13;27:462–72.

31. Gill SE, Gharib SA, Bench EM, Sussman SW, Wang RT, Rims C, et al. Tissue inhibitor of metalloproteinases-3 moderates the proinflammatory status of macrophages. Am J Respir Cell Mol Biol. 2013 Nov;49:768–77.

32. Thai SN-M, Iruela-Arispe ML. Expression of ADAMTS1 during murine development. Mech Dev. 2002 Jul;115:181–5.

33. Lu X, Wang Q, Hu G, Van Poznak C, Fleisher M, Reiss M, et al. ADAMTS1 and MMP1 proteolytically engage EGF-like ligands in an osteolytic signaling cascade for bone metastasis. Genes Dev. 2009;23:1882–94.

34. Rocks N, Paulissen G, Quesada-Calvo F, Munaut C, Gonzalez ML, Gueders M, et al. ADAMTS-1 metalloproteinase promotes tumor development through the induction of a stromal reaction in vivo. Cancer Res. 2008;68:9541–50.

35. Mittaz L, Russell DL, Wilson T, Brasted M, Tkalcevic J, Salamonsen LA, et al. Adamts-1 is essential for the development and function of the urogenital system. Biol Reprod. 2004;70:1096–105.

36. Qiu TH, Chandramouli GVR, Hunter KW, Alkharouf NW, Green JE, Liu ET. Global expression profiling identifies signatures of tumor virulence in MMTV-PyMT-transgenic

mice: correlation to human disease. Cancer Res. 2004 Sep 1;64:5973–81.

37. Liu Y, Jang S, Xie L, Sowa G. Host deficiency in caveolin-2 inhibits lung carcinoma tumor growth by impairing tumor angiogenesis. Cancer Res. 2014 Nov 15;74:6452–62.

38. Goetz JG, Minguet S, Navarro-Lérida I, Lazcano JJ, Samaniego R, Calvo E, et al. Biomechanical remodeling of the microenvironment by stromal caveolin-1 favors tumor invasion and metastasis. Cell. 2011;146:148–63.

39. Itoh T, Tanioka M, Yoshida H, Yoshioka T, Nishimoto H, Itohara S. Reduced angiogenesis and tumor progression in gelatinase A-deficient mice. Cancer Res. 1998 Mar 1;58:1048–51.

40. Boulay A, Masson R, Chenard MP, El Fahime M, Cassard L, Bellocq JP, et al. High cancer cell death in syngeneic tumors developed in host mice deficient for the stromelysin-3 matrix metalloproteinase. Cancer Res. 2001 Mar 1;61:2189–93.

41. Cruz-Muñoz W, Kim I, Khokha R. TIMP-3 deficiency in the host, but not in the tumor, enhances tumor growth and angiogenesis. Oncogene. 2006 Jan 26;25:650–5.

42. Vences-Catalan F, Rajapaksa R, Srivastava MK, Marabelle A, Kuo C-C, Levy R, et al. Tetraspanin CD81 promotes tumor growth and metastasis by modulating the functions of T regulatory and myeloid-derived suppressor cells. Cancer Res. 2015 Sep 1;75:4517–26.

43. Alizadeh AA, Aranda V, Bardelli A, Blanpain C, Bock C, Borowski C, et al. Toward understanding and exploiting tumor heterogeneity. Nat Med. 2015 Aug 6;21:846–53.

44. Rodríguez-Manzaneque JC, Fernández-Rodríguez R, Rodríguez-Baena FJ, Iruela-Arispe ML. ADAMTS proteases in vascular biology. Matrix Biol. 2015 Jan;44-46C:38–45.

45. Baluk P, Morikawa S, Haskell A, Mancuso M, McDonald DM. Abnormalities of basement membrane on blood vessels and endothelial sprouts in tumors. Am J Pathol. 2003;163:1801–15.

46. Lee N V, Sato M, Annis DS, Loo JA, Wu L, Mosher DF, et al. ADAMTS1 mediates the release of antiangiogenic polypeptides from TSP1 and 2. EMBO J. 2006;25:5270–83.

47. Baker M, Robinson SD, Lechertier T, Barber PR, Tavora B, D'Amico G, et al. Use of the mouse aortic ring assay to study angiogenesis. Nat Protoc. 2012;7:89–104.

171

α   **Contribution of ADAMTS1 as a tumor suppressor gene in human breast carcinoma. Linking its tumor inhibitory properties to its proteolytic activity on nidogen-1 and nidogen-2.** Martino-Echarri, E., Fernández-Rodríguez, R., Rodríguez-Baena, F.J., Barrientos-Durán, A., Torres-Collado, A.X., Plaza-Calonge, M. del C., Amador-Cubero, S., Cortés, J., Reynolds, L.E., Hodivala-Dilke, K.M., et al. (2013). Int. J. Cancer *133*, 2315–2324. Impact factor: 5,531. Q1

α   **ADAMTS proteases in vascular biology.** Rodríguez-Manzaneque, J.C., Fernández-Rodríguez, R., Rodríguez-Baena, F.J., and Iruela-Arispe, M.L. (2015). Matrix Biol. *44*, 38–45. Impact factor: 4,47. Q1

ABSTRACTS AND PUBLICATIONS TO CONFERENCES AROSE FROM THIS THESIS

FJ Rodríguez-Baena, R Fernández-Rodríguez, MD Plaza-Calonge, and JC Rodríguez-Manzaneque. *Study of the extracellular protease ADAMTS1 and its substrates in the vasculature: relevance for tumour progression and neo-vascularization. Angiogenesis and vascular remodelling - new perspectives*. The biochemical society conference, 14-16 July 2014, Chester, United Kingdom. **Oral presentation and poster.**

FJ Rodríguez-Baena, S Redondo-Garcia, D. L. Russell and JC Rodríguez-Manzaneque. *Study of the extracellular protease ADAMTS1 and its substrates in the vasculature: relevance for tumour progression and neo-vascularization*. Ph.D conference of the University of Adelaide, Australia. 16 october 2015. **Poster.**

FJ Rodríguez-Baena, S Redondo-Garcia, D. L. Russell and JC Rodríguez-Manzaneque. *Study of the extracellular protease ADAMTS1 and its substrates in the vasculature: relevance for tumour progression and neo-vascularization*. Australian New Zealand Bone & Mineral Society Annual Scientific Meeting 2015. Hobart, Tasmania, Australia. 1 – 4 November 2015. **Poster.**

FJ Rodríguez-Baena, S Redondo-Garcia, D. L. Russell and JC Rodríguez-Manzaneque. *Study of the extracellular protease ADAMTS1 and its substrates in the vasculature: relevance for tumour progression and neo-vascularization*. 5th Adelaide Cell and Developmental Biology Meeting, Adelaida, Australia. 17 November 2015. **Oral presentation and Poster.**

FJ Rodríguez-Baena, S Redondo-Garcia, C Peris-Torres, O Serrano-Garrido, R Fernández-Rodríguez, MD Plaza-Calonge, D. L. Russell and JC Rodríguez-Manzaneque. *Study of the extracellular protease ADAMTS1 and its substrates in the vasculature: relevance for tumour progression and neo-vascularization*. ASMB 2016 Biennial conference. The ECM microenvironment: A regulatory force in aging and disease. 13-16 November 2016, St. Petersburg, Florida, EE.UU. **Oral presentation and Poster.**

FJ Rodríguez-Baena, S Redondo-Garcia, C Peris-Torres, O Serrano-Garrido, R Fernández-Rodríguez, MD Plaza-Calonge, and JC Rodríguez-Manzaneque. *Elucidating the actions of ADAMTS1, from stromal and/or tumour origin, in distinct tumour models*. ASMB 2016 Biennial conference. The ECM microenvironment: A regulatory force in aging and disease. 13-16 November 2016, St. Petersburg, Florida, EE.UU. **Oral presentation and poster.**

BIBLIOGRAPHY

A

Adams, R.H., and Alitalo, K. (2007). Molecular regulation of angiogenesis and lymphangiogenesis. Nat. Rev. Mol. Cell Biol. *8*, 464–478.

Alexander, C.M., Howard, E.W., Bissell, M.J., and Werb, Z. (1996). Rescue of mammary epithelial cell apoptosis and entactin degradation by a tissue inhibitor of metalloproteinases-1 transgene. J. Cell Biol. *135*.

Apte, S.S. (2009). A disintegrin-like and metalloprotease (reprolysin-type) with thrombospondin type 1 motif (ADAMTS) superfamily: functions and mechanisms. J. Biol. Chem. *284*, 31493–31497.

De Arao Tan, I., Ricciardelli, C., and Russell, D.L. (2013). The metalloproteinase ADAMTS1: A comprehensive review of its role in tumorigenic and metastatic pathways. Int. J. Cancer *133*, 2263–2276.

Armulik, A., Genové, G., Mäe, M., Nisancioglu, M.H., Wallgard, E., Niaudet, C., He, L., Norlin, J., Lindblom, P., Strittmatter, K., et al. (2010). Pericytes regulate the blood–brain barrier. Nature *468*, 557–561.

Arroyo, A.G., and Iruela-Arispe, M.L. (2010). Extracellular matrix, inflammation, and the angiogenic response. Cardiovasc. Res. *86*, 226–235.

Asahara, T., Murohara, T., Sullivan, A., Silver, M., van der Zee, R., Li, T., Witzenbichler, B., Schatteman, G., and Isner, J.M. (1997). Isolation of Putative Progenitor Endothelial Cells for Angiogenesis. Science (80-.). *275*.

Auld, D.S. (2013). Metalloproteases. In Encyclopedia of Biological Chemistry, pp. 86–89.

B

Bader, B.L., Smyth, N., Nedbal, S., Miosge, N., Baranowsky, A., Mokkapati, S., Murshed, M., and Nischt, R. (2005). Compound genetic ablation of nidogen 1 and 2 causes basement membrane defects and perinatal lethality in mice. Mol. Cell. Biol. *25*, 6846–6856.

Balkwill, F., and Mantovani, A. (2001). Inflammation and cancer: back to Virchow? Lancet *357*, 539–545.

Baluk, P., Morikawa, S., Haskell, A., Mancuso, M., and McDonald, D.M. (2003). Abnormalities of basement membrane on blood vessels and endothelial sprouts in tumors. Am. J. Pathol. *163*, 1801–1815.

Baranowsky, A., Mokkapati, S., Bechtel, M., Krügel, J., Miosge, N., Wickenhauser, C., Smyth, N., and Nischt, R. (2010). Impaired wound healing in mice lacking the basement membrane protein nidogen 1. Matrix Biol. *29*, 15–21.

Bender, B.L., Jaffe, R., Carlin, B., and Chung, A.E. (1981). Immunolocalization of entactin, a sulfated basement membrane component, in rodent tissues, and comparison with GP-2 (laminin). Am. J. Pathol. *103*, 419–426.

Bender, B.L., Carlin, B., Jaffe, R., Temple, T., and Chung, A.E. (1982). Production and distribution of entactin and GP-2 in M1536-B3 cells. Exp. Cell Res. *137*, 415–425.

Bercsenyi, K., Schmieg, N., Bryson, J.B., Wallace, M., Caccin, P., Golding, M., Zanotti, G., Greensmith, L., Nischt, R., and Schiavo, G. (2014). Tetanus toxin entry. Nidogens are therapeutic targets for the

prevention of tetanus. Science *346*, 1118–1123.

Bergers, G., and Hanahan, D. (2008). Modes of resistance to anti-angiogenic therapy. Nat. Rev. Cancer *8*, 592–603.

Bertram, J.S., and Janik, P. (1980). Establishment of a cloned line of Lewis Lung Carcinoma cells adapted to cell culture. Cancer Lett. *11*, 63–73.

Bhowmick, N.A., Neilson, E.G., and Moses, H.L. (2004). Stromal fibroblasts in cancer initiation and progression. Nature *432*, 332–337.

Bissell, M.J., and Hines, W.C. (2011). Why don't we get more cancer? A proposed role of the microenvironment in restraining cancer progression. Nat. Med. *17*, 320–329.

De Bock, K., Cauwenberghs, S., and Carmeliet, P. (2011). Vessel abnormalization: another hallmark of cancer? Molecular mechanisms and therapeutic implications. Curr. Opin. Genet. Dev. *21*, 73–79.

Bode, W., Grams, F., Reinemer, P., Gomis-Rüth, F.-X., Baumann, U., McKay, D.B., and Stöcker, W. (1996). The Metzincin-Superfamily of Zinc-Peptidases. (Springer US), pp. 1–11.

Boettcher, S., Gerosa, R.C., Radpour, R., Bauer, J., Ampenberger, F., Heikenwalder, M., Kopf, M., and Manz, M.G. (2014). Endothelial cells translate pathogen signals into G-CSF-driven emergency granulopoiesis. Blood *124*, 1393–1403.

Bonnet, D., and Dick, J.E. (1997). Human acute myeloid leukemia is organized as a hierarchy that originates from a primitive hematopoietic cell. Nat. Med. *3*, 730–737.

Bourd-Boittin, K., Bonnier, D., Leyme, A., Mari, B., Tuffery, P., Samson, M., Ezan, F., Baffet, G., and Theret, N. (2011). Protease profiling of liver fibrosis reveals the ADAM metallopeptidase with thrombospondin type 1 motif, 1 as a central activator of transforming growth factor beta. Hepatology *54*, 2173–2184.

Bronte, V., Apolloni, E., Cabrelle, A., Ronca, R., Serafini, P., Zamboni, P., Restifo, N.P., and Zanovello, P. (2000). Identification of a CD11b(+)/Gr-1(+)/CD31(+) myeloid progenitor capable of activating or suppressing CD8(+) T cells. Blood *96*, 3838–3846.

Brooks, P.C., Montgomery, A.M.P., Rosenfeld, M., Reisfeld, R.A., Hu, T., Klier, G., and Cheresh, D.A. (1994). Integrin αvβ3 antagonists promote tumor regression by inducing apoptosis of angiogenic blood vessels. Cell *79*, 1157–1164.

Brown, H.M., Dunning, K.R., Robker, R.L., Boerboom, D., Pritchard, M., Lane, M., and Russell, D.L. (2010). ADAMTS1 cleavage of versican mediates essential structural remodeling of the ovarian follicle and cumulus-oocyte matrix during ovulation in mice. Biol. Reprod. *83*, 549–557.

Bruce Alberts, Alexander Johnson, J.L., Martin Raff, K.R., and Peter, W. (2002). Molecular Biology of the Cell, 4th edition (New york: Garland Science).

C

Cal, S., and Lopez-Otin, C. (2015). ADAMTS proteases and cancer. Matrix Biol. *44–46*, 77–85.

Canals, F., Colomé, N., Ferrer, C., Plaza-Calonge, M.D.C., and Rodríguez-Manzaneque, J.C. (2006).

Identification of substrates of the extracellular protease ADAMTS1 by DIGE proteomic analysis. Proteomics *6 Suppl 1*, S28-35.

Cao, Z., Bao, M., Miele, L., Sarkar, F.H., Wang, Z., and Zhou, Q. (2013). Tumour vasculogenic mimicry is associated with poor prognosis of human cancer patients: A systemic review and meta-analysis. Eur. J. Cancer *49*, 3914–3923.

Carlin, B., Jaffe, R., Bender, B., and Chung, A.E. (1981). Entactin, a novel basal lamina-associated sulfated glycoprotein. J. Biol. Chem. *256*, 5209–5214.

Carmeliet, P., and Jain, R.K. (2011a). Principles and mechanisms of vessel normalization for cancer and other angiogenic diseases. Nat. Rev. Drug Discov. *10*, 417–427.

Carmeliet, P., and Jain, R.K. (2011b). Molecular mechanisms and clinical applications of angiogenesis. Nature *473*, 298–307.

Casal, C., Torres-Collado, A.X., Plaza-Calonge, M.D.C., Martino-Echarri, E., Ramón Y Cajal, S., Rojo, F., Griffioen, A.W., and Rodríguez-Manzaneque, J.C. (2010). ADAMTS1 contributes to the acquisition of an endothelial-like phenotype in plastic tumor cells. Cancer Res. *70*, 4676–4686.

Casimiro, S., Luis, I., Fernandes, A., Pires, R., Pinto, A., Gouveia, A.G., Francisco, A.F., Portela, J., Correia, L., and Costa, L. (2012). Analysis of a bone metastasis gene expression signature in patients with bone metastasis from solid tumors. Clin. Exp. Metastasis *29*, 155–164.

Chaffer, C.L., and Weinberg, R.A. (2011). A perspective on cancer cell metastasis. Science *331*, 1559–1564.

Chai, A.W.Y., Cheung, A.K.L., Dai, W., Ko, J.M.Y., Ip, J.C.Y., Chan, K.W., Kwong, D.L.-W., Ng, W.T., Lee, A.W.M., Ngan, R.K.C., et al. (2016). Metastasis-suppressing NID2, an epigenetically-silenced gene, in the pathogenesis of nasopharyngeal carcinoma and esophageal squamous cell carcinoma. Oncotarget *7*, 78859–78871.

Chang, M.Y., Tanino, Y., Vidova, V., Kinsella, M.G., Chan, C.K., Johnson, P.Y., Wight, T.N., and Frevert, C.W. (2014). A rapid increase in macrophage-derived versican and hyaluronan in infectious lung disease. Matrix Biol. *34*, 1–12.

Cheng, Z.-X., Huang, X.-H., Wang, Q., Chen, J.-S., Zhang, L.-J., and Chen, X.-L. (2012). Clinical significance of decreased nidogen-2 expression in the tumor tissue and serum of patients with hepatocellular carcinoma. J. Surg. Oncol. *105*, 71–80.

Cochrane, A.W., Chen, C.-H., and Rosen, C.A. (1990). Specific interaction of the human immunodeficiency virus Rev protein with a structured region in the env mRNA. Biochemistry *87*, 1198–1202.

Crawford, Y., and Ferrara, N. (2009a). VEGF inhibition: insights from preclinical and clinical studies. Cell Tissue Res. *335*, 261–269.

Crawford, Y., and Ferrara, N. (2009b). Tumor and stromal pathways mediating refractoriness/resistance to anti-angiogenic therapies. Trends Pharmacol. Sci. *30*, 624–630.

Crawford, Y., Kasman, I., Yu, L., Zhong, C., Wu, X., Modrusan, Z., Kaminker, J., and Ferrara, N. (2009). PDGF-C Mediates the Angiogenic and Tumorigenic Properties of Fibroblasts Associated with Tumors Refractory to Anti-VEGF Treatment. Cancer Cell *15*, 21–34.

Cross, N.A., Chandrasekharan, S., Jokonya, N., Fowles, A., Hamdy, F.C., Buttle, D.J., and Eaton, C.L. (2005). The expression and regulation of ADAMTS-1, -4, -5, -9, and -15, and TIMP-3 by TGFb1 in prostate

cells: relevance to the accumulation of versican. Prostate *63*, 269–275.

D

Darbro, B.W., Mahajan, V.B., Gakhar, L., Skeie, J.M., Campbell, E., Wu, S., Bing, X., Millen, K.J., Dobyns, W.B., Kessler, J. a, et al. (2013). Mutations in extracellular matrix genes NID1 and LAMC1 cause autosomal dominant Dandy-Walker malformation and occipital cephaloceles. Hum. Mutat. *34*, 1075–1079.

Dedhar, S., Jewell, K., Rojiani, M., and Gray, V. (1992). The receptor for the basement membrane glycoprotein entactin is the integrin alpha 3/beta 1. J. Biol. Chem. *267*, 18908–18914.

Dick, J.E. (2008). Stem cell concepts renew cancer research. Blood *112*.

Dick, J.E. (2009). Looking ahead in cancer stem cell research. Nat. Biotechnol. *27*, 44–46.

Dong, L., Chen, Y., Lewis, M., Hsieh, J.-C., Reing, J., Chaillet, J.R., Howell, C.Y., Melhem, M., Inoue, S., Kuszak, J.R., et al. (2002). Neurologic defects and selective disruption of basement membranes in mice lacking entactin-1/nidogen-1. Lab. Invest. *82*, 1617–1630.

Duffy, M.J., Mullooly, M., O'Donovan, N., Sukor, S., Crown, J., Pierce, A., and McGowan, P.M. (2011). The ADAMs family of proteases: new biomarkers and therapeutic targets for cancer? Clin. Proteomics *8*, 9.

Dunleavey, J.M., Xiao, L., Thompson, J., Kim, M.M., Shields, J.M., Shelton, S.E., Irvin, D.M., Brings, V.E., Ollila, D.W., Brekken, R.A., et al. (2014). Vascular channels formed by subpopulations of PECAM1(+) melanoma cells. Nat. Commun. *5*, 5200.

Dunn, J.R., Reed, J.E., du Plessis, D.G., Shaw, E.J., Reeves, P., Gee, A.L., Warnke, P., and Walker, C. (2006). Expression of ADAMTS-8, a secreted protease with antiangiogenic properties, is downregulated in brain tumours. Br. J. Cancer *94*, 1186–1193.

E

Eble, J.A., and Niland, S. (2009). The extracellular matrix of blood vessels. Curr. Pharm. Des. *15*, 1385–1400.

Edwards, I.J. (2012). Proteoglycans in prostate cancer. Nat. Rev. Urol. *9*, 196–206.

Egeblad, M., Nakasone, E.S., and Werb, Z. (2010). Tumors as Organs: Complex Tissues that Interface with the Entire Organism. Dev. Cell *18*, 884–901.

Ellis, L.M., and Hicklin, D.J. (2008). Pathways Mediating Resistance to Vascular Endothelial Growth Factor–Targeted Therapy. Clin. Cancer Res. *14*.

Esselens, C., Malapeira, J., Colomé, N., Casal, C., Rodríguez-Manzaneque, J.C., Canals, F., and Arribas, J. (2010). The cleavage of semaphorin 3C induced by ADAMTS1 promotes cell migration. J. Biol. Chem. *285*, 2463–2473.

F

Fang, M., Yuan, J., Peng, C., and Li, Y. (2014). Collagen as a double-edged sword in tumor progression. Tumor Biol. *35*, 2871–2882.

Fernández-Rodríguez, R., Rodríguez-Baena, F.J., Martino-Echarri, E., Peris-Torres, C., Del Carmen Plaza-Calonge, M., and Rodríguez-Manzaneque, J.C. (2016). Stroma-derived but not tumor ADAMTS1 is a main driver of tumor growth and metastasis. Oncotarget *7*, 34507–34519.

Ferrara, N., and Henzel, W.J. (1989). Pituitary follicular cells secrete a novel heparin-binding growth factor specific for vascular endothelial cells. Biochem. Biophys. Res. Commun. *161*, 851–858.

Ferrara, N., Hillan, K.J., and Novotny, W. (2005). Bevacizumab (Avastin), a humanized anti-VEGF monoclonal antibody for cancer therapy. Biochem. Biophys. Res. Commun. *333*, 328–335.

Flamme, I., Frölich, T., and Risau, W. (1997). Molecular mechanisms of vasculogenesis and embryonic angiogenesis. J. Cell. Physiol. *173*, 206–210.

Folberg, R., Kadkol, S.S., Frenkel, S., Valyi-Nagy, K., Jager, M.J., Pe'er, J., and Maniotis, A.J. (2008). Authenticating cell lines in ophthalmic research laboratories. Invest. Ophthalmol. Vis. Sci. *49*, 4697–4701.

Folkman, J. (1971). Tumor Angiogenesis: Therapeutic Implications. N. Engl. J. Med. *285*, 1182–1186.

Folkman, J., and Hanahan, D. (1991). Switch to the angiogenic phenotype during tumorigenesis. Princess Takamatsu Symp. *22*, 339–347.

Frantz, C., Stewart, K.M., and Weaver, V.M. (2010). The extracellular matrix at a glance. J. Cell Sci. *123*.

G

Gallina, G., Dolcetti, L., Serafini, P., De Santo, C., Marigo, I., Colombo, M.P., Basso, G., Brombacher, F., Borrello, I., Zanovello, P., et al. (2006). Tumors induce a subset of inflammatory monocytes with immunosuppressive activity on CD8+ T cells. J. Clin. Invest. *116*, 2777–2790.

Gao, D., Joshi, N., Choi, H., Ryu, S., Hahn, M., Catena, R., Sadik, H., Argani, P., Wagner, P., Vahdat, L.T., et al. (2012). Myeloid Progenitor Cells in the Premetastatic Lung Promote Metastases by Inducing Mesenchymal to Epithelial Transition. Cancer Res. *72*.

Gargett, T., Christo, S.N., Hercus, T.R., Abbas, N., Singhal, N., Lopez, A.F., and Brown, M.P. (2016). GM-CSF signalling blockade and chemotherapeutic agents act in concert to inhibit the function of myeloid-derived suppressor cells in vitro. Clin. Transl. Immunol. *5*, e119.

Giebeler, N., and Zigrino, P. (2016). A Disintegrin and Metalloprotease (ADAM): Historical Overview of Their Functions. Toxins (Basel). *8*, 122.

Goel, S., Duda, D.G., Xu, L., Munn, L.L., Boucher, Y., Fukumura, D., and Jain, R.K. (2011). Normalization of the vasculature for treatment of cancer and other diseases. Physiol Rev. *91*, 1071–1121.

Gomis-Rüth, F.X. (2009). Catalytic domain architecture of metzincin metalloproteases. J. Biol. Chem. *284*, 15353–15357.

Gordon, M.K., and Hahn, R.A. (2010). Collagens. Cell Tissue Res. *339*, 247–257.

Gorter, A., Zijlmans, H.J., van Gent, H., Trimbos, J.B., Fleuren, G.J., and Jordanova, E.S. (2010). Versican expression is associated with tumor-infiltrating CD8-positive T cells and infiltration depth in cervical cancer. Mod. Pathol. *23*, 1605–1615.

Greaves, M. (2010). Cancer stem cells: back to Darwin? Semin. Cancer Biol. *20*, 65–70.

Greaves, M., and Maley, C.C. (2012). Clonal evolution in cancer. Nature *481*, 306–313.

Gupta, K., and Zhang, J. (2005). Angiogenesis: a curse or cure? Postgrad. Med. J. *81*, 236–242.

Gustavsson, H., Tesan, T., Jennbacken, K., Kuno, K., Damber, J.-E.E., Welen, K., and Welén, K. (2010). ADAMTS1 alters blood vessel morphology and TSP1 levels in LNCaP and LNCaP-19 prostate tumors. BMC Cancer *10*, 288.

$\mathcal{H}$

Han, G., Li, F., Singh, T.P., Wolf, P., and Wang, X.-J. (2012). The Pro-inflammatory Role of TGFβ1: A Paradox? Int. J. Biol. Sci. *8*, 228–235.

Hanahan, D., and Coussens, L.M. (2012). Accessories to the Crime: Functions of Cells Recruited to the Tumor Microenvironment. Cancer Cell *21*, 309–322.

Hanahan, D., and Weinberg, R.A. (2000). The Hallmarks of Cancer Review. *100*, 57–70.

Hanahan, D., Weinberg, R.A., Adams, J.M., Cory, S., Aguirre-Ghiso, J.A., Ahmed, Z., Bicknell, R., Al-Hajj, M., Wicha, M.S., Benito-Hernandez, A., et al. (2011). Hallmarks of cancer: the next generation. Cell *144*, 646–674.

Hatipoglu, O.F., Hirohata, S., Cilek, M.Z., Ogawa, H., Miyoshi, T., Obika, M., Demircan, K., Shinohata, R., Kusachi, S., and Ninomiya, Y. (2009). ADAMTS1 is a unique hypoxic early response gene expressed by endothelial cells. J. Biol. Chem. *284*, 16325–16333.

Held-Feindt, J., Paredes, E.B., Blömer, U., Seidenbecher, C., Stark, A.M., Mehdorn, H.M., and Mentlein, R. (2006). Matrix-degrading proteases ADAMTS4 and ADAMTS5 (disintegrins and metalloproteinases with thrombospondin motifs 4 and 5) are expressed in human glioblastomas. Int. J. Cancer *118*, 55–61.

Hendrix, M.J.C., Seftor, E.A., Hess, A.R., and Seftor, R.E.B. (2003). Vasculogenic mimicry and tumour-cell plasticity: lessons from melanoma. Nat. Rev. Cancer *3*, 411–421.

Hendrix, M.J.C., Seftor, E.A., Seftor, R.E.B., Chao, J.-T., Chien, D.-S., and Chu, Y.-W. (2016). Tumor cell vascular mimicry: Novel targeting opportunity in melanoma. Pharmacol. Ther. *159*, 83–92.

Herbert, S.P., and Stainier, D.Y.R. (2011). Molecular control of endothelial cell behaviour during blood vessel morphogenesis. Nat. Rev. Mol. Cell Biol. *12*, 551–564.

Hess, A.R., Seftor, E.A., Gardner, L.M.G., Carles-Kinch, K., Schneider, G.B., Seftor, R.E.B., Kinch, M.S., and Hendrix, M.J.C. (2001). Molecular Regulation of Tumor Cell Vasculogenic Mimicry by Tyrosine Phosphorylation. Cancer Res. *61*.

Hess, A.R., Seftor, E.A., Seftor, R.E.B., and Hendrix, M.J.C. (2003). Phosphoinositide 3-Kinase Regulates Membrane Type 1-Matrix Metalloproteinase (MMP) and MMP-2 Activity during Melanoma Cell

Vasculogenic Mimicry. Cancer Res. *63*.

Hillen, F., and Griffioen, A.W. (2007). Tumour vascularization: sprouting angiogenesis and beyond. Cancer Metastasis Rev. *26*, 489–502.

Ho, M.S.P., Böse, K., Mokkapati, S., Nischt, R., and Smyth, N. (2008). Nidogens-Extracellular matrix linker molecules. Microsc. Res. Tech. *71*, 387–395.

Holash, J., Maisonpierre, P.C., Compton, D., Boland, P., Alexander, C.R., Zagzag, D., Yancopoulos, G.D., and Wiegand, S.J. (1999). Vessel Cooption, Regression, and Growth in Tumors Mediated by Angiopoietins and VEGF. Science (80-.). *284*.

Hope, C., Foulcer, S., Jagodinsky, J., Chen, S.X., Jensen, J.L., Patel, S., Leith, C., Maroulakou, I., Callander, N., Miyamoto, S., et al. (2016). Immunoregulatory roles of versican proteolysis in the myeloma microenvironment. Blood *128*, 680–685.

Hu, F. (1965). The developmental cycle of B16 melanoma cell in culture. Tex. Rep. Biol. Med. *23*, Suppl 1:308-20.

Huuzer, J.C., Uhlenkott, C.E., and Meadows, G.G. (1995). Differences in expression of metalloproteinases and plasminogen activators in murine melanocytes and B16 melanoma variants: Lack of association withIn vitro invasion. Int. J. Cancer *63*, 92–99.

J

Jain, R.K. (2005). Normalization of Tumor Vasculature: An Emerging Concept in Antiangiogenic Therapy. Science (80-.). *307*.

Jang, S.K., Davies, M. V, Kaufman, R.J., and Wimmer, E. (1989). Initiation of protein synthesis by internal entry of ribosomes into the 5' nontranslated region of encephalomyocarditis virus RNA in vivo. J. Virol. *63*, 1651–1660.

Junttila, M.R., and de Sauvage, F.J. (2013). Influence of tumour micro-environment heterogeneity on therapeutic response. Nature *501*, 346–354.

K

Kalluri, R. (2003). Angiogenesis: Basement membranes: structure, assembly and role in tumour angiogenesis. Nat. Rev. Cancer *3*, 422–433.

Kang, Y., Siegel, P.M., Shu, W., Drobnjak, M., Kakonen, S.M., Cordón-Cardo, C., Guise, T.A., and Massagué, J. (2003). A multigenic program mediating breast cancer metastasis to bone. Cancer Cell *3*, 537–549.

Kelly, P.N., Dakic, A., Adams, J.M., Nutt, S.L., and Strasser, A. (2007). Tumor Growth Need Not Be Driven by Rare Cancer Stem Cells. Science (80-.). *317*.

Kelwick, R., Desanlis, I., Wheeler, G.N., Edwards, D.R., Porter, S., Clark, I., Kevorkian, L., Edwards, D., Apte, S., Gomis-Ruth, F., et al. (2015). The ADAMTS (A Disintegrin and Metalloproteinase with Thrombospondin motifs) family. Genome Biol. *16*, 113.

Kerkar, S.P., and Restifo, N.P. (2012). Cellular Constituents of Immune Escape within the Tumor Microenvironment. Cancer Res. *72*.

Kern, C.B., Wessels, A., McGarity, J., Dixon, L.J., Alston, E., Argraves, W.S., Geeting, D., Nelson, C.M., Menick, D.R., and Apte, S.S. (2010). Reduced versican cleavage due to Adamts9 haploinsufficiency is associated with cardiac and aortic anomalies. Matrix Biol. *29*, 304–316.

Kimura, N., Toyoshima, T., Kojima, T., and Shimane, M. (1998). Entactin-2: a new member of basement membrane protein with high homology to entactin/nidogen. Exp. Cell Res. *241*, 36–45.

Klein, T., and Bischoff, R. (2011). Physiology and pathophysiology of matrix metalloproteases. Amino Acids *41*, 271–290.

Kodama, J., Hasengaowa, Kusumoto, T., Seki, N., Matsuo, T., Ojima, Y., Nakamura, K., Hongo, A., and Hiramatsu, Y. (2006). Prognostic significance of stromal versican expression in human endometrial cancer. Ann. Oncol. *18*, 269–274.

Kohfeldt, E., Sasaki, T., Göhring, W., and Timpl, R. (1998). Nidogen-2: a new basement membrane protein with diverse binding properties. J. Mol. Biol. *282*, 99–109.

Krishna Priya, S., Nagare, R.P., Sneha, V.S., Sidhanth, C., Bindhya, S., Manasa, P., and Ganesan, T.S. (2016). Tumour angiogenesis-Origin of blood vessels. Int. J. Cancer *139*, 729–735.

Kruegel, J., and Miosge, N. (2010). Basement membrane components are key players in specialized extracellular matrices. Cell. Mol. Life Sci. *67*, 2879–2895.

Kuk, C., Gunawardana, C.G., Soosaipillai, A., Kobayashi, H., Li, L., Zheng, Y., and Diamandis, E.P. (2010). Nidogen-2: a new serum biomarker for ovarian cancer. Clin. Biochem. *43*, 355–361.

Kumar, S., Rao, N., and Ge, R. (2012). Emerging Roles of ADAMTSs in Angiogenesis and Cancer. Cancers (Basel). *4*, 1252–1299.

Kuno, K., Kanada, N., Nakashima, E., Fujiki, F., Ichimura, F., and Matsushima, K. (1997a). Molecular cloning of a gene encoding a new type of metalloproteinase-disintegrin family protein with thrombospondin motifs as an inflammation associated gene. J. Biol. Chem. *272*, 556–562.

Kuno, K., Iizasa, H., Ohno, S., and Matsushima, K. (1997b). The Exon/Intron Organization and Chromosomal Mapping of the Mouse ADAMTS-1 Gene Encoding an ADAM Family Protein with TSP Motifs. Genomics *46*, 466–471.

Kuno, K., Bannai, K., Hakozaki, M., Matsushima, K., and Hirose, K. (2004). The carboxyl-terminal half region of ADAMTS-1 suppresses both tumorigenicity and experimental tumor metastatic potential. Biochem. Biophys. Res. Commun. *319*, 1327–1333.

L

Lai, C.-Y., Schwartz, B.E., and Hsu, M.-Y. (2012). CD133+ Melanoma Subpopulations Contribute to Perivascular Niche Morphogenesis and Tumorigenicity through Vasculogenic Mimicry. Cancer Res. *72*, 5111–5118.

Lai, K.K.Y., Shang, S., Lohia, N., Booth, G.C., Masse, D.J., Fausto, N., Campbell, J.S., Beretta, L., El-Serag, H., Rudolph, K., et al. (2011). Extracellular Matrix Dynamics in Hepatocarcinogenesis: a Comparative

Proteomics Study of PDGFC Transgenic and Pten Null Mouse Models. PLoS Genet. *7*, e1002147.

Lapidot, T., Sirard, C., Vormoor, J., Murdoch, B., Hoang, T., Caceres-Cortes, J., Minden, M., Paterson, B., Caligiuri, M.A., and Dick, J.E. (1994). A cell initiating human acute myeloid leukaemia after transplantation into SCID mice. Nature *367*, 645–648.

Lee, H.K., Seo, I.A., Park, H.K., and Park, H.T. (2006a). Identification of the basement membrane protein nidogen as a candidate ligand for tumor endothelial marker 7 in vitro and in vivo. FEBS Lett. *580*, 2253–2257.

Lee, N. V, Rodriguez-Manzaneque, J.C., Thai, S.N.-M., Twal, W.O., Luque, A., Lyons, K.M., Argraves, W.S., and Iruela-Arispe, M.L. (2005). Fibulin-1 acts as a cofactor for the matrix metalloprotease ADAMTS-1. J. Biol. Chem. *280*, 34796–34804.

Lee, N.V.N., Sato, M., Annis, D.S.D., Loo, J.A., Wu, L., Mosher, D.F.D., Iruela-Arispe, M.L., Agah, A., Kyriakides, T., Lawler, J., et al. (2006b). ADAMTS1 mediates the release of antiangiogenic polypeptides from TSP1 and 2. EMBO J. *25*, 5270–5283.

Lee, Y., Koch, M., Karl, D., Torres-collado, A.X., Namali, T., Rothrock, C., Kuruppu, D., Ryeom, S., Iruela-, M.L., and Yoon, S.S. (2010). Variable inhibition of Thrombospondin 1 against liver and lung metastases through differential activation of metalloproteinase ADAMTS1. Cancer Res. *70*, 948–956.

Li, L., Zhang, Y., Li, N., Feng, L., Yao, H., Zhang, R., Li, B., Li, X., Han, N., Gao, Y., et al. (2015). Nidogen-1: a candidate biomarker for ovarian serous cancer. Jpn. J. Clin. Oncol. *45*, 176–182.

Liang, J., Yang, B., Cao, Q., and Wu, X. (2016). Association of Vasculogenic Mimicry Formation and CD133 Expression with Poor Prognosis in Ovarian Cancer. Gynecol. Obstet. Invest. *81*, 529–536.

Lin, E.Y., Li, J., Bricard, G., Wang, W., Deng, Y., Sellers, R., Porcelli, S.A., and Pollard, J.W. (2007). Vascular endothelial growth factor restores delayed tumor progression in tumors depleted of macrophages. Mol. Oncol. *1*, 288–302.

Lind, T., Birch, M.A., and McKie, N. (2006). Purification of an insect derived recombinant human ADAMTS-1 reveals novel gelatin (type I collagen) degrading activities. Mol. Cell. Biochem. *281*, 95–102.

Liu, R., Yang, K., Meng, C., Zhang, Z., and Xu, Y. (2012). Vasculogenic mimicry is a marker of poor prognosis in prostate cancer. Cancer Biol. Ther. *13*, 527–533.

Liu, T., Xie, C., Ma, H., Zhang, S., Liang, Y., Shi, L., Yu, D., Feng, Y., Zhang, T., and Wu, G. (2014a). Gr-1+CD11b+ cells facilitate Lewis lung cancer recurrence by enhancing neovasculature after local irradiation. Sci. Rep. *4*, 4833.

Liu, T., Sun, B., Zhao, X., Li, Y., Gu, Q., Dong, X., and Liu, F. (2014b). OCT4 Expression and Vasculogenic Mimicry Formation Positively Correlate with Poor Prognosis in Human Breast Cancer. Int. J. Mol. Sci. *15*, 19634–19649.

Liu, Y.J., Xu, X., and Q, Y. (2006). Full-Length ADAMTS-1 and the ADAMTS-1 fragments display pro- and antimetastatic activity, respectively. Oncogene 2452.67.

López-Otín, C., and Overall, C.M. (2002). Protease degradomics: a new challenge for proteomics. Nat. Rev. Mol. Cell Biol. *3*, 509–519.

Lu, P., Li, L., Kuno, K., Wu, Y., Baba, T., Li, Y.-Y., Zhang, X., and Mukaida, N. (2008). Protective roles of the

fractalkine/CX3CL1-CX3CR1 interactions in alkali-induced corneal neovascularization through enhanced antiangiogenic factor expression. J. Immunol. *180*, 4283–4291.

Lu, P., Takai, K., Weaver, V.M., and Werb, Z. (2011). Extracellular matrix degradation and remodeling in development and disease. Cold Spring Harb. Perspect. Biol. *3*, a005058.

Lu, P., Weaver, V.M., and Werb, Z. (2012). The extracellular matrix: A dynamic niche in cancer progression. J. Cell Biol. *196*, 395–406.

Lu, X., Wang, Q., Hu, G., Van Poznak, C., Fleisher, M., Reiss, M., Massagué, J., Kang, Y., Poznak, C. Van, Fleisher, M., et al. (2009). ADAMTS1 and MMP1 proteolytically engage EGF-like ligands in an osteolytic signaling cascade for bone metastasis. Genes Dev. *23*, 1882–1894.

Luque, A., Carpizo, D.R., and Iruela-Arispe, M.L. (2003). ADAMTS1/METH1 inhibits endothelial cell proliferation by direct binding and sequestration of VEGF165. J. Biol. Chem. *278*, 23656–23665.

M

Makatsori, E., Lamari, F.N., Theocharis, A.D., Anagnostides, S., Hjerpe, A., Tsegenidis, T., and Karamanos, N.K. (2003). Large matrix proteoglycans, versican and perlecan, are expressed and secreted by human leukemic monocytes. Anticancer Res. *23*, 3303–3309.

Maniotis, A.J., Folberg, R., Hess, A., Seftor, E.A., Gardner, L.M., Pe'er, J., Trent, J.M., Meltzer, P.S., and Hendrix, M.J. (1999). Vascular channel formation by human melanoma cells in vivo and in vitro: vasculogenic mimicry. Am. J. Pathol. *155*, 739–752.

Mantovani, A., Sozzani, S., Locati, M., Allavena, P., Sica, A., Stein, M., al., et, Goerdt, S., al., et, Mantovani, A., et al. (2002). Macrophage polarization: tumor-associated macrophages as a paradigm for polarized M2 mononuclear phagocytes. Trends Immunol. *23*, 549–555.

Mantovani, A., Allavena, P., Sica, A., and Balkwill, F. (2008). Cancer-related inflammation. Nature *454*, 436–444.

Manzur, M., Hamzah, J., and Ganss, R. (2008). Modulation of the "blood-tumor" barrier improves immunotherapy. Cell Cycle *7*, 2452–2455.

Maquart, F.-X., Pasco, S., Ramont, L., Hornebeck, W., and Monboisse, J.-C. (2004). An introduction to matrikines: extracellular matrix-derived peptides which regulate cell activity: Implication in tumor invasion. Crit. Rev. Oncol. Hematol. *49*, 199–202.

Martino-Echarri, E., Fernández-Rodríguez, R., Rodríguez-Baena, F.J., Barrientos-Durán, A., Torres-Collado, A.X., Plaza-Calonge, M. del C., Amador-Cubero, S., Cortés, J., Reynolds, L.E., Hodivala-Dilke, K.M., et al. (2013). Contribution of ADAMTS1 as a tumor suppressor gene in human breast carcinoma. Linking its tumor inhibitory properties to its proteolytic activity on nidogen-1 and nidogen-2. Int. J. Cancer *133*, 2315–2324.

Martino-Echarri, E., Fernández-Rodríguez, R., Bech-Serra, J.J., Plaza-Calonge, M. del C., Vidal, N., Casal, C., Colomé, N., Seoane, J., Canals, F., Rodríguez-Manzaneque, J.C., et al. (2014). Relevance of IGFBP2 proteolysis in glioma and contribution of the extracellular protease ADAMTS1. Oncotarget *5*, 4295–4304.

Marusyk, A., and Polyak, K. (2010). Tumor heterogeneity: causes and consequences. Biochim. Biophys.

Acta *1805*, 105–117.

Masui, T., Hosotani, R., Tsuji, S., Nakajima, S., and Kawaguchi, M. (2001). Expression of METH-1 and METH-2 in Pancreatic Cancer. Clin. Cancer Res. *7*, 3437–3443.

Matthews, R.T., Gary, S.C., Zerillo, C., Pratta, M., Solomon, K., Arner, E.C., and Hockfield, S. (2000). Brain-enriched Hyaluronan Binding (BEHAB)/Brevican Cleavage in a Glioma Cell Line Is Mediated by a Disintegrin and Metalloproteinase with Thrombospondin Motifs (ADAMTS) Family Member. J. Biol. Chem. *275*, 22695–22703.

Mayer, U., Mann, K., Timpl, R., and Murphy, G. (1993). Sites of nidogen cleavage by proteases involved in tissue homeostasis and remodelling. Eur. J. Biochem. *217*, 877–884.

McCulloch, D.R., Nelson, C.M., Dixon, L.J., Silver, D.L., Wylie, J.D., Lindner, V., Sasaki, T., Cooley, M.A., Argraves, W.S., and Apte, S.S. (2009). ADAMTS Metalloproteases Generate Active Versican Fragments that Regulate Interdigital Web Regression. Dev. Cell *17*, 687–698.

McMahon, M., Ye, S., Izzard, L., Dlugolenski, D., Tripp, R.A., Bean, A.G.D., McCulloch, D.R., Stambas, J., Lakadamyali, M., Rust, M., et al. (2016). ADAMTS5 Is a Critical Regulator of Virus-Specific T Cell Immunity. PLOS Biol. *14*, e1002580.

Meulmeester, E., and ten Dijke, P. (2011). The dynamic roles of TGF-β in cancer. J. Pathol. *223*, 206–219.

Miosge, N., Sasaki, T., and Timpl, R. (2002). Evidence of nidogen-2 compensation for nidogen-1 deficiency in transgenic mice. Matrix Biol. *21*, 611–621.

Misra, R.M., Bajaj, M.S., and Kale, V.P. (2012). Vasculogenic Mimicry of HT1080 Tumour Cells In Vivo: Critical Role of HIF-1α-Neuropilin-1 Axis. PLoS One *7*, e50153.

Mittaz, L., Russell, D.L., Wilson, T., Brasted, M., Tkalcevic, J., Salamonsen, L.A., Hertzog, P.J., and Pritchard, M.A. (2004). Adamts-1 is essential for the development and function of the urogenital system. Biol. Reprod. *70*, 1096–1105.

Mokkapati, S., Baranowsky, A., Mirancea, N., Smyth, N., Breitkreutz, D., and Nischt, R. (2008). Basement membranes in skin are differently affected by lack of nidogen 1 and 2. J. Invest. Dermatol. *128*, 2259–2267.

Mokkapati, S., Bechtel, M., Reibetanz, M., Miosge, N., and Nischt, R. (2012). Absence of the basement membrane component nidogen 2, but not of nidogen 1, results in increased lung metastasis in mice. J. Histochem. Cytochem. *60*, 280–289.

Monahan-Earley, R., Dvorak, A.M., and Aird, W.C. (2013). Evolutionary origins of the blood vascular system and endothelium. J. Thromb. Haemost. *11*, 46–66.

Mott, J.D., and Werb, Z. (2004). Regulation of matrix biology by matrix metalloproteinases. Curr. Opin. Cell Biol. *16*, 558–564.

Mullooly, M., McGowan, P.M., Crown, J., and Duffy, M.J. (2016). The ADAMs family of proteases as targets for the treatment of cancer. Cancer Biol. Ther. *17*, 870–880.

Murshed, M., Smyth, N., Miosge, N., Karolat, J., Krieg, T., Paulsson, M., and Nischt, R. (2000). The absence of nidogen 1 does not affect murine basement membrane formation. Mol. Cell. Biol. *20*, 7007–7012.

N

Naba, A., Clauser, K.R., Whittaker, C.A., Carr, S.A., Tanabe, K.K., Hynes, R.O., Rustgi, A., Network, C., Hanash, S., Taguchi, A., et al. (2014). Extracellular matrix signatures of human primary metastatic colon cancers and their metastases to liver. BMC Cancer *14*, 518.

Nagase, H., Visse, R., and Murphy, G. (2006). Structure and function of matrix metalloproteinases and TIMPs. Cardiovasc. Res. *69*.

Nagy, J., Chang, S.-H., Shih, S.-C., Dvorak, A., and Dvorak, H. (2010). Heterogeneity of the Tumor Vasculature. Semin. Thromb. Hemost. *36*, 321–331.

Nan, H., Xu, M., Zhang, J., Zhang, M., Kraft, P., Qureshi, A.A., Chen, C., Guo, Q., Hu, F.B., Rimm, E.B., et al. (2011). Genome-wide association study identifies nidogen 1 (NID1) as a susceptibility locus to cutaneous nevi and melanoma risk. Hum. Mol. Genet. *20*, 2673–2679.

Nandadasa, S., Foulcer, S., and Apte, S.S. (2014). The multiple, complex roles of versican and its proteolytic turnover by ADAMTS proteases during embryogenesis. Matrix Biol. *35*, 34–41.

Naso, M.F., Morgan, J.L., Buchberg, A.M., Siracusa, L.D., and Iozzo, R. V. (1995). Expression Pattern and Mapping of the Murine Versican Gene (Cspg2) to Chromosome 13. Genomics *29*, 297–300.

Ng, Y.H., Zhu, H., Pallen, C.J., Leung, P.C.K., and MacCalman, C.D. (2006). Differential effects of interleukin-1beta and transforming growth factor-beta1 on the expression of the inflammation-associated protein, ADAMTS-1, in human decidual stromal cells in vitro. Hum. Reprod. *21*, 1990–1999.

Nguyen, L. V., Vanner, R., Dirks, P., and Eaves, C.J. (2012). Cancer stem cells: an evolving concept. Nat. Rev. Cancer *12*, 133.

Nicosia, R.F., Bonanno, E., Smith, M., and Yurchenco, P. (1994). Modulation of angiogenesis in vitro by laminin-entactin complex. Dev. Biol. *164*, 197–206.

Nikitovic, D., Zafiropoulos, A., Katonis, P., Tsatsakis, A., Theocharis, A.D., Karamanos, N.K., and Tzanakakis, G.N. (2006). Transforming Growth Factor-β as a key molecule triggering the expression of versican isoforms v0 and v1, Hyaluronan Synthase-2 and synthesis of Hyaluronan in Malignant Osteosarcoma cells. IUBMB Life *58*, 47–53.

Nowell, P. (1976). The clonal evolution of tumor cell populations. Science (80-.). *194*, 23–28.

O

Oivula, J., Lohi, J., Tani, T., Kangas, L., Kiviluoto, T., Kivilaakso, E., Butkowski, R., and Virtanen, I. (1999). Renal cell carcinomas and pancreatic adenocarcinomas produce nidogen in vitro and in vivo. J. Pathol. *187*, 455–461.

Oller, J., Méndez-Barbero, N., Ruiz, E.J., Villahoz, S., Renard, M., Canelas, L.I., Briones, A.M., Alberca, R., Lozano-Vidal, N., Hurlé, M.A., et al. (2017). Nitric oxide mediates aortic disease in mice deficient in the metalloprotease Adamts1 and in a mouse model of Marfan syndrome. Nat. Med. *23*, 200–212.

Onken, J., Moeckel, S., Leukel, P., Leidgens, V., Baumann, F., Bogdahn, U., Vollmann-Zwerenz, A., and Hau, P. (2014). Versican isoform V1 regulates proliferation and migration in high-grade gliomas. J.

Neurooncol. *120*, 73–83.

Ostrand-Rosenberg, S. (2008). Immune surveillance: a balance between protumor and antitumor immunity. Curr. Opin. Genet. Dev. *18*, 11–18.

Oveland, E., Karlsen, T. V., Haslene-Hox, H., Semaeva, E., Janaczyk, B., Tenstad, O., and Wiig, H. (2012). Proteomic Evaluation of Inflammatory Proteins in Rat Spleen Interstitial Fluid and Lymph during LPS-Induced Systemic Inflammation Reveals Increased Levels of ADAMST1. J. Proteome Res. *11*, 5338–5349.

Overwijk, W.W., and Restifo, N.P. (2001). B16 as a mouse model for human melanoma. Curr. Protoc. Immunol. *Chapter 20*, Unit 20.1.

Owens, G.K., Kumar, M.S., and Wamhoff, B.R. (2004). Molecular regulation of vascular smooth muscle cell differentiation in development and disease. Physiol. Rev. *84*, 767–801.

𝒫

Paulsson, M. (1992). Basement membrane proteins: structure, assembly, and cellular interactions. Crit. Rev. Biochem. Mol. Biol. *27*, 93–127.

Paulsson, M., Deutzmann, R., Dziadek, M., Nowack, H., Timpl, R., Weber, S., and Engel, J. (1986). Purification and structural characterization of intact and fragmented nidogen obtained from a tumor basement membrane. Eur. J. Biochem. *156*, 467–478.

Paulus, W., Baur, I., Dours-Zimmermann, M.T., and Zimmermann, D.R. (1996). Differential expression of versican isoforms in brain tumors. J. Neuropathol. Exp. Neurol. *55*, 528–533.

Pedrola, N., Devis, L., Llauradó, M., Campoy, I., Martinez-Garcia, E., Garcia, M., Muinelo-Romay, L., Alonso-Alconada, L., Abal, M., Alameda, F., et al. (2015). Nidogen 1 and Nuclear Protein 1: novel targets of ETV5 transcription factor involved in endometrial cancer invasion. Clin. Exp. Metastasis *32*, 467–478.

Pickup, M.W., Mouw, J.K., and Weaver, V.M. (2014). The extracellular matrix modulates the hallmarks of cancer. EMBO Rep. *15*, 1243–1253.

Pirinen, R., Leinonen, T., Böhm, J., Johansson, R., Ropponen, K., Kumpulainen, E., and Kosma, V.-M. (2005). Versican in nonsmall cell lung cancer: relation to hyaluronan, clinicopathologic factors, and prognosis. Hum. Pathol. *36*, 44–50.

Porta, C., Riboldi, E., Totaro, M.G., Strauss, L., Sica, A., and Mantovani, A. (2011). Macrophages in cancer and infectious diseases: the "good" and the "bad." Immunotherapy *3*, 1185–1202.

Porter, S., Scott, S.D., Sassoon, E.M., Williams, M.R., Jones, J.L., Girling, A.C., Ball, R.Y., and Edwards, D.R. (2004). Dysregulated expression of adamalysin-thrombospondin genes in human breast carcinoma. Clin. Cancer Res. *10*, 2429–2440.

Poste, G., Doll, J., Hart, I.R., and Fidler, I.J. (1980). In vitro selection of murine B16 melanoma variants with enhanced tissue-invasive properties. Cancer Res. *40*, 1636–1644.

Potente, M., Gerhardt, H., and Carmeliet, P. (2011). Basic and therapeutic aspects of angiogenesis. Cell *146*, 873–887.

Puente, X.S., Sánchez, L.M., Overall, C.M., and López-Otín, C. (2003). Human and mouse proteases: a comparative genomic approach. Nat. Rev. Genet. *4*, 544–558.

Pujuguet, P., Simian, M., Liaw, J., Timpl, R., Werb, Z., and Bissell, M.J. (2000). Nidogen-1 regulates laminin-1-dependent mammary-specific gene expression. J. Cell Sci. *113 (Pt 5*, 849–858.

Quesada, V., Ordóñez, G.R., Sánchez, L.M., Puente, X.S., and López-Otín, C. (2009). The Degradome database: mammalian proteases and diseases of proteolysis. Nucleic Acids Res. *37*, D239-43.

$\mathcal{R}$

Rahbari, N.N., Kedrin, D., Incio, J., Liu, H., Ho, W.W., Nia, H.T., Edrich, C.M., Jung, K., Daubriac, J., Chen, I., et al. (2016). Anti-VEGF therapy induces ECM remodeling and mechanical barriers to therapy in colorectal cancer liver metastases. *135*, 1–12.

Rahmani, M., Wong, B.W., Ang, L., Cheung, C.C., Carthy, J.M., Walinski, H., and McManus, B.M. (2006). Versican: signaling to transcriptional control pathwaysThis paper is one of a selection of papers published in this Special Issue, entitled Young Investigator's Forum. Can. J. Physiol. Pharmacol. *84*, 77–92.

Raymond, K., Deugnier, M.-A., Faraldo, M.M., and Glukhova, M.A. (2009). Adhesion within the stem cell niches. Curr. Opin. Cell Biol. *21*, 623–629.

Rehn, A.P., Birch, M.A., Karlström, E., Wendel, M., and Lind, T. (2007). ADAMTS-1 increases the three-dimensional growth of osteoblasts through type I collagen processing. Bone *41*, 231–238.

Rensen, S.S.M., Doevendans, P.A.F.M., and van Eys, G.J.J.M. (2007). Regulation and characteristics of vascular smooth muscle cell phenotypic diversity. Neth. Heart J. *15*, 100–108.

Reynolds, L.E., Watson, A.R., Baker, M., Jones, T.A., D'Amico, G., Robinson, S.D., Joffre, C., Garrido-Urbani, S., Rodriguez-Manzaneque, J.C., Martino-Echarri, E., et al. (2010). Tumour angiogenesis is reduced in the Tc1 mouse model of Down's syndrome. Nature *465*, 813–817.

Ribatti, D., Nico, B., and Crivellato, E. (2011). The role of pericytes in angiogenesis. Int. J. Dev. Biol. *55*, 261–268.

Ricciardelli, C., Mayne, K., Sykes, P.J., Raymond, W.A., McCaul, K., Marshall, V.R., and Horsfall, D.J. (1998). Elevated levels of versican but not decorin predict disease progression in early-stage prostate cancer. Clin. Cancer Res. *4*, 963–971.

Ricciardelli, C., Brooks, J.H., Suwiwat, S., Sakko, A.J., Mayne, K., Raymond, W.A., Seshadri, R., LeBaron, R.G., and Horsfall, D.J. (2002). Regulation of stromal versican expression by breast cancer cells and importance to relapse-free survival in patients with node-negative primary breast cancer. Clin. Cancer Res. *8*, 1054–1060.

Ricciardelli, C., Sakko, A.J., Ween, M.P., Russell, D.L., and Horsfall, D.J. (2009). The biological role and regulation of versican levels in cancer. Cancer Metastasis Rev. *28*, 233–245.

Ricciardelli, C., Frewin, K.M., Tan, I. de A., Williams, E.D., Opeskin, K., Pritchard, M.A., Ingman, W. V, and Russell, D.L. (2011). The ADAMTS1 Protease Gene Is Required for Mammary Tumor Growth and Metastasis. Am. J. Pathol. *179*, 3075–3085.

Risau, W. (1997). Mechanisms of angiogenesis. Nature *386*, 671–674.

Robker, R.L., Russell, D.L., Espey, L.L., Lydon, J.P., O'Malley, B.W., and Richards, J.S. (2000). Progesterone-regulated genes in the ovulation process: ADAMTS-1 and cathepsin L proteases. Proc Natl Acad Sci U S A *97*, 4689–4694.

Rodriguez-Manzaneque, J.C., Milchanowski, A.B., Dufour, E.K., Leduc, R., and Iruela-Arispe, M.L. (2000). Characterization of METH-1/ADAMTS1 Processing Reveals Two Distinct Active Forms. J. Biol. Chem. *275*, 33471–33479.

Rodríguez-Manzaneque, J.C., Westling, J., Thai, S.N.-M., Luque, A., Knauper, V., Murphy, G., Sandy, J.D., and Iruela-Arispe, M.L. (2002). ADAMTS1 cleaves aggrecan at multiple sites and is differentially inhibited by metalloproteinase inhibitors. Biochem. Biophys. Res. Commun. *293*, 501–508.

Rodríguez-Manzaneque, J.C., Carpizo, D., Plaza-Calonge, M. del C., Torres-Collado, A.X., Thai, S.N.-M., Simons, M., Horowitz, A., and Iruela-Arispe, M.L. (2009). Cleavage of syndecan-4 by ADAMTS1 provokes defects in adhesion. Int. J. Biochem. Cell Biol. *41*, 800–810.

Rodríguez-Manzaneque, J.C.J.C., Fernández-Rodríguez, R., Rodríguez-Baena, F.J.F.J., and Iruela-Arispe, M.L.L. (2015). ADAMTS proteases in vascular biology. Matrix Biol. *44*, 38–45.

Rozario, T., and DeSimone, D.W. (2010). The extracellular matrix in development and morphogenesis: A dynamic view. Dev. Biol. *341*, 126–140.

Ruffell, B., Au, A., Rugo, H.S., Esserman, L.J., Hwang, E.S., and Coussens, L.M. (2012). Leukocyte composition of human breast cancer. Proc. Natl. Acad. Sci. U. S. A. *109*, 2796–2801.

S

Sage, J., Leblanc-Noblesse, E., Nizard, C., Sasaki, T., Schnebert, S., Perrier, E., Kurfurst, R., Brömme, D., Lalmanach, G., and Lecaille, F. (2012). Cleavage of nidogen-1 by cathepsin S impairs its binding to basement membrane partners. PLoS One *7*, e43494.

Salmivirta, K., Talts, J.F., Olsson, M., Sasaki, T., Timpl, R., and Ekblom, P. (2002a). Binding of mouse nidogen-2 to basement membrane components and cells and its expression in embryonic and adult tissues suggest complementary functions of the two nidogens. Exp. Cell Res. *279*, 188–201.

Salmivirta, K., Talts, J.F., Olsson, M., Sasaki, T., Timpl, R., and Ekblom, P. (2002b). Binding of Mouse Nidogen-2 to Basement Membrane Components and Cells and Its Expression in Embryonic and Adult Tissues Suggest Complementary Functions of the Two Nidogens. Exp. Cell Res. *279*, 188–201.

Sandy, J.D., Westling, J., Kenagy, R.D., Iruela-Arispe, M.L., Verscharen, C., Rodriguez-Mazaneque, J.C., Zimmermann, D.R., Lemire, J.M., Fischer, J.W., Wight, T.N., et al. (2001). Versican V1 Proteolysis in Human Aorta in Vivo Occurs at the Glu441-Ala442 Bond, a Site That Is Cleaved by Recombinant ADAMTS-1 and ADAMTS-4. J. Biol. Chem. *276*, 13372–13378.

Sasaki, M., Seo-Kiryu, S., Kato, R., Kita, S., and Kiyama, H. (2001). A disintegrin and metalloprotease with thrombospondin type1 motifs (ADAMTS-1) and IL-1 receptor type 1 mRNAs are simultaneously induced in nerve injured motor neurons.

Schmitt, M., Hope, C., Foulcer, S., Jagodinsky, J., Wang, L., Jin, N., Schmitt, A., Schmitt, M., Schmitt, A., Rojewski, M., et al. (2016). Versican vs versikine: tolerance vs attack. Blood *128*, 612–613.

Schoenenberger, C.A., Andres, A.C., Groner, B., van der Valk, M., LeMeur, M., and Gerlinger, P. (1988). Targeted c-myc gene expression in mammary glands of transgenic mice induces mammary tumours with constitutive milk protein gene transcription. EMBO J. *7*, 169–175.

Schrimpf, C., Xin, C., Campanholle, G., Gill, S.E., Stallcup, W., Lin, S.-L., Davis, G.E., Gharib, S.A., Humphreys, B.D., and Duffield, J.S. (2012). Pericyte TIMP3 and ADAMTS1 modulate vascular stability after kidney injury. J. Am. Soc. Nephrol. *23*, 868–883.

Schymeinsky, J., Nedbal, S., Miosge, N., Pöschl, E., Rao, C., Beier, D.R., Skarnes, W.C., Timpl, R., and Bader, B.L. (2002). Gene structure and functional analysis of the mouse nidogen-2 gene: nidogen-2 is not essential for basement membrane formation in mice. Mol. Cell. Biol. *22*, 6820–6830.

Seewaldt, V. (2014). ECM stiffness paves the way for tumor cells. Nat. Med. *20*, 332–333.

Seftor, R.E., Seftor, E.A., Koshikawa, N., Meltzer, P.S., Gardner, L.M., Bilban, M., Stetler-Stevenson, W.G., Quaranta, V., and Hendrix, M.J. (2001). Cooperative interactions of laminin 5 gamma2 chain, matrix metalloproteinase-2, and membrane type-1-matrix/metalloproteinase are required for mimicry of embryonic vasculogenesis by aggressive melanoma. Cancer Res. *61*, 6322–6327.

Semkova, I., Kociok, N., Karagiannis, D., Nischt, R., Smyth, N., Paulsson, M., Strauß, O., and Joussen, A.M. (2014). Anti-angiogenic effect of the basement membrane protein nidogen-1 in a mouse model of choroidal neovascularization. Exp. Eye Res. *118*, 80–88.

Shamir, E.R., and Ewald, A.J. (2014). Three-dimensional organotypic culture: experimental models of mammalian biology and disease. Nat. Rev. Mol. Cell Biol. *15*, 647–664.

Shindo, T., Kurihara, H., Kuno, K., Yokoyama, H., Wada, T., Kurihara, Y., Imai, T., Wang, Y., Ogata, M., Nishimatsu, H., et al. (2000). ADAMTS-1: A metalloproteinase-disintegrin essential for normal growth, fertility, and organ morphology and function. J. Clin. Invest. *105*, 1345–1352.

Shiomi, T., Lemaître, V., D'Armiento, J., and Okada, Y. (2010). Matrix metalloproteinases, a disintegrin and metalloproteinases, and a disintegrin and metalloproteinases with thrombospondin motifs in non-neoplastic diseases. Pathol. Int. *60*, 477–496.

Shojaei, F., Wu, X., Malik, A.K., Zhong, C., Baldwin, M.E., Schanz, S., Fuh, G., Gerber, H.-P., and Ferrara, N. (2007). Tumor refractoriness to anti-VEGF treatment is mediated by CD11b+Gr1+ myeloid cells. Nat. Biotechnol. *25*, 911–920.

Shozu, M., Minami, N., Yokoyama, H., Inoue, M., Kurihara, H., Matsushima, K., and Kuno, K. (2005). ADAMTS-1 is involved in normal follicular development, ovulatory process and organization of the medullary vascular network in the ovary. J. Mol. Endocrinol. *35*, 343–355.

Srivastava, M.M.K., Zhu, L., Harris-White, M., Kar, U.U., Huang, M., Johnson, M.F., Lee, J.M.J., Elashoff, D., Strieter, R., Dubinett, S., et al. (2012). Myeloid Suppressor Cell Depletion Augments Antitumor Activity in Lung Cancer. PLoS One *7*, e40677.

Stankunas, K., Hang, C.T., Tsun, Z.-Y., Chen, H., Lee, N. V., Wu, J.I., Shang, C., Bayle, J.H., Shou, W., Iruela-Arispe, M.L., et al. (2008). Endocardial Brg1 Represses ADAMTS1 to Maintain the Microenvironment for Myocardial Morphogenesis. Dev. Cell *14*, 298–311.

Stapor, P.C., Sweat, R.S., Dashti, D.C., Betancourt, A.M., and Murfee, W.L. (2014). Pericyte dynamics during angiogenesis: new insights from new identities. J. Vasc. Res. *51*, 163–174.

Sternlicht, M.D., Lochter, A., Sympson, C.J., Huey, B., Rougier, J.P., Gray, J.W., Pinkel, D., Bissell, M.J., and Werb, Z. (1999). The stromal proteinase MMP3/stromelysin-1 promotes mammary carcinogenesis.

Cell *98*, 137–146.

Stewart, T.A., Pattengale, P.K., and Leder, P. (1984). Spontaneous mammary adenocarcinomas in transgenic mice that carry and express MTV/myc fusion genes. Cell *38*, 627–637.

Stover, D.G., Bierie, B., and Moses, H.L. (2007). A delicate balance: TGF-beta and the tumor microenvironment. J. Cell. Biochem. *101*, 851–861.

Stratman, A.N., Malotte, K.M., Mahan, R.D., Davis, M.J., and Davis, G.E. (2009). Pericyte recruitment during vasculogenic tube assembly stimulates endothelial basement membrane matrix formation. Blood *114*, 5091–5101.

Stylianopoulos, T., Martin, J.D., Snuderl, M., Mpekris, F., Jain, S.R., and Jain, R.K. (2013). Coevolution of solid stress and interstitial fluid pressure in tumors during progression: Implications for vascular collapse. Cancer Res. *73*, 3833–3841.

Su, S.-C., Mendoza, E.A., Kwak, H.-I., and Bayless, K.J. (2008). Molecular profile of endothelial invasion of three-dimensional collagen matrices: insights into angiogenic sprout induction in wound healing. Am. J. Physiol. Cell Physiol. *295*, C1215-29.

Sumpio, B.E., Riley, J.T., and Dardik, A. (2002). Cells in focus: endothelial cell. Int. J. Biochem. Cell Biol. *34*, 1508–1512.

T

Tang, B.L., and Hong, W. (1999). ADAMTS: a novel family of proteases with an ADAM protease domain and thrombospondin 1 repeats. FEBS Lett. *445*, 223–225.

Tanjore, H., and Kalluri, R. (2006). The role of type IV collagen and basement membranes in cancer progression and metastasis. Am. J. Pathol. *168*, 715–717.

Tennant, M., and McGeachie, J.K. (1990). BLOOD VESSEL STRUCTURE AND FUNCTION: A BRIEF UPDATE ON RECENT ADVANCES. ANZ J. Surg. *60*, 747–753.

Thai, S.N.-M., and Iruela-Arispe, M.L. (2002). Expression of ADAMTS1 during murine development. Mech. Dev. *115*, 181–185.

Thienel, U., Loike, J., and Yellin, M.J. (1999). CD154 (CD40L) induces human endothelial cell chemokine production and migration of leukocyte subsets. Cell. Immunol. *198*, 87–95.

Thompson, W.D., Shiach, K.J., Fraser, R.A., McIntosh, L.C., and Simpson, J.G. (1987). Tumours acquire their vasculature by vessel incorporation, not vessel ingrowth. J. Pathol. *151*, 323–332.

Titz, B., Dietrich, S., Sadowski, T., Beck, C., Petersen, A., and Sedlacek, R. (2004). Activity of MMP-19 inhibits capillary-like formation due to processing of nidogen-1. Cell. Mol. Life Sci. *61*, 1826–1833.

del Toro, R., Prahst, C., Mathivet, T., Siegfried, G., Kaminker, J.S., Larrivee, B., Breant, C., Duarte, A., Takakura, N., Fukamizu, A., et al. (2010). Identification and functional analysis of endothelial tip cell-enriched genes. Blood *116*, 4025–4033.

Touab, M., Villena, J., Barranco, C., Arumí-Uría, M., and Bassols, A. (2002). Versican is differentially expressed in human melanoma and may play a role in tumor development. Am. J. Pathol. *160*, 549–557.

Tyan, S.-W., Hsu, C.-H., Peng, K.-L., Chen, C.-C., Kuo, W.-H., Lee, E.Y.-H.P., Shew, J.-Y., Chang, K.-J., Juan, L.-J., and Lee, W.-H. (2012). Breast cancer cells induce stromal fibroblasts to secrete ADAMTS1 for cancer invasion through an epigenetic change. PLoS One *7*, e35128.

U

Ulazzi, L., Sabbioni, S., Miotto, E., Veronese, A., Angusti, A., Gafà, R., Manfredini, S., Farinati, F., Sasaki, T., Lanza, G., et al. (2007). Nidogen 1 and 2 gene promoters are aberrantly methylated in human gastrointestinal cancer. Mol. Cancer *6*, 17.

V

Valente, P., Noonan, D.M., Ogle, R.C., and Albini, A. (1996). Altered production of laminin and nidogen by high and low metastatic variants of murine melanoma cells. Oncol Res *8*, 131–138.

Vasudevan, A., Ho, M.S.P., Weiergräber, M., Nischt, R., Schneider, T., Lie, A., Smyth, N., and Köhling, R. (2010). Basement membrane protein nidogen-1 shapes hippocampal synaptic plasticity and excitability. Hippocampus *20*, 608–620.

Vázquez, F., Hastings, G., Ortega, M.A., Lane, T.F., Oikemus, S., Lombardo, M., and Iruela-Arispe, M.L. (1999). METH-1, a human ortholog of ADAMTS-1, and METH-2 are members of a new family of proteins with angio-inhibitory activity. J. Biol. Chem. *274*, 23349–23357.

Voron, T., Marcheteau, E., Pernot, S., Colussi, O., Tartour, E., Taieb, J., and Terme, M. (2014). Control of the Immune Response by Pro-Angiogenic Factors. Front. Oncol. *4*, 70.

Voron, T., Colussi, O., Marcheteau, E., Pernot, S., Nizard, M., Pointet, A.-L., Latreche, S., Bergaya, S., Benhamouda, N., Tanchot, C., et al. (2015). VEGF-A modulates expression of inhibitory checkpoints on CD8+ T cells in tumors. J. Exp. Med. *212*.

W

Wang, H., Lin, H., Pan, J., Mo, C., Zhang, F., Huang, B., Wang, Z., Chen, X., Zhuang, J., Wang, D., et al. (2016). Vasculogenic Mimicry in Prostate Cancer: The Roles of EphA2 and PI3K. J. Cancer *7*, 1114–1124.

Wang, Z., Li, Z., Wang, Y., Cao, D., Wang, X., Jiang, M., Li, M., Yan, X., Li, Y., Liu, Y., et al. (2015). Versican silencing improves the antitumor efficacy of endostatin by alleviating its induced inflammatory and immunosuppressive changes in the tumor microenvironment. Oncol. Rep. 2981–2991.

Wei, S.C., Fattet, L., Tsai, J.H., Guo, Y., Pai, V.H., Majeski, H.E., Chen, A.C., Sah, R.L., Taylor, S.S., Engler, A.J., et al. (2015). Matrix stiffness drives epithelial–mesenchymal transition and tumour metastasis through a TWIST1–G3BP2 mechanotransduction pathway. Nat. Cell Biol. *17*, 678–688.

Weis, S.M., and Cheresh, D.A. (2011). Tumor angiogenesis: molecular pathways and therapeutic targets. Nat. Med. *17*, 1359–1370.

Wight, T.N. (2002). Versican: a versatile extracellular matrix proteoglycan in cell biology. Curr. Opin. Cell Biol. *14*, 617–623.

Wu, Y.J., Pierre, D.P. La, Wu, J., Yee, A.J., and Yang, B.B. (2005). The interaction of versican with its binding partners. Www.cell-Research.com | Cell Res. *15*, 483–494.

Y

Yang, J.P., Liao, Y.D., Mai, D.M., Xie, P., Qiang, Y.Y., Zheng, L.S., Wang, M.Y., Mei, Y., Meng, D.F., Xu, L., et al. (2016). Tumor vasculogenic mimicry predicts poor prognosis in cancer patients: a meta-analysis. Angiogenesis *19*, 191–200.

Yang, L., DeBusk, L.M., Fukuda, K., Fingleton, B., Green-Jarvis, B., Shyr, Y., Matrisian, L.M., Carbone, D.P., and Lin, P.C. (2004). Expansion of myeloid immune suppressor Gr+CD11b+ cells in tumor-bearing host directly promotes tumor angiogenesis. Cancer Cell *6*, 409–421.

Yao, X., Ping, Y., Liu, Y., Chen, K., Yoshimura, T., Liu, M., Gong, W., Chen, C., Niu, Q., Guo, D., et al. (2013). Vascular endothelial growth factor receptor 2 (VEGFR-2) plays a key role in vasculogenic mimicry formation, neovascularization and tumor initiation by Glioma stem-like cells. PLoS One *8*, e57188.

Yegin, Z., Gunes, S., and Buyukalpelli, R. (2013). Hypermethylation of TWIST1 and NID2 in tumor tissues and voided urine in urinary bladder cancer patients. DNA Cell Biol. *32*, 386–392.

Z

Zennou, V., Petit, C., Guetard, D., Nerhbass, U., Montagnier, L., and Charneau, P. (2000). HIV-1 Genome Nuclear Import Is Mediated by a Central DNA Flap. Cell *101*, 173–185.

Zhang, D., Sun, B., Zhao, X., Ma, Y., Ji, R., Gu, Q., Dong, X., Li, J., Liu, F., Jia, X., et al. (2014). Twist1 expression induced by sunitinib accelerates tumor cell vasculogenic mimicry by increasing the population of CD133+ cells in triple-negative breast cancer. Mol. Cancer *13*, 207.

Zhang, Y., Xu, B., Liu, Y., Yao, H., Lu, N., Li, B., Gao, J., Guo, S., Han, N., Qi, J., et al. (2012). The ovarian cancer-derived secretory/releasing proteome: A repertoire of tumor markers. Proteomics *12*, 1883–1891.

Zhao, E., Xu, H., Wang, L., Kryczek, I., Wu, K., Hu, Y., Wang, G., and Zou, W. (2012). Bone marrow and the control of immunity. Cell. Mol. Immunol. *9*, 11–19.

Zhou, Y., Damsky, C.H., and Fisher, S.J. (1997). Preeclampsia is associated with failure of human cytotrophoblasts to mimic a vascular adhesion phenotype. One cause of defective endovascular invasion in this syndrome? J. Clin. Invest. *99*, 2152–2164.

Zhu, D., Xie, H., Li, H., Cai, P., Zhu, H., Xu, C., Chen, P., Sharan, A., Xia, Y., and Tang, W. (2015). Nidogen-1 is a common target of microRNAs MiR-192/215 in the pathogenesis of Hirschsprung's disease. J. Neurochem. *134*, 39–46.

Ziyad, S., and Iruela-Arispe, M.L. (2011). Molecular mechanisms of tumor angiogenesis. Genes Cancer *2*, 1085–1096.

TAKE YOUR NOTES!

NOTES

NOTES

NOTES

-